UNIVERSITY OF BIRMINGHAM

Self-Assembled Nanorods and Nanowires from Oxide Functional Materials Grown by Pulsed Laser Deposition

By

Ye Wang

A thesis submitted for the degree

of

Doctor of Philosophy

School of Metallurgy and Materials

The University of Birmingham

Birmingham, B15 2TT

United Kingdom

June, 2014

UNIVERSITY OF BIRMINGHAM

University of Birmingham Research Archive

e-theses repository

Abstract

In this study, ZnO, MgO, In_2O_3, SnO_2, iron oxide nanowires and nanorods were successfully produced by using Pulsed Laser Deposition. It was observed that the parameters, such as gold nanodots, number of pulses on the targets, temperature, oxygen pressure and substrate, contribute to various results.

For the growth of MgO nanorods, gold nanodots are essential. Increasing the pulses on gold target will increase the average width of MgO nanorods instead of increasing the average length. However, increasing the pulses on MgO target will only result in increasing the length.

The morphology of ZnO nanowires is highly influenced by the plasma plume. A high oxygen pressure (1.2Torr), a high laser energy density ($1J/cm^2$) and a proper temperature (600-700°C) are also necessary for ZnO nanorods and nanowires growth. In a higher temperature (800°C), ZnO tends to follow the Volmer-Weber (3D island) growth mode and for lower temperatures (600°C), the growth tends to be the Stranski-Krastanov growth mode. Au and Pd can be the catalyst for ZnO nanowires growth. By increasing the number of pulses on gold target, the distribution of the sizes and dimensions of ZnO nanorods become smaller. It was also observed that MgO and Si single crystalline substrates and glass can be used for ZnO nanowires growth.

For the growth of In_2O_3 nanorods, a temperature range of 500-700°C and an oxygen pressure of 1.2Torr is needed. In order to maintain a uniform size of the In_2O_3 one dimensional nanostructures formed, it was observed that the total numbers of gold shots should not be less than 5 shots and no more than 25 shots. When compared with gold, the

average width of nanorods grown with the assist from silver is smaller. Increasing the number of pulses on In_2O_3 will not only result in increasing the nanorods length, but also increases the average width. Regarding SnO_2 nanorods growth, either gold nanodots must be present or high oxygen pressure (1.2Torr) is needed when the temperature is set to at 700°C.

Nanowires made from the Fe_3O_4 target were produced with an oxygen pressure of 1.2Torr and substrate temperature of 700-800°C. On MgO substrate, the nanowires were formed parallel to the surface. However, on Al_2O_3 ceramic and single crystal substrates, the nanowires formed were perpendicular to the surface.

Acknowledgements

Contents

5

Chapter 1

Introduction

1.1 One-Dimensional Structures of Functional Oxides

One-dimensional (1D) nanostructures, recently, have had an increase in study, as they provide a suitable base for a variety of different applications such as nanodevices in electronics [1-3], photonics [4,5] and ultrasensitive biomolecular sensors [6,7]. Conventional semiconductors have been traditionally utilized as the primary source of nanowire materials. However, through the recent advancements in this field of study, it has been observed that additional functionality and improved efficiency can be obtained, if these nanowires are integrated, in conjunction with other materials such as transitional metal oxides. These materials offer a wide range of physical properties and are currently being utilized in a variety of different applications of ferromagnetism [9], ferroelectricity [10], and superconductivity [8].

One of the more widely used transitional metal oxides is MgO. Its versatility has allowed this material to be utilized in several types of applications such as insulation of layers in tunnel magnetoresistance junctions [11,12] and catalysis. It has also been utilized as a substrate for several thin films composed of other transition metal oxides such as magnetite [13], spinel ferrites [14] and perovskite oxides [15]. MgO nanowires have primarily been produced utilizing the method of catalysis-assisted chemical vapour deposition. However, currently the uses of pulsed laser deposition (PLD) on substrates with an Au catalyst [16] have been producing significant results. This has resulted in the further study of these techniques and the production of MgO nanorods and nanowires via PLD on MgO (100) single crystal substrates decorated with Au nanodots [17] have shown successful results as well. This is a significant improvement in production as previous successful results was due to a different method of PLD substrate decoration that created artificial pinning centers in superconducting films [18].

ZnO is another material that has had extensive study done as this material has several unique piezoelectric, optical, and mechanical properties [19]. Nanowires produced from ZnO have been widely utilized in a variety of different nanodevices and have been highly considered in the development of nanogenerators and nanolasers [20-22]. As ZnO nanowires have a large surface to volume ratio, it has been commonly utilized in applications in nanoscale sensing devices [22-28].

In_2O_3 has been used in a variety of different microelectronic applications, such as flat-panel displays, solar cells, window heaters, as this material is a transparent semiconductor [29]. This material will be utilized, in important roles in several applications such as field effect transistors [31], gas sensors [30] and optoelectronics devices [32]. Up to currently a variety different synthesis methods have been utilized for fabrication. These methods include solution [34], chemical vapor deposition [36], template-based method [35], thermal evaporation [37] and laser ablation [33].

SnO_2 has been widely utilized in a variety of different fields. These applications include transparent conducting electrodes [44], dye-sensitized solar cells [43], catalyst supports and electrochemical modifiers on electrodes, etc [45-48], and gas sensors for detecting leakage [38-41]. 1D nanostructures along with SnO_2 can be used as semiconductor sensors with a high expectation of performance. These 1D SnO_2 nanostructure materials have been successfully produced through several methods such as chemical vapor deposition (CVD) [49], hydrothermal synthesis [47], the sol–gel template method [50], the reaction sintering method [51], the molten-salt method [42] and the co-precipitation method [52].

Fe_3O_4, also known as magnetite, has been a major topic of study in the field of magnetic materials. Magnetite has been considered to be used in a variety of applications such as magnetic recording media [53], ferrofluids [55], photo-catalysis [54], and pigments

[56]. However, the ability to control growth with 1D morphology has yet to be determined due to the material's complicated spinel structures [57]. Production of single-crystalline Fe_3O_4 1D nanostructures are currently based on solution-phase chemical methods. Some of these methods include hydrothermal process [58] [60], one-step sol–gel route [59], and the solvothermal treatment [61].

Chemical or direct evaporation are currently the primary methods for the fabrication of functional nanowires. However, no studies have been conducted regarding the use of different oxides and the varying of parameters within a PLD system. In this work, PLD was utilized in order to prepare MgO, ZnO, In_2O_3, SnO_2 and iron oxide nanostructure samples. It was observed that the influence of a variety of different experimental parameters were utilized for the growth of MgO, ZnO, In_2O_3, SnO_2 and iron oxide nanowires and nanorods. The observed parameters included substrate temperature, different metal catalysts and substrates, target to substrate distance, laser energy, plasma plume, number of pulses on an oxide target, number of pulses on a catalyst target, and oxygen pressure. Also, previous research has not compared the evenness of the samples produced via PLD, but this particular topic was studied and observed within this thesis.

1.2 Aim and Objective

Within this thesis, the main aim was to optimize the pulsed laser deposited functional oxide nanowires. To achieve this aim, the objectives of this thesis intended to establish a correlation between the morphology and the deposition parameters of oxygen pressure, substrate temperature, catalyst, substrate, laser energy, plasma plume, number of pulses on catalyst, number of pulses on oxides and target-to-substrate distance.

References

[1] F. Patolsky, B.D. Timko, G. Yu, Y. Fang, A.B. Greytak, G. Zheng, and C.M. Lieber, Science 313 (2006) 1100.

[2] J. Xiang, W. Lu, Y. Hu, Y. Wu, H. Yan and C.M. Lieber, Nature, 441 (2006) 489

[3] R.S. Friedman, M.C. McAlpine, D.S. Ricketts, D. Ham and C.M. Lieber, Nature 434, (2005)1085.

[4] O. Hayden, R. Agarwal and C.M. Lieber, Nat. Mater. 5 (2006) 352.

[5] C.J. Barrelet, J. Bao, M. Loncar, H.G. Park, F. Capasso and C.M. Lieber, Nano Lett. 6, (2006) 11.

[6] F. Patolsky, G. Zheng and C.M. Lieber, Anal. Chem. 78 (2006) 4260.

[7] G. Zheng, F. Patolsky, Y. Cui, W.U. Wang and C.M. Lieber, Nat. Biotechnol. 23,(2005) 1294.

[8] M. I. Faley, S. B. Mi, A. Petraru, C. L. Jia, U. Poppe, and K. Urban, Appl. Phys. Lett. 89, (2006)082507.

[9] M. Ishikawa, H. Tanaka, and T. Kawai, Appl. Phys. Lett. 86, (2005) 222504.

[10] H. Tian, Y. Wang, D. Wang, J. Miao, J. Qi, H. L.W. Chan, and C. L. Choy, Appl. Phys. Lett. 89, (2006)142905.

[11] H. Tsuji, F. Yagi, H. Hattori, and H. Kita, J. Catal. 148, (1994)759.

[12] Y. M. Lee, J. Hayakawa, S. Ikeda, F. Matsukura, and H. Ohno, Appl. Phys. Lett. 89, (2006)042506.

[13] D. M. Lind, S. D. Berry, G. Chern, H. Mathias, and L. R. Testardi, Phys. Rev. B 45, (1992)1838.

[14] X. ZuO, A. Yang, S. D. Yoon, J. A. Christodoulides, V. G. Harris, and C. Vittoria, J. Appl. Phys. 97 (2005) 10G103.

[15] I. B. Misirlioglu, S. P. Alpay, F. He, and B. O. Wells, J. Appl. Phys. 99(2006) 104103.

[16] K. Nagashima, T. Yanagida, H. Tanaka and T.Kawai, J. Appl. Phys. 101(2007)124304.

[17] A.Crisan, J.L.Tanner, P. Mikheenko, J.S. Abell, Optoelectronics and Advanced Materials- Rapid Communications, 3(2009)231.

[18] A. Crisan, S. Fujiwara, J.C. Nie, A.Sundaresan, H. Ihara, Appl. Phys. Lett. 79(2001) 4547.

[19] M.H. Huang, Y.Wu, H. Feick, N. Tran, E.Weber, P. Yang, Adv. Mater. 13(2001)113.

[20] C. Klingshirn, Chem. Phys. Chem. 8(2007)782.

[21] Özgür Ü, Alivov Y I, Liu C, Teke A, Reshchikov M A, Dogan S, Avrutin V, Cho S J and Morkoc H J. Appl. Phys. 98(2005) 041301.

[22] Tsukazaki A et al Nat. Mater. 4 (2005)42.

[23] Kang B S, Heo Y W, Tien L C, Norton D P, Ren F, Gila B P and Pearton S J Appl. Phys. A 80 (2005) 1029.

[24] P Yang, H Yan, S Mao, R Russo, J Johnston, R Saykally, N Morris, Pham, J, He R and H-J Choi Adv. Funct. Mater. 12 (2002)323.

[25] X Duan, Y Huang, R Agarwal and C M Lieber, Nature 421(2003) 241.

[26] J Xiang, W Lu, Y Hu, Y Wu, H Yan and C M Lieber Nature 441(2006) 489.

[27] C Thelander, T Martensson, M T Bjork, B J Ohlsson, M WLarsson, Wallenberg L R and Samuelson L Appl. Phys. Lett. 83(2003) 2052.

[28] C Levy-Clement, R Tena-Zaera, M A Ryan, A Katty and G Hodes Adv. Mater. 17, (2005)1512.

[29] I. Hamburg, C.G. Granqvist, J. Appl. Phys. 60(1986) 123.

[30] X.C. Wu, J.M. Hong, Z.J. Han, Y.R. Tao, Chem. Phys. Lett., 373(2003) 28.

[31] C. Li, D. Zhang, S. Han, T. Tang, J. Han, W. Jin, C. Zhou, Appl. Phys. Lett., 82, (2003)112.

[32] D.S. Ginley, C. Bright, Mater. Res. Soc. Bull., 25(2000) 15

[33] M.H. Huang, Y. Wu, H. Feick, N. Tran, E. Weber, P. Yang, Adv. Mater., 13(2001)113

[34] J.D. Holmes, K.P. Johnson, R.C. Doty, B.A. Korgel, Science, 287(2000)1471

[35] J.S. Jeong, J.Y. Lee, C.J. Lee, S.J. An, G.C. Yi, Chem. Phys . Lett., 384,(2004)246.

[36] M.J. Zheng, L.D. Zhang, G.H. Li, X.Y. Zhang, X.F. Wang, Appl. Phys. Lett., 79(2001) 839.

[37] N.G. Patel, K.K. Makhija, C.J. Panchal, D.B. Dave, V.S. Vaishnav, Sens. Actuators B, 23(1995)49

[38] X. Song, L. Liu, Sens. and Actuators A: Physical, 154(2009) 175

[39] Y. Shimizu, S. Kai, Y. Takao, T. Hyodo, M. Egashira, Sensors and Actuators B, 65(2000) 349.

[40] Q. Qi, T. Zhang, L. Liu, X. Zheng, Sens. Actuators B, 137(2009) 471.

[41] M. Matsuguchi, T. Uno, T. Aoki, M. Yoshida, Sens. Actuators B, 131(2008) 652.

[42] D. Wang, X. Chu, M. Gong, Sens. Actuators B, 117(2006) 183.

[43] A.Y. El-Etre, S.M. Reda, Appl.Surf. Sci., 256 (2010) 6601.

[44] Y.P. Yadava, G. Denicoló, A.C. Arias, L.S. Roman, I.A. Hümmelgen, Materials Chemistry and Physics, 48(1997) 263.

[45] J. Lee, S. Sim, B. Min, K. Cho, S.W. Kim, S.J. Kim, Journal of Crystal Growth, 267, (2004)145.

[46] I.T. Weber, A. Valentini, L.F.D. Probst, E. Longo, E.R. Leite, Materials Letters, 62 (2008) 1677–1680

[47] Y. Wang, M. Guo, M. Zhang, X. Wang, Thin Solid Films, 518 (2010), pp. 5098–5103

[48] Zh. Wang, L. Liu, Materials Letters, 63 (2009) 917–919

[49] Y.C. Lee, H. Huang, O.K. Tan, M.S. Tse, Sensors and Actuators B:Chemical, 132 (2008) 239–242

[50] N. Yang, J. Wang, Y. Guo, X. Zhou, Rare Metal Materials and Engineering, 37 (2008) 694–696

[51] X. Hou, Z. Yu, Z. Chen, B. Zhao, K. Chou, Dalton Transactions, 41 (2012), pp. 7127–7133

[52] X. Huang, Z. Liu, Y. Zheng, Q. Nie, Chinese Chemical Letters, 21 (2010)999–1002

[53] Y.K. Kim, M. Oliveria, J. Appl. Phys., 75 (1994)431

[54] D. Beydoun, R. Amal, Mater. Sci. Eng., B, Solid-State Mater. Adv. Technol., 94 (2002)71

[55] S.H. Sun, H. Zeng, J. Am. Chem. Soc., 124 (2002), 8204

[56] I.M. Bell, P.J.H. Clark, P.J. Gibbs, Spectrochim. Acta, Part A: Mol. Biomol. Spectrosc., 53 (1997)2159

[57] T.A. Crowley, K.J. Ziegler, D.M. Lyons, D. Erts, H. Olin, M.A. Morris, J.D. Holmes, Chem. Mater., 15 (2003) 3518

[58] J. Wang, Q.W. Chen, C. Zeng, B.Y. Hou, Adv. Mater., 16 (2004)137

[59] Z.B. Huang, Y.Q. Zhang, F.Q. Tang, Chem. Commun., 3 (2005)342

[60] S.Y. Lian, E.B. Wang, L. Gao, Z.H. Kang, D. Wu, Y. Lan, L. Xu, Solid State Commun., 132 (2004) 375

[61] S.Y. Lian, Z.H. Kang, E.B. Wang, M. Jiang, C.W. Hu, L. Xu, Solid State Commun., 127 (2003)605

Chapter 2

Literature Review

2.1 Nanostructures

An object, that is of intermediate size, between molecular and microscopic (micrometer-sized) structures, is defined as a nanostructure [1]. The production of such nanostructures contributes to the advancement and development of several modern and technological applications. These nanostructures provide many new opportunities, to a variety of industries, by developing new types of nanostructures or taking an existing microstructure and reducing the size that can be utilized in a variety of electronics used every day. The rapid development, within the microelectronics industry, is attributed to the development and use of integrated circuits [2]. The miniaturization of these components has resulted in improved performance, greater efficiency, faster operation, cost reduction, and reduction in power consumption. This has proved to be highly beneficial in the scientific and technological communities throughout the world. The current drive of the development of nanotechnology, is the advancement of smaller devices within the semiconductor industry. This is further supported by the various fabrication methods and techniques at the nanometer level. As the trend continues to indicate the decrease in the dimensions of devices, Moore's Law [3] becomes much more evident, as displayed in Fig. 2.1.1. Moore's Law expresses that the number of transistors and circuits per unit area will double approximately every two years, which was detailed in Gordon E. Moore's 1965 paper.
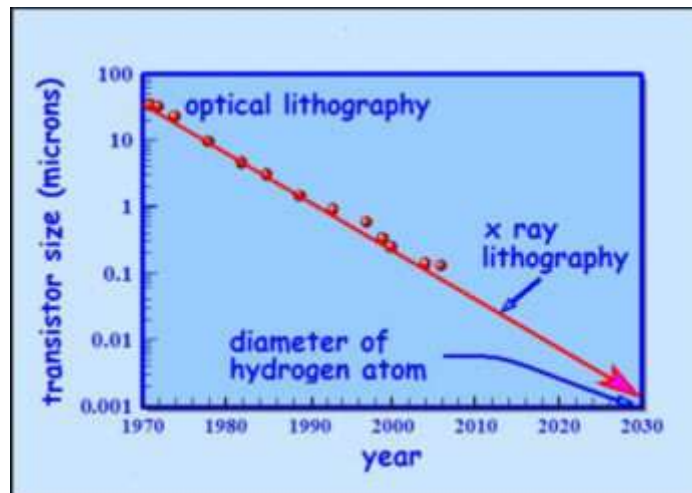
Fig. 2.1.1 "Moore's Law" [4]

Nanotechnology can be defined as the manipulation of matter on an atomic and molecular scale and its application in the design and production of nanostructures and nanomaterials [5]. Nanomaterials and nanostructures provide the foundation for nanotechnology. Nanomaterials are materials that contain at least one dimension in the nanometer scale. These materials also include nanoparticles (zero-dimensional nanostructures), nanorods/nanowires (one-dimensional nanostructures), thin films (two-dimensional nanostructures), and three-dimensional bulk materials. The processes in which these materials are fabricated can be categorized as top-down approach or bottom-up approach, but can also, in addition, be considered as a spontaneous process or forced process.

Despite many of the foundations of nanotechnology have been established in various scientific fields, there are still many obstacles and challenges that need to be overcome that are unique to this field of study. Some of these challenges consist of developing tools to observe the on goings within the nanometer scale that are specifically occurring at the macro scale. This poses another challenge that is opposite, as there are situations that only occur within the nanometer scale but do not appear at the macro scale. Therefore, the following challenges must overcome in order for the fabrication and processing of nanomaterials and

nanostructures [5]:

(1) Overcoming the huge surface energy, this is a result of a large surface area or large surface to volume ratio.

(2) Ensure that all nanomaterials produced with the desired size, uniform size distribution, morphology, crystallinity, chemical composition, and microstructure, are all resulting with the desired physical properties.

(3) The prevention of nanomaterials and nanostructures from coarsening through dissolution of small crystals and the redeposition of the dissolved crystals, on the surfaces of larger crystals (Ostwald ripening) or the mass grouping of these materials (agglomeration) over the progression of time.

2.2 One-Dimensional Nanostructures

One-dimensional (1D) nanostructures have been identified by a variety of different names which include the following: whiskers, fibers or fibrils, nanowires and nanorods, nanobelts and nanotubes. However, whiskers and nanorods are generally considered to be shorter, in length, than fibers and nanowires. It should also be noted that early study of one-dimensional structures described whiskers and fibers to have diameters that ranged from several nanometers to several hundred microns. However, current studies primarily label nanowires and nanorods as structures with diameters that do not exceed a few hundred nanometers [6].

Nanowires are one-dimensional single crystals with surface structural properties that are well defined. The utilization of these one-dimensional nanostructures can be found in a multitude of various applications such as nanoscale electronics, optoelectronics, electrochemical devices as well as electromechanical devices. These applications are possible due to the nanostructure's properties when compared to their bulk counterparts [8]. The number of topics regarding one-dimensional nanowires have significantly increased over the

19

past 10 years, as shown in Fig. 2.2.1.
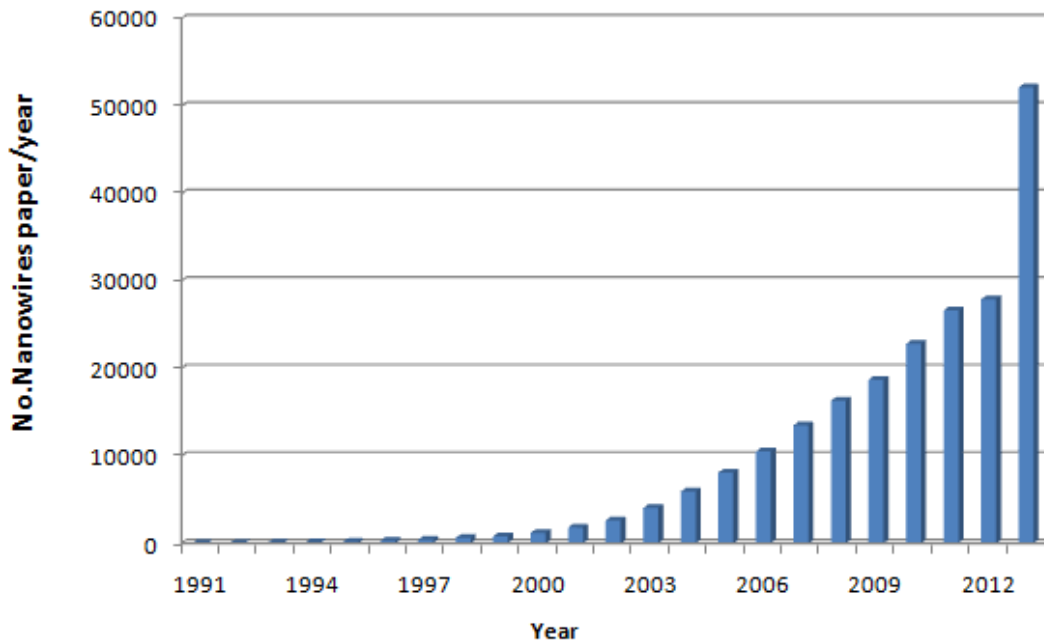
Fig. 2.2.1 Number of publications on nanowires related topics from 1991-2013 based on Google scholar

2.3 One-Dimensional Nanostructures Growth

2.3.1 One-dimensional nanostructures growth techniques

There are several key requirements for growing one-dimensional nanostructures. A pathway that is reversible or a condition that is near equilibrium between a fluid phase and a solid phase is one such requirement. Another requirement requires that, in the solid phase, the adsorbed atom or adatom, should have a high surface or bulk mobility [10]. The various current techniques for the synthesis and formation of one-dimensional nanostructure materials are simply displayed in Fig. 2.3.1. [7]. When comparing top-down and bottom-up techniques, the bottom-up techniques are far superior as they exceed the limits of top-down technology in regards to future applications [11]. Therefore, bottom-up techniques should be utilized as they are capable of producing nanoscale features [12].
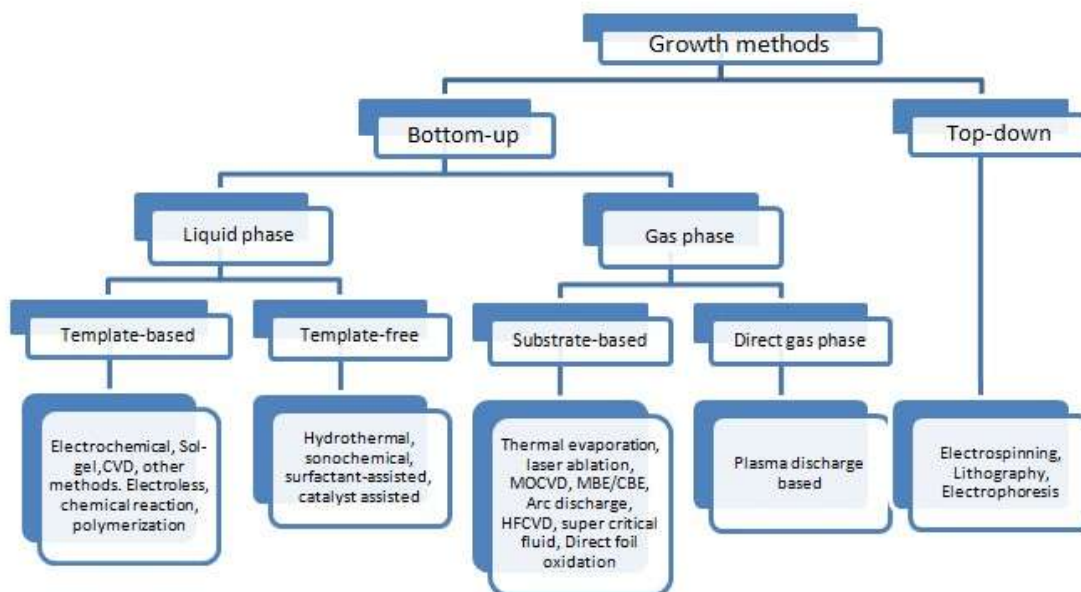
Fig. 2.3.1 Summary tree of the growth techniques [5]

2.3.2 Self-assembly of nanoparticles and nanowires

Self-assembly is the ordered arrangement of molecules and small components when referring to nanomaterials. These small particles may spontaneously form from the influence of chemical reactions, electrostatic attraction, and/or capillary forces. Between the assembled molecules and the surface of the substrate, chemical bonds are formed. These same chemical bonds can also be found between the molecules in the adjacent layers. It can be assumed that the reduction of chemical potential is the primary cause of this phenomenon. Therefore, the final assembly tends to form spontaneously when approaching near or at a thermodynamic equilibrium [16].

Self-assembly methods allow access to a larger variety and selection of structures than are accessible through non-self-assembly structures. The formation of self-assembled structures utilized the various interactions between the substrate and the layers on the substrate, as well as the interactions between the layers. One such example, molecular self-

assembly, utilizes noncovalent interactions, hydrophobic, electrostatic interaction along with coordination and hydrogen bonds [17]. Regarding the self-assembly of nanostructures within mesoscopic and macroscopic objects, several other forces are utilized such as shear force, electromagnetic field, gravitation, capillary, and entropy [18].

In the self-assembly of nanoclusters, nanocrystals [19] [20], and nanorods [21], the most commonly used approaches include electric-field assisted assembly [24], gravitational field assisted assembly [26], dispersion interactions [23], shear force assisted assembly [20], capillary forces [22], covalently linked assembly [25], and template assisted assembly [27].

2.3.2.1 Template assisted assembly

Template assisted assembly is a method that introduces surface or spatial confinement to self-assembly [5]. Several methods have been utilized, for instance, the process provides surface confinement by use of aqueous dispersions to assemble colloidal particles into an array of templates [28] [29]. These patterned arrays, on solid substrates, have been utilized to form colloidal crystals [30] [31].

Harald Brune *et al.* [32] describes template assisted assembly as "the fabrication of highly ordered, two-dimensional nanostructure arrays through nucleation of deposited metal atoms on substrates with periodic patterns defined by dislocations that form to relieve strain".
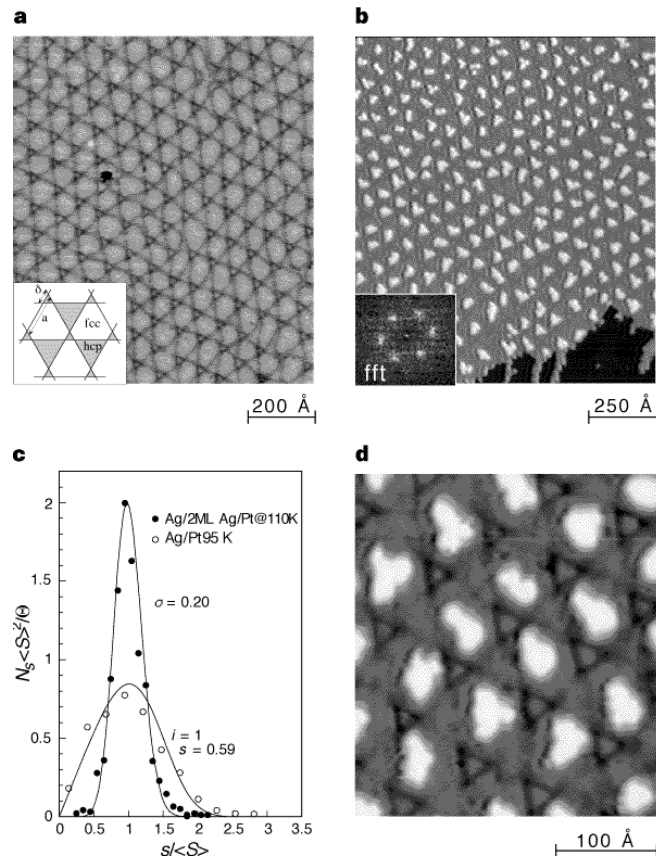
STM images showing the confined nucleation of adatom islands on a dislocation network. **a**, STM image of the ordered (25 × 25) dislocation network formed by the second Ag monolayer on Pt(111) on deposition at 400 K and subsequent annealing to 800 K. The inset shows a model of this trigonal strain-relief pattern. **b**, A superlattice of islands is formed on Ag deposition onto this network at 110 K (coverage $\Theta = 0.10$ ML). Inset, the Fourier transform of the STM image shows the high degree of order and the hexagonal symmetry of the nanostructure array. **c**, Island size distributions for random and ordered nucleation (curves, theory; dots, experiment). The curve for ordered nucleation is a binomial fit. The curve labelled $i = 1$ shows the size distribution from scaling theory for random nucleation on an isotropic substrate. Size distributions were normalized according to scaling theory (s is the island size in atoms, $\langle S \rangle$ its mean value, and N_s the density of islands with size s per substrate atom). **d**, Detail of STM image **b**.

Fig. 2.3.2 STM images in Harald et al. [32] report

The strain-relief pattern is spontaneously created when a monolayer or one of the two materials, with a different lattice constant, is deposited on the substrate. As the dislocations can often repel the adsorbed atoms, which are diffusing over the surface, they will be utilized as templates for the confined nucleation of nanostructures from the adatoms. This technique was utilized to produce ordered arrays of silver and iron nanostructures on metal substrates,

as seen in Fig.2.3.2. In this project, metal catalyst nanodots served as the template for one-dimensional oxides nanostructures growth and formation.

2.3.3 Growth mechanisms

There are several types of growth mechanisms utilized in the formation of nanostructures, but two commonly used ones were conducted within the scope of this project. These growth mechanisms include vapor-liquid-solid (VLS), vapor-solid-solid (VVS), low-melting metal mediated, and self-catalytic.

2.3.3.1 Vapor- liquid-solid (VLS) mechanism

Several types of semiconductor nanowires have been fabricated by means of vapor deposition utilizing a vapor-liquid-solid (VLS) model, as shown in Fig. 2.3.2. Vapor-liquid-solid whisker growth can be described through the equation established by R.S. Wagner:

$$R_{min} = [(2V_l)/(RT \ln s)]\sigma_{lv},$$

R_{min} represents the minimum whisker radius, V_l represents the molar volume of the metal droplet, σ_{lv} represents the liquid-vapor surface energy, and lastly s represents the degree of supersaturation of the vapor [14]. In order to enhance the selectivity of vapor phase reactions, catalyst metal clusters are utilized. While maintaining a constant synthesis temperature, a continuous dissolution from the gas phase allows the supersaturation of the solute within the alloy cluster. At the droplet-substrate surface interface, the precipitation of solute becomes evident [15]. Applications of this equation have allowed the fabrication of semiconductor nanowire-based prototype devices, such as logic circuits, light emitters and gas sensors [33-35].
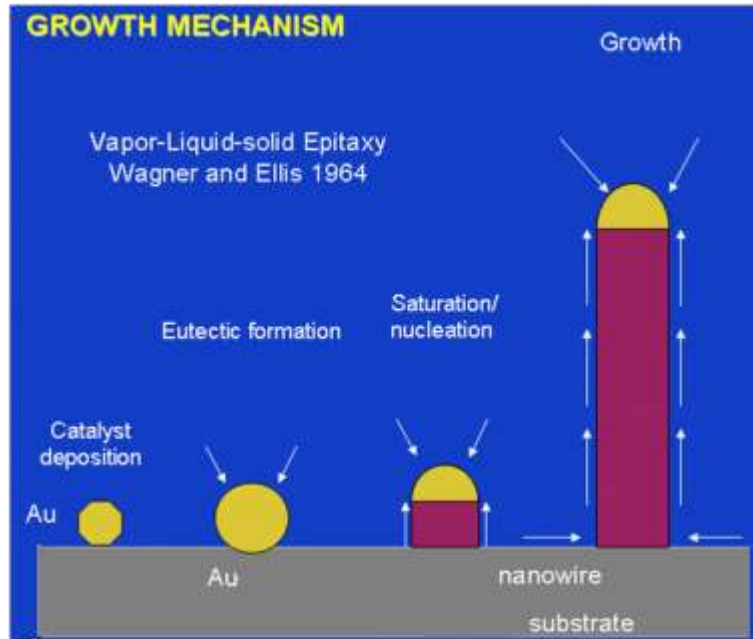
Fig. 2.3.3 Vapor-liquid-solid (VLS) model [14, 15]

Wagner et al. first proposed the VLS theory over 40 years ago, although an extensive research in this field has been carried out in the recent years, fundamentals of the VLS method have not been changed significantly. The VLS model is a classic and the most common one-dimensional nanostructure growth mechanism found in CVD and PVD methods. PLD is also considered as a PVD method. However, in this study there was no sufficient evidence that indicated that the nanostructures produced within PLD system were according to the VLS model, such as a liquid-like globule that was found in the tip of nanostructure on only one sample within this entire study. The ZnO growth mode is discussed in section 4.2.10.

2.3.3.2 Vapor- solid (VS) mechanism

The vapor-solid (VS) mechanism is a process of nanowire production that does not utilize a catalyst. This process directly vaporizes the solid at high temperatures. The deposition of the nanowires is conducted at a much lower temperature. As no catalyst is

utilized in the VS growth process, the nanowires are grown directly on the solid particles. This method has been commonly used to produce many different semiconducting oxide nanowires [36, 38].

2.3.4 Pulsed laser deposition (PLD)

Pulsed laser deposition (PLD) is the currently preferred method of nanowire production. This process provides an environment, that is nonequilibrium, easily controlled, rapidly condensing, low pressured, and of high energy [13]. The PLD method utilized and monitored the following variables: temperature, pressure, target composition, gas phase composition, laser power, substrate conditions, and residence time of the vapor-phase species.

The PLD setup is very similar to thermal evaporation, with the exception of the laser beam and the target. One of the major differences between the two methods relates to the manner of which the target is heated. The vapor-phase composition will fluctuate during the process of thermal evaporation. This fluctuation is caused by different materials in the source that can generate a different amount of vapors due to the various melting points and vapor pressures of the source components. However, in PLD, the vapor-phase composition will be the same as the source composition. This due to the vaporization of the targeted spot and is regardless of the difference in the constituent elements evaporation points. Complete vaporization can be achieved by heating a small confined spot on the target at an extremely high heating rate. Therefore, the utilization of laser ablation allows the retention of the deposited structure's target stoichiometry. However, this may result in a large size distribution of nanowire materials [39].

In accordance to the VLS growth model, the size of the catalyst is the basis for the growth of the nanowires and also affects the diameter as well. Due to the vaporization of the catalyst target during the laser ablation, large particulates, with sizes that can reach several microns, may eject from the target's surface. Due to this, the varying sizes of the deposited

catalyst can also affect the size distribution on the substrate, which in turn can cause the lack of uniformity in the nanowire diameters. In order for these structures to have practical use in electronic and photonic applications, the nanowire diameter must maintain uniformity as the electronic energy band structures are dependent on size.

Due to the high heating rate of the target, laser ablation requires a lower substrate temperature than thermal evaporation. Therefore, within PLD, it permits the ability to selectively heat a small portion of the target. This increases efficiency and saves energy. In the case of thermal evaporation, the entire material absorbs the heat as it increases in temperature. However, the yield in nanowires is relatively small, as only a small amounts of vapors are generated through the process [7].

2.4 Functional Oxides

The various properties of nanowires allow them to be utilized in a variety of different applications. Some of these uses are listed in Table 2.4.1. Nanowires can also be utilized in other functions where they play a central role within a system. Future applications of these materials are illustrated in Fig. 2.4.1.

Table 2.4.1 Application of functional oxides

| Material	Application
MgO	Substrates for functional oxide thin film growth,
ZnO [7]	UV lasers, photodetectors, UV light-emitting diodes (LEDs), field emission device, Frequency converter, solar cell,
In$_2$O$_3$ [7]	Chemical sensors, biosensors, solar cell,
SnO$_2$ [40]	Gas sensor, magnetic data storage and magnetic resonance imaging (MRI), electrodes, optoelectronic devices and resistors, field-effect transistor, UV and polarized UV detector, waveguide, evanescent wave optical sensor
Indium tin oxide [7]	Transparent conductive film in display electrodes, solar cells, organic LEDs
Fe$_3$O$_4$ [41]	Nanocatalysis, biosensor, MRI contrast agents and drug delivery
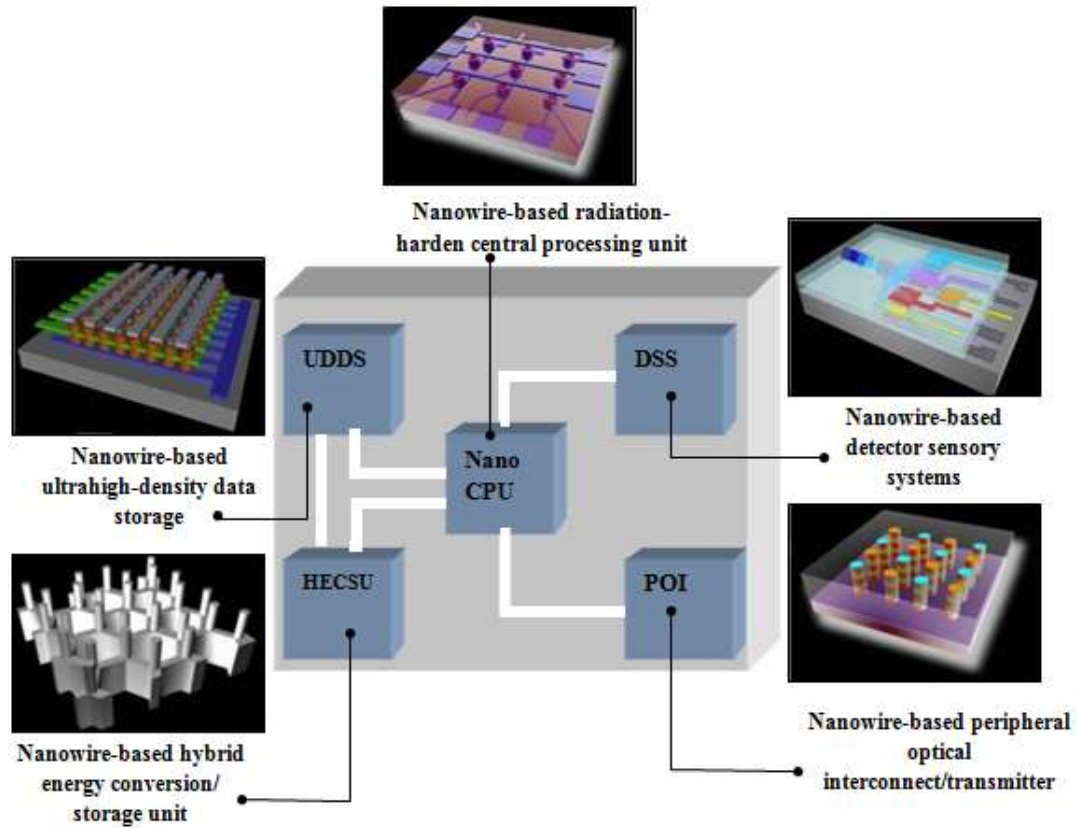
Fig. 2.4.1 Future of nanowires (Courtesy of H.T. Ng)

2.4.1 Solid-state MgO and MgO nanowires

MgO, also known as Magnesium Oxide, is a rock salt crystal that has a lattice constant of 4.21Å [42], as seen in Fig.2.4.2. It is commonly used as a substrate for transition metal oxide film growth as it provides a lattice mismatch for several transition metal oxides, such as ferromagnets [44], ferroelectrics [43], and superconductors [45]. MgO has also been utilized in a variety of applications such as catalysis, additives in refractory paint, and insulating (band gap = 7.8 eV) layers in tunnel magnetoresistance junctions [46, 47].

MgO is also a common material that is taken into consideration as an oxide nanowire substrate [48]. It contains several favorable properties such as chemical inertness, thermal stability, and electrical insulation. Nanowires fabricated from MgO are highly preferred as it

allows the integration of the transitional metal oxide functionalities onto the MgO nanowires through the heterostructures [49, 50]. In order to further integrate the functionalities of other metal oxides while utilizing MgO nanowires, control over the morphologies of MgO nanowires is crucial.
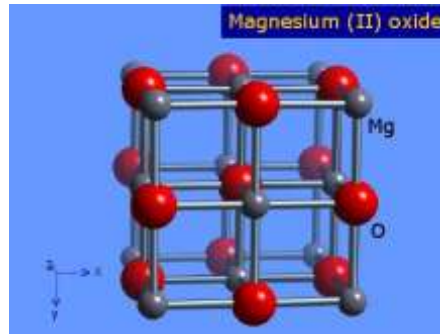
Fig. 2.4.2 A unit cell of MgO with a rock salt (cubic) structure.

Marcu *et al.* [51] studied the effect of PLD ablated particle flux on MgO nanowire growth. It was observed that when the distance between the ablated material and the substrate varied, it primarily influences the growth rate while maintaining the growth system. This is due to the small variation in the ablated particle flux, which is generated by the different plume expansion time. However, changing the laser energy affects both the growth rate and system. If the laser energy is below a critical value, the surface morphology will tend to display an island growth rather than any evident nanowire growth. Yanagida *et al.* [52] also indicated that longer nanowire length was due to high ambient oxygen pressures. This same phenomena was also observed with the use of an argon atmosphere. It was also noted that as the oxygen pressures increased in value, the crystallinity also increased.

**Table 2.4.2** Fabrication methods and applications of MgO nanostructures

Structure	Method	Application
MgO/Fe$_{3-\delta}$O$_4$ core-shell heterostructured nanowires [49], MgO/LaCaMnO$_3$ and MgO/LaSrMnO$_3$ core-shell nanowires [54]	MgO nanowires were grown on single-crystalline MgO (100) substrates and Si/SiO$_2$ substrates by the Au catalyst-assisted thermal CVD approach. Fe$_{3-\delta}$O$_4$ and LAMOshell layer deposition was performed in a PLD system consisting of a tube furnace and a solid-state Nd:YAG laser. The repetition rate was 10 Hz. The laser energy was15 mJ. The substrate-to-target distance was 45 mm. The substrate temperature and oxygen pressure during the shell depositions were varied from room temperature to 800 °C and 10^{-4}–10 Pa.	ferromagnetic behavior [49], colossal magnetoresistance [54]
MgO nanowires [55][56][52]	Substrate was MgO (100) single crystal. Au catalyst was patterned on the substrate by sputtering with metal mask. The thickness of Au catalyst was controlled from 1 to 10 nm. ArF excimer laser (λ=193nm), was used for the laser ablation by varying the pulse repetition rate 3 to 10 Hz and the laser energy from 10 to 80 mJ. MgO single crystals were used as source of ablation. Distance between the substrate and the target *Dst* was varied from 25 to 50 mm. Oxygen and/ or argon gas was introduced into the chamber at the constant ambient pressure of 10^{-2} Pa-10 Pa. The substrate temperature for growth was varied from 400 to 800 °C. The laser ablation was performed for 60 min.	
MgO nanowires [57]	Substrates were MgO(001) and Si substrates, with gold as a catalyst. The substrates were placed back into the tube furnace along with the magnesium nitride (Mg$_3$N$_2$) powder precursor to synthesize the MgO nanowires. A fixed flow rate of 100 SCCM ultrapure argon gas is mixed with a 60 SCCM flow of Ar/0.02% O$_2$ mixture and together introduced into the furnace at atmospheric pressure. The furnace temperature is then raised to 925 °C,	
MgO nanowires [58]	MgO nanowires were produced by the thermal evaporation of MgB$_2$ powders at 900°C.	photoluminescence
ZnO and MgO nanowires [59,60]	2 Mg(vapor)+O$_2$(gas)→2 MgO(solid) The reaction was carried out in a conventional tube furnace with a horizontal quartz glass tube by directly heating metal powder in appropriate oxygen atmospheres.	

A.Crisan *et al.* [53] was successful in the fabrication of all-self-assembled MgO nanorods and nanowires via PLD on MgO (100) single crystal substrates decorated with Au nanodots by PLD deposition. Superconducting films also previously utilized this method of substrate decoration of artificial pin centers on the film. Bo Lei *et al.* [54] studied the PLD

process in the synthesis of colossal magnetoresistive MgO/LaCaMnO$_3$ and MgO/LaSrMnO$_3$ core-shell nanowires. Within their study, a process was developed by depositing an epitaxial layer of magnetite onto randomly oriented MgO nanowires grown on SiO$_2$/Si substrates. It was also discovered that the target to substrate distance was critical in the quality of the core-shell nanowires produced.

2.4.2 Solid-state ZnO and ZnO nanowires

The use of ZnO has three primary advantages. It is a semiconductor that is a functional oxide [61] with direct bandgap energy of 3.37 eV at room temperature and a large exciton binding energy of 60 meV, which exhibits a nearly ultraviolet emission and is a transparent conductor [62]. This enhances the efficiency of luminescence and the sensitivity of photo response which is due to the formation of stable exciton. ZnO is piezoelectric due to its noncentral symmetry. Lastly, the material is biologically safe and can be used in various biomedical applications without the use of a coating [63]. In addition, ZnO nanowires have been fabricated to be utilized in a variety of sensors that detect a wide range of gases (i.e. ethanol, O$_2$, NO$_2$[64-66], ammonia, hydrogen and carbon monoxide[67-69]).
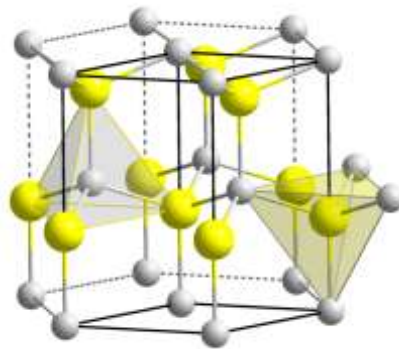
Fig. 2.4.3 ZnO wurtzite structure

Table 2.4.3 Fabrication methods and applications of ZnO nanostructures

Structure	Method	Application
ZnO nanorods[8]	ZnO nanorods have been grown on Si(001) substrates at 600°C by a catalyst free PLD method by using ArF excimer laser, (λ=193nm, 10 Hz repetition rate) on a rotating ceramic ZnO target. The target –substrate separation was maintained in the range of 40–60 mm. A continuous working (cw) CO_2 laser was employed to heat the substrate by illuminating its rear surface. Temperature of the substrate was varied from room temperature to >700 °C, in the presence of a slowly flowing low background pressure of oxygen(>99.99% purity, 10 sccm, $p(O_2) \sim 10$ mTorr).	photoluminescence
ZnO nanorods [70]	ZnO nanorods were produced by KrF eximer laser (λ=193nm, energy 3 J/cm^2, 20 Hz) on a sapphire substrate, without metal catalyst. The target-substrate distance was set from 20 to 70 mm and the chamber pressure was set to be relatively high of more than 3 Torr. The substrate temperature was more than 600°C.	photoluminescence
ZnO nanobelt [71]	RF sputtering technique without the presence of a metal catalyst	H_2, NO_2, and hydrocarbon gas sensor
ZnO nanowires [72] [73]	Vapor-phase epitaxy	photoluminescence [72], nanolasers [73]
1D ZnO nanowires/ nanoflakes, 2D ZnO nanosheets, and 3D ZnO networks [74]	Directly heating a CuZn alloy (brass) on a hotplate in ambient conditions	electron field emission
ZnO nanowires [75]	Thermal evaporation	photoluminescence, field emission
ZnO nanorods [76]	Vapor-phase transport, using different types of ZnO thin films as seed layers	
ZnO nanobelts [77]	Direct evaporating commercial metal oxide powders at high temperature	
ZnO and SnO_2 nanowires[78] [79]	Using template-assisted method, hard templates such as porous anodic aluminum oxide membranes (AAOM)	photoluminescence
Cone shaped ZnO nanowires [80]	Hydrothermal reaction of $ZnCl_2$, NaOH in water	
ZnO nanowires [64]	Microelectromechanical system technology	ethanol sensors
ZnO nanowires [81]	ZnO nanowires were produced by high power femtosecond laser system (Nd:YAG laser, λ=266 nm 10 mJ per pulse, 10 Hz repetition rate) on sapphire or silicon substrate. Au catalyst was pre-deposited on the surface of the substrate by thermal evaporation. All growth experiments were conducted at 1 atm pressure and 900 °C.	photoluminescence
ZnO nanowires [82]	ZnO nanowires were produced by selective	fluorescence (FL),

	electrodeposition of Zn in 10-, 25- and 50-nm pores of a porous anodic alumina film, followed by chemical oxidation.	infrared absorption (IR) spectra
ZnO nanowires [83]	Using a typical carbothermal reduction process	
ZnO nanowires [84]	On STO substrates by the vapour condensation method using a mixture of equal amounts of ZnO and graphite powders	
ZnO nanowires [85]	On a Si (100) substrate via a free-catalyst chemical vapor deposition method	photoluminescence
ZnO nanowires [86]	The process begins in a tube furnace with the melting of dispersed metallic nanocrystals or thermally evaporated metallic thin on single-crystalline substrates by introduction of various process gases.	photonic circuitry
ZnO nanowires [87]	On c plane–oriented α-Al_2O_3 substrate, using Au particles as a catalyst, by the chemical vapor deposition (CVD) of vapor liquid- solid (VLS) process	piezoelectric nanogenerators
ZnO nanowires [88]	By CVD with a base pressure of 5 torr using high-purity (99.999%) Zn metal and an O_2/Ar flux as source chemicals	hydrogen gas nanosensor
ZnO nanowires [89]	ZnO films were firstly grown by a pulsed laser deposition technique under different ambient oxygen pressures. A ZnO target was irradiated by a focused Nd:YAG laser. ZnO nanowires were grown by the sol–gel process on the ZnO films. Aqueous solution of [$Zn(NO_3)_2 \cdot 6H_2O$] and ($C_6H_{12}N_4$) was prepared, while keeping the same molar ratio of 1:1. The ZnO thin film grown on Si substrate by pulsed laser deposition was floated facing downward in the solution for longer than 12 h, which was sealed and kept at 95°C in a furnace.	photoluminescence
ZnO nanowires [90]	ZnO nanowires were thermally grown on the GaN(2 μ m)/sapphire substrate, on which 3 nm of an Au thin film catalyst was deposited using a thermal evaporator, using a horizontal quartz tube by vaporizing mixed ZnO and graphite (1:1) powder.	sound-driven piezoelectric nanowire-Based nanogenerators
ZnO/$ZnGa_2O_4$ core–shell nanorods [91]	By reactive evaporation on ZnO/glass templates at 600 °C	photoluminescence
ZnO nanoneedles [92]	Metal-organic chemical vapor deposition (MOCVD) on Si substrates, Et_2Zn and oxygen were the reactants.	photoluminescence
ZnO nanowires [93]	Produced by using PLD on 0001 single crystal alumina at 1 Pa oxygen pressure and 750°C substrate temperature. Laser energy was up to 100 mJ/pulse and repetition frequency was 10 Hz. Substrate-target distance was 5 cm.	

Y. Zhang *et al.* [81] successfully fabricated ZnO nanowires in a Nd:YAG laser system

under 1atm pressure. It was observed that ZnO nanowires grown under high oxygen partial

pressure contained significant morphology imperfections along with a short carrier recombination lifetime.

C. Li *et al.* [76] discovered that the growth methods, deposition temperature, and thickness of ZnO seed layer greatly affect the growth of ZnO nanorods, in the vapor-phase synthesized process. It was also observed that a variety of polycrystalline ZnO seed layers can yield ZnO nanorods. Another key observation noted was that, the self-assembled growth of a network layer, formed on a highly c-axis-oriented seed layer, is ideal for nanorod arrays of high quality. The primary characteristic that influences the growth of nanorods, is the crystal quality of the ZnO seed layer. Seed layers, with a thicknesses of 200 nm or more and deposited at a temperature of 500 °C via PLD results in arrays with large nanorod densities, a narrow diameter distribution, preferable alignments, and of higher quality. It was concluded that the formation of ZnO nanorod arrays were the result of ZnO seed layers with a smooth surface, favorable crystallinities, reduced lattice stress, and a high c-axis orientation.

A.Marcu *et al.* [93] deposited ZnO nanowires on single crystal alumina substrates using a PLD/VLS technique. The resulting nanowires were very sensitive to plume variation. It was observed that flux optimization has influence in nanowire morphology. Further testing, with the use an optimized penetration rate helical mask, resulted in uniform ZnO nanowire growth on area as large as $1 \times 1 \text{cm}^2$.

Okada *et al* [70] indicated that the formation of smaller nanorods can be achieved from lower gas pressure. This is due to the nanoparticles that are formed, in the gas phase, become smaller. As the target to substrate distance increases, the densities of nanoparticles that participate in the growth of the nanorods, reduces in size. Addition testing was conducted to synthesize nanorods and the following parameters were utilized included gas pressure of 3 Torr, a vertical target to substrate distance of 70 cm, a horizontal target to substrate distance

of 20 cm, 30 min deposition time, and a substrate temperature of 700 °C. The resulting nanorods displayed an average size of 122 nm and more than 1/3 of the nanorods were less than 100 nm in size.

2.4.3 Solid-state In$_2$O$_3$ and SnO$_2$, In$_2$O$_3$ and SnO$_2$ nanowires

2.4.3.1 In$_2$O$_3$

In$_2$O$_3$ is a transparent semiconductor, with a wide bandgap of approximately 3.6eV and an indirect bandgap of approximately 2.5 eV, that is widely used in solar cells and organic light emitting diodes (OLED) [94,95]. In addition to these types of common applications, In$_2$O$_3$ films have also been used in toxic gas (i.e. NO$_2$) detectors [96].

2.4.3.2 SnO$_2$

An important n-type semiconductor with a large bandgap (Eg=3.6 eV at 300K) [97] is SnO$_2$. This material is utilized as transparent conducting electrodes for a variety of different applications such as organic light emitting diodes (OLED) and solar cells [98-100]. In addition, SnO$_2$ nanowires can be utilized as building blocks for nanoelectronics, while SnO$_2$ thin films have current environmental and industrial applications within chemical sensors [98-100].

2.4.3.3 Gas sensor

The oxygen vacancies, on the oxide surfaces, are electrically and chemically active which primarily controls the sensing mechanism of oxide materials. Two specific types of sensing responses were studied. In the first case, a notable reduction of conductivity was

observed and was caused by the withdrawal and depletion of electrons within metal oxides from the adsorption of charge accepting molecules, at the vacancy sites, on the conduction band. However, in environments that are rich in oxygen, chemical molecules will react with the adsobed oxygen on the surface of the substrate. This releases the electrons and results in an increase of conductance in the metal oxide [101, 102]. The sensing responses are represented in the following equations:

$$\text{Reducing response: } CO + O \rightarrow CO_2 + e^-$$

$$\text{Oxidizing response: } NO + e^- \rightarrow NO^-$$

The increased sensitivity of one-dimensional systems to a chemical environment is typically caused by the large surface to volume ratio, when comparing bulk and thin film materials. However, bulk materials that exhibit a large surface to volume ratio and a comparable Debye length to the radius of the nanowire, typically will have improved sensitivity when compared to thin films. This is due to the heavy influence of the surface processes that affects the electronic properties of the materials.

Table 2.4.4 Fabrication methods and applications of In_2O_3 and SnO_2 nanostructures

Structure	Method	Application
In_2O_3 nanowires [103]	Laser ablation on indium target with gold catalyst, base pressure was 220Torr, at 770°C, 150 standard cubic centimeters per minute of Ar mixed with 0.02% O_2	field-effect transistors (FETs)
SnO_2, In_2O_3 nanobelts [77]	Direct evaporating commercial metal oxide powders at high temperature	
SnO_2 nanoribbons [104]	Thermal deposition process	NO_2 gas detector
SnO_2 nanowires [105]	Laser ablation, with 20nm gold catalystic clusters on Si-SiO_2 substrates, in the quartz tube furnace, purged with 0.02% oxygen diluted in argon, heating the furnace to 900°C, Nd:YAG laser ablated Sn target. chamber was maintained at 400Torr. Reaction time used was 10-30min.	field-effect transistors, polarized UV detectors
SnO_2 nanowires [106]	Pulsed laser deposition method on Si (100) substrates at room temperature. KrF excimer laser (λ= 248 nm, energy of 150 mJ), the duration of every excimer laser pulse was 34 ns, repetition rate of 5 Hz, SnO_2 target, The base oxygen pressure in the deposition chamber was about 3×10^{-4} mbar.	
Sn-doped In_2O_3 (ITO) and Mo-doped In_2O_3 (IMO) nanowires [107][108]	ITO (In:Sn =95:5) buffer layer was first deposited on a YSZ(100) substrate by PLD. A 10nm gold film was then deposited on the ITO/YSZ substrate by sputter deposition. The mixture of In and SnO_2 (atomic ratio of 90:10) powders and substrates were then loaded in an alumina boat and placed at the center of an alumina tube that was inserted into a horizontal tube furnace. The temperature was kept at 900°C and the growth lasted 2 h under a 0.5 L/min flux of nitrogen and oxygen.	optical transmittance field emission
SnO_2 nanowires [109]	Self-catalysis-grown nanowires by the thermal evaporation process	application in lithium-ion Batteries
Epitaxial ZnO/SnO_2 core-shell heterostructure [110]	A two-step deposition process based on the chemical vapor deposition technique	luminescence properties

2.4.4 Solid-state Fe$_3$O$_4$ nanowires

Fe_3O_4, commonly known as magnetite, has a Curie temperature of Tc~850 K and, at room temperature, nearly a full spin polarization. Due to these characteristics, Fe_3O_4 is ideal for use in large magnetoresistance and spin valve devices [111]. J.R. Morber [112] was the

first to document a systematic synthesis and characterization of aligned Fe_3O_4 nanowires grown on alumina substrates utilizing a PLD method.

Magnetite nanoparticles have a wide range of biomedical applications which include gene therapy [113], targeted drug delivery [113], hyperthermic cancer treatment [113], ultra-sensitive bio-agent detection [114], and magnetic resonance imaging (MRI) contrast enhancement [113]. Hematite (α-Fe_2O_3) has been utilized as a photocatalyst as well as a photoelectrode in solar energy conversion applications [115] due to material's stability, electronic properties, and availability. Exploration of other uses in various applications such as the focused development of ferrite nanoparticles for use in high density memory storage [116] [117] and advanced communications devices[118] are currently under way. Also, ferrite nanoscale materials are preferred over other rare-earth alloys to address superparamagnetic limits in conventional recording. These materials are taken in consideration due to its stability, low cost, and low toxicity. In addition, these materials also exhibit high resistivity and reduction of unfavorable eddy current energy loss [119].

Recent studies have indicated that the high aspect ratio of magnetic nanowires is capable of producing a large magnetic moment [120]. This has several significant benefits in a wide range of applications. Unique ferrite properties have the potential use in various applications in communications, defense, memory storage, and energy technologies to name a few.

Table 2.4.5 Fabrication methods and applications of Fe_3O_4 nanostructures

Structure	Method	Application
Fe_3O_4 nanowires[112]	PLD: laser (20Hz, 30 kV, ~300 mJ, laser spot of $1\times5mm^2$), on polycrystalline alumina wafer substrates coated with 2 nm of Au film, base pressure of 10^{-2} mbar, argon flow gas introduced into the system at 50 sccm, and maintained throughout the duration of the synthesis. Pressure inside the tube was 10^{-2} ~500mbar. Temperature was 700~1000°C.	SQUID (superconducting quantum interference device)
Fe_3O_4 nanowires [121]	Microwave-hydrothermal approach	anode in lithium ion batteries
Fe_3O_4 nanowires [122]	Synthesized from ferrous chloride ($FeCl_2\cdot4H_2O$) and diamine hydrate ($H_4N_2\cdot H_2O$) via the surfactant-assisted redox hydrothermal process induced by low magnetic field.	

2.4.5 One-dimensional nanostructures of other materials fabricated by PLD

As there are a variety of different one-dimensional materials that are produced by PLD, several of these materials are listed in the table below.

Table 2.4.6 PLD fabrication methods and applications of other materials

Structure	Method	Application
$Mg_xZn_{1-x}O$ nanowires with Mg-content x from 0 to 0.2 [123]	KrF excimer laser,2 J /cm2. From ZnO and $Mg_{0.26}Zn_{0.74}O$ targets, 12 000–48 000 laser pulses with 3–10 Hz repetition frequency. Temperature was 870–950 °C. A downstream argon flow of 0.05 to 0.2 l /min resulted in a gas pressure from 25 to 200 mbar. The target to substrate distance was varied between 5 and 35 mm. on a-plane or c-plane sapphire substrates	cathodoluminescence (CL)
GaN nanowires [124]	KrF excimer laser (248 nm, 23 ns), GaN target, Si (100) substrates, a base pressure of 6.67×10^{-5} Pa, the chamber was filled with 99.999% purified nitrogen (N_2) at a flow rate of 100 sccm. Chamber pressures of 26.66 and 66.66 Pa for the growth of nanowires and nanodots, The temperature was kept at 700 ± 10°C. After the nanowire growth, the substrates were allowed to cool down to $100°$ in N_2 ambient to prevent oxidation.	field emission

References

[1] H.S. Nalwa, Handbook of Nanostructured Materials and Nanotechnology, Academic Press,New York (2000).

[2] S. Luryi, J.Xu, A.Zaslavsky, Future Trends in Microelectronics: The Nano Millennium, Wiley-Interscience, New York (2002).

[3] B.E. Deal, Interface 6 (1976) 18

[4] Moore, Gordon E.,Cramming more components onto integrated circuits, Electronics Magazine. (1965)4.

[5]G. Z. Cao, Nanostrcutures and nanomaterials: synthesis, properties and applications, Imperial college press (2004) 11

[6] Z.L.Wang, Adv. Mater. 12(2000) 1295

[7] M. Meyyappan, M.K.Sunkara, Inorganic nanowires: applications, properties and characterization, CRC press, 17(2010)

[8] Y. Sun, G. M. Fuge, M.l N.R. Ashfold, Chemical Physics Letters 396 (2004) 21–26

[9] H.S. Nalwa, Handbook of Nanostructured Materials and Nanotechnology, Academic Press,New York(2000).

[10] T.J.Trentler, K.M.Hickman and W.E.Buhro, Science 270 (1995) 1791

[11] Y. N. Xia, P. D. Yang, Y. G. Sun, Y. Y. Wu, B. Mayers, B. Gates, Y. D. Yin, F. Kim, H. Q.Yan, 15 5 (2003) 353-389 .

[12] J.S. Wan, H.X.Liu, semiconducting oxide nanowires: growth, doping and device applications, chapter 4, (2011)

[13] Douglas B. Chrisey, Graham K. Hubler, Pulsed Laser Deposition of Thin Films, (1994) John Wiley & Sons, Inc.

[14] R. S. Wagner, Ellis, W. C. Trans. Metall. Soc. AIME 233 (1965)1053.

[15] R. S. Wagner, W. C. Ellis, Appl. Phys. Lett., 4 4 5 (1964) 89-90 .

[16] Z.L.Wang (ed.), Characterization of nanophase materials, Wiley-VCH, New York, (2000)

[17]J.Z.Zhang, J.Liu, chemistry of Self-assembled nanostructures, Kluwer, New York, (2002)

[18] C.N.Reinhoudt, Supermolecular Technology, John Wiley & Sons, New York,(1999)

[19]Y. Lin, H. Skaff, A.D.Dinsmore, and T.P.Russell, Science 299 (2003) 226
[20] W.R.Bowen and A.O.Sharif, Nature 393 (1998) 663

[21] Y. Huang, X.Duan, and C.M. Lieber, Science 291 (2001) 630

[22] P.A. Kralchevsky and N.D.Denkov, Curr. Opin. Colloid Interf. Sci.6 (2001) 383

[23]P.C. Ohara, D.V. Leff, J.R.Heath, and W.M.Gelbart, Phys. Rev. Lett. 75 (1995) 3466

[24] P.A.Smith, C.D.Nordquist, T.N. Jackson, T.S.Mayer,Appl. Phys. Lett.77 (2000) 1399

[25] T.Vossmeyer, E.Delonno, and J.R. Heath, Angew. Chem. int. Ed. Engl. 36 (1997) 1080

[26] A.K.Arora and B.R.V.Tata, Ordering and Phase Transitions in Colloidal Systems, VCH, Weinheim, (1996)

[27] Y.Lin, Y.Lu,B.Gates and Y.Xia, J.Am. Chem. Soc. 123 (2001) 8718

[28]W.T.S. Huck, J.Tien, and G.M.Whitesides, J.Am.Chem.Soc.120 (1998) 8267

[29]O.D.Velev. A.M. Lenhoff, and E.W.Kaler,Science 287 (2000) 2240

[30]A. van Blaaderen, R. Ruel, and P. Wiltzius, Nature 385 (1997) 321

[31] K.H. Lin, J.C.Crocker, V.Prasad, and A.G. Yodh, Phys. Rev.Lett. 85 (2000) 1770

[32] H. Brune, M. Giovannini, K. Bromann , K. Kern. 394 (1998) 451

[33] Yazawa, M. Koguchi, M. Muto, A. Ozawa, M. Hiruma, K. Appl. Phys. Lett.,61, (1992)2051

[34] M.Yazawa, M.Koguchi, A.Muto, K.Hiruma, Adv. Mater. 5(1993)577.

[35] K. Haraguchi, T. Katsuyama, K. Hiruma, J. Appl. Phys. 75(1994)4220.

[36] Q. Wan, Q. H. Li, Y. J. Chen, T. H. Wang, X. L. He, J. P. Li, C. L. Lin, Phys. Lett.,84 (2004)3654-3656

[37] Q. H. Li, Q. Wan, Y. X. Liang, T. H.Wang, Appl. Phys. Lett., 22 (2004) 4556-4558 .

[38] Y. J. Chen, M. S. Cao, T. H. Wang, Q.. Wan. Appl. Phys. Lett., 17 (2004) 3367-3369 .

[39] M.Alfredo, Morales, M Charles. Lieber, Science, 279 (1998)208-211.

[40] P. J. Pauzauskie and P. Yang, Materialstoday,9 (2006) 36

[41] C, Yang, J. Wu and Y. Hou, Chem. Commun.47 (2011)5130-5141

[42] M. Ishikawa, H. Tanaka, and T. Kawai, Appl. Phys. Lett. 86 (2005)222504.

[43] H. Tian, Y. Wang, D. Wang, J. Miao, J. Qi, H. L.W. Chan, and C. L. Choy, Appl. Phys. Lett.89(2006)142905.

[44] M. Ishikawa, H. Tanaka, and T. Kawai, Appl. Phys. Lett. 86(2005)222504.

[45] M. I. Faley, S. B. Mi, A. Petraru, C. L. Jia, U. Poppe, and K. Urban, Appl. Phys. Lett. 89,(2006) 082507

[46] H. Tsuji, F. Yagi, H. Hattori, and H. Kita, J. Catal. 148(1994)759.

[47] Y. M. Lee, J. Hayakawa, S. Ikeda, F. Matsukura, and H. Ohno, Appl. Phys. Lett. 89(2006)042506.

[48] T. Yanagida, K.Nagashima, H.Tanaka and T.Kawai. Appl. Phys. Lett. 91 (2007) 061502

[49] B. Lei, C. Li, D. Zhang, S. Han, and C. Zhou, J. Phys. Chem. B 109(2005)18799

[50] C. Li, B. Lei, Z. Luo, S. Han, Z. Liu, D. Zhang, and C. Zhou, Adv. Mater.Weinheim, Ger.17(2005) 1548

[51] A. Marcu,T. Yanagida, K. Nagashima, APPL. PHYS.LET. 92 (2008) 173119

[52] T. Yanagida, K. Nagashima, H. Tanaka, and T. Kawai, APPLIED PHYSICS LETTERS 91,(2007)061502

[53]A.Crisan,J.L.Tanner,P.Mikheenko,J.S.Abell,Opt.andAdv.Mater.RapidCommun.3(2009)231-235

[54] B. Lei, C. Li, D. Zhang, S. Han, and C. Zhou, J. Phys. Chem. B, 109(2005) 18799-18803

[55] T.Yanagida, K. Nagashima, H. Tanaka, and T. Kawai, JOURNAL OF APPLIED PHYSICS102 (2007) 016102

[56] K. Nagashima, T. Yanagida, H. Tanaka, and T. Kawai, JOURNAL OF APPLIED PHYSICS101 (2007) 124304

[57] G. Kim, R. L. Martens, G. B. Thompson, B. C. Kim, and A. Gupta, JOURNAL OF APPLIED PHYSICS 102(2007) 104906

[58] H. W. Kim, and S. H. Shim, phys. stat. sol. (a) 204(2007)563–568

[59] M. Zhao, X.L. Chen, W.J. Wang, Y.J. Ma, Y.P. Xu, H.Z. Zhao. Materials Letters 60 (2006)2017–2019

[60] H. Y. Dang, J.Wang and S. S. Fan, Nanotechnology 14 (2003) 738–741

[61] M.H. Huang, Y.Wu, H. Feick, N. Tran, E.Weber, P. Yang, Adv. Mater. 13(2001) 113.

[62] N. Saito, H. Haneda, T. Sekiguchi, N. Ohashi, I. Sakuguchi, K. Koumoto, Adv.14(2002),418.
[63] P. Yang, R.Yan, and M. Fardy, Nanoletters, Semiconductor Nanowire: What's Next?(2010)

[64] Wan Q, Li Q.H., Chen Y.J., Wang T.H. Appl. Phys. Lett. 84 (2004) 3654-3656

[65] Fan Z., Wang D., Chang P., Tseng W., Lu J.G. Appl. Phys. Lett. 85 (2004) 5923-5925.

[66] Fan Z., Lu J.G. Appl. Phys. Lett. 86 (2005)123510.

[67] Tien L.C, Sadik P.W, Norton D.P, Appl. Phys. Lett. 87 (2005) 222106.

[68] Wang H.T, Kang B.S, Ren F. Appl. Phys. Lett. 86 (2005) 243503.

[69] Wan Q., Li Q.H., Chen Y.J., *et al*. Appl. Phys. Lett. 84 (2004) 3085-3087

[70] B. Q. Cao, T. Matsumoto, M. Matsumoto, M. Higashihata, D. Nakamura and T. Okada, *J*.Phys. Chem. *C*,113(2009) 10975–10980

[71] Abu Z. Sadek*,* IEEE SENS. JOURNAL, 7(2007) 919

[72] L. Wischmeier, T. Voss, I R¨uckmann, J. Gutowski, Nanotechnology 19 (2008) 135705

[73] M. H. Huang, S.l Mao, H. Feick, H. Yan,Y. Wu, H. Kind, E. Weber, R. Russo, P. Yang, SCIENCE, 292(2001) 8

[74] Y. Zhu, C.Sow, Adv. Funct. Mater.16 (2006)2415–2422

[75]T. Ghoshal, S. Biswas, Nanotechnology 19 (2008) 065606

[76] C. Li, G. Fang, J. Li, L. Ai, B. Dong, and X. Zhao, J. Phys. Chem. C, 112, (2008)990-995

[77] Pan ZW, Dai ZR, Wang ZL. Science, 291 (2001) 1947-1949.

[78] Zhang J., Sun L.D., Jiang X.C., Liao C.S., Yan C.H. Cryst Growth Design. 4(2004)309-313

[79] Y. Li, G. W. Meng, and L. D. Zhang Appl. Phys. Lett., 76 (2000) 15

[80] Guozhen Shen, Recent Patents on Nanotechnology 2(2008) 161

[81] Y. Zhang, R. E. Russo, and S. S. Mao, APPLIED PHYSICS LETTERS 87 (2005) 133115

[82] S. Ramanathan , S. Patibandla , S. Bandyopadhyay ,J. D. Edwards , J. Anderson J Mater Sci:Mater Electron 17(2006) 651–655

[83] C.Kim, Y.Chung, W.Youn, and N.Hwang, Aerosol Sci. and Tech., 43(2009)120–125

[84] D.W. Kima, S. Shin, Y. Kim, S.H. Chang, Y.J. Chang, M. Kim, H. Jeong, Solid State Communications 143 (2007) 140–143

[85] Y. Liang, X.T. Zhang, Z. Liub, L. Qin, E. Zhang, C.Z. Zhao, H. Gaoa,, Z.G. Zhang, PhysicaE 33 (2006) 191–195

[86] Huang, M. H., et al., Science 292 (2001) 1897

[87] Z. L. Wang, and J. Song, Science 312 (2006) 242

[88] O. Lupana, V.V. Ursaki, G. Chai, L. Chow, G.A. Emelchenko, I.M. Tiginyanu, A.N. Gruzintsev, A.N. Redkin, Sensors and Actuators B 144 (2010) 56–66

[89] C. H. Bae, S. M. Park, S.Ahn, D.Oh ,G. T. Kim, J. S. Ha, Applied Surface Science 253 (2006) 1758–1761

[90] S. N. Cha , J.S. Seo , S. M. Kim , H. J. Kim , Y. J. Park , S.W. Kim , and J. M. Kim, Adv.Mater.234 (2010) 1–5

[91] C.L. Hsu, Y.R. Lin, S.J. Chang , T.S. Lin, S.Y. Tsai, IC. Chen, Chemical Physics Letters 411 (2005) 221–224

[92]W.Park, G.Yi, M.Kim and S. Pennycook, Adv. Mater, 14(2002)1841

[93] A. Marcu, M.Goyat, T. Yanagida and T.Kawai, JOURNAL OF OPTOELECTRONICS AND ADVANCED MATERIALS,11(2009) 421 - 424

[94] K.Sreenivas, T.S. Rao,A.Mansingh, J.Appl.Phys. 57 (1985)384

[95]Y.Shigesato, S.Takaki, T.Haranoh, J.Appl.Phys. 71 (1992)3356.

[96] J.Tamaki, C.Naruo, Y.Yamamoto, M.Mastuoka, Sens.Actuators B, 83 (2002)190

[97] P. Camagni, G. Faglia, P.Gallinetto, C.Perego, G. Samoggia, G.Sberveglieri, Sen. ActuatorB 31(1996)99

[98] E.Comini, G. Faglia, G. Sberveglieri, Sens, Actuators B 78 (2001)73

[99]N.Amin, T.Isaka, A.Yamada, M.Konagai: Sol. Energy mater. Sol.Cells 67(2001)195

[100]M.Law, H.Kind, B.Messer, F.Kim, P.Yang, Angew. Chem. Int.Ed.41(2002)2405

[101] Kolmakov A, Zhang, YX, Cheng, GZ, Moskovits, M. Adv Mater. 15(2003)997-1000.

[102] Baratto C, Comini E, Faglia G, Sberveglieri G, Zha M, Zappettini A. Sens Actuators B Chem; 109(2005)2-6.

[103]C.Li, D.Zhang,S.Han,Adv.Mater, 2 (2003) 15

[104] Law M., Kind H., Kim F., Messer B., Yang P.D. Angew Chem. Int. Ed.41(2002) 2405-2408.

[105] Z.Liu, D.Zhang, S.Han.C.Li, T.Tang, W.Jin, X.Liu, adv. Mater. 15(2003)20.

[106] Z.W. Chen, J.K.L. Lai, C.H. Shek, Physics Letters A 345 (2005) 391–397

[107] Qing W., Eric N. Dattoli, Wayne Y. Fung,W. Guo,Y. Chen,X. Pan, and W. Lu,Nano Lett.,6,(2006) 12

[108] Q. Wan, P. Feng and T. H. Wang, APPLIED PHYSICS LETTERS 89(2006)123102

[109] M.Park, G.Wang, Y.Kang, D. Wexler, S.Dou, and H.Liu, Angew. Chem. Int. Ed. 46(2007)750 –753

[110] Q. Kuang, Z.Y. Jiang, Z.X. Xie, S.C. Lin, Z.W. Lin, S.Y. Xie, R.B. Huang and L.S. Zheng,J. AM. CHEM. SOC. 127 (2005) 11777-11784

[111] Goya G. F., Berquo T. S., Fonseca F. C., Morales M. P., J. Appl.Phys. 94(2003) 3520.

[112] J. R. Morber, Y. Ding, M.S. Haluska, Y. Li, J. P. Liu, Z. L. Wang, R. L. Snyder, J. Phys.Chem. B 110 (2006) 21672-21679

[113] Pankhurst, Q. A., Connolly, J., Jones, S. K., Dobson, J. J. Phys. D: Appl. Phys. 36(2003)167.

[114] Fang B., Wang G. F., Zhang W. Z., Li M. G., Kan X. W., Electroanalysis 17(2005) 744.

[115] Ohmori T., Takahashi H., Mametsuka H., Suzuki, E. Phys. Chem.Chem. Phys.2 (2000)3519

[116] Fried T., Shemer G., Markovich G., AdV. Mater. 13 (2001) 1158.

[117] Gubin S. P., Spichkin Y. I., Yurkov G. Y., Tishin A. M., Russ.J. Inorg. Chem. 47(2002)S32.

[118] Chen R. S., Yung E. K. N., Ji F., Dou W. B. Int. J. Infrared Millimeter Waves 24(2003) 813.

[119] Jin J., Hashimoto K., Ohkoshi S. J. Mater. Chem. 15 (2005) 1067.

[120] Gould, P. Mater. Today (2004).

[121] T. Muraliganth, A. V. Murugan, A. Manthiram, Chem. Commun. (2009) 7360-7362

[122] J. Zhang, J. Chen, Z. Wang, Materials Letters, 61(2007) 1629–1632

[123] M. Lorenz, E. M. Kaidashev, A. Rahm, Th. Nobis, J. Lenzner, G. Wagner, APPLIED PHYSICS LETTERS 86 (2005)143113

[124] D.K.T. Ng, M.H. Hong, L.S. Tan, Y.W. Zhu, C.H. Sow, Appl Phys A 93 (2008) 685–689

Chapter 3

Experimental

3.1 Pulsed Laser Deposition Growth

The growth of functional metallic oxide nanowires and nanorodes (ZnO, MgO, In_2O_3, SnO_2 and Fe_3O_4) was performed by Pulsed Laser Deposition (PLD). The deposition was conducted in a vacuum chamber, in which the base pressure of about 2×10^{-6} Torr was achieved prior to the deposition, and using a KrF (λ=248 nm) excimer laser (Lambda Physics LPX 300) system. Within the system, high purity O_2 gas was introduced through independent mass flow controllers and the pressure was kept in the range from 7.5 to 3000 mTorr during growth. A schematic diagram of PLD system used in this experiment is shown in Fig.3.1.
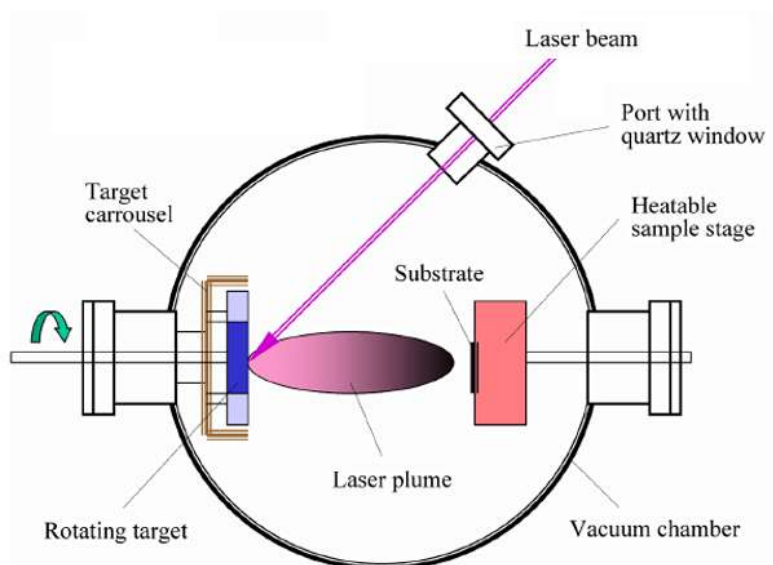
Fig. 3.1 Schematic diagram of a PLD system (Photo from
http://groups.ist.utl.pt/rschwarz/rschwarzgroup_files/PLD_files/PLD.htm)

The laser beam has a typical energy of 100 mJ, when measured inside the chamber, for the depositions used within this report. Optical instruments, such as lenses, mirrors and apertures, are needed to steer and focus the laser beam at an incident angle of 45° towards the target through a chamber window, were placed before the port of the deposition chamber.

During the depositions, the targets were rotated at 10 rpm, while being exposed to a 10Hz pulsed laser, to remove the top layer of the target and ensure uniform ablation of the targets. Pulsed laser frequencies of 1Hz and 4Hz were chosen for depositing gold nanodots and metallic oxide nanowires, respectively, while the power density of the laser beam at the target surface was about 1 J/cm^2.

Catalytic nanodots, made of metals, such as gold, palladium and silver, and metallic oxide nanowires were deposited from commercial targets (1" diameter $\times$ 0.25" thick, in the case of oxides, while catalyst metal target being thinner) with the purity of 99.99%, supplied by Pi-Kem. The target surface was exposed to 1000 laser pulses before the deposition to clean it. The target-to-substrate distance was set at several distances between 65 and 55 mm.

All the substrates were supplied by Pi-Kem, including MgO(100), MgO(001), Si(100), glass, Al$_2$O$_3$ ceramic, STO(100). Before the deposition, 5 mm $\times$ 5 mm substrates were cleaned first using acetone for 10 minutes, then ethanol for another 10 minutes in an ultrasonic bath. The substrates were then rinsed with deionized water and dried by compressed air or pure nitrogen. Once dry, the substrates were fixed to the heater by using silver paste. This insures good thermal conductivity which can set the substrate's temperature in the range from room temperature up to 800°C.

Gold nanodots, used as a catalyst for nanowires, are first deposited on the substrate by 5 laser shots. Then a deposition was conducted, using the metallic oxide target, using the same temperatures settings for depositing the gold nanodots on the substrate. After the deposition, the substrate was cooled down to room temperature, at a rate of 8°C/min in an oxygen atmosphere of 450 Torr.

Three different PLD chambers were utilized in this project. Two of these chambers, were located in Metallurgy and Material Science department and will be labeled as Chamber

#1 and Chamber #2. The other chamber was located in the basement of Electrical Engineering department, which is aptly named Chamber #3.

The three chambers that were used have distinct differences in physical configuration. The first major difference is the shape of main chamber. Chamber #1 and chamber #2, shown in Fig.3.2 and 3.3, have a spherical main chamber, while Chamber #3, shown in Fig.3.5, is cylindrical. Another difference concerns the positioning of the gas inlet opening. In chamber #2, the gas inlet opening is on top of the heater, as is shown in Fig.3.4, which is located in the center of the chamber. However, the gas inlet openings in chamber #1 and #3 are located at the bottom of the chambers. This is a significant difference as the position of gas inlet opening will affect the flow of gas and may influence the final result of the deposition. In chamber #1 and #2, the shutter covers the substrate, as shown in Fig. 3.4, while in chamber #3, shown in Fig. 3.7, the shutter covers the target. The optical instruments setup, shown in Fig.3.3, for chamber #1, the laser is steered by two tracked lenses, which move back and forth during the deposition. This allows the laser shots to cover the entire target, which removes the need to polish the targets before deposition. While, in Fig.3.3 and 3.6, for chamber #2 and #3, the lens and mirrors are fixed and do not move during the deposition and causes the laser to not cover the entire target. Therefore, after several depositions the targets need to be polished to ensure that the surface of the targets is flat and even enough for each deposition. Lastly, there is a water cooling system located in the target carrousel of chamber #3, which cools down the target during the deposition.

It was discovered that due to the differences from these three different laser-chambers system setups can affect the morphology of the samples. Therefore, in order to discuss the influence of a specific parameter, it is important to keep the other parameters at the same constant setting, and varying the observational parameter at different values in the same laser-chamber system.
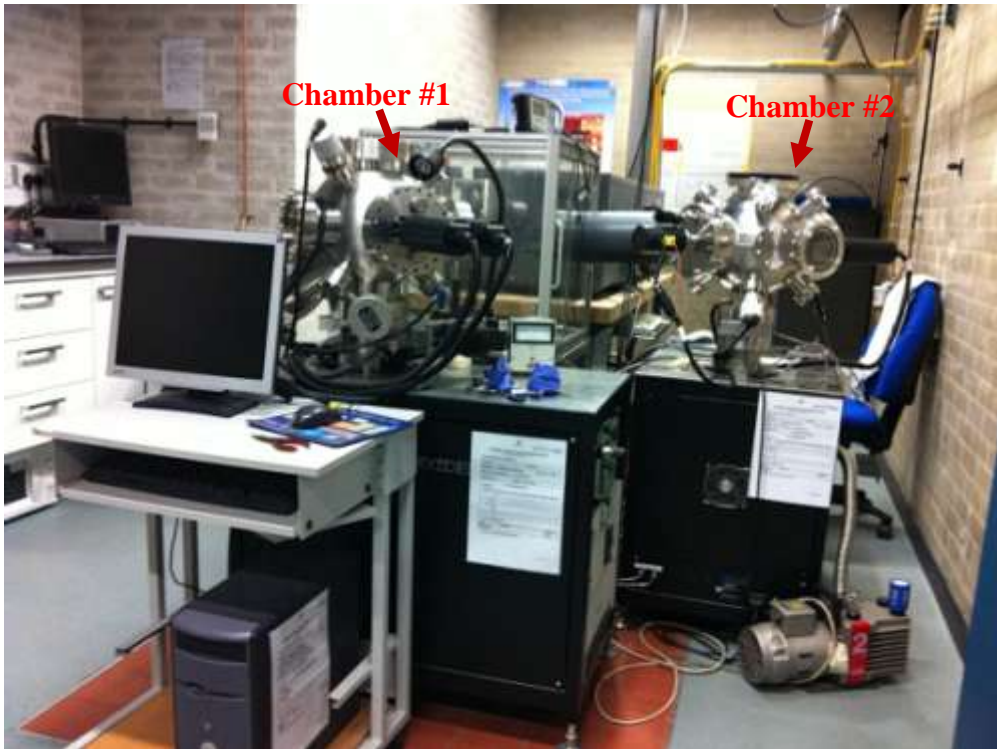
Fig. 3.2 Laser lab in Material and Metallurgy Department
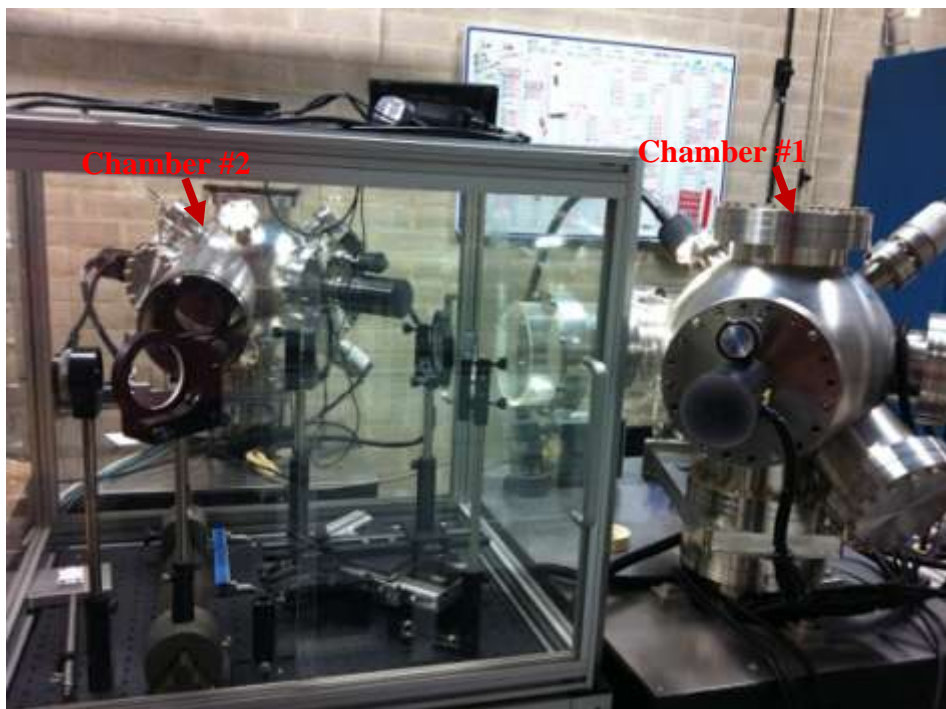
Fig. 3.3 Optical instruments set-up of chamber #1 and #2

Fig. 3.4 Inside Chamber #2: the gas inlet opening on top of the heater and the shutter covering the substrate
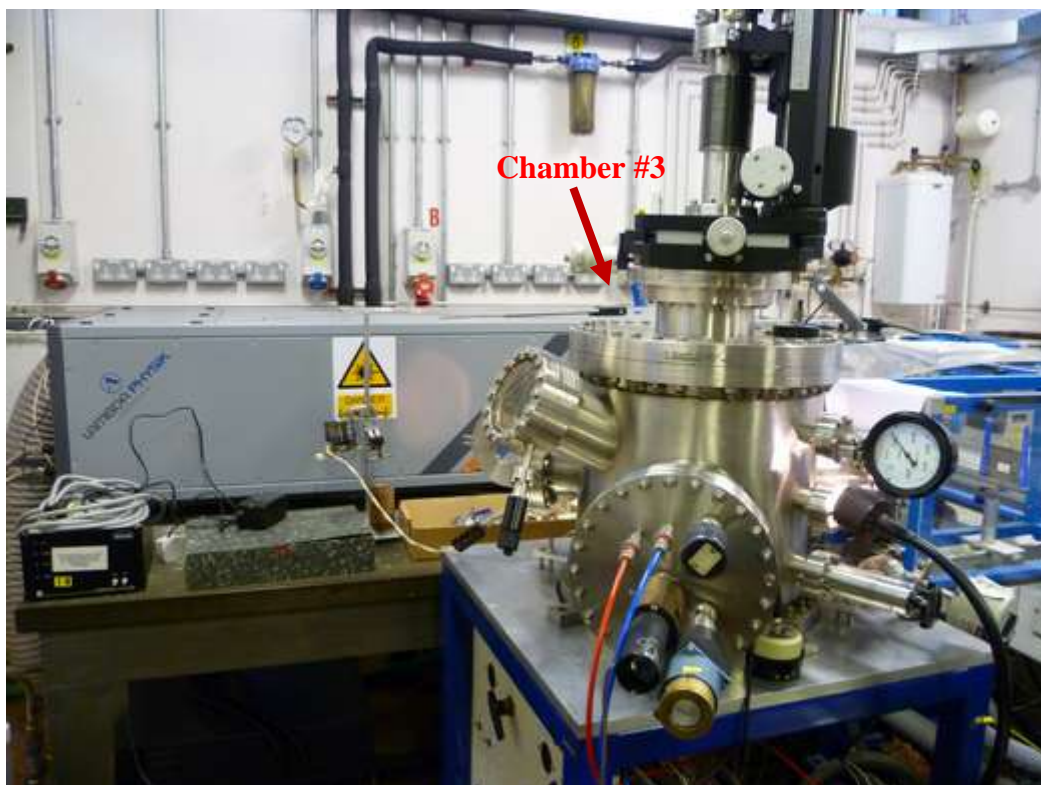
Fig. 3.5 Laser lab in the basement of Electrical Engineer Department
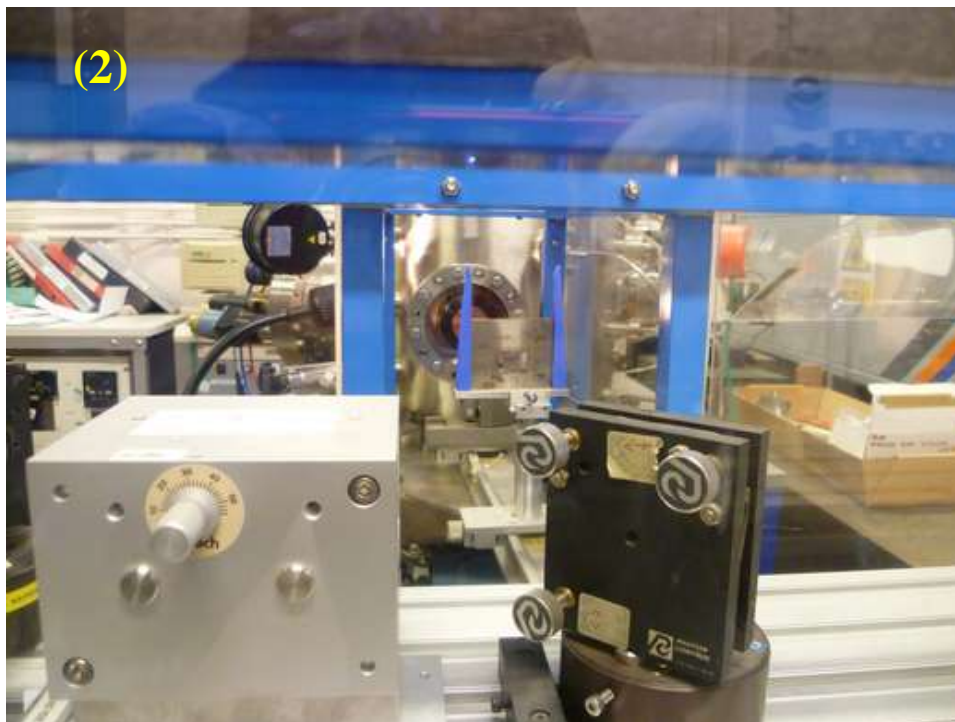
Fig. 3.6 Optical instruments set-up of chamber #3

Fig. 3.7 Inside of Chamber #3: shutter covering the target

3.2 Scanning Electron Microscopy (SEM)

In order to observe the results of the depositions conducted, Scanning Electron Microscopy (SEM) was utilized, at high magnifications, in all the samples. The SEM that was used for all the results and observations was a JEOL-7000 Scanning Electron Microscope. The specific one that was used is located in the Centre for Electron Microscopy, School of Metallurgy and Materials, shown in Fig.3.8.

Fig. 3.8 Jeol JSM-7000F FE-SEM

The Scanning Electron Microscope generates a beam of electrons from a tungsten filament. This filament is a looped and functions as a cathode. Once voltage is applied, the loop heats up and the anode begins to attract electrons. As the process continues, the electrons start to accelerate toward the anode and onto the sample that is being observed. The beam of electrons is then focused by an array of lenses and then scanned across the surface of the sample. Electrons that are released by the sample are detected by a material that causes flashes of light from the electrons. These flashes are detected and then amplified by a photomultiplier tube. This produces an image that can show the topography of the sample in a manner similar to an optical microscope [1]. The electron microscope used was equipped with an x-ray, Energy dispersive spectroscopy (EDS) detector which allows the detection of specific elements that are found within the sample.

In order to produce a clear and concise image of the sample, a conducting coating is utilized when doing cross section analysis. This was the case for all the samples being analyzed and a coating of Au was used on the samples after each deposition. This provided the needed conductivity that was needed to create cross section images within the SEM.

3.3 Atomic Force Microscopy (AFM)

Atomic Force Microscopy (AFM) was used to observe the surface morphology of the all the Au coated samples created from the depositions. The DI AFM Nanoscope III, located in the Metallurgy and Material Science department, was used for the observations of all the Au coated samples. The nanoscope was set to "Tapping Mode" which is an imaging technique that is widely when using AFM. In this mode, the cantilever oscillates at various frequencies near its resonance frequency by the probe's tip. An electronic servo uses a piezoelectric actuator to control the height of the cantilever, while maintaining constant oscillation amplitude while scanning over the sample. The image is produced when the oscillating tip touches the sample and is measured by a laser that is reflected off the cantilever into a photodiode detector [2].

In order to study the morphology of the Au nanodots, 1nm diameter ultra-fine AFM tips were utilized. The AFM pictures, that were generated, were further analyzed by using WSXM 4.0 and Image Tool 3.0.

3.4 Structure

3.4.1 X-ray diffraction

In order to understand the structure of the samples produced, X-Ray-Diffraction (XRD) analysis was conducted by using a Siemens Goniometer with a Cu Kα radiation source to investigate the phase of the samples. Bragg's Law is defined as:

$$n\lambda = 2d \sin(\theta)$$

n is an integer, λ is the wavelength of a beam of x-rays incident on a crystal with lattice planes separated by distance d, and θ is the Bragg angle.

The interference (constructive) between the waves scattering, from two adjacent rows of atoms, in a crystal is illustrated in Fig. 3.9. The effect of scattering waves from a single row is equivalent to the partial reflection from a mirror imagined to be aligned with the row. Therefore, the angle of reflection is equal to the Angle of Incidence for each individual row. Interference will then occur between the beams reflecting off different rows of atoms within the crystal.
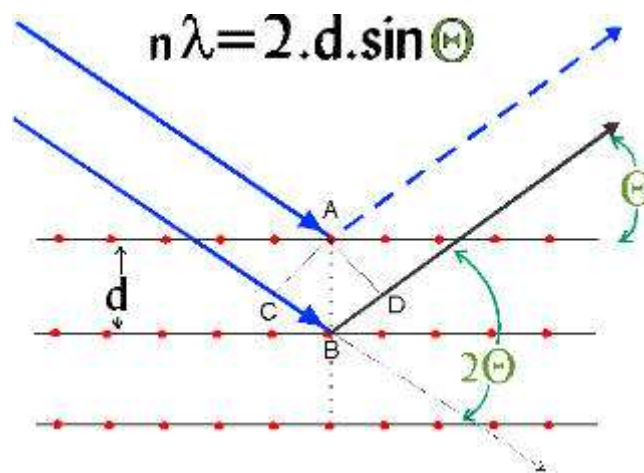
Fig. 3.9 A graphical representation of X-ray Radiation Diffracting from crystal planes and what Bragg's law represents

When X-rays are scattered from a crystal lattice, peaks of scattered intensity are observed which correspond to the following conditions:

1. The Angle of Incidence = Angle of Scattering.

2. The difference in path length is equal to an integer number of wavelengths.

If the wavelengths (λ), that allow the X-rays diffracting from the lower crystal plane to cover the distance from CB to BD, can be determined and still be in constructive interference with the upper X-rays, then Bragg's Law can be upheld. The condition for

maximum intensity contained in Bragg's law provides the ability to calculate details regarding the crystal structure or to determine the wavelength of the X-rays incident upon the crystal, if the crystal structure is known.

Therefore, to determine the spacing between the lattice planes, the *d* variable from Bragg's Law, the variable that needs to be controlled is the wavelength (λ) of the X-rays. This variable can be controlled the target that is being used to create the beam. The angle (θ) is measured by the angle between the arms of the diffractometer as it moves. The integer "n", appears due to the periodicity of the wave and can be any positive integer [3].

3.4.2 Phi-scan

The intensity data for various settings of Chi and Phi needed to be collected and analyzed. Therefore a Phi-scan was utilized to obtain intensity information of the various samples produced. Phi is the angle of rotation of the sample on the axis normal to the sample surface, through the center of the sample holder (in Fig. 3.10). The systematic change in angular orientation of the sample is normally achieved by utilizing an X-Ray diffractometer. All Phi values were measured by a given setting of Chi.
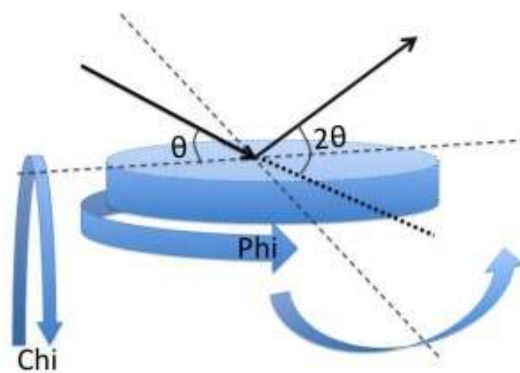
Fig. 3.10 Schematic diagram of phi-scan[3]

57

References

[1] Oliver C. Wells, Scanning Electron Microscopy, (1974) McGraw Hill

[2] Geisse, Nicholas A. AFM and Combined Optical Techniques. Materials Today 12/7(2009) 40

[3] Rupp B. Biomolecular Crystallography: Principles, Practice and Application to Structural Biology. (2009) New York: Garland Science

Chapter 4

Results and Discussion

4.1 MgO Nanowires and Nanorods

Depositing MgO layers on MgO(100) substrates is homoepitaxial growth. All the samples mentioned, in this section, were conducted in chamber #2, under the heater temperature of 800°C and the laser energy density was kept around 1.15J/cm^2 (spot size of 1.2×7mm^2). The other parameters and results are listed in the table below.

Table 4.1.1 Detailed parameters of the samples AMG-001,002,003 and 004

Sample Number	Number of pulses on Au target (shots)	Number of pulses on MgO target (shots)	Oxygen Pressure (mTorr)	Length of nanowires (nm)	Planar Dimension (nm)
AMG-001	N/A (1-2nm)	120,000	165	1000~2000	700~800
AMG-002	5	10,000	120	100~200	20
AMG-003	5	60,000	120	1000	20
AMG-004	25	60,000	120	1000	100

4.1.1 Catalytic effect of gold on MgO nanowires and nanorods growth

In order to investigate the catalytic effect of gold for MgO nanowires and nanorods, it is necessary to compare the morphology of deposited material with and without gold at exactly the same deposition conditions. To achieve this, the substrate was partially coated by an ultrathin gold layer, with a thickness of 1-2 nm, using a shadow mask during the thermal evaporation of gold. The region 1 in Fig.4.1.1.1 is thick film, numbered as AMG-001, with 120,000 pulses of MgO grown on bare substrate without a gold layer. This thick film shows a plate-like misoriented morphology with some large particulates. However, in region 2, above the layer of gold, shows growth of nanostructures in the form of cuboids or nanorods with a

length of 1-2 micrometers and square cross-section with planar size of 700-800 nm. Most of these nanorods are grown perpendicularly to the surface. However, there are many oblique ones with variable lengths (see Fig.4.1.1.1c). This may be related to the specific morphology of the thermally evaporated gold layer or reflect the particular oxygen flow during the MgO deposition.
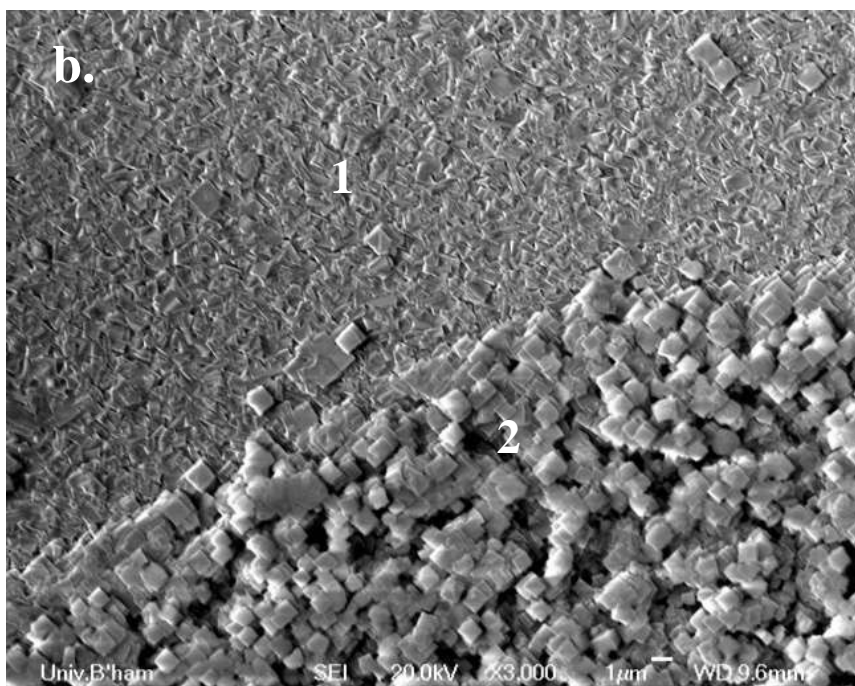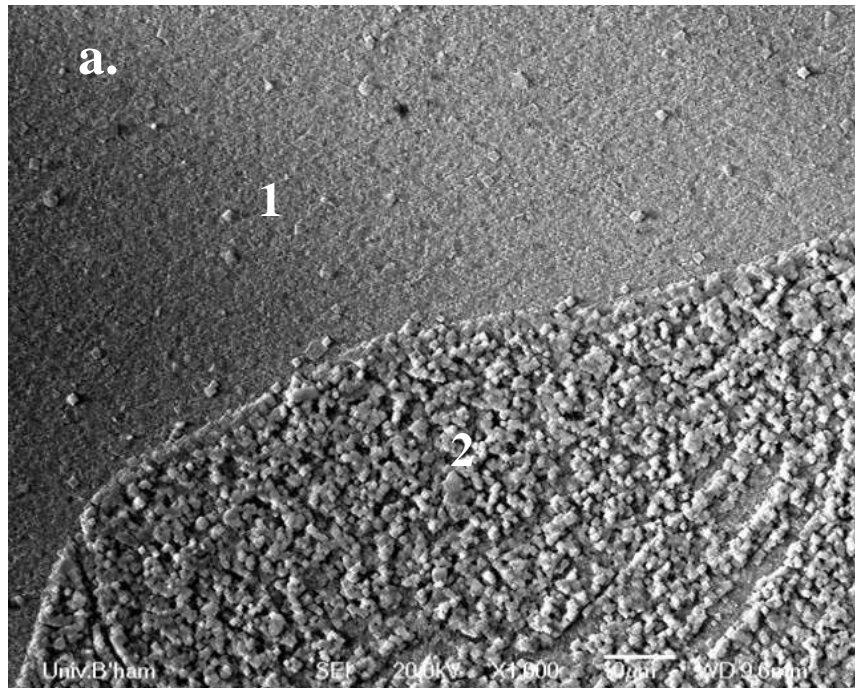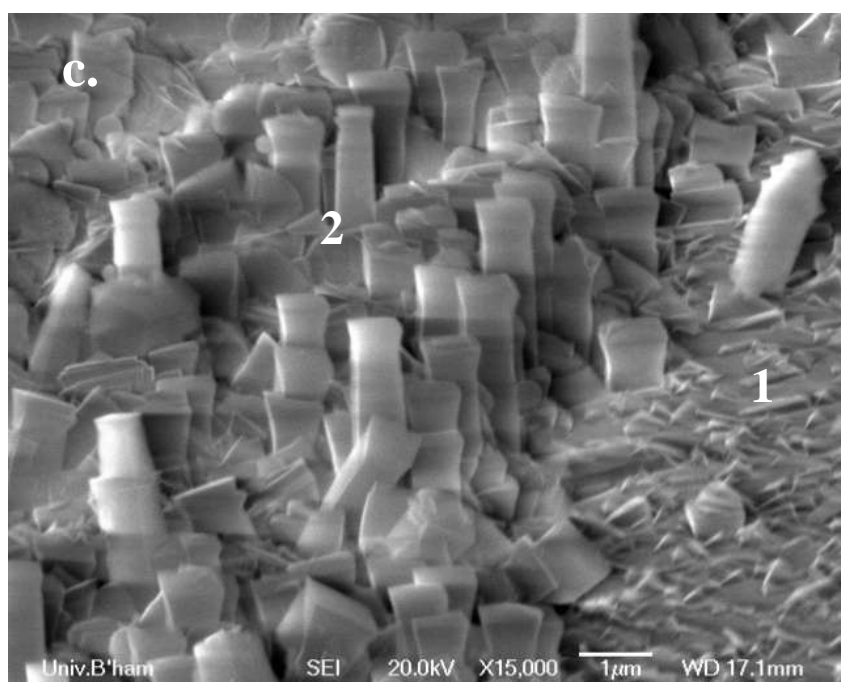
Fig. 4.1.1.1 Scanning electron microscopy (SEM) images of PLD grown MgO deposited by 120,000 laser pulses in 165 mTorr oxygen pressure without (region 1) and with (region 2) a 1-2 nm gold layer at different tilt and magnification:
a) top view, magnification of 1000; b) top view, magnification of 3000 ;
c) 70˚ tilt, magnification of 15,000.

4.1.2 Influence on morphology of the number of pulses on MgO target

In order to understand the growth of MgO and active formation of MgO nanowires, gold was deposited by PLD, in the form of nanoparticles. The number of laser pulses on the MgO target has been changed comparable with that used in section 4.1.1 to 10,000 pulses (Fig.4.1.2.1) and 60,000 pulses (Fig.4.1.2.2). These samples were deposited using the same parameters of deposition, such as 5 pulses on gold target and 120mTorr of oxygen pressure. It was observed that nanowires were formed and their length increased with the number of pulses on MgO target while retaining a similar cross-section. The length of nanowires, grown by 10,000 laser pulses, were between 100 and 200 nm, while the length of nanowires grown

by 60,000 laser pulses was about 1 micrometer. In both ablations, the planar dimensions of nanowires were about 20 nm.

It was also observed that the increase in the length of the nanowires was accompanied by the appearance and growth of boulders, which are larger and more common among longer nanowires as seen in Fig.4.1.2.2. The formation of these boulders may be due to the gold agglomeration on the substrate. However, they are almost spherical with an indication that they are formed without or having little contact with the substrate. Hence, the gold agglomeration may be not a direct cause of the boulders formation. It suggests that the boulders are formed from the large particles within the plasma plume, during the ablation of MgO. The appearance of similar spheres has been found when conducting the ablation of Indium Tin Oxide by using the same PLD system [1].

15.0kV X10,000 1μm

15.0kV X20,000 1μm

64
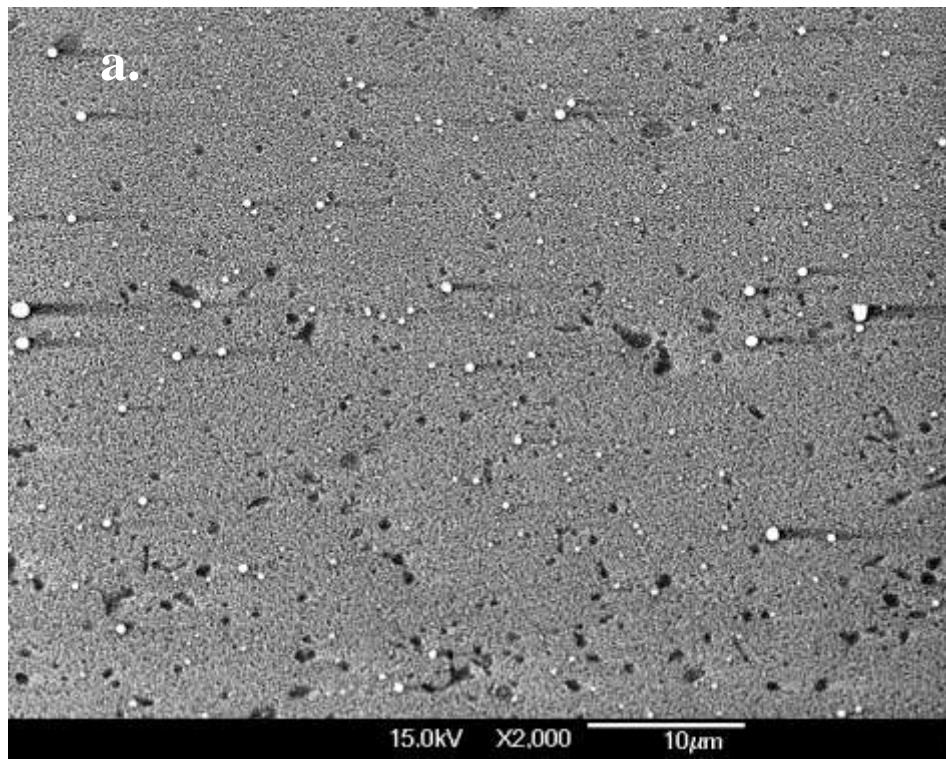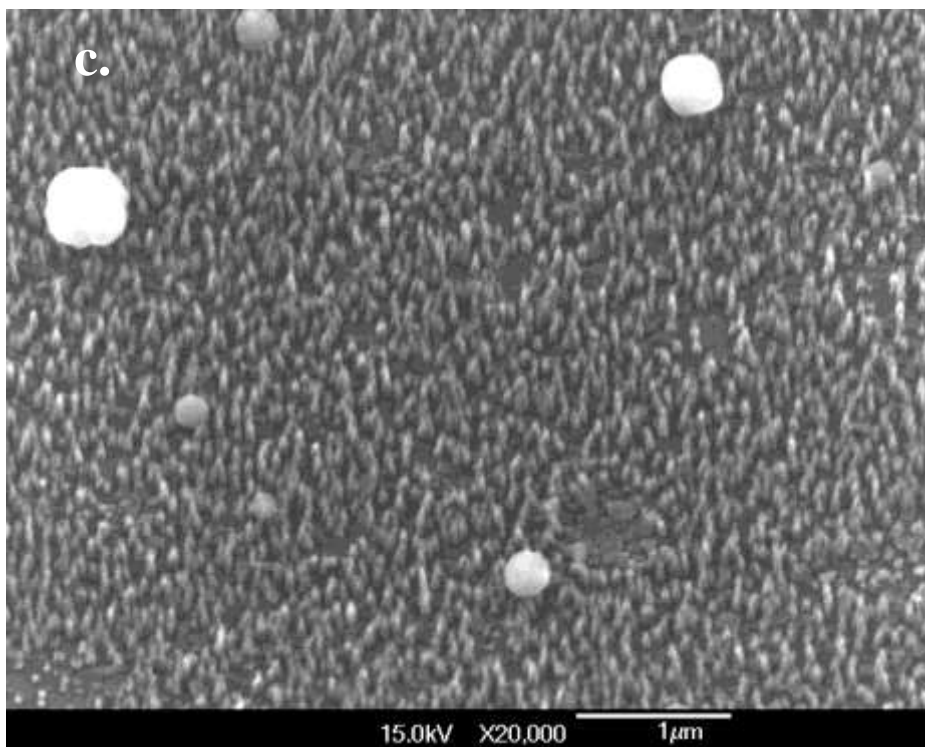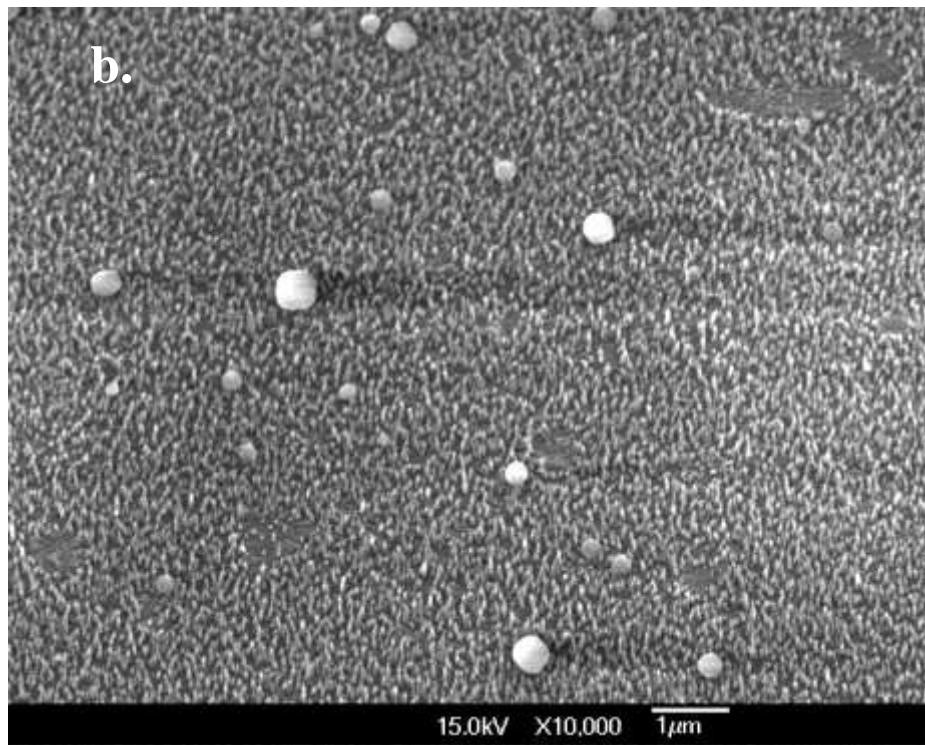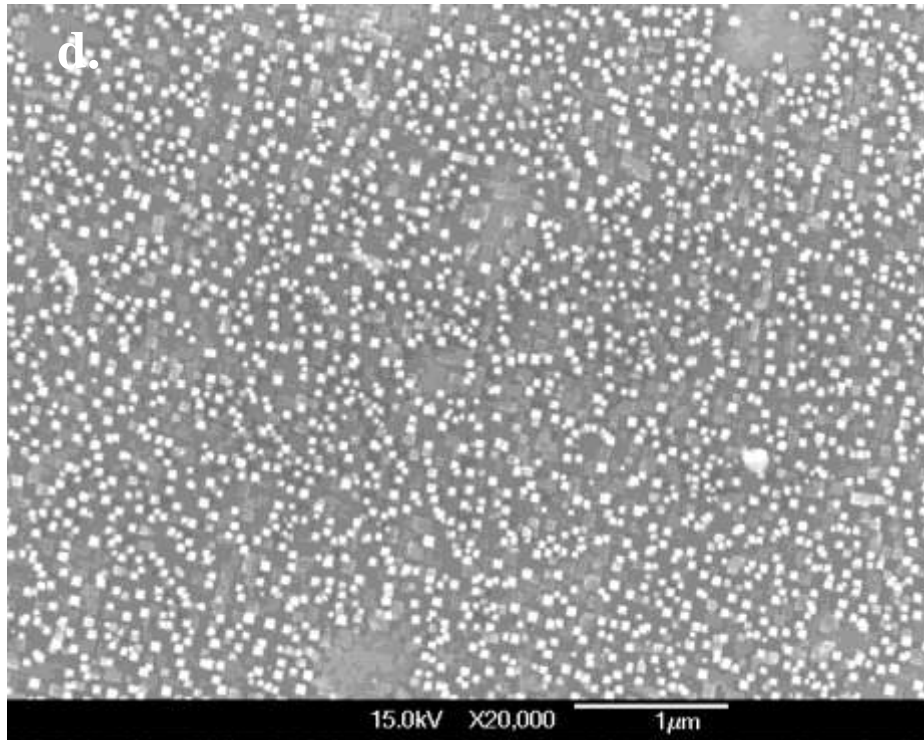
Fig. 4.1.2.1 SEM images of PLD grown MgO deposited by 10,000 laser pulses in 120 mTorr oxygen pressure

a) 45˚ tilt, magnification of 2000; b) 45˚ tilt, magnification of 10,000; c) 45˚ tilt, magnification of 20,000; d) top view, magnification of 20,000.
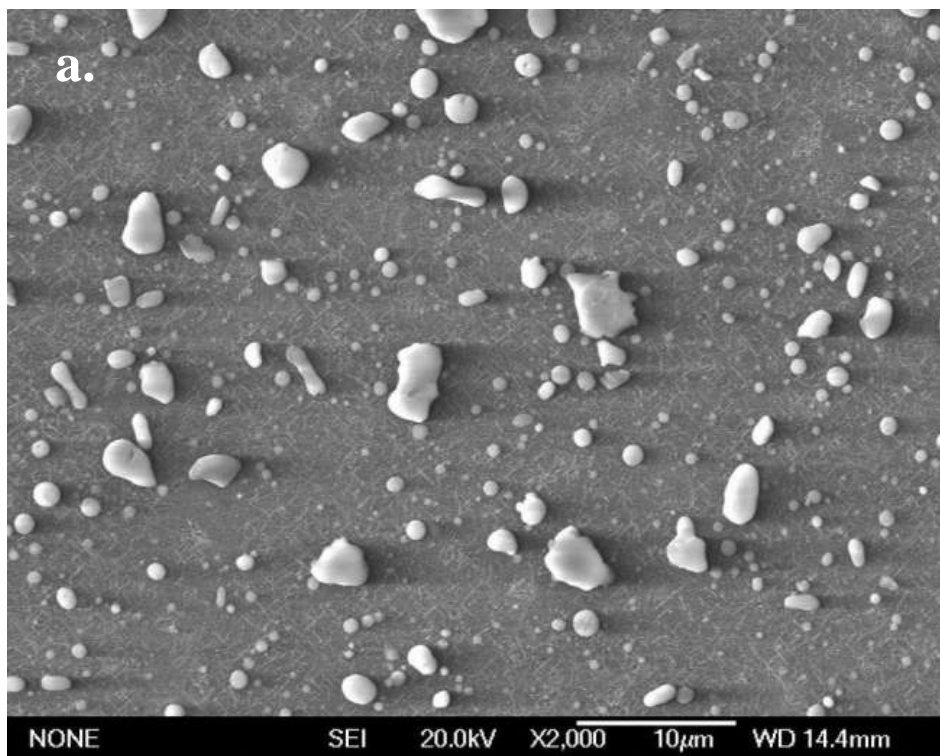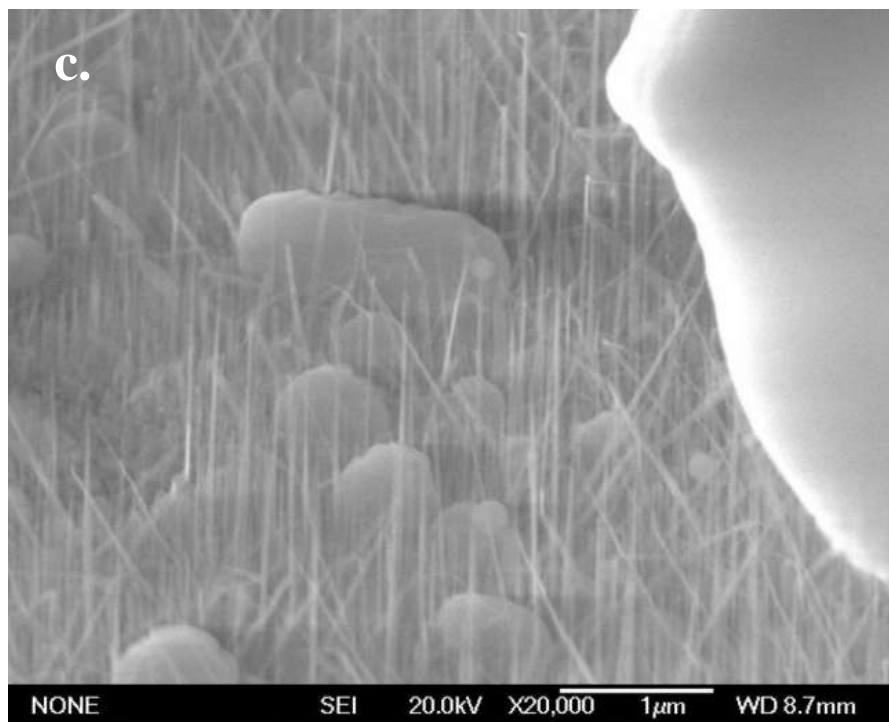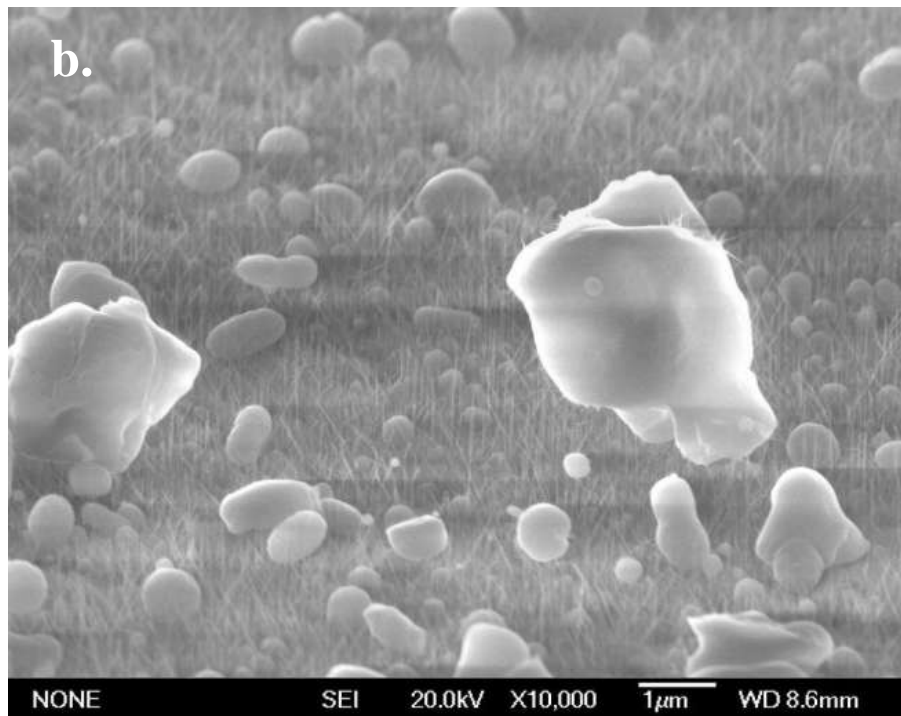
Fig. 4.1.2.2 SEM images of PLD grown MgO deposited by 60,000 laser pulses in 120 mTorr oxygen pressure

a) top view, magnification of 2000; b) 70˚ tilt, magnification of 10,000;
c) 70˚ tilt, magnification of 20,000.

4.1.3 Influence on MgO growth of the number of pulses on gold target

As the number of laser pulses on MgO target has an effect to change the length in nanowires, their morphology may also be varied by the number of laser pulses on the gold target. To investigate this, two samples were prepared on MgO single crystal substrates using 5 and 25 pulses on the gold target, respectively. The morphology of the gold cover was studied by Atomic Force Microscopy (AFM) as shown in Fig.4.1.3.1 and Fig.4.1.3.2. It was observed that, as the number of pulses increased from 5 to 25, the average diameter of the gold nanodots increased from 7 nm to 15 nm and their height increased from 1 nm to 2.5 nm. The gold agglomerations were found on the sample with 5 pulse nanodots, which are marked by the circles in Fig.4.1.3.1. The gold melting point decreases from its bulk material melting point, if the gold was deposited as a very thin layer towards the atomic scale [4] and this is how the gold nanodots are formed. According to Oswald Ripening, when increasing the thickness of the gold layer, small gold nanodots will redeposit onto larger particles. Therefore, the gold nanodots' average diameter increases as the pulses on gold increase.
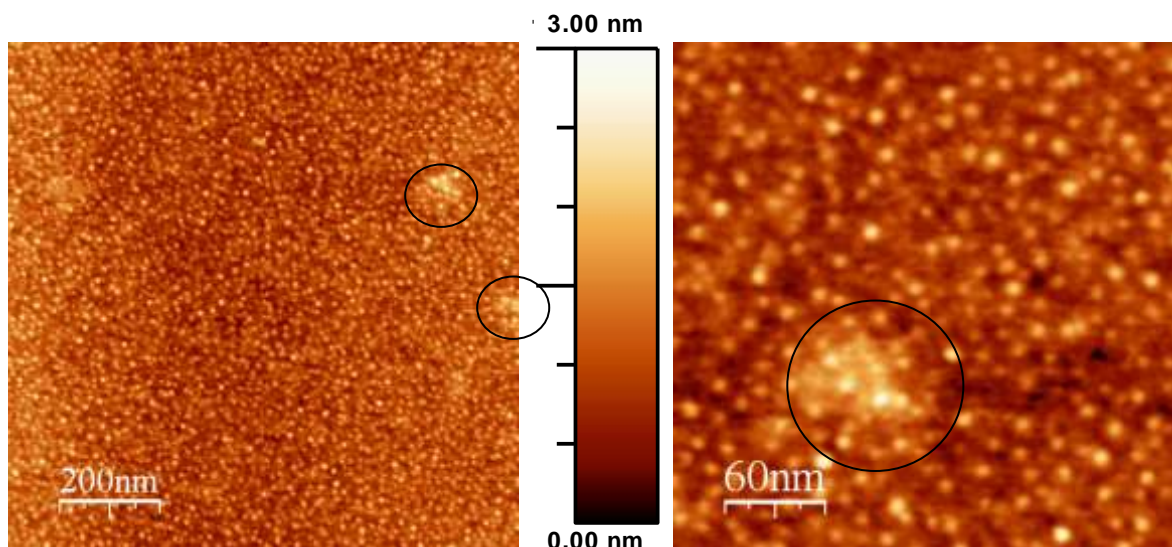
Fig. 4.1.3.1 AFM images of the surface of MgO substrate covered with gold nanodots deposited by 5 laser pulses at different magnifications. The circled areas are gold agglomerations formed by nanodots.
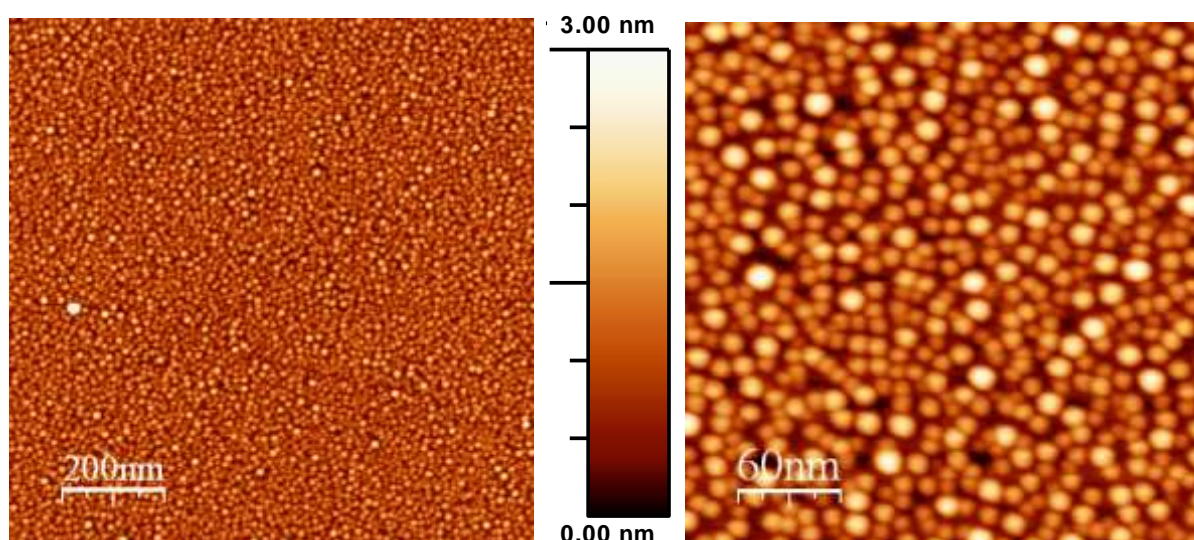
Fig. 4.1.3.2 AFM images of the surface of MgO substrate covered with gold nanodots deposited by 25 laser pulses at different magnifications.

If the number of gold pulses were increased from 5 shots to 25, the dimension of nanorods cross section also increased from 20 nm to 100 nm, as shown in Fig.4.1.3.3. From this observation, it can assume that the width of nanowires is related to the size of gold nanodots formed on the substrate.
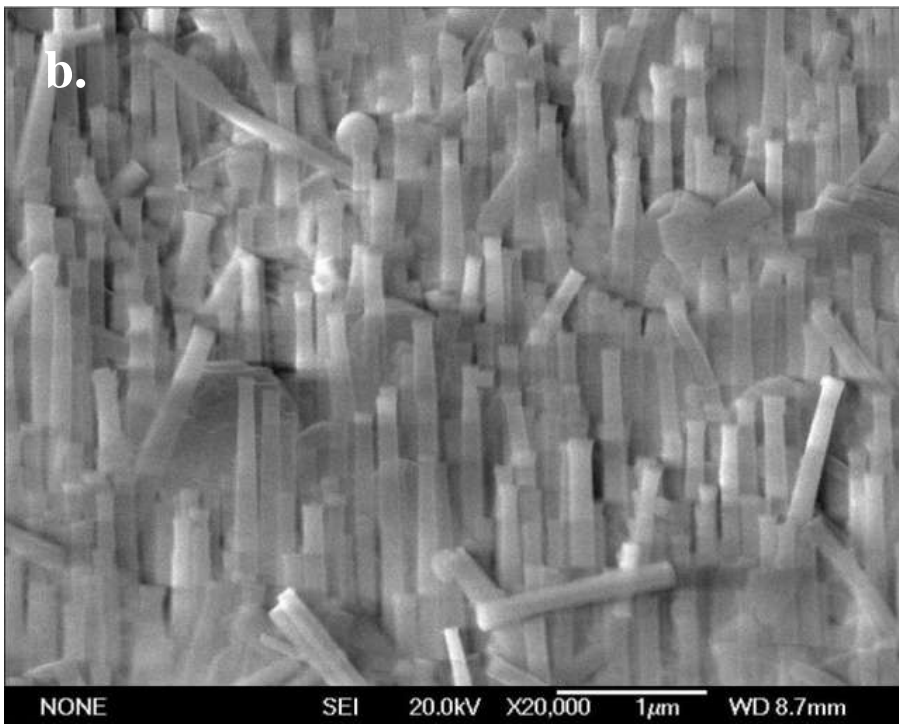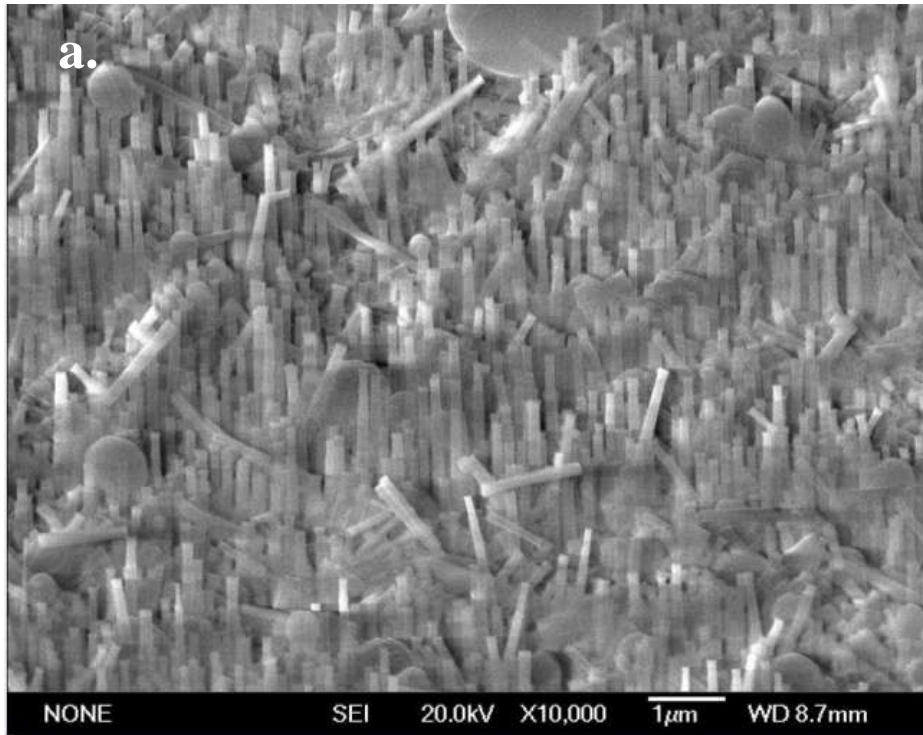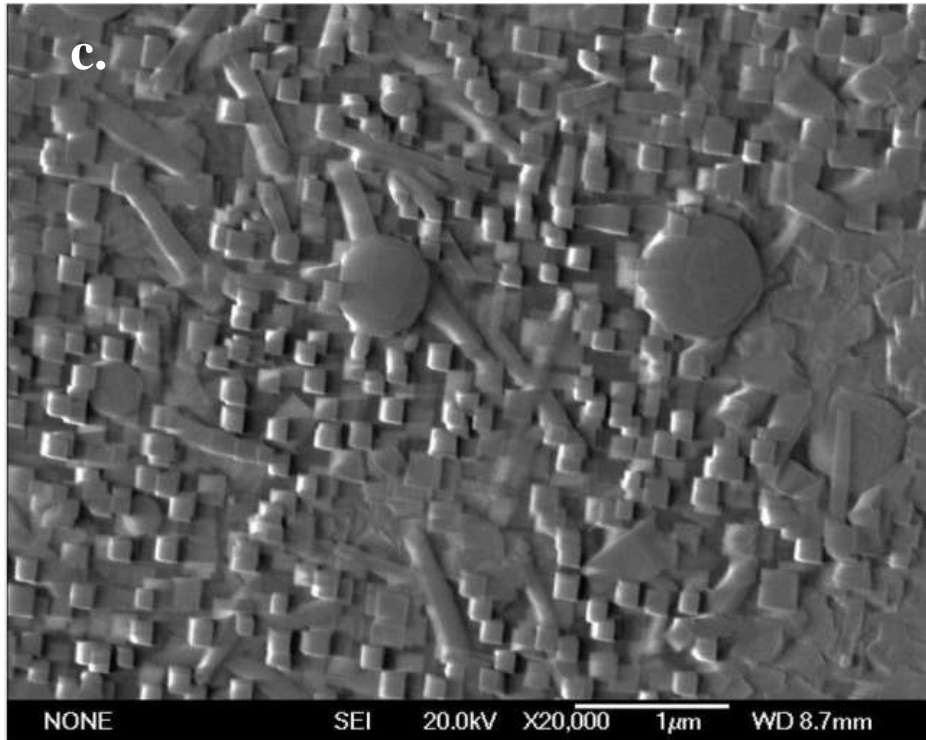
Fig. 4.1.3.3 SEM images of PLD grown MgO deposited by 25 laser pulses on gold, 60,000 laser pulses on MgO in 120 mTorr oxygen pressure

a) 70˚ tilt, magnification of 10,000; b) 70˚ tilt, magnification of 20,000; c) top view, magnification of 20,000.

4.2 ZnO One Dimensional Nanostructures

4.2.1 Influence of oxygen pressure

An important factor, when conducting oxide PLD depositions, is oxygen pressure. It can affect the shape of the plasma plume as well as react with the oxide used. In some instances, a higher oxygen pressure is needed when compared with the growth of other oxides. This is especially the case for the growth of ZnO nanowires and nanorods.

The samples, which are taken into consideration, are listed in Table 4.2.1, 4.2.2, 4.2.3 and 4.2.4. All of the substrates used in this section are MgO(100). 5 pulses were shot on the gold target and the laser energy density inside the chamber was kept around 1 J/cm^2.

Table 4.2.1 Detailed parameters of the samples AZO-004,003 and 002

Sample Number	Temperature (°C)	Chamber number	Distance of Target-Substrate (mm)	Number of pulses on ZnO target (shots)	**Oxygen Pressure (mTorr)**
AZO-004	800	#1	58	10000	**150**
AZO-003	800	#1	58	10000	**250**
AZO-002	800	#1	58	10000	**350**

Table 4.2.2 Detailed parameters of the samples AZO-009 and 013

Sample Number	Temperature (°C)	Chamber number	Distance of Target-Substrate (mm)	Number of pulses on ZnO target (shots)	**Oxygen Pressure (mTorr)**
AZO-009	800	#1	55	5000	**1200**
AZO-013	800	#1	55	5000	**3000**

Table 4.2.3 Detailed parameters of the samples AZO-017,016,018 and 015

Sample Number	Temperature (˚C)	Chamber number	Distance of Target-Substrate (mm)	Number of pulses on ZnO target (shots)	**Oxygen Pressure (mTorr)**
AZO-017	750	#2	55	5000	**7.5**
AZO-016	750	#2	55	5000	**150**
AZO-018	750	#2	55	5000	**350**
AZO-015	750	#2	55	5000	**1200**

Table 4.2.4 Detailed parameters of the samples AZO-024 and 058

Sample Number	Temperature (˚C)	Chamber number	Distance of Target-Substrate (mm)	Number of pulses on ZnO target (shots)	**Oxygen Pressure (mTorr)**
AZO-024	700	#3	55	5000	**1200**
AZO-058	700	#3	55	5000	**2000**

The morphology of the samples observed was directly influenced by the oxygen pressure within the chamber. The sample AZO-004 was exposed to a high temperature of 800°C with a lower oxygen pressure of 150mTorr produced a lattice-like surface without any granular objects and peaks, as seen in Fig.4.2.1.1.a. However, in sample AZO-002, shown in Fig.4.2.1.1.c, the oxygen pressure was increased to 350mTorr and it produced a surface that is rough and uneven with peaks of various sizes. Round and granular objects with occasional peaks of various sizes can be found on the surface of sample AZO-003, shown in Fig.4.2.1.1.b, which were made with an oxygen pressure of 250mTorr. It is clear that the surface becomes rougher as the oxygen pressure increases. This indicates that under higher oxygen pressure, growth tends to be one dimensional rather than two dimensional.

a.

SEI 15.0kV X4,000 1μm WD 11.0mm

b.

1μm
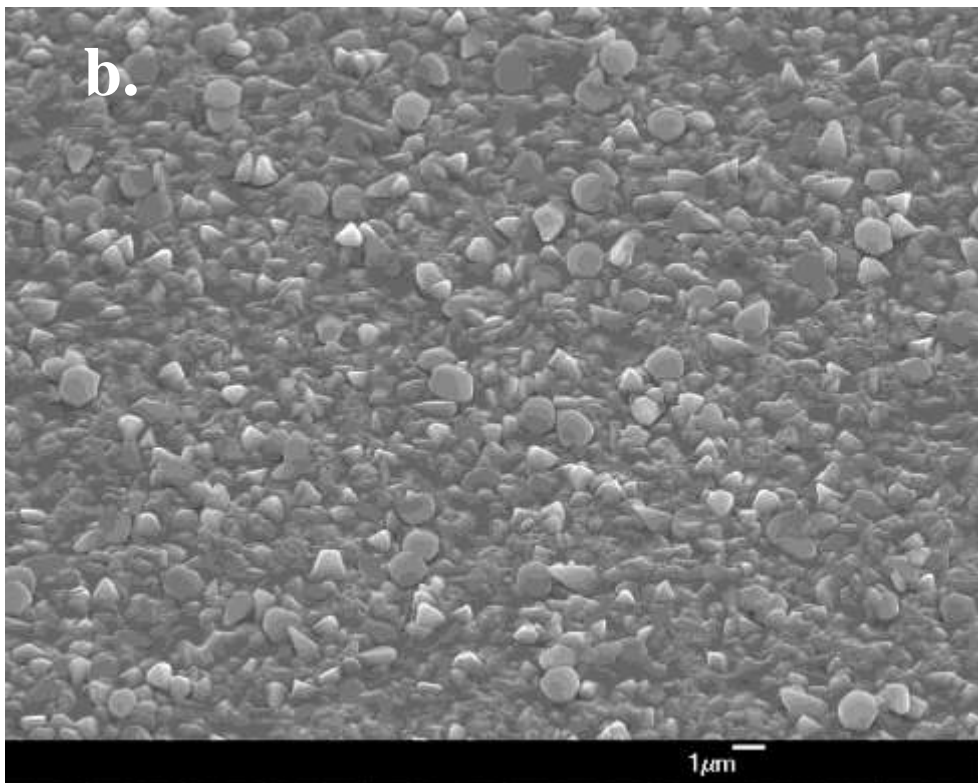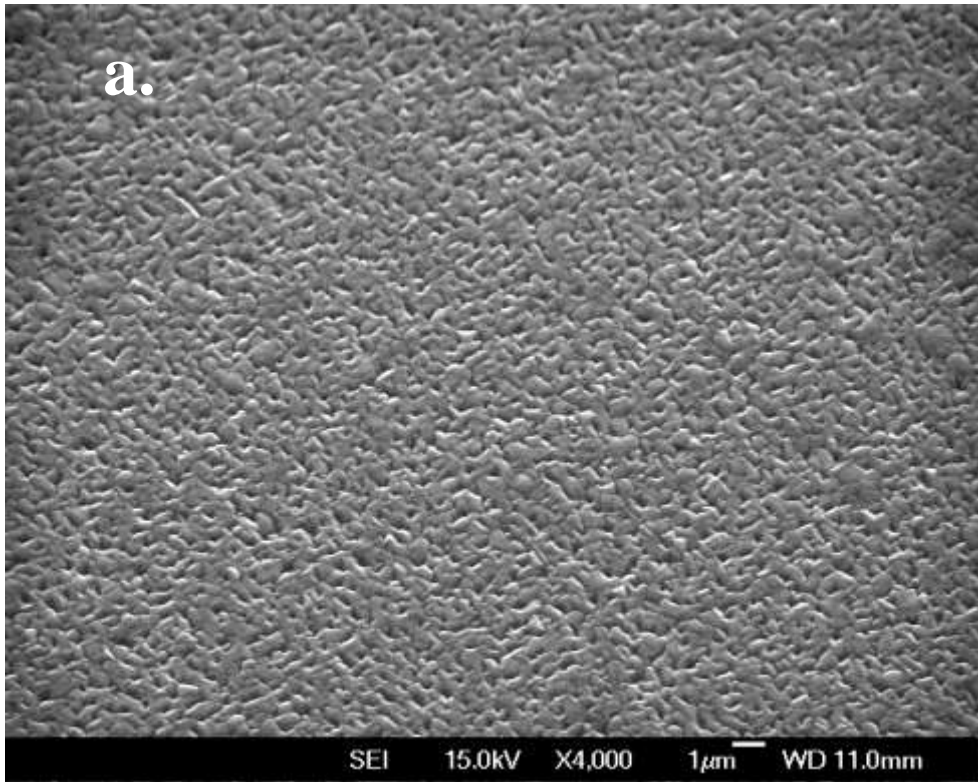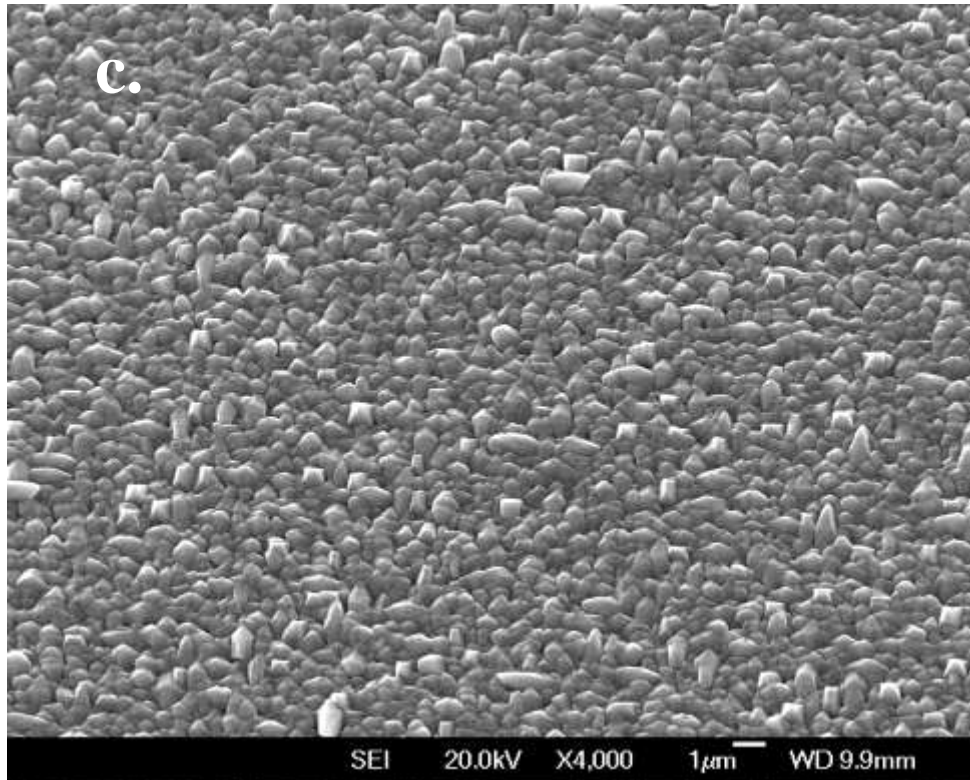
Fig. 4.2.1.1 SEM images of PLD grown on MgO (100) deposited by 10,000 laser shots under 800°C

a) AZO-004, 150mTorr oxygen pressure, magnification of 4,000;
b) AZO-003, 250mTorr oxygen pressure, 30˚ tilt, magnification of 4,000;
c) AZO-002, 350mTorr oxygen pressure, 30˚ tilt, magnification of 4,000.

It was observed that if the temperature is kept at a constant 800˚C, reduce the number of laser pulses to 5000 shots, and increase the oxygen pressure from 1200mTorr to 3000mTorr, there were no significant structures detected and no change in the morphology, as shown in the Fig.4.2.1.2. Under high temperatures, regardless how high the oxygen pressure is, no identifiable nanostructures can be produced.
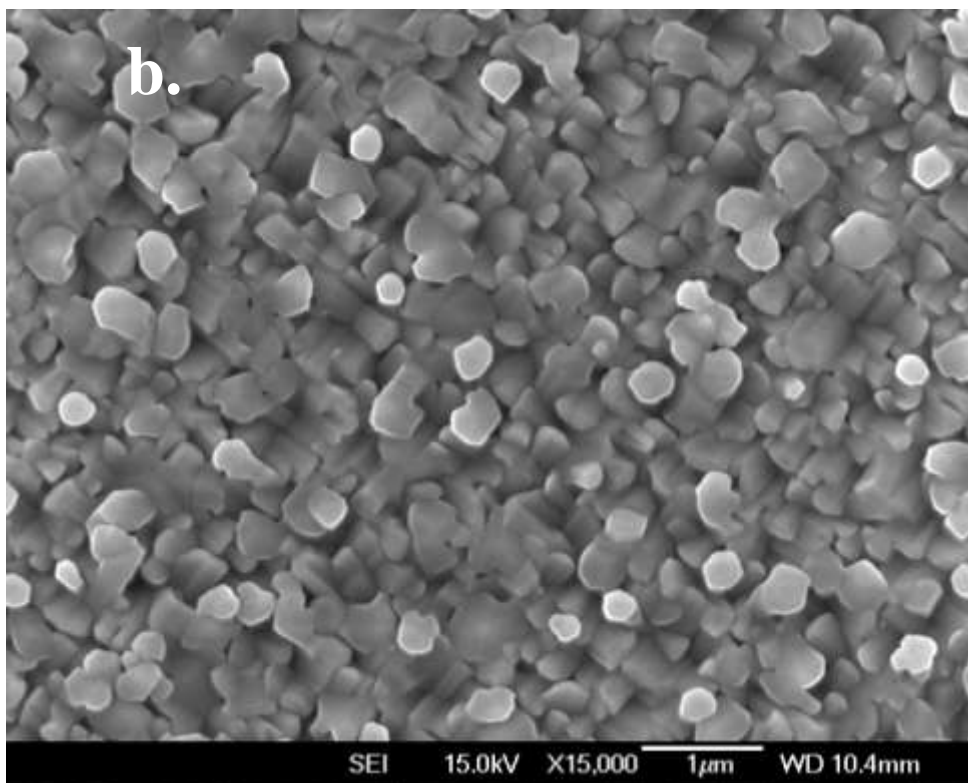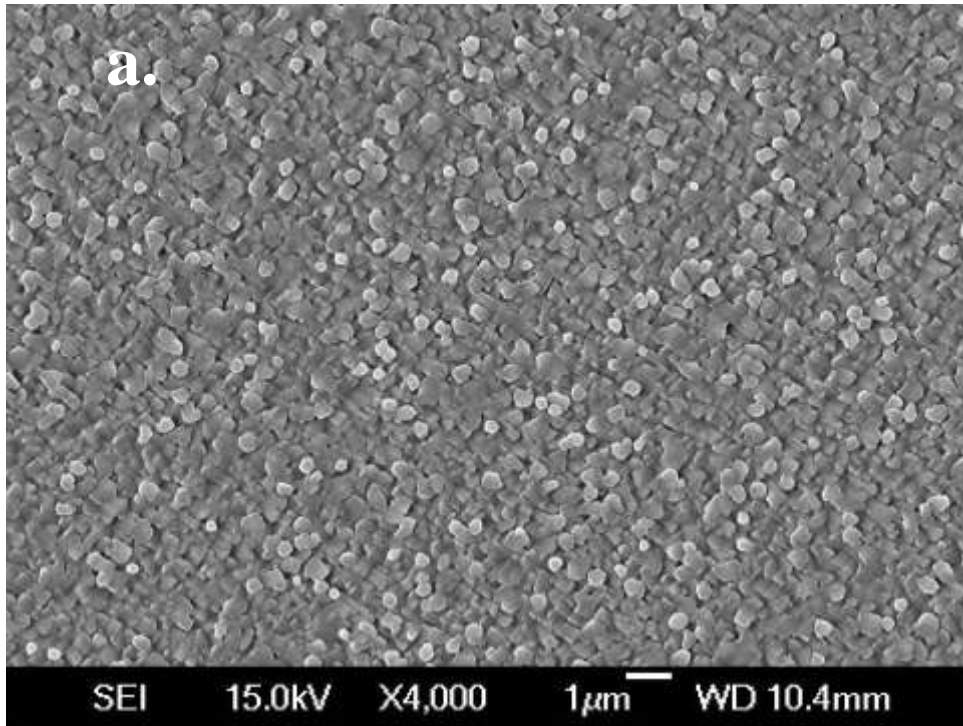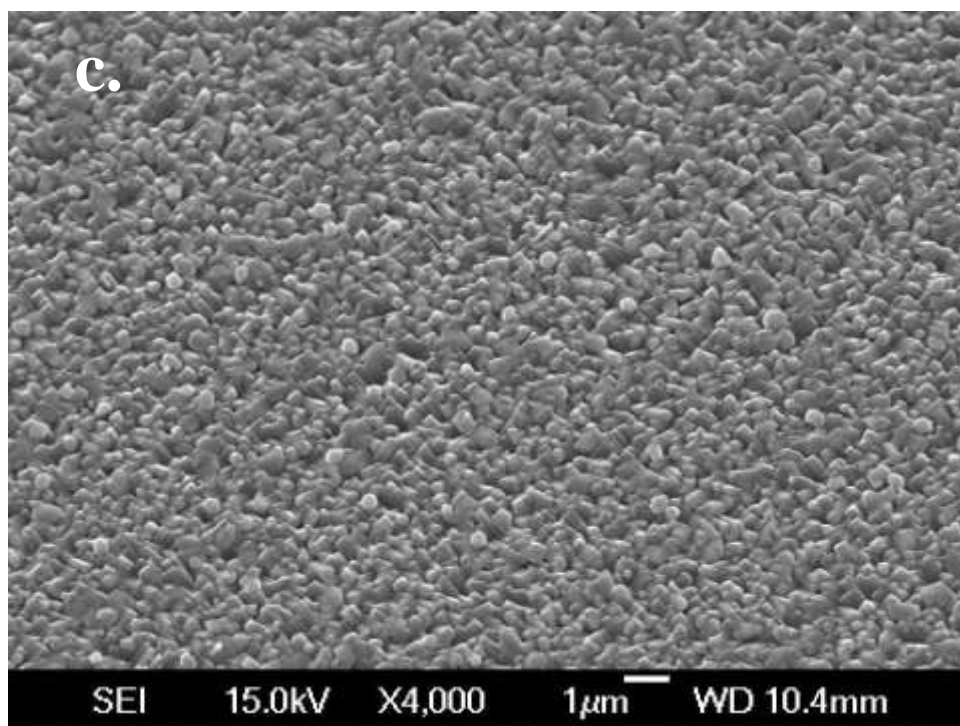
Fig. 4.2.1.2 SEM images of PLD grown MgO(100) deposited by 5,000 laser shots under 800°C

a) AZO-009, 1200mTorr oxygen pressure, magnification of 4000;
b) AZO-009, 1200mTorr oxygen pressure, magnification of 15,000;
c) AZO-013, 3000mTorr oxygen pressure, 30˚ tilt, magnification of 4000.

In chamber #2, the temperature was decreased to 750°C and the samples were produced in varying oxygen pressures of 7.5, 150, 350, 1200mTorr. In Fig.4.2.1.3, the sample AZO-017 produced in oxygen with a pressure of 7.5 mTorr. No nanowires or nanorods are present in this sample. The surface is smooth, when compared with the other three samples. The grain boundaries are very clear and some bud-shaped structures can be found at the grain boundaries.

When the oxygen pressure is increased to 150 mTorr, nanowires with dimensions between 30~50nm begin to appear, as shown in Fig.4.2.1.4 of sample AZO-016. At these conditions, the nanowires are grown in clusters in an overlapping manner with four different orientations parallel to the surface. Compared with Fig.4.2.1.2.b, both of samples have the

76

same overlapping pattern. However, sample AZO-009 shows large structures overlapping one another as opposed to the sample AZO-016 with individual clusters of nanowires overlapping in Fig.4.2.1.4.b, which is due to the different temperature.

When the oxygen pressure is increased to 350mTorr, as shown in Fig.4.2.1.5, granular crystals with size of approximately 200~360nm are formed on the surface. Also some very thin nanowires, with dimensions between 10 to 20nm, start to form on these crystals as well as between them. As the oxygen pressure is increased to 1200 mTorr, nanowires with dimensions from 10 to 20nm, nanorods with thickness around 50~100nm, nanoplates and granular crystals with size from 280 to 420nm appear on the substrate, as seen in Fig.4.2.1.6 of sample AZO-015. Most of the nanowires have a granular crystal or plate-like structure at the nanowire base. In some cases, nanorod structures can be seen in various areas along with the nanowires.

When comparing these four samples, as the oxygen pressure is increased to 350mTorr, granular crystals begin to form. The average sizes of these crystals also increase as the oxygen pressure increases. The presence of very thin nanowires also appears between the granular crystals but remain the same diameter despite the increase of oxygen pressure. This indicates that these very thin nanowires growth mode is different from perpendicular nanorods, which will be discussed in the nanowires and nanorods growth mode section. Clusters of nanowires can be grown in lower oxygen pressure, such as 150mtorr, while perpendicular nanowires and nanorods can only be grown when the pressure is higher.
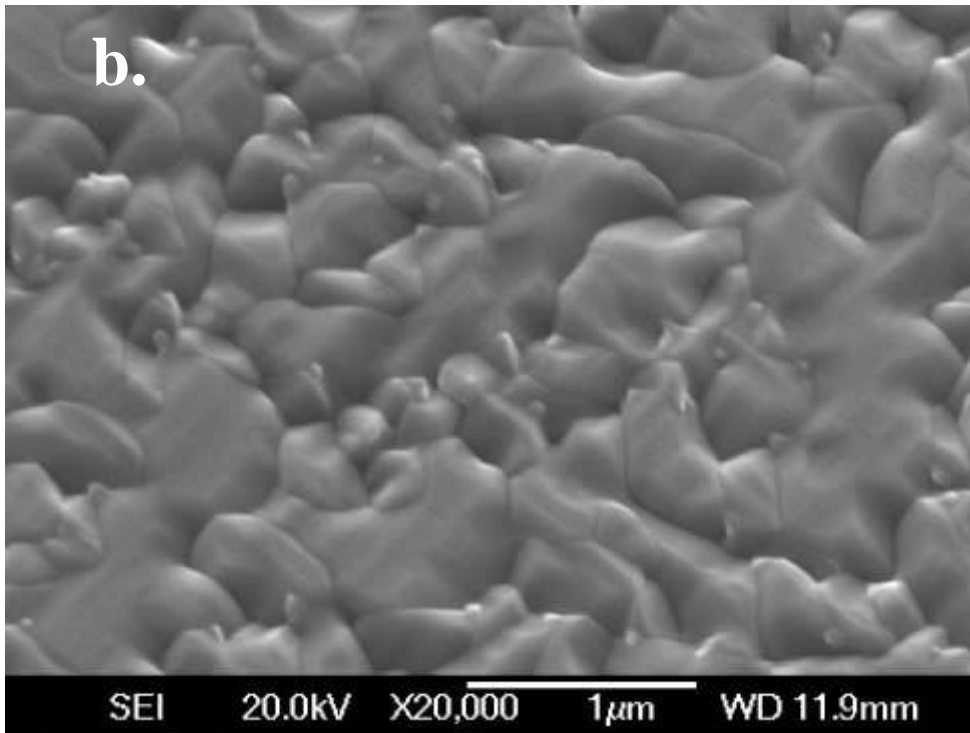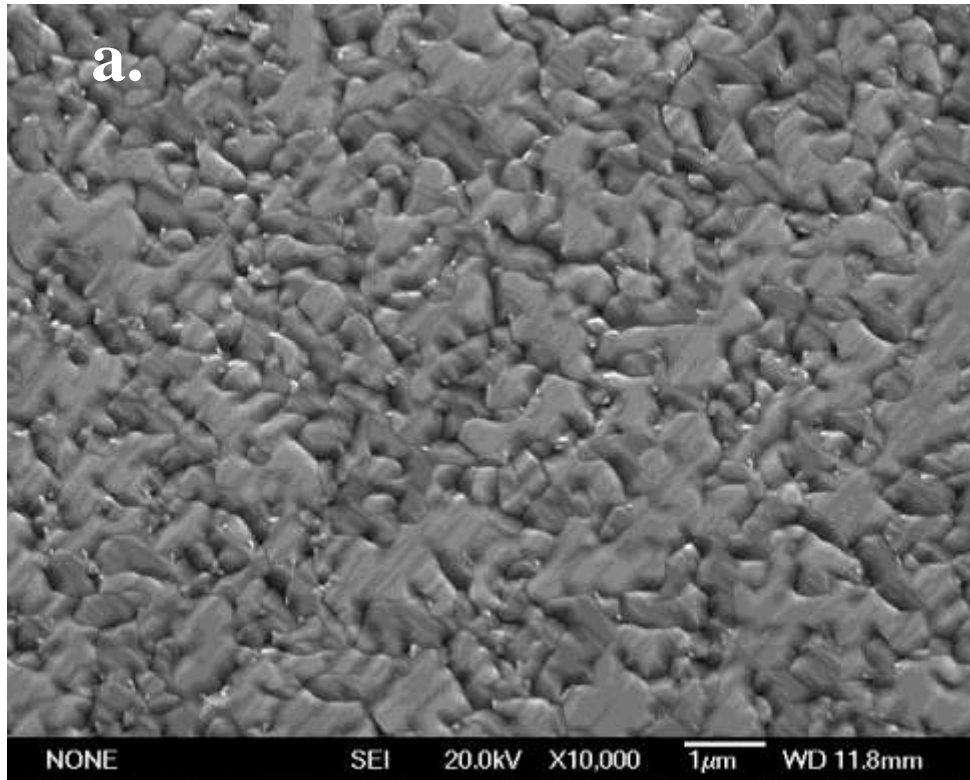
Fig.4.2.1.3 SEM images of PLD grown MgO(100) deposited by 5,000 laser shots under 750°C, 7.5mTorr oxygen pressure, marked as AZO-017

a) magnification of 10,000; b) magnification of 20,000.
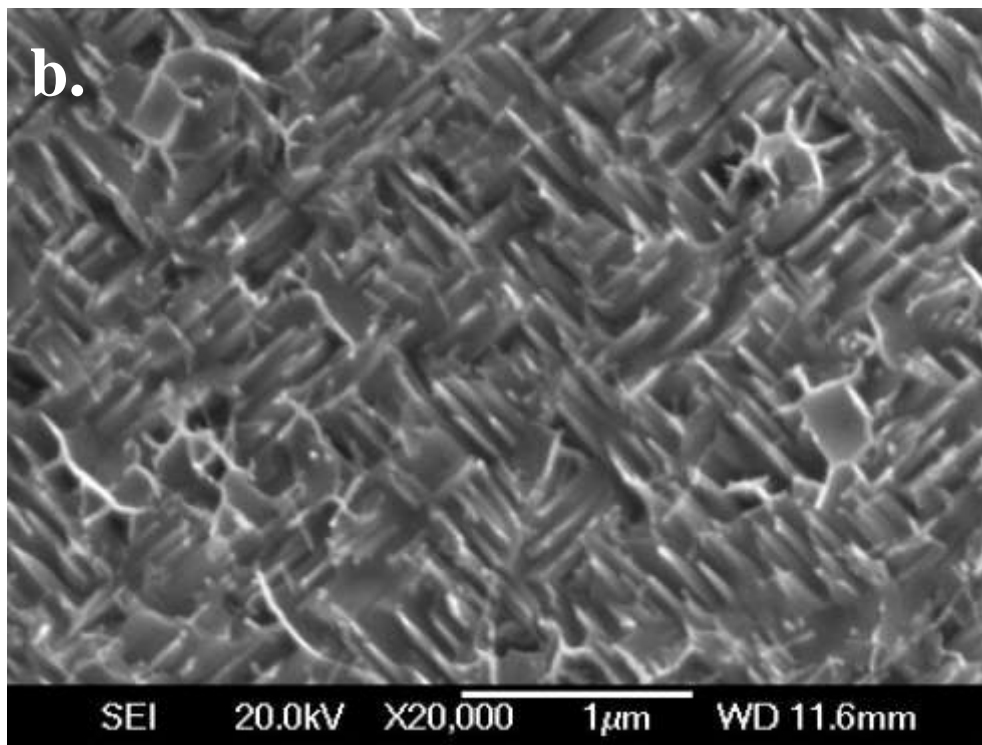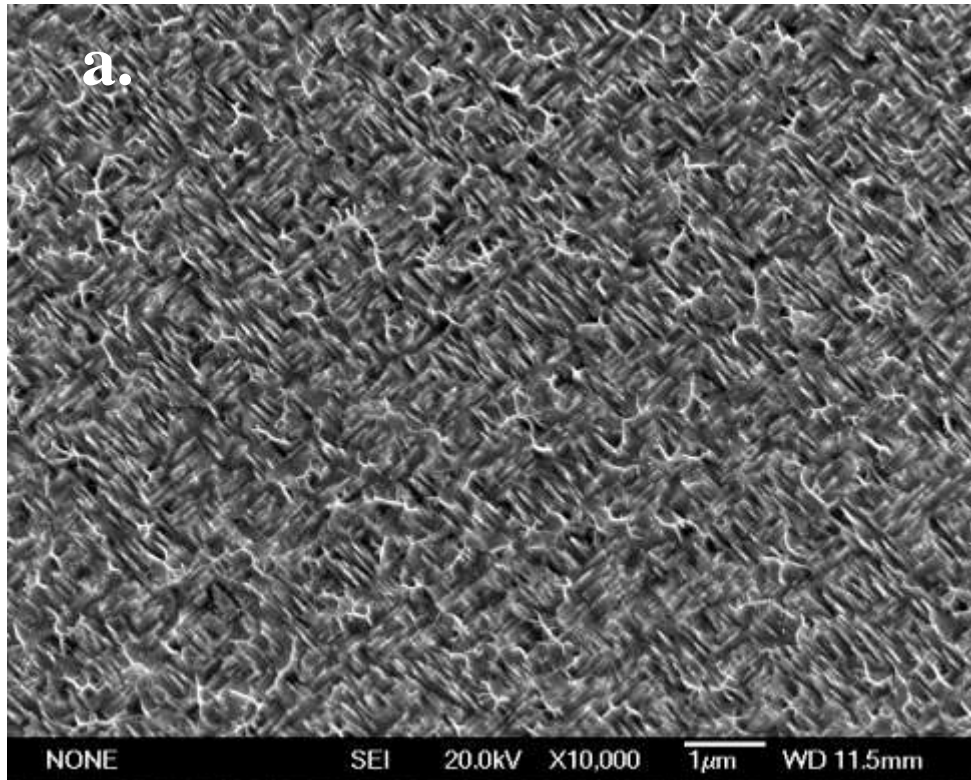
Fig.4.2.1.4 SEM images of PLD grown MgO(100) deposited by 5,000 laser shots under 750°C, 150mTorr oxygen pressure, marked as AZO-016

a) magnification of 10,000; b) magnification of 20,000.
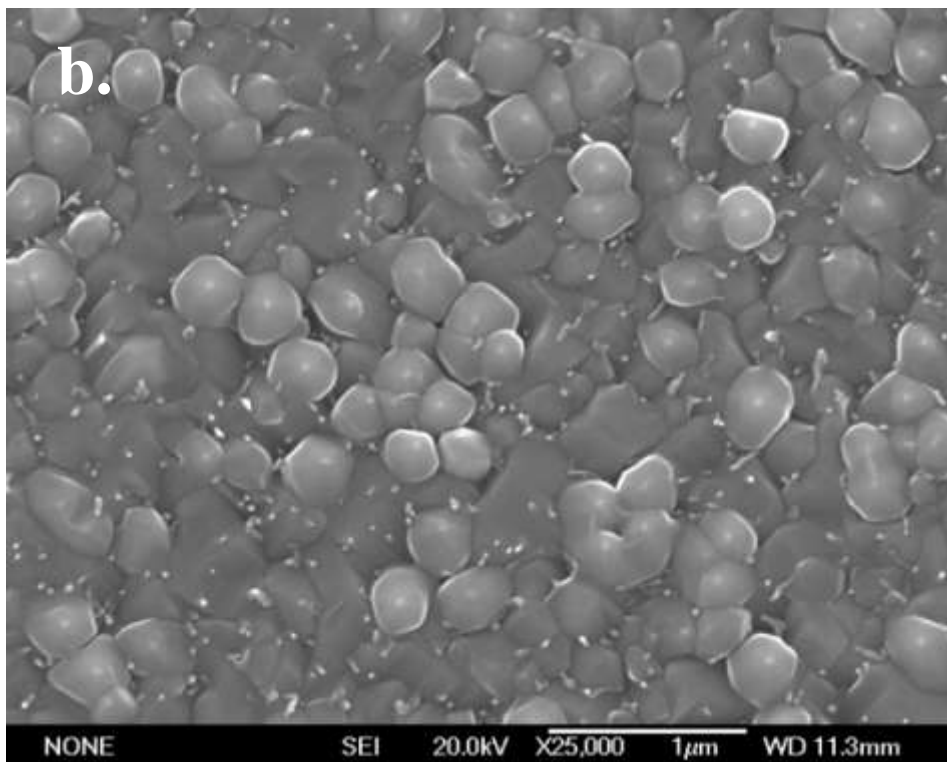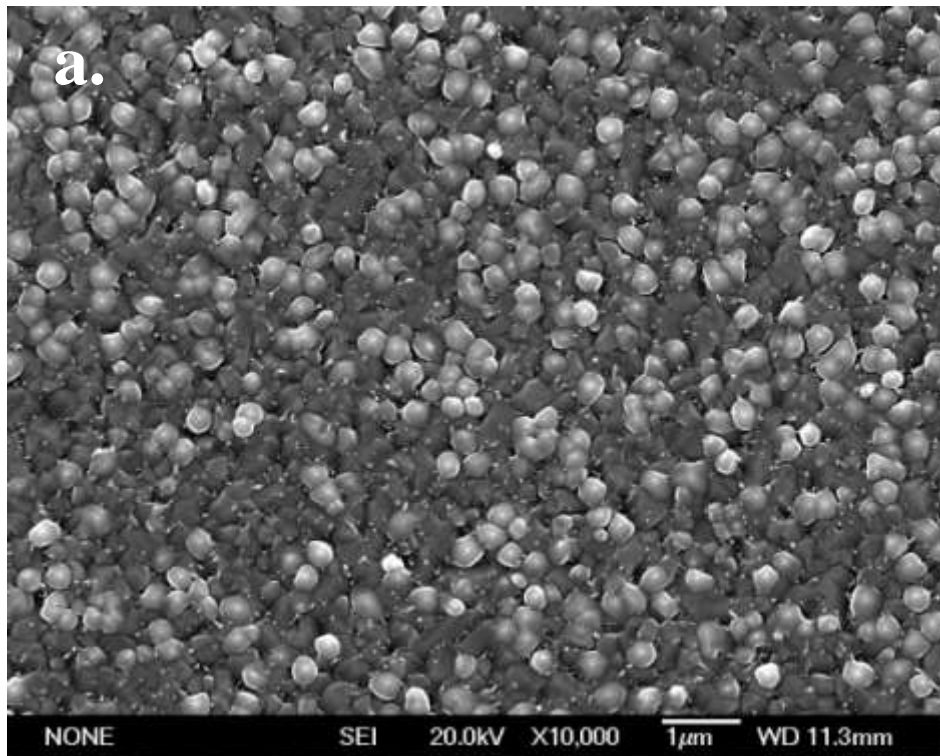
Fig.4.2.1.5 SEM images of PLD grown MgO(100) deposited by 5,000 laser shots under 750°C, 350mTorr oxygen pressure, marked as AZO-018

a) magnification of 10,000; b) magnification of 25,000.
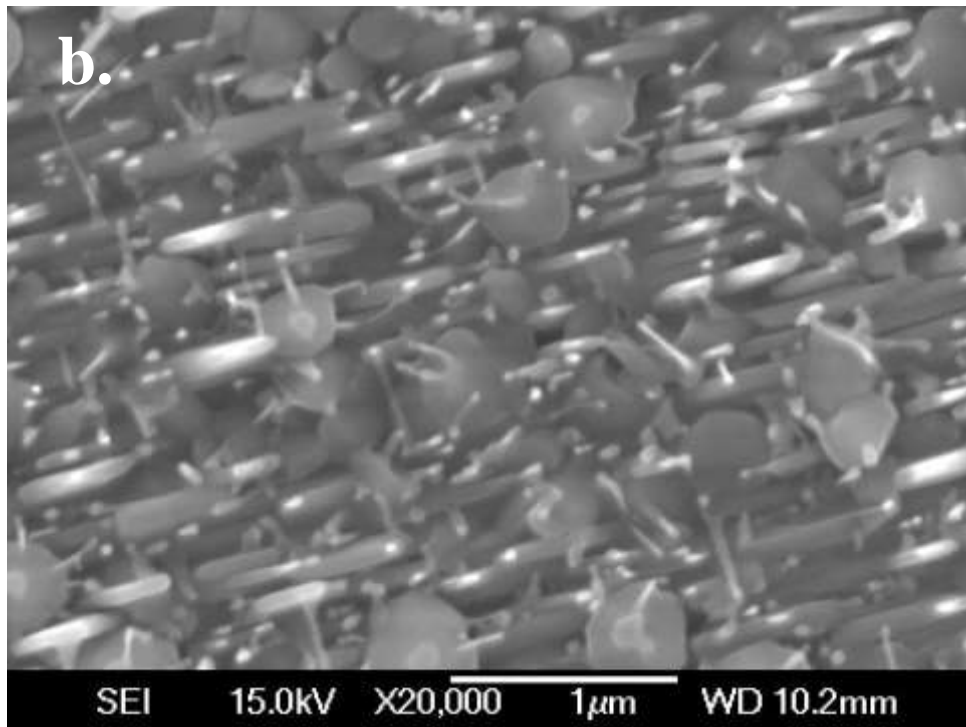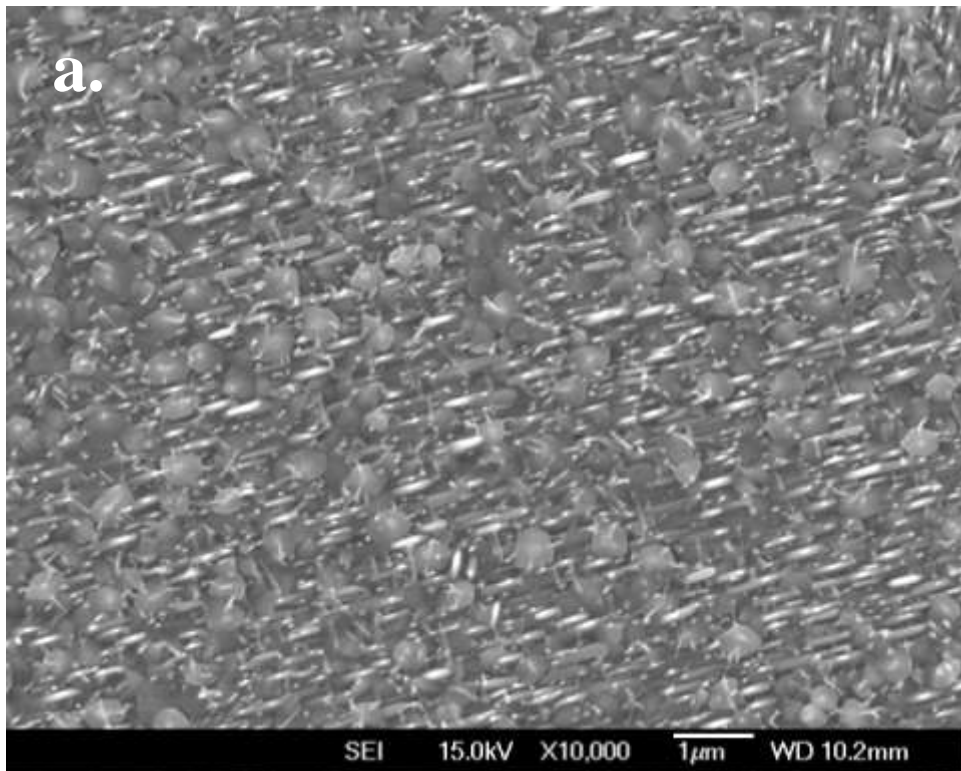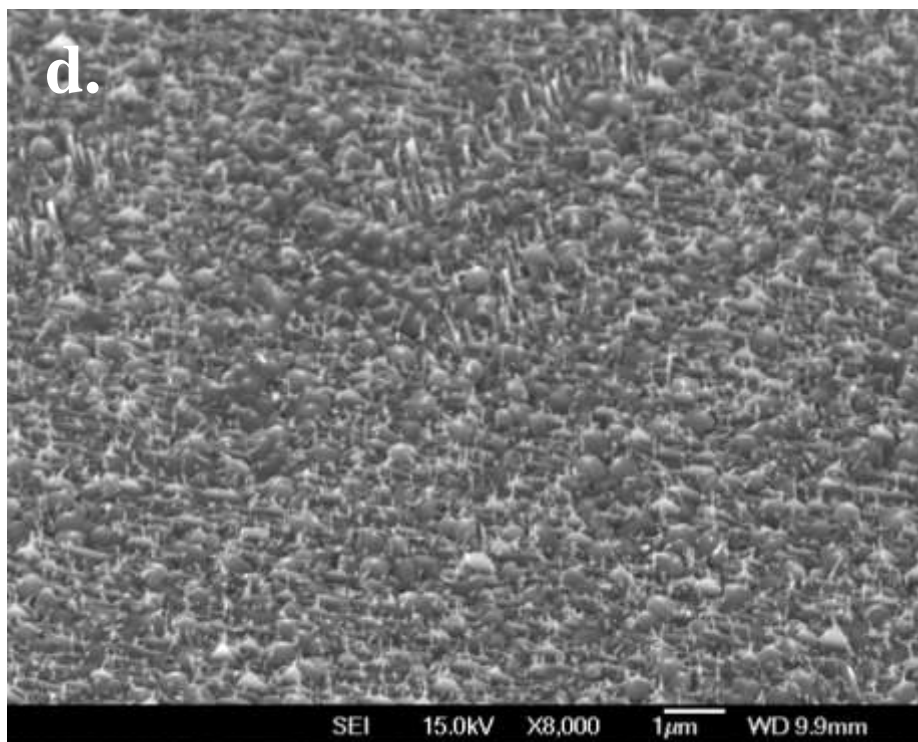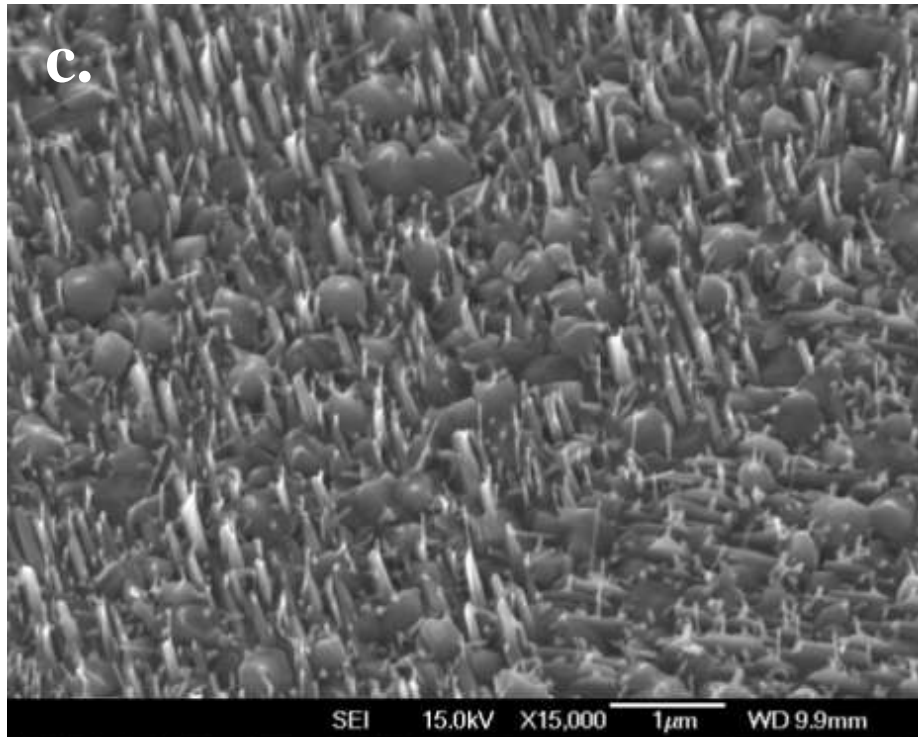
Fig.4.2.1.6 SEM images of PLD grown MgO(100) deposited by 5,000 laser shots under 750°C, 1200mTorr oxygen pressure, marked as AZO-015

a) magnification of 10,000; b) magnification of 20,000;
c) 45°tilt, magnification of 15,000; d) 45°tilt, magnification of 8000.

Reducing the temperature to 700°C, in chamber #3, samples AZO-024 and AZO-058 were produced in the oxygen pressure of 1200mTorr and 2000mTorr respectively. On sample AZO-024, shown in Fig.4.2.1.7, nanorods and nanoplates in various dimensions ranging from 60 to 280nm with five orientations can be found. It was observed that there were no significant changes, but the density of the nanorods, which are perpendicular to the surface, reduce in number towards the edge of the sample. If compared with morphology of the centre of AZO-024, the centre AZO-058's surface is mainly covered by perpendicular nanorods, with a wider dimension ranging from 210 to 420nm, as shown in Fig.4.2.1.8.a. The further away from the center of the sample, the density of perpendicular nanorods decrease and the presence of nanocones in different orientations are formed. Upon approaching the edge of the sample, all nanostructures, similar to the nanostructures observed in areas closer to the center of the sample, become much more rare and sparse. This unevenness may have be caused by the plume.

One of the well-known PLD limitations is that it can only produce a uniform deposition on a small substrate (10×10mm maximum, In this case 5×5mm samples were used). These samples are normally placed, in a small area, in the direct centre of the plume, where the energy level should be the highest. However, it was found that the plume affects the distribution of nanostructures on the sample, this influence will be discussed in the "influence of plasma plume" section, and locations with lower energy levels may be better suited for production of nanowires and nanorods. Therefore, substrates, used in these depositions, were placed in an area, on the heater, that would not be at the direct centre of the plume during the deposition. As it is known the higher pressure would result the smaller size of the plume. This would result in a higher chance for an uneven deposition. For sample AZO-058, the environment pressure was set as high as 2Torr, so the varied structure distribution may have been caused from the smaller sized plume.
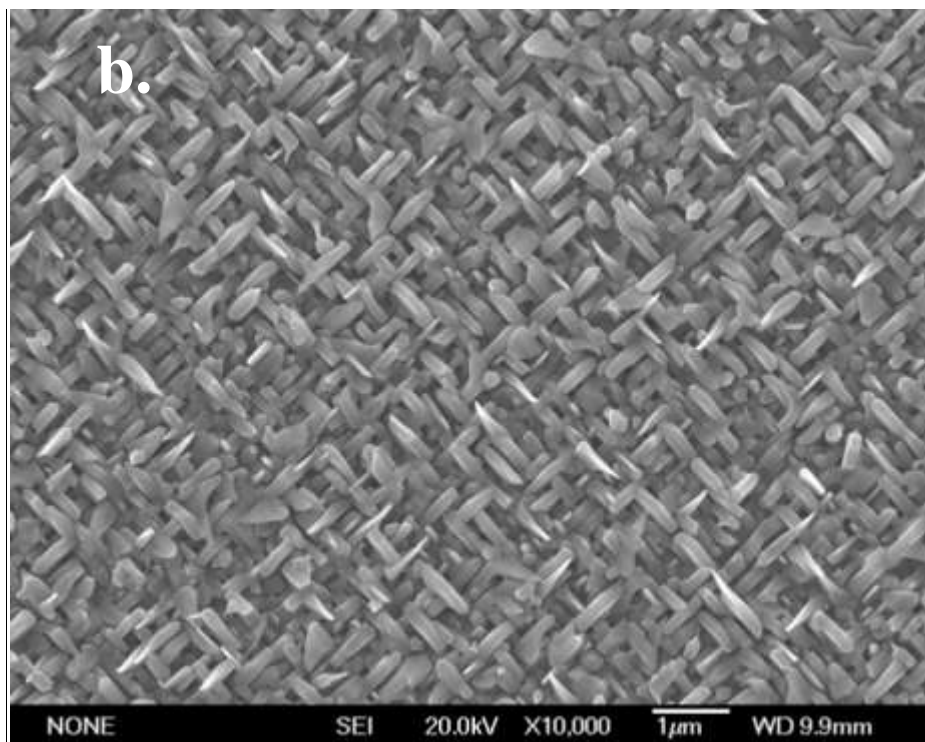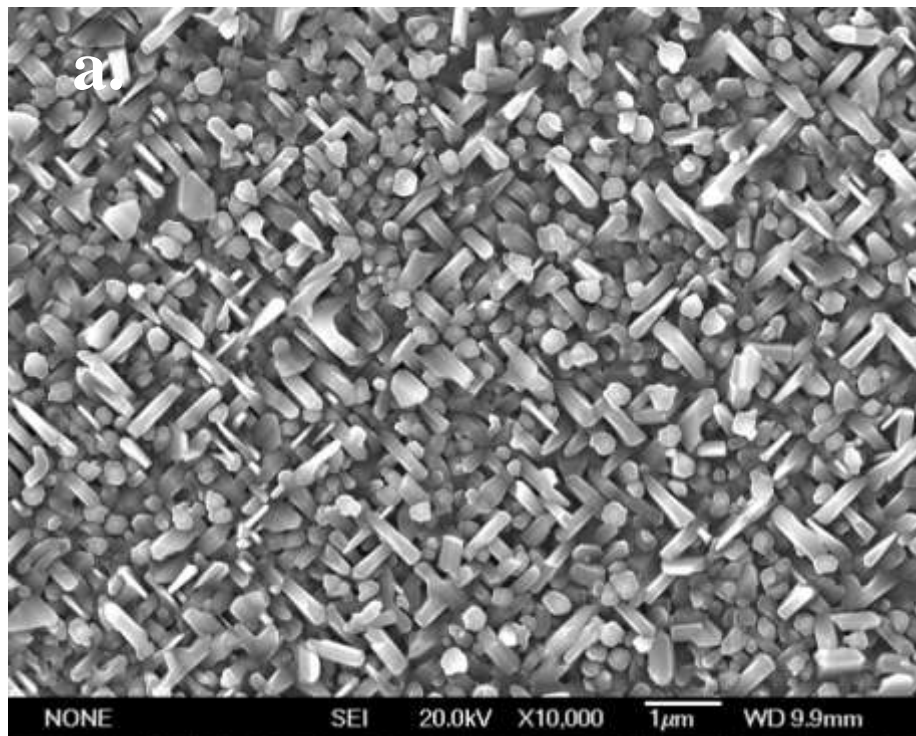
Fig. 4.2.1.7 SEM images of PLD grown MgO(100) deposited by 5,000 laser shots under 700°C, 1200mTorr oxygen pressure, marked as AZO-024

a) centre of the sample, magnification of 10,000;
b) area close to the edge, magnification of 10,000.
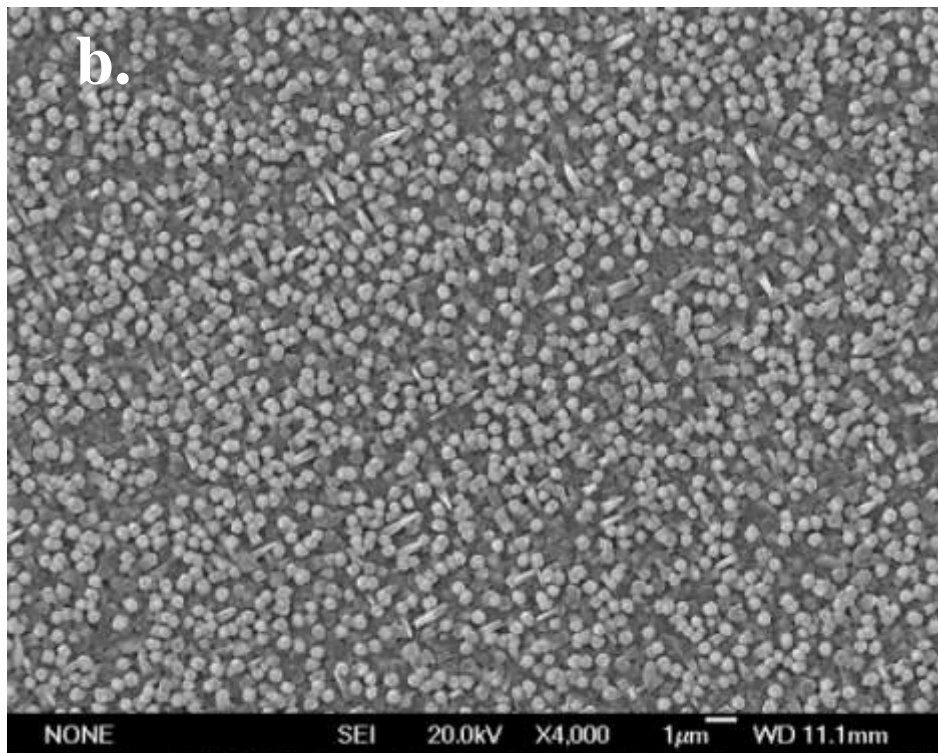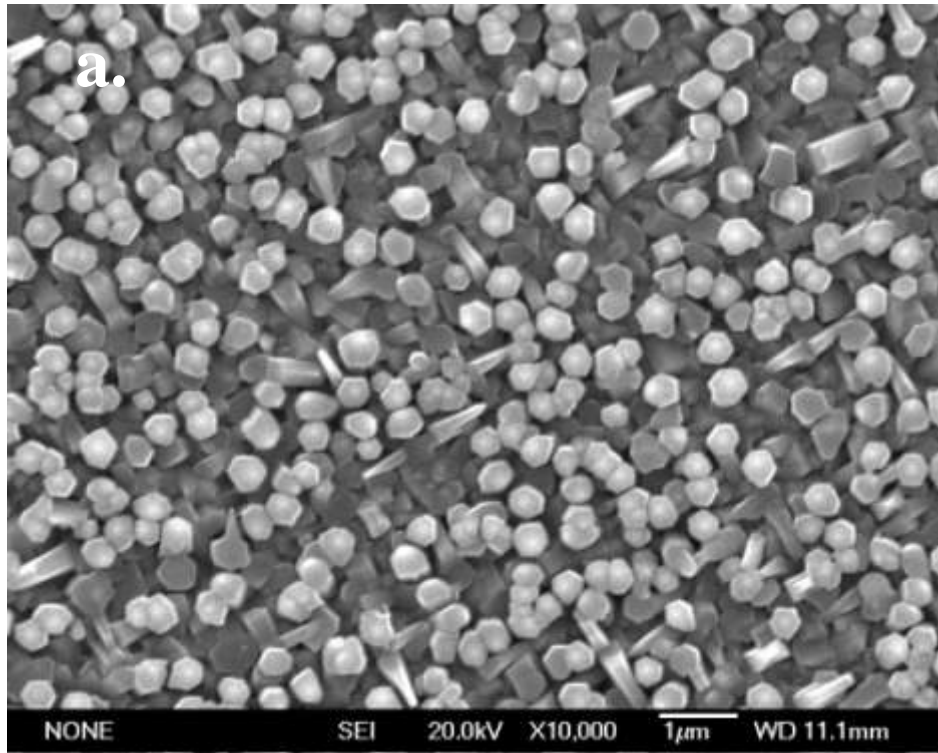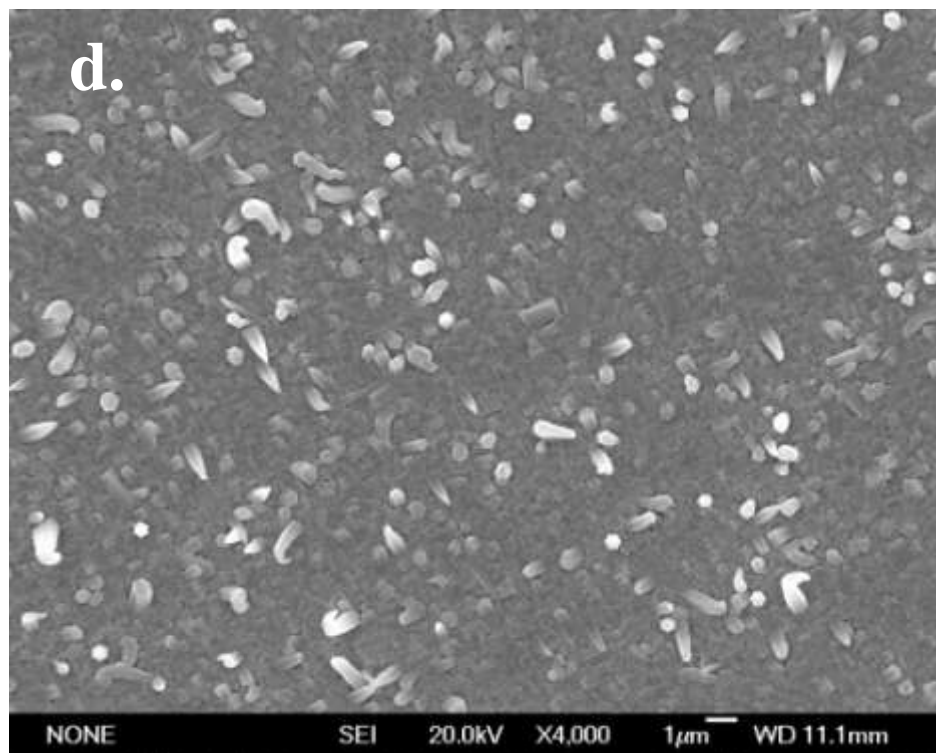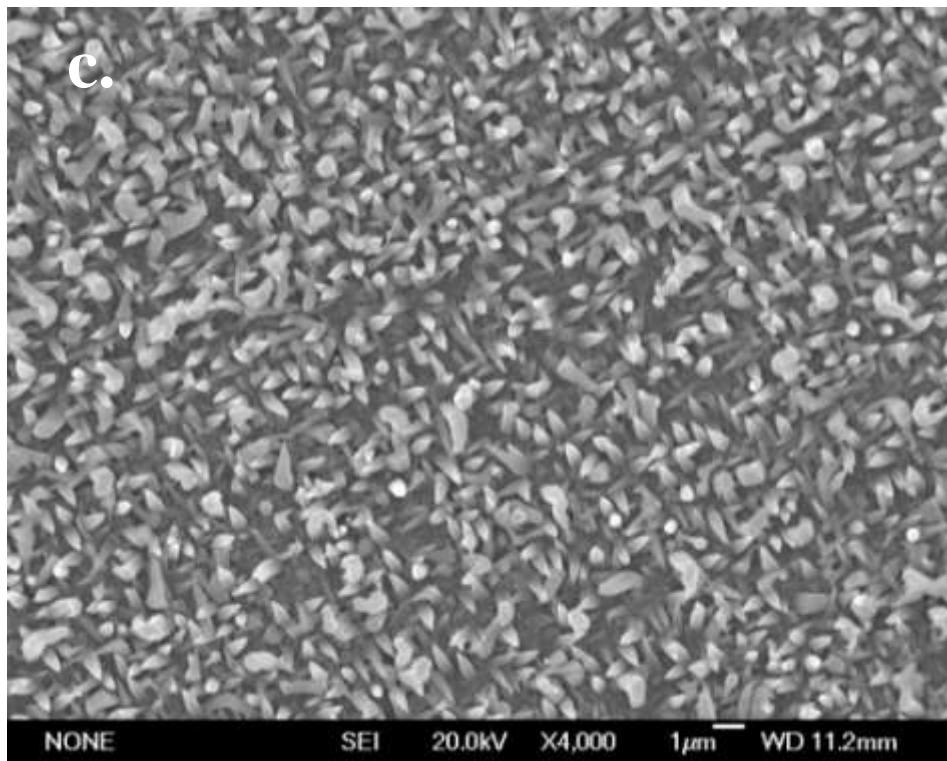
Fig. 4.2.1.8 SEM images of PLD grown MgO (100) deposited by 5,000 laser shots under 700°C, 2000mTorr oxygen pressure, marked as AZO-058

a) centre of the sample, magnification of 10,000; b) centre of the sample, magnification of 4000; c) area close to the edge of the sample, magnification of 4000; d) area closer to the edge of the sample, magnification of 4000.

Comparing these four groups of samples, as the growth temperature decreases, the difference between each sample, in the same temperature group, becomes more tremendous. This indicates that in lower temperature ranges, oxygen pressure can be significant influence during the deposition.

According to the theory of how ambient gas pressure influences the particulates in book [3], diffusion is the deposition growth mechanism and the size of the particulate is controlled by the residence time. Introducing ambient gas into the PLD system during the deposition would result in increasing the residence time, hence it would increase the size of the particulate. This may explain why the surface becomes progressively rougher as the oxygen pressure increases. This is especially true for sample AZO-018 in Fig.4.2.1.5 and AZO-015 in Fig.4.2.1.6. Larger granular crystals can be found on the surface and the average size increases when increasing the oxygen pressure. As for the samples produced in lower oxygen pressure, the size of the particulates will be smaller as well as the size distribution would be narrower. This results in a smoother surface.

It is also found that in higher oxygen pressure, the deposition tends to make an 1-dimensional growth mode (nanowires or nanorods), rather than 2-dimentional growth (thin film). As there are more oxygen molecules in the high oxygen pressure chamber, the chance of collisions in the plume increases. This may reduce the energy of the particles before residence. Lower energy may be the main reason for the formation of nanorods and nanowires.

It was observed that in higher temperatures, the uniformity and distribution of nanostructures was not influenced by the oxygen pressure. However, in low temperatures, the oxygen pressure directly affects the uniformity and distribution of nanostructures. As the oxygen pressure increases, the surface becomes more uneven. In the instance of very high

oxygen pressure, the energy of single particles may be reduced as well as gas flows within the chamber during the deposition. This is due to the matter that the apparatus that was used, in this project, was designed for low ambient gas pressure. When set at higher pressures, it may cause "blowing" of the plume and could be the reason for the unevenness of the surface in very high oxygen pressures.

In conclusion, regardless of the temperature value, higher oxygen pressure directly affects the growth of various nanostructures, such as nanoplates, nanowires and nanorods. However, in terms of evenness of the samples, at higher temperatures, regardless of the value of the oxygen pressure, the sample produced will always have more uniform structures and morphology. Therefore, by reducing the temperature and increasing the oxygen pressure, the surface becomes more uneven with different structures and morphologies at various areas within the sample.

4.2.2 Influence of number of pulses on ZnO target

Thin film growth can be expressed as Thickness = Deposition Rate $\times$ Deposition Time. The thickness is directly proportional by the deposition rate and time. At specific distances between the target and substrate, the increase of the number of depositing pulses can increase the thickness of the film by extending the time of the deposition. By investigating the influence of the number of depositing pulses, it can be an effective way on understanding how nanostructures are formed and grown. Two groups of samples, which are taken into consideration, are listed in Table 4.2.5 and 4.2.6. In each group, each sample was subjected to a different number of pulses in order to observe the changes in morphology. The energy density was at 1J/cm^2.

Table 4.2.5 Detailed parameters of the samples AZO-010,009 and 007

Sample Number	Temperature (˚C)	Chamber number	Number of pulses on Au target (shots)	Substrate	Distance of Target to Substrate	**Number of pulses on ZnO target (shots)**	Oxygen Pressure (mTorr)
AZO-010	800	#1	5	MgO(100)	55	**2000**	1200
AZO-009	800	#1	5	MgO(100)	55	**5000**	1200
AZO-007	800	#1	5	MgO(100)	55	**10000**	1200

Table 4.2.6 Detailed parameters of the samples AZO-210812-1, 160812-1, 210812-2 and 160812-2

Sample Number	Temperature (˚C)	Chamber number	Number of pulses on Au target (shots)	Substrate	Distance of Target to Substrate	**Number of pulses on ZnO target (shots)**	Oxygen Pressure (mTorr)
AZO-210812-1	600	#2	5	MgO(100)	40	**2000**	1200
AZO-160812-1	600	#2	5	MgO(100)	40	**5000**	1200
AZO-210812-2	600	#2	5	MgO(001)	40	**2000**	1200
AZO-160812-2	600	#2	5	MgO(001)	40	**5000**	1200

When the producing temperature was set to 800°C, in which there were no identifiable nanostructures, it was observed that the deposition growth tends to be a Volmer-Weber (island formation) nucleation and growth mode. As the number of pulses fired on the ZnO target increase, the surface of the sample starts off rough, but eventually becomes smoother as the grains grow larger. This comparison can be seen from AZO-010, with 2000 pulses being fired at the target, AZO-009, with 5000 pulses and AZO-007, with 10,000 pulses, in Fig.4.2.2.1. In AZO-010, the grains have begun to form. By increasing the number

of pulses to 5000, the surface becomes more rough and overlapping pattern forms. However, in AZO-007, the grains are much larger and the surface appears to be more even and uniform.

Upon further observation of AZO-007, the deposition has an average thickness of 1.313 µm and the grains have grown to be more like column shaped but not separate with each other. This can be seen in the cross section of AZO-007 in Fig.4.2.2.2, which shows a typical crystallized structure.

SEI   15.0kV   X10,000   1μm   WD 10.4mm

SEI   15.0kV   X10,000   1μm   WD 10.2mm
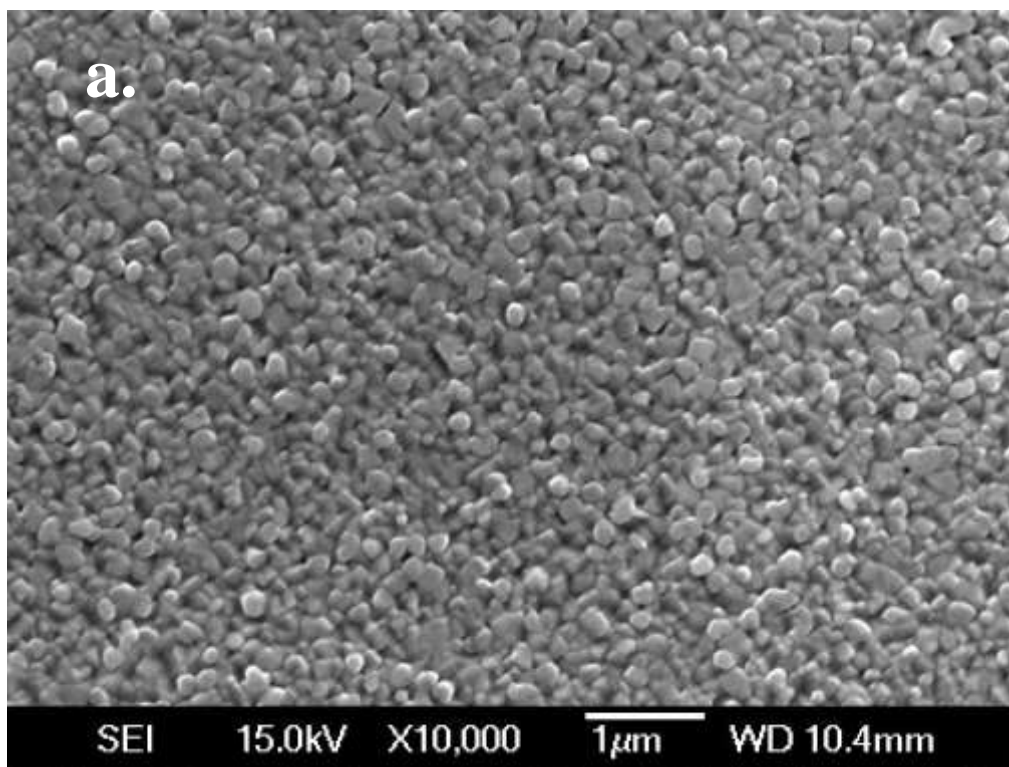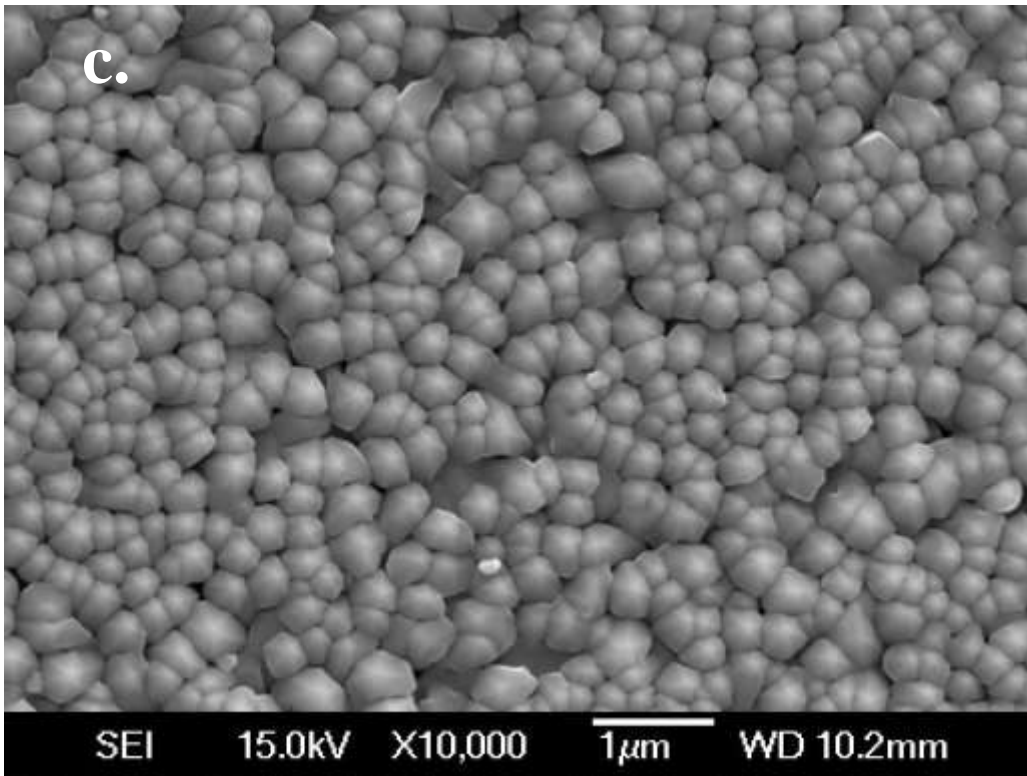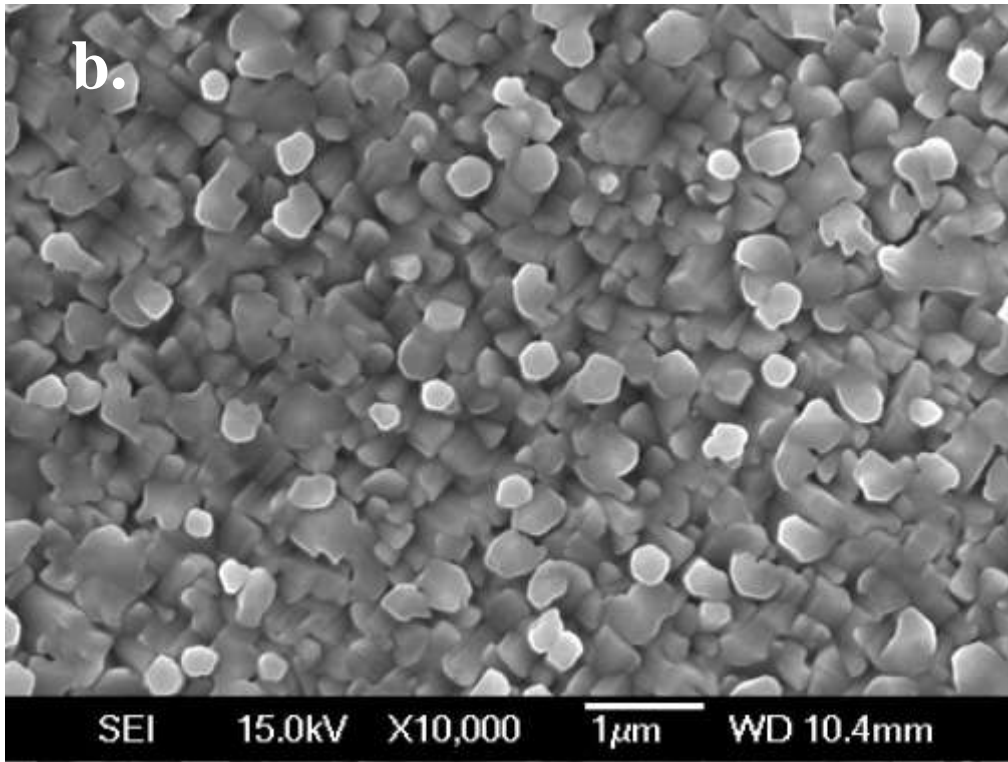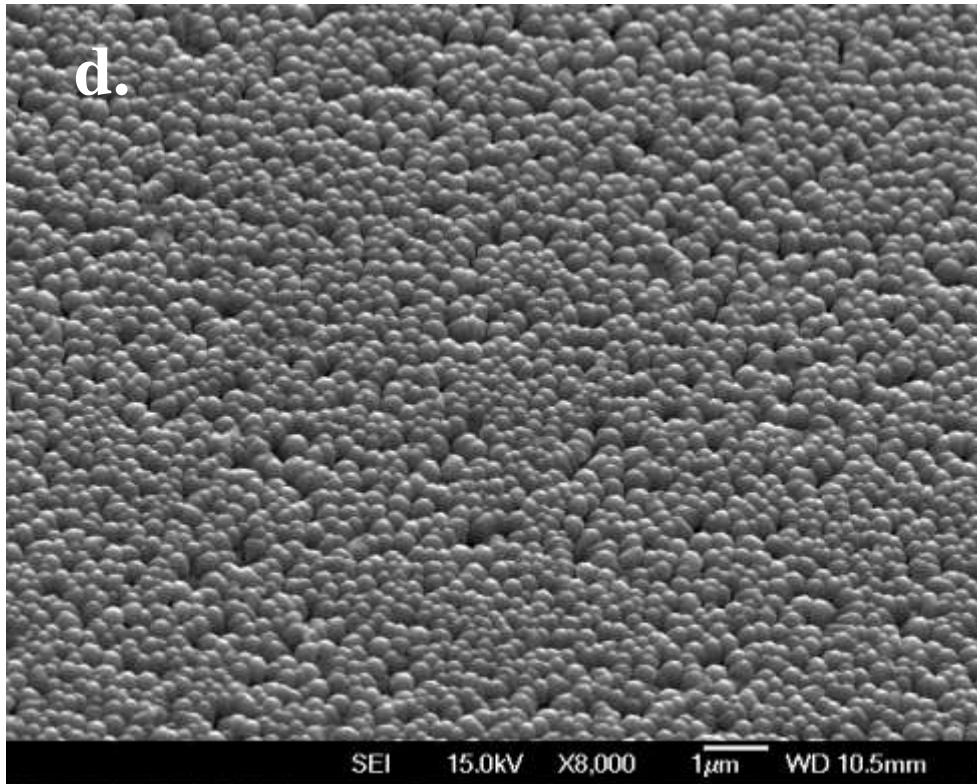
Fig. 4.2.2.1 SEM images of PLD grown on MgO(100) deposited under 800°C
a) AZO-010, with 2000 pulses, magnification of 10,000;
b) AZO-009, with 5000 pulses, magnification of 10,000;
c) AZO-007, with 10,000 pulses, magnification of 10,000;
d) AZO-007, 30°tilt, magnification of 8000.
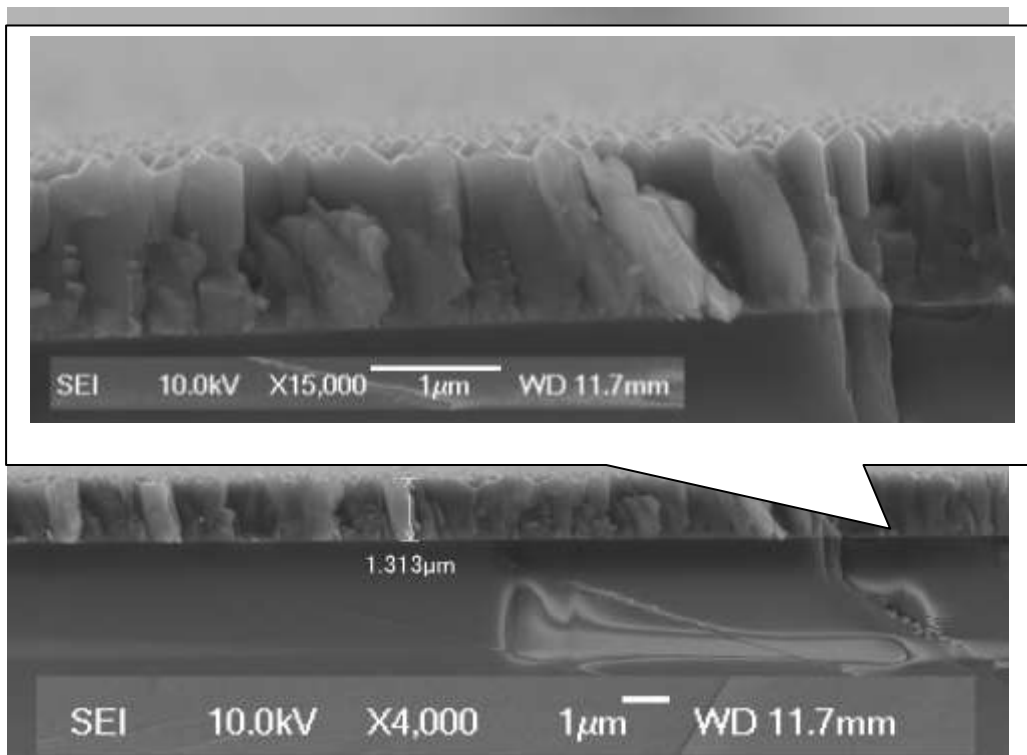
Fig. 4.2.2.2 SEM images of cross-section structure of AZO-007 magnification of 4000 and 15,000.

Decreasing the temperature to 600°C in chamber #2, 2000 and 5000 pulses of ZnO were deposited on the substrates MgO(100) and MgO(001) respectively. It was observed that there wasn't any significant difference on the samples made by 2000 pulses on two different substrates, as shown in Fig.4.2.2.3, and Fig.4.2.2.5. From the detailed image shown in Fig.4.2.2.5.c, on the solid base, nucleation starts, indicating that the growth mode tends to be the Stranski-Krastanov mode. This mode is a growth mode combining the Frank-van der Merwe mode (2-dimensional growth mode) and the Volmer-Weber mode (Island growth mode). In Fig.4.2.2.4 and Fig. 4.2.2.6, the densities of the nanostructures on both samples are similar with the perpendicular length varying from 1μm to 2.5μm. The difference between the two samples is that there are more nanowires growing parallel to the substrate on MgO(001) than on MgO(100). Since MgO(100) substrates have identical crystallography to MgO(001), this difference should be related to different manufacturers, or growth and surface finishing techniques.

In the literature [3], if the growth mode is considered to be layer-by-layer growth, it can be expressed by Bauer and Van der Merwe's simplified form, assuming there is equilibrium between the film components in the gas phase and the components of the substrate.

$$\Delta\gamma = \gamma_A + \gamma_i - \gamma_B \leq 0$$

In this representation, γ_A is the surface free energy of film components, γ_B represents the substrate surface free energy, and γ_i is the interfacial free energy. Since the temperature for producing the samples of first group is higher, the γ_B is smaller than the second group. Therefore, the first group of samples tends to grow in the Volmer-Weber (3D island) mode, while the second group, the deposition tends to have the Frank-van der Merwe (layer-by-

layer) growth mode until it reaches the thickness where $\gamma_A + \gamma_i$ exceeds γ_B. The growth mode then transforms to Stranski-Krastanov mode, resulting in 3D nucleation on a 2D coating.
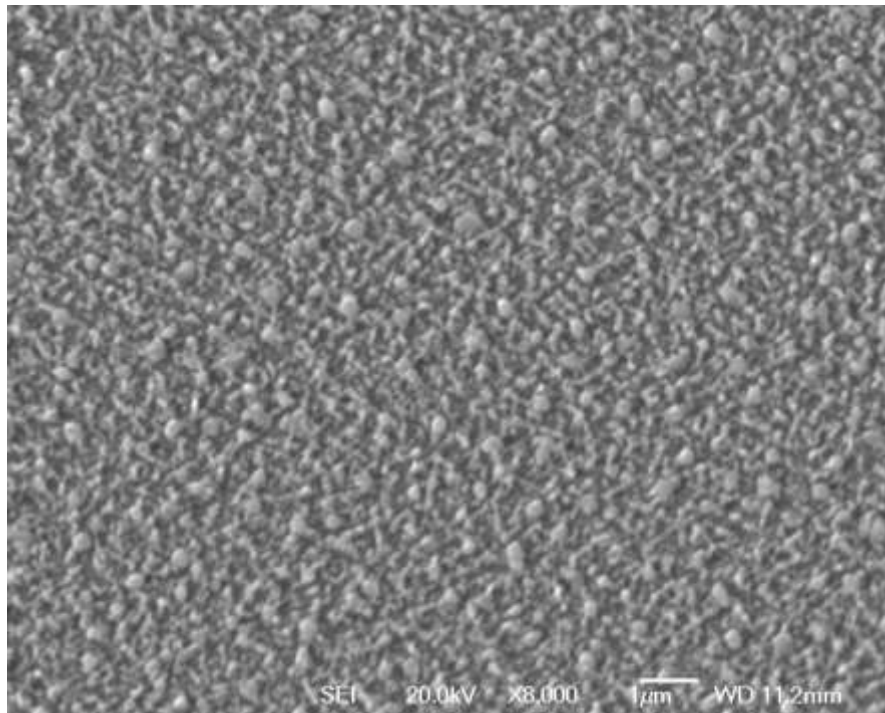
Fig. 4.2.2.3 SEM image of PLD grown on MgO(100) deposited under 600°C, AZO-210812-1, with 2000 pulses, magnification of 8000
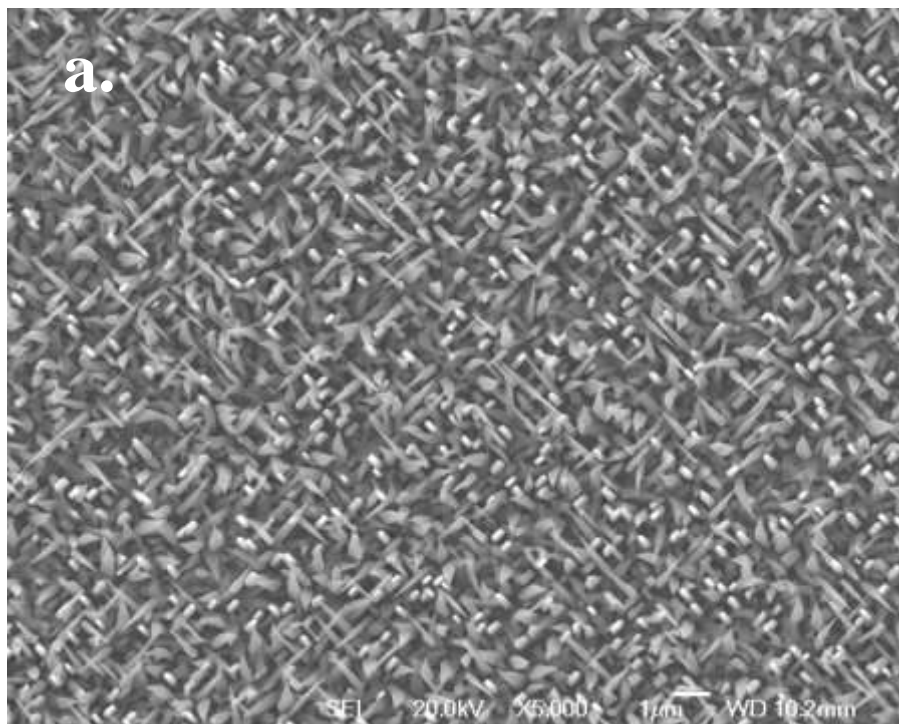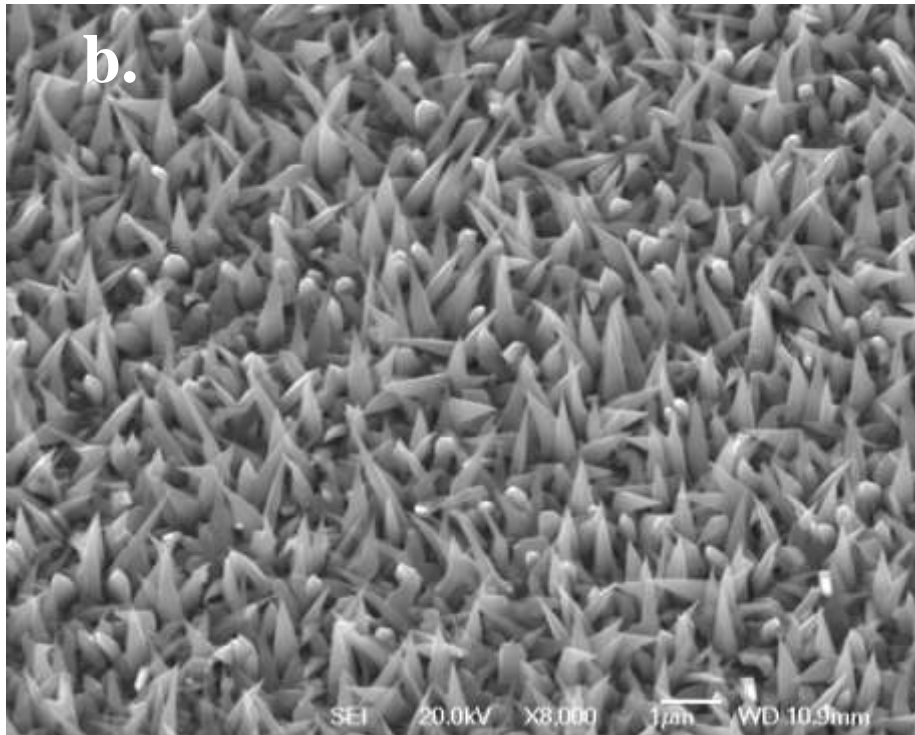
Fig. 4.2.2.4 SEM images of PLD grown on MgO(100) deposited under 600°C, AZO-160812-1, with 5000 pulses,

a) top view, magnification of 5000; b) 30° tilt, magnification of 8000.
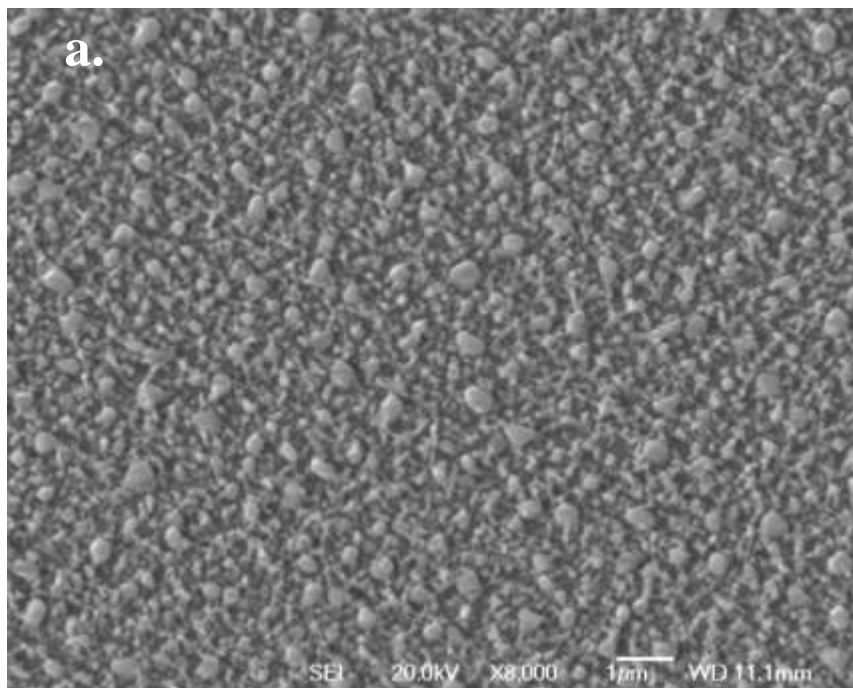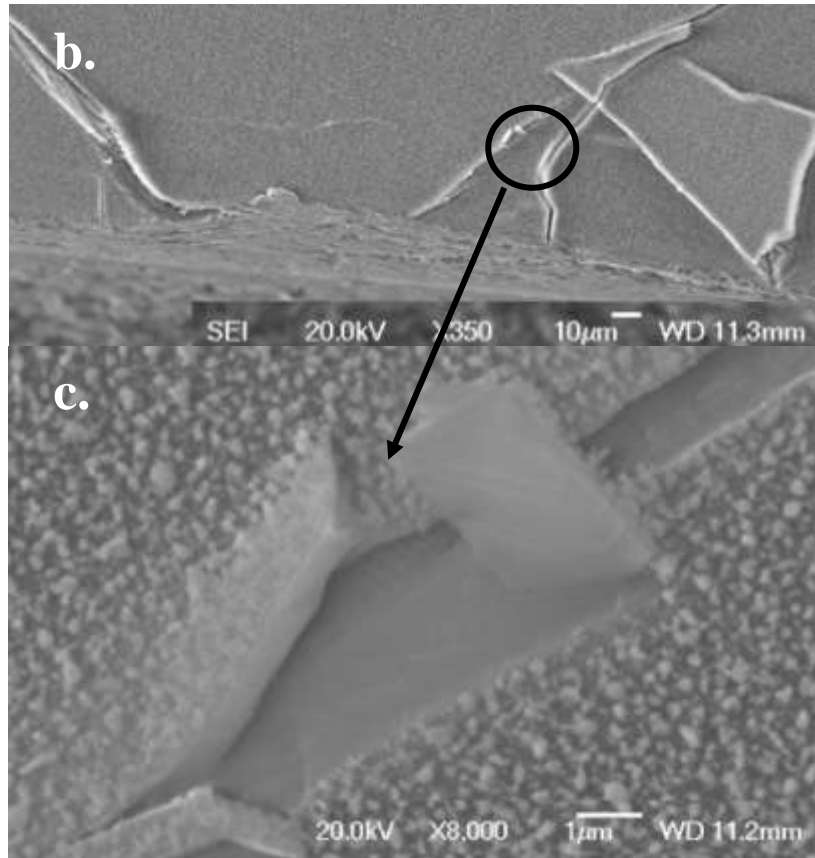
Fig. 4.2.2.5 SEM images of PLD grown on MgO(001) deposited under 600°C, AZO-210812-2, with 2000 pulses, a) top view, magnification of 8000; b)30° tilt, magnification of 350; c)detail image, magnification of 8000.
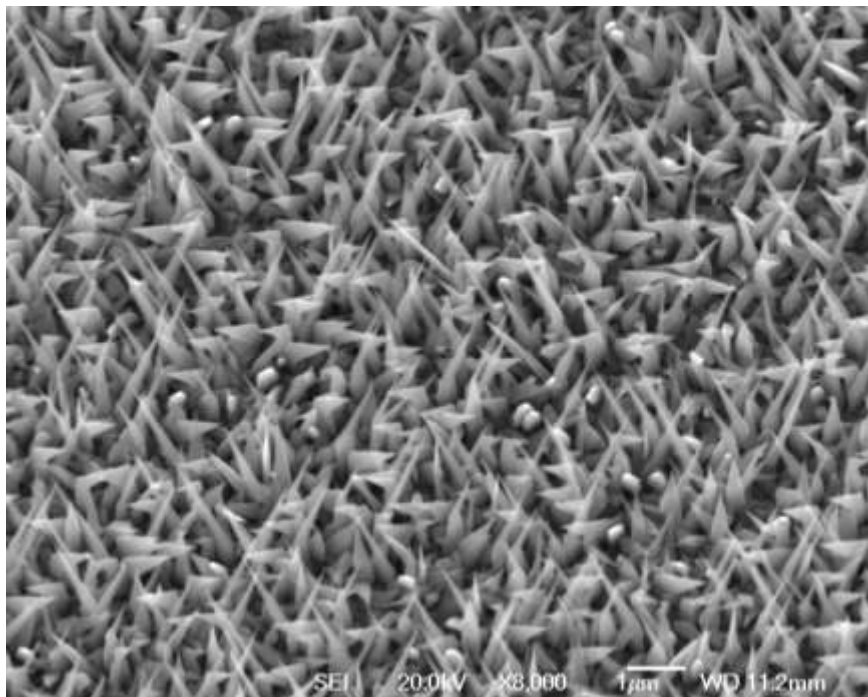
Fig. 4.2.2.6 SEM image of PLD grown on MgO(001) deposited under 600°C,AZO-160812-2, with 5000 pulses, magnification of 8000.

In conclusion, by studying the influence of the number of pulses used on ZnO helps to determine growth modes. For higher temperatures, it tends to be the Volmer-Weber (3D island) growth mode and for lower temperatures, the growth tends to be the Stranski-Krastanov growth mode. 5000 pulses on a ZnO target was used for the remainder of this thesis.

4.2.3 Influence of pulses on gold targets

In the previous section, it was found that gold acts as catalyst of MgO nanorods and nanowires, where MgO nanorods and nanowires only were grown on the area coated by gold nanodots and increasing the pulses on gold targets increased the average diameter of MgO nanorods or nanowires. As in the ZnO case, in chamber #3, sample AZO-023, AZO-024 and AZO-025 were made by being deposited 0, 5, 20 shots on the gold target and followed by depositing 5000 pulses on ZnO target. The parameters are shown below, in Table 4.2.7. The energy density was set at 1 J/cm^2.

Table 4.2.7 Detailed parameters of the samples AZO-023, 024 and 025

Sample Number	Chamber	Substrate	Temperature (°C)	**Au pulses**	ZnO pulses	Oxygen Pressure (mBar)	Distance of Target-Substrate (mm)
AZO-023	#3	MgO(100)	700	**0**	5k	1.6	55
AZO-024	#3	MgO(100)	700	**5**	5k	1.6	55
AZO-025	#3	MgO(100)	700	**20**	5k	1.6	55

Without the gold nanodot coating, sample AZO-023, in Fig.4.2.3.1 shows a typical ZnO thin film morphology, which is a smoother surface with crystallized granular objects on the surface, when compared with the other two samples. By increasing the gold coating from 5 shots to 20 shots, the samples AZO-024 and AZO-025 are grown in five main directions

marked by the yellow arrows, shown in the top view image of Fig.4.2.3.2a and Fig.4.2.3.3a. The dimensions and lengths of the nanorods on sample AZO-024 (thickness ranging from 15nm to 230nm and length ranging from 500nm to 1μm) are not as even as the dimensions of those nanorods found on sample AZO-025 (thickness ranging from 50nm to 170nm and length ranging from 800nm to 1μm). Therefore, the number of gold shots directly affects the morphology of the nanorods being grown. As shown in Fig.4.1.3.1 and Fig.4.1.3.2, as more of the substrate becomes covered by the gold coating and the average size of the gold nanodots increase, it results in narrowing the distribution of size and length of the ZnO nanorods. Where as in the case of MgO nanorods/nanowire growth, discussed the previous section, the width of nanowires is related to the size of gold nanodots formed on the substrate. This was due to the substrate also being MgO which is homoepitaxial growth.
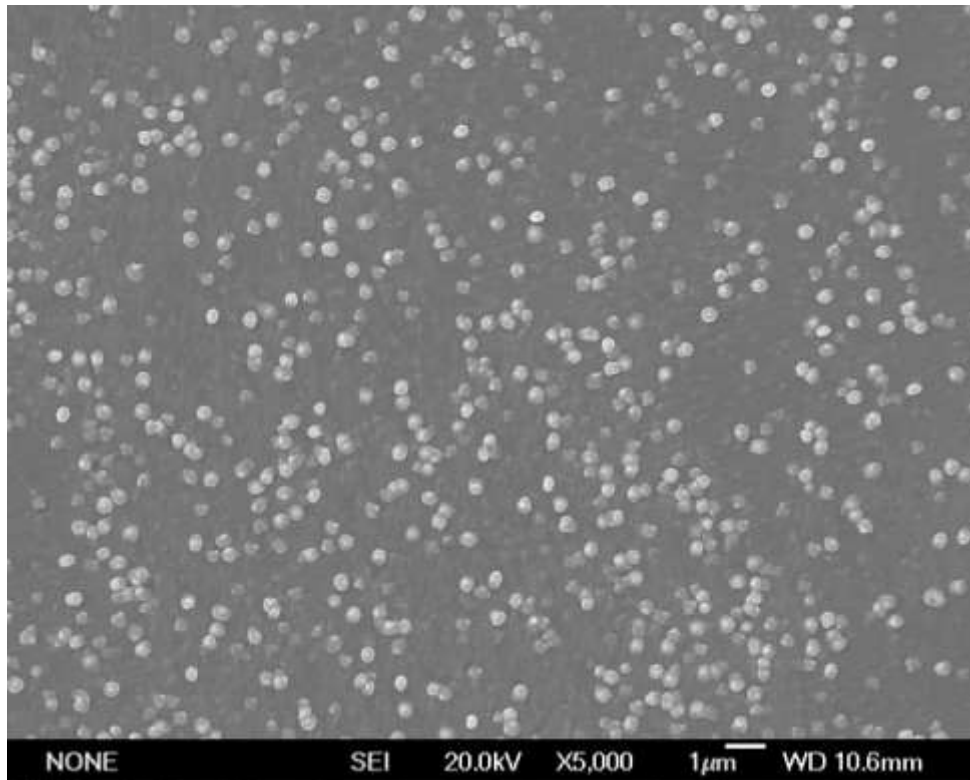
Fig.4.2.3.1 SEM image of AZO-023, without gold shots, with 5000 pulses of ZnO, top view, magnification of 5000.
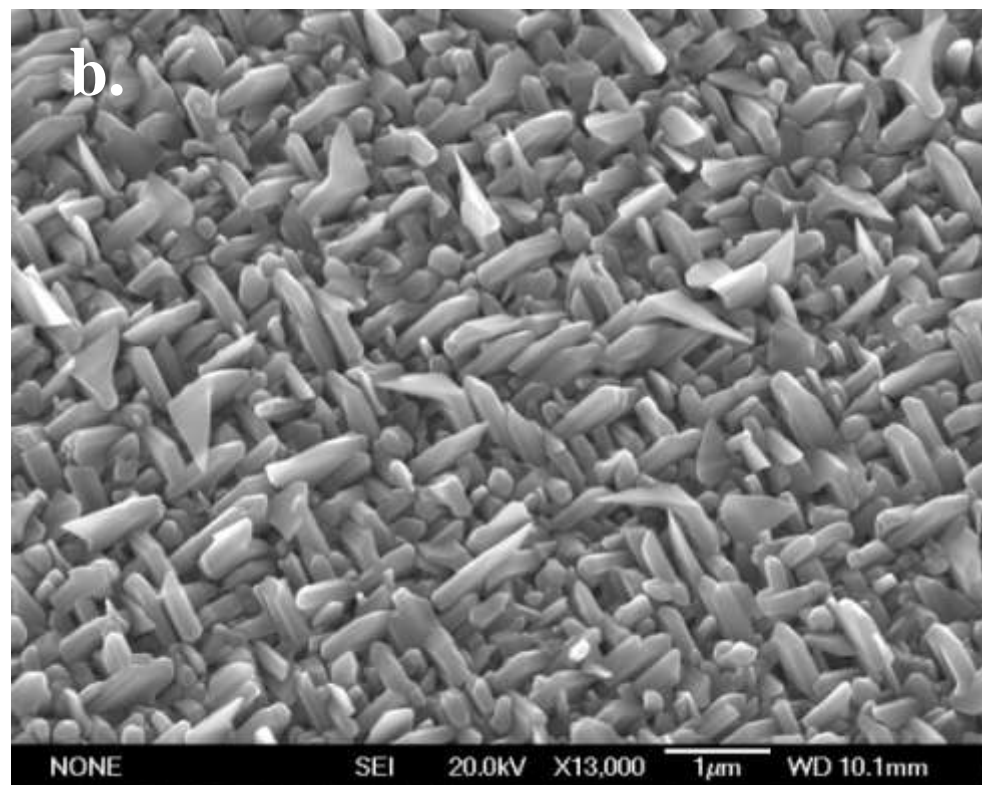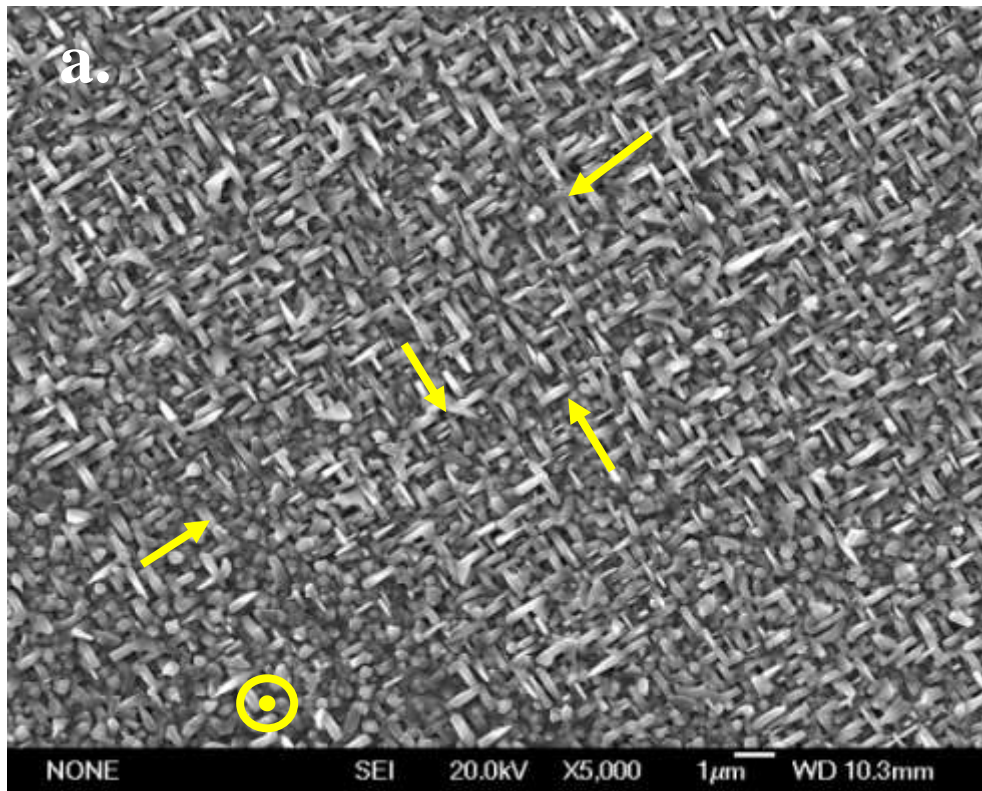
Fig.4.2.3.2 SEM images of AZO-024, with 5 shots on gold and 5000 pulses of ZnO, a) top view, magnification of 5000; b) 30° tilt, magnification of 13,000
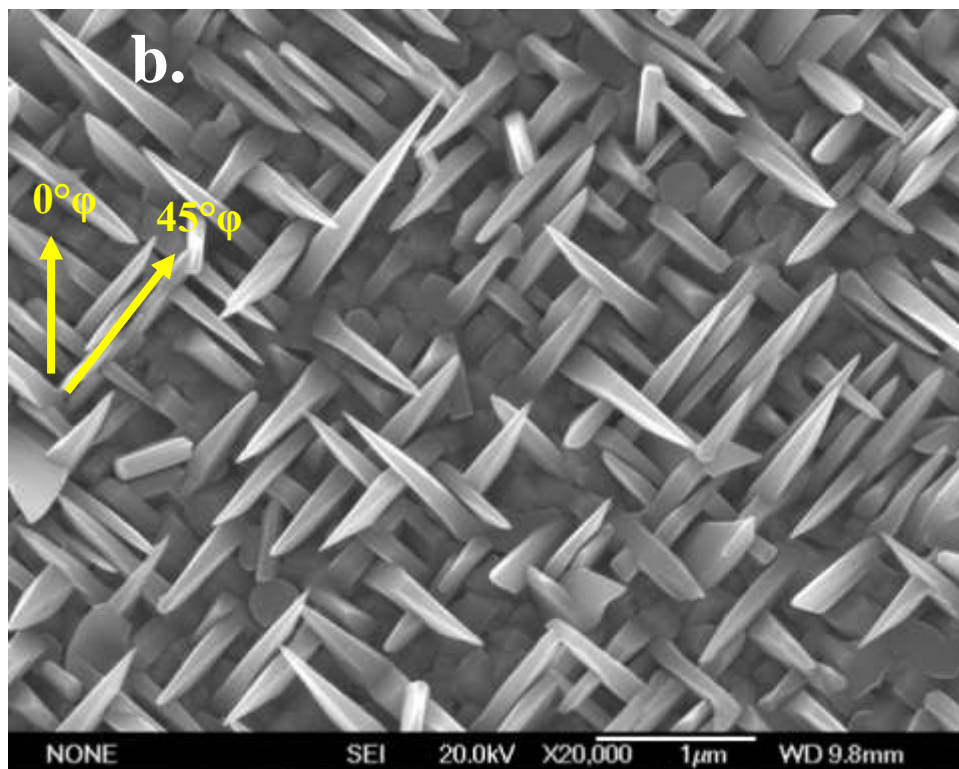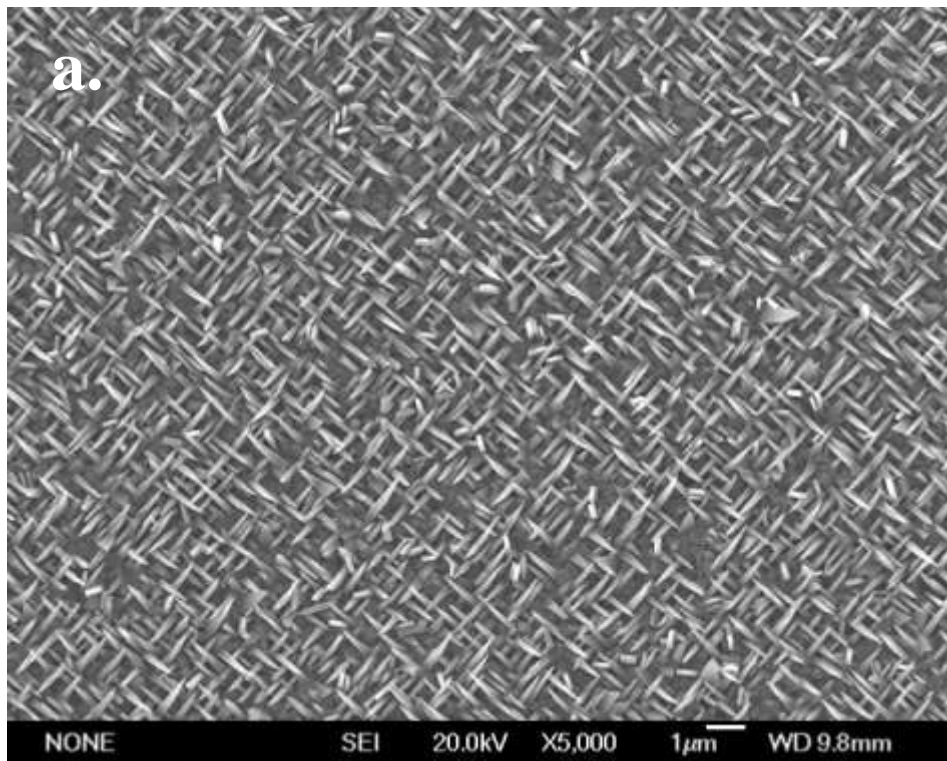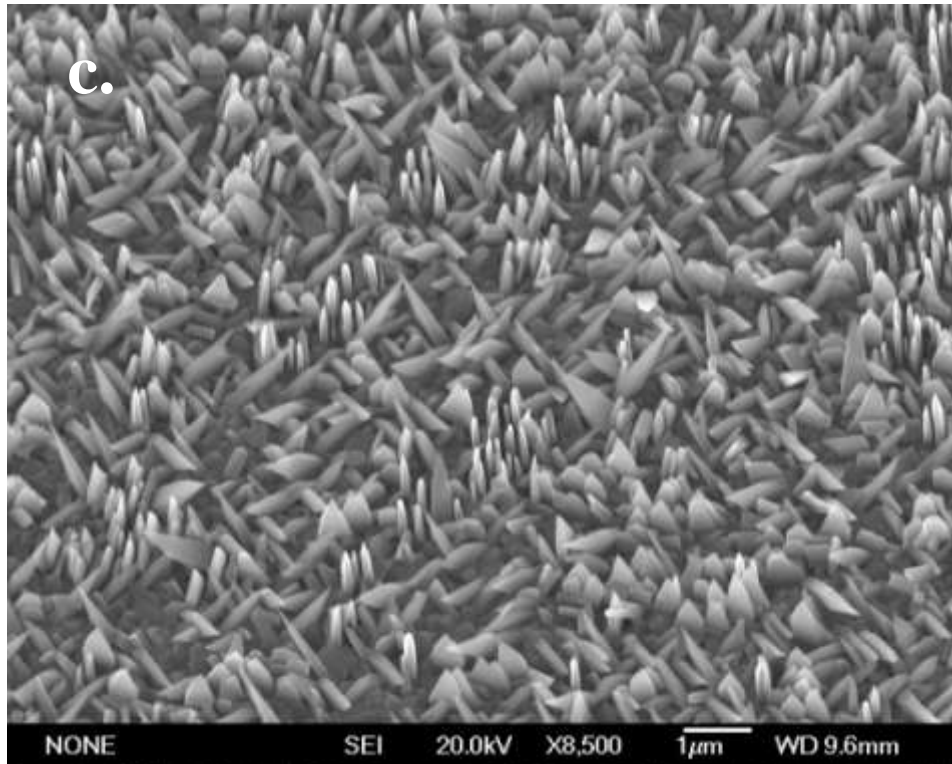
Fig.4.2.3.3 SEM images of AZO-025, with 20 shots on gold and 5000 pulses of ZnO,

a) top view, magnification of 5000, produced in the centre of the plume;
b) top view, magnification of 20,000, produced in the direct centre of the plume;
c) 30° tilt, magnification of 8500, produced away from the centre of plume.

Fig.4.2.3.4. is the phi scan patterns of AZO-025. The ZnO(002) peak is around 45° (θ=15.5732, χ=88.1175) and ZnO(100) peak is around 0° (θ=15.2376, χ=87.6175), which indicates the tilted nanostructures are grown in the orientation (002) while the parallel nanostrcutres are (100) as shown in Fig.4.2.3.5 and marked yellow in Fig.4.2.3.3b.

Another phenomenon was discovered when investigating the deposition of sample AZO-025, the number and density of perpendicular nanorods became larger by moving the substrate's location out from the direct centre of the plume, which will be further discussed in the Influence of Plasma Plume section. The depositions being discussed here were produced in the same location within the plume, which is in the centre of the plume but not the direct centre of the plume.

a.
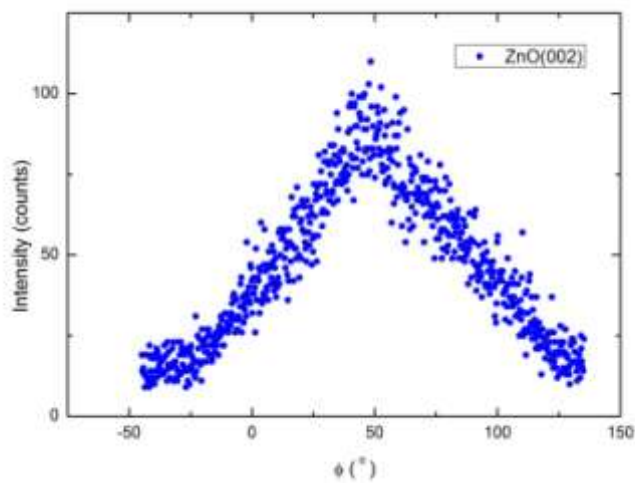
b.
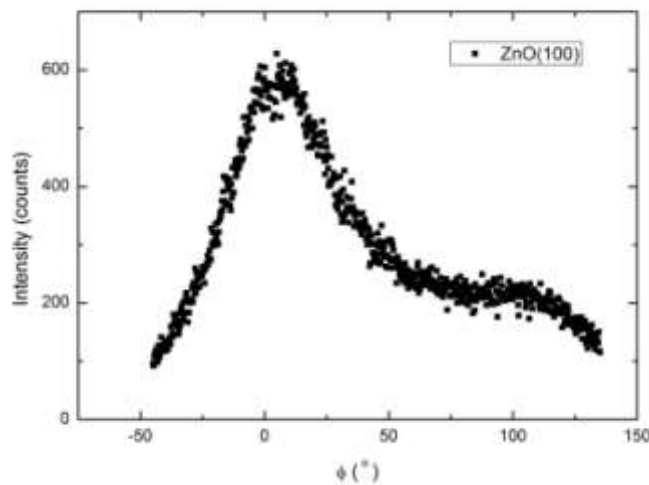
Fig. 4.2.3.4 XRD Phi scans of sample AZO-025 a) ZnO(002) peak; b) ZnO(100) peak.
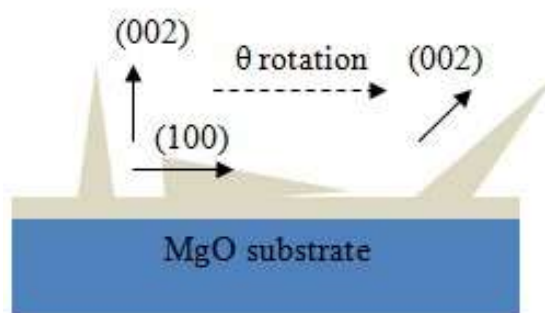
Fig. 4.2.3.5 Schematic diagram of ZnO sample AZO-025 nanorods

102

In conclusion, gold nanodots can influence on the growth of ZnO nanorods. As the gold nanodots more evenly cover the substrate, by increasing the number of pulses on gold target, the distribution of the sizes and dimensions of ZnO nanorods become smaller.

4.2.4 Influence of plasma plume

When investigating the sample of AZO-025, it was found that the morphology can be different due to the substrate location in the plasma plume. The thickness variation of the thin film on the sample is determined by the intensity of the plume [3], as shown in Fig.4.2.4.1. In the direct centre of the plume, the thickness is larger when compared with the other areas. Fig.4.2.4.3a and b are images of the morphology of deposition produced in the direct center of the plume at site A, shown in Fig.4.2.4.2. The nanorods were formed in four orientations and not perpendicular to the substrate. As the deposition location moves away from the direct center of the plume, significantly more vertical nanorods form on the substrate as shown in Fig.4.2.4.4. When the deposition location moves to site B, as seen in Fig.4.2.4.2, the density of perpendicular nanorods reaches its maximum, shown in Fig.4.2.4.5. However as the location approaches the edge of the plume (site C, in Fig.4.2.4.2), the nanorods become rarer on the surface.
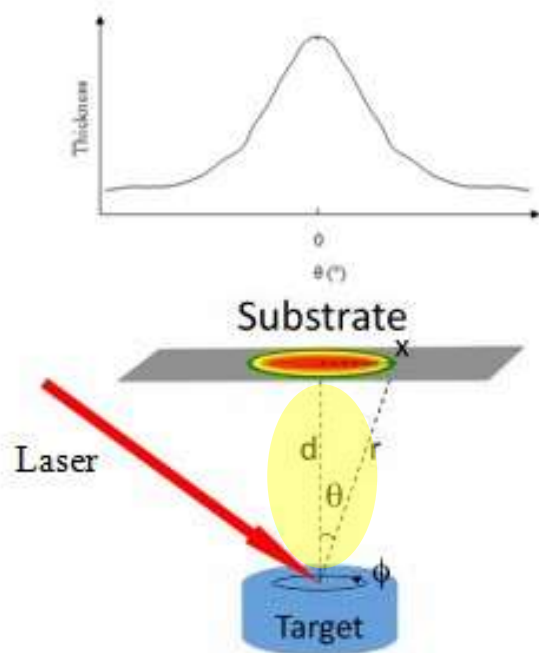
Fig.4.2.4.1 Schematic diagram of the target-substrate-plume geometry [3]
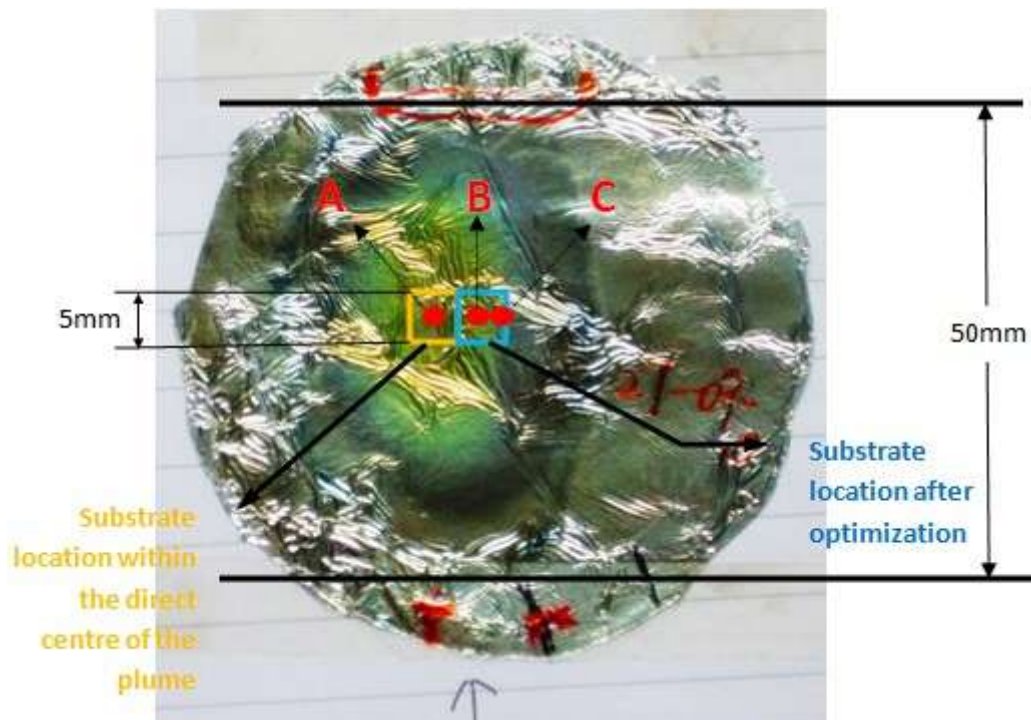
Fig.4.2.4.2 Diagram of plume shown on aluminum foil
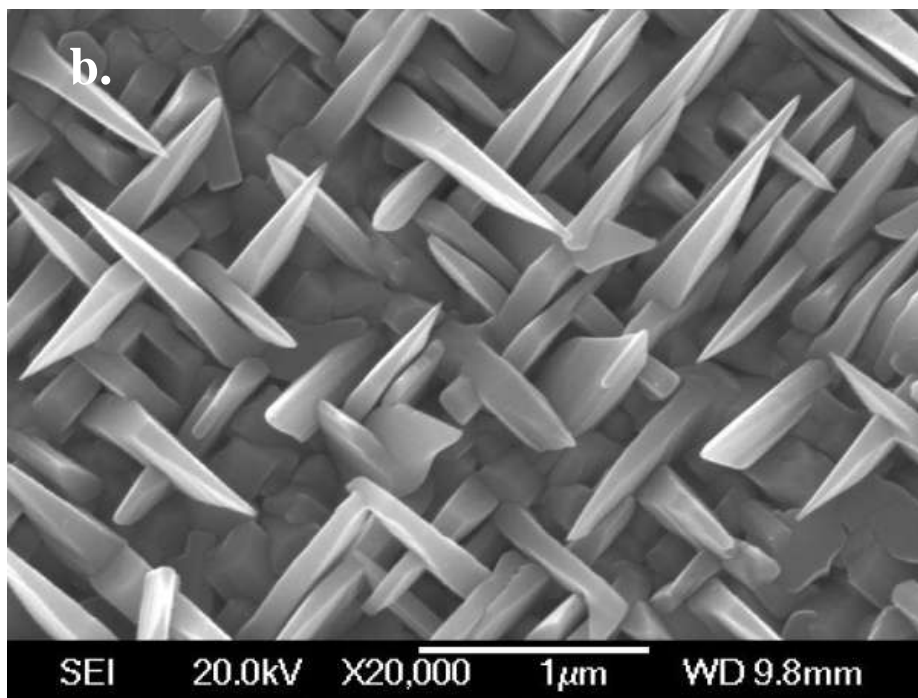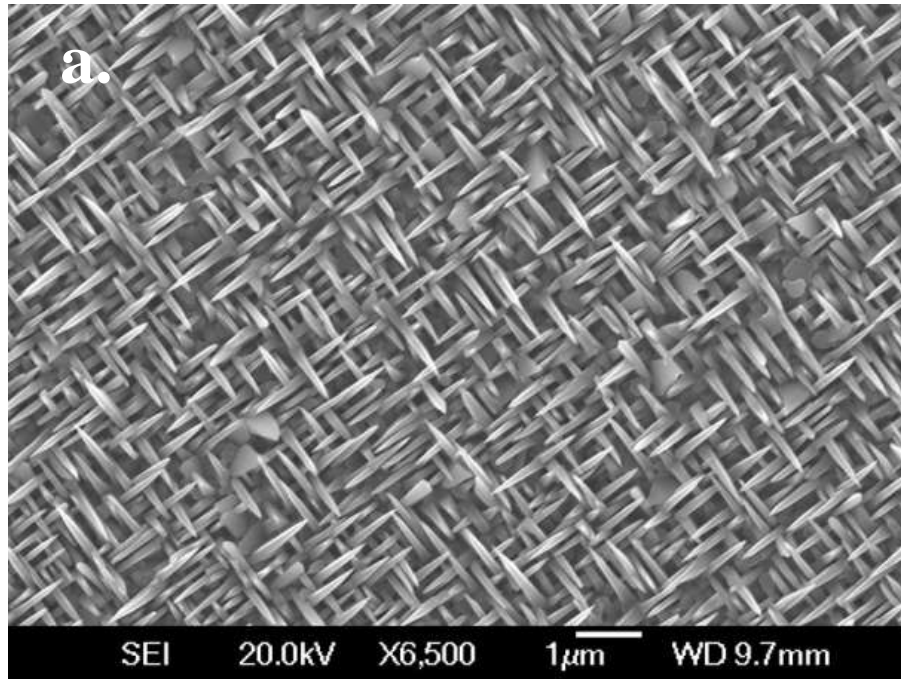
Fig.4.2.4.3 SEM images of AZO-025 on MgO(100), under 700°C and 1.2Torr oxygen pressure, with 20 shots on gold and 5000 pulses of ZnO,

a) top view, magnification of 6500, at site A in Fig.4.2.4.2;
b) top view, magnification of 20,000, at site A in Fig.4.2.4.2.
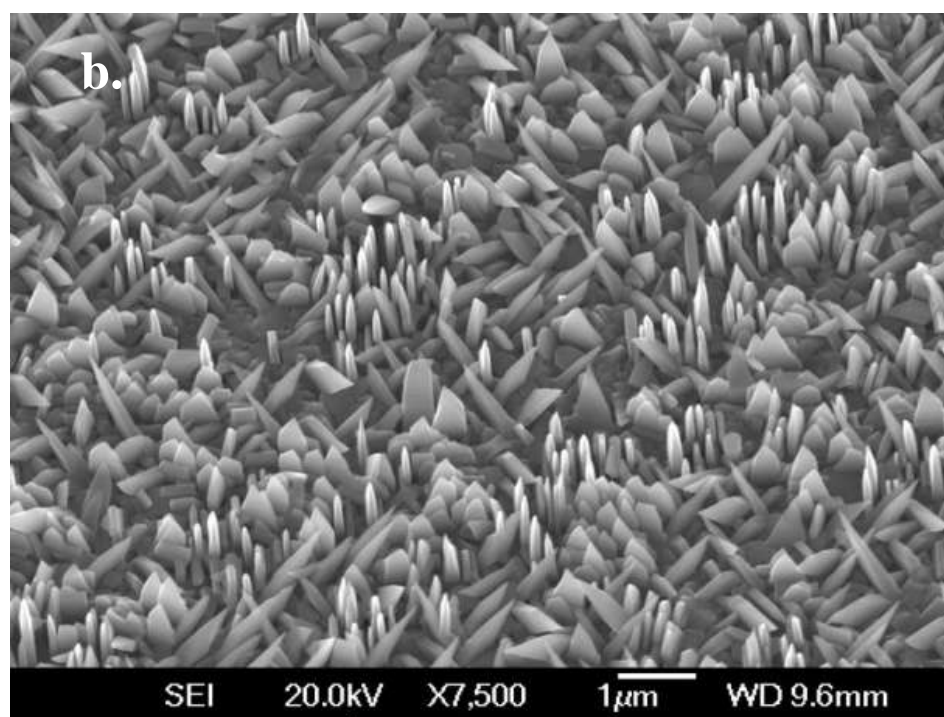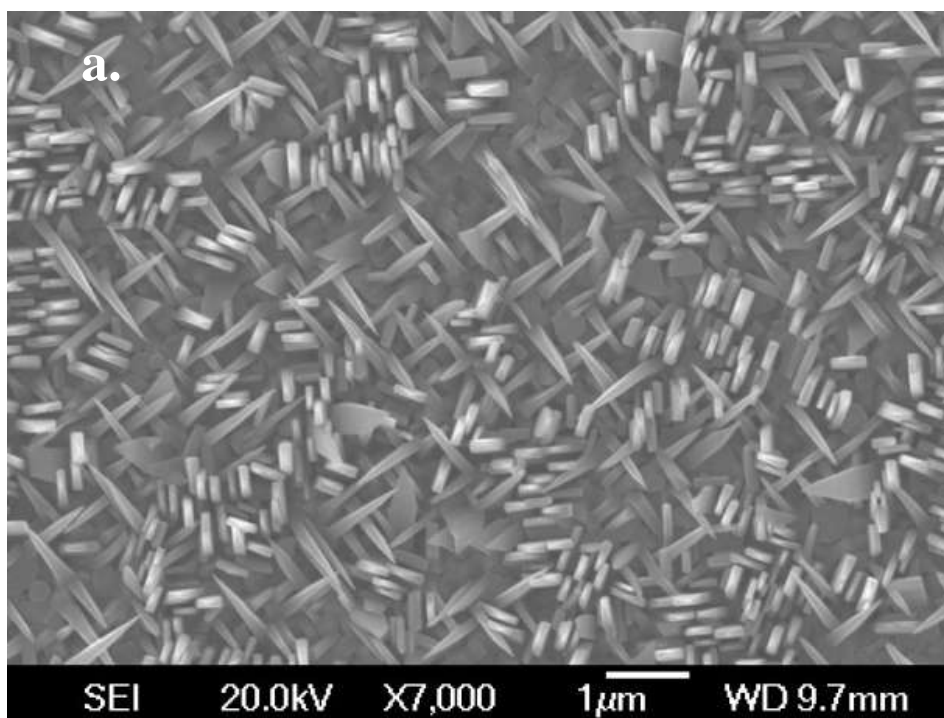
Fig.4.2.4.4 SEM images of AZO-025 on MgO(100), under 700°C and 1.2Torr oxygen pressure, with 20 shots of gold and 5000 pulses of ZnO,

a) top view, magnification of 7000, at site between A and B in Fig.4.2.4.2;
b) 30° tilt, magnification of 7500, at site between A and B in Fig.4.2.4.2.
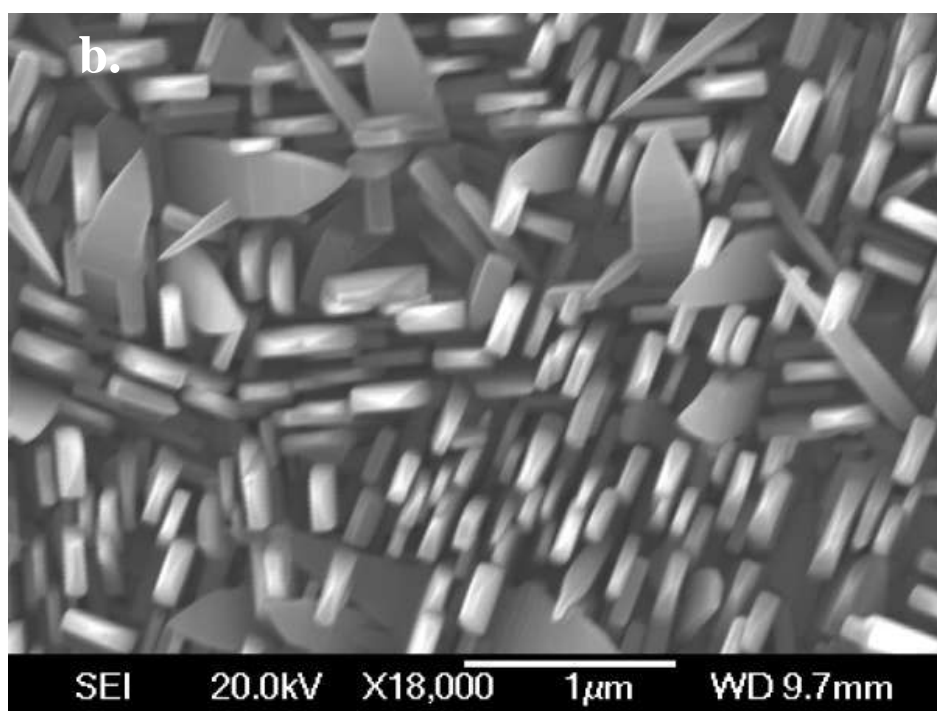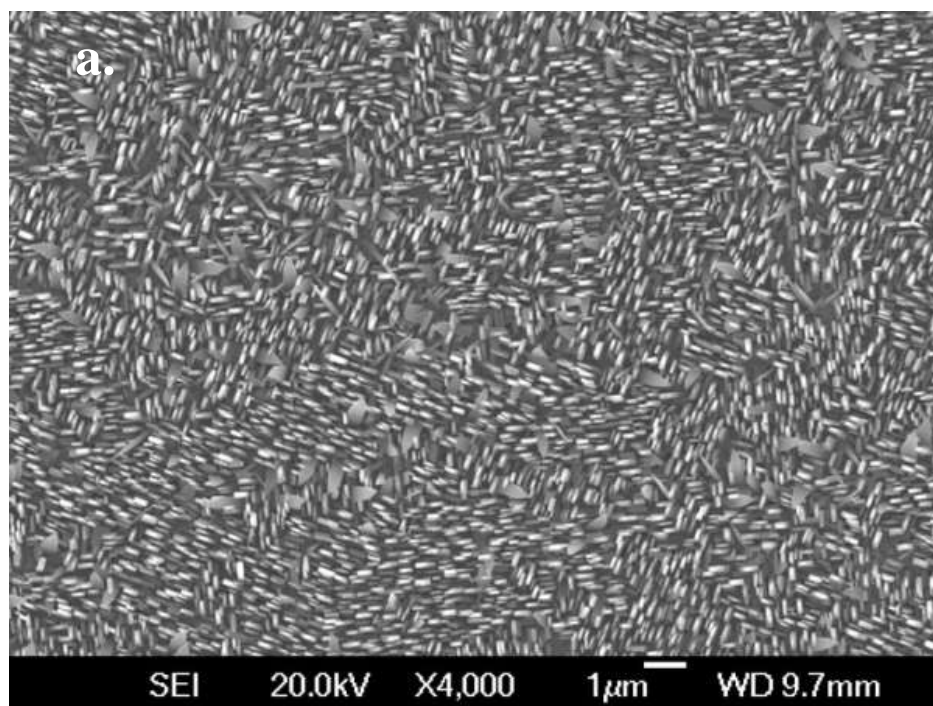
Fig.4.2.4.5 SEM images of AZO-025 on MgO(100), under 700°C and 1.2Torr oxygen pressure, with 20 shots of gold and 5000 pulses of ZnO,

a) top view, magnification of 4000, at site B in Fig.4.2.4.2;
b) top view, magnification of 18,000, at site B in Fig.4.2.4.2.
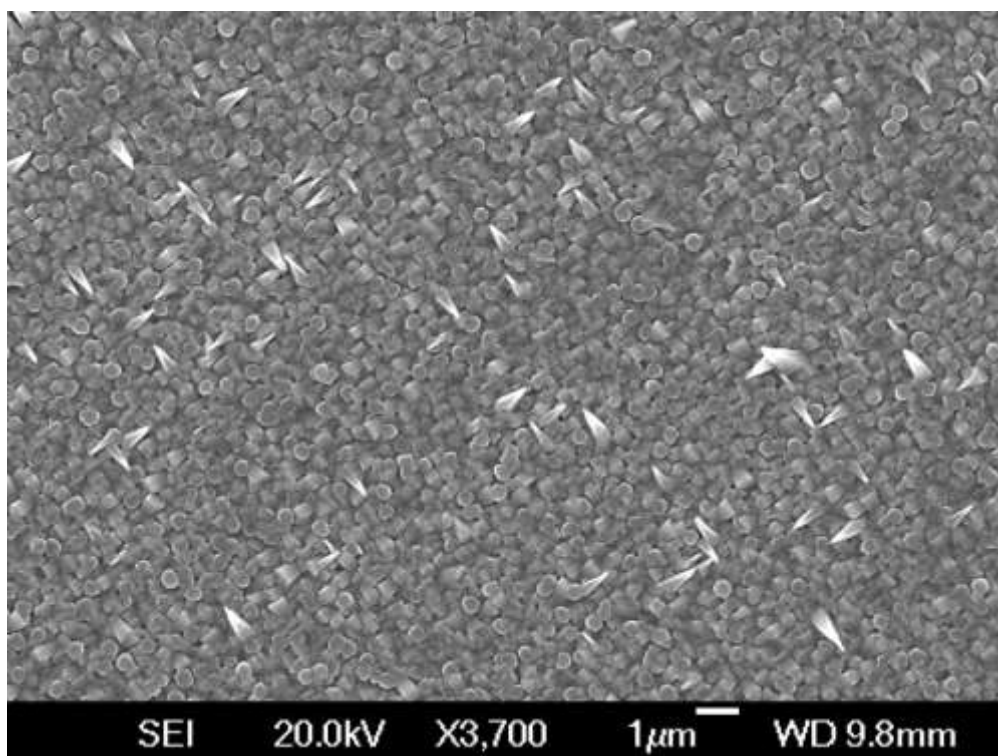
Fig.4.2.4.6 SEM image of AZO-025 on MgO(100), under 700°C and 1.2Torr oxygen pressure, with 20 shots of gold and 5000 pulses of ZnO, top view, magnification of 3700, at site C in Fig.4.2.4.2.

In order to investigate this phenomenon, several more samples were made on a tilted heater (substrate) with an angle within the plume. The heater (substrate) was positioned away from the centre of the plume. The details of the samples discussed in this section are listed in Table 4.2.8. The schematic of laser, plume, heater, substrate and target, from the top view of the chamber, is shown below, in Fig.4.2.4.7.

Table 4.2.8 Detailed parameters of the samples AZO-050,051,052 and 057

Schematic	Sample Number	Temperature (°C)	Chamber number	Number of pulses on Au	Number of pulses on ZnO	Oxygen Pressure (mTorr)
A	AZO-050	700	#3	5	5000	1200
B	AZO-051	700	#3	5	5000	1200
C	AZO-052	700	#3	5	5000	1200
B	AZO-057	700	#3	0	5000	1200
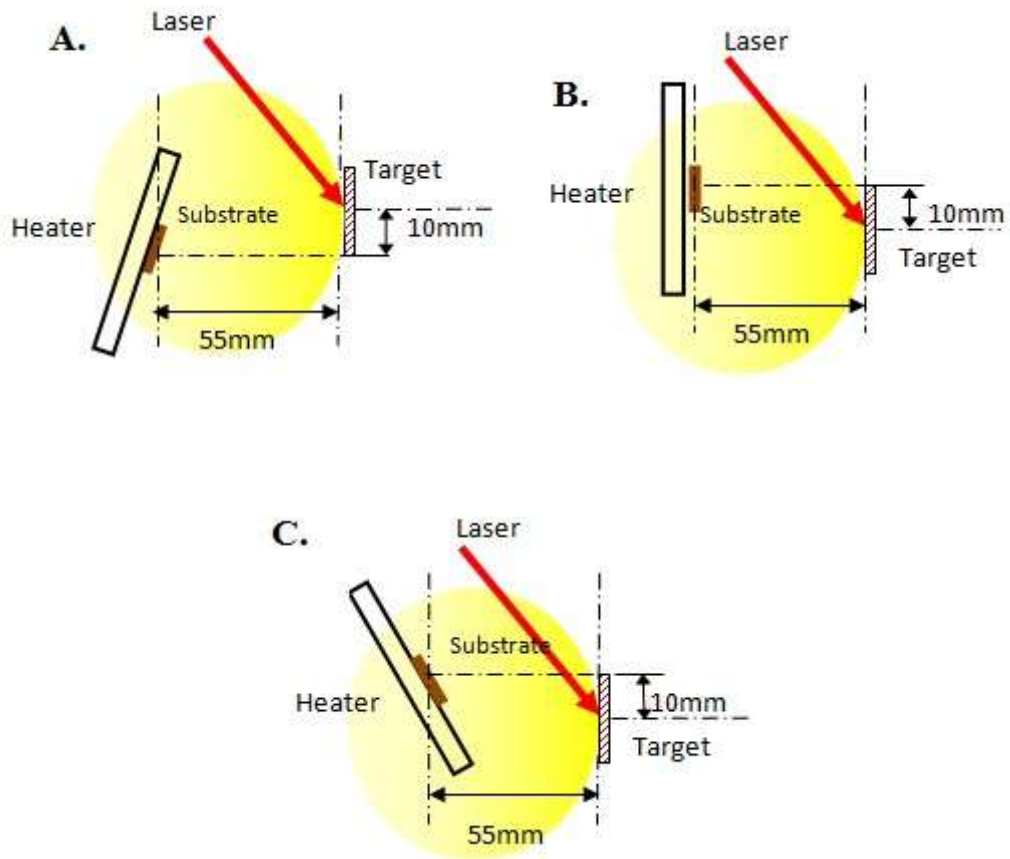
Fig.4.2.4.7 Schematics of heater (substrate) positions

Fig.4.2.4.8 and Fig.4.2.4.9 show the morphologies of sample AZO-050 and AZO-052 made in the position drawn in schematic A and C, where the heater was tilted with an angle within the plume. There were no nanowires or nanorods present on the samples produced at both positions. Also there were no signs of any significant structures to indicate nanowires or nanorods are forming either. Instead, the surface of sample is quite smooth, only decorated by a few crystallized granular objects, as shown in Fig.4.2.4.8a, where grain boundaries are starting to form in Fig.4.2.4.8b and Fig.4.2.4.9a and b. Due to the substrate being tilted during the deposition, the particles would have a different distribution when deposited on the substrate from the plume. The areas closer to the centre of the plume are coated by thicker

layer when compared with the areas further from the centre of the plume. As a result, the depositions on both samples are not even. Fig.4.2.4.8c and Fig.4.2.4.9c show images of the area closer to the center of the plume. Here, a thicker layer, where grain boundaries have been formed and grains become larger, the surface is rougher.
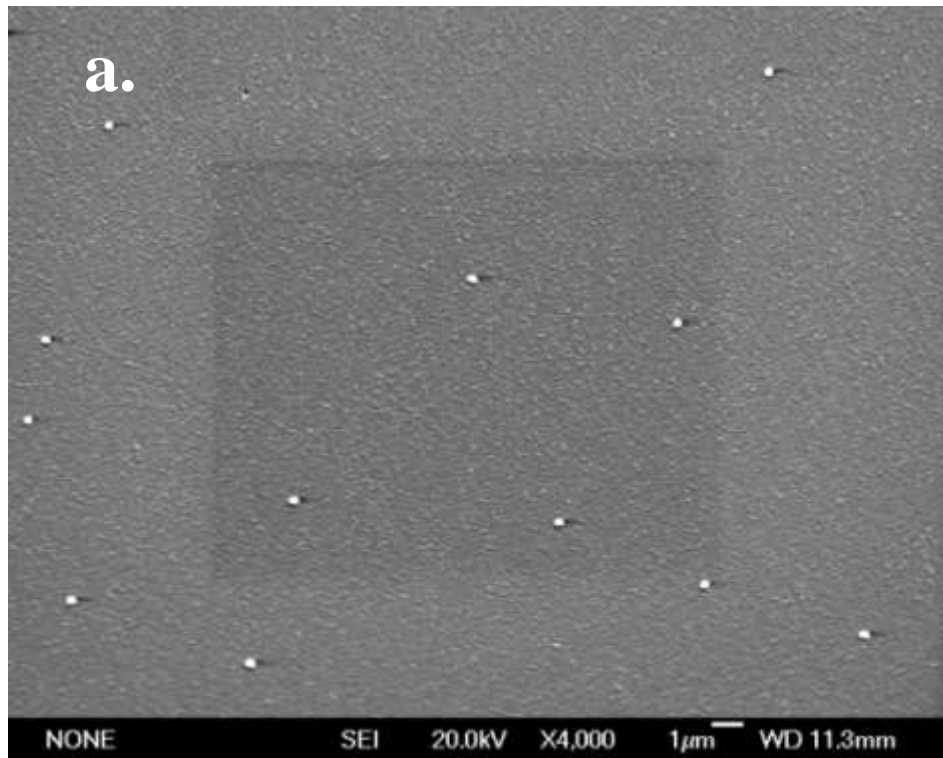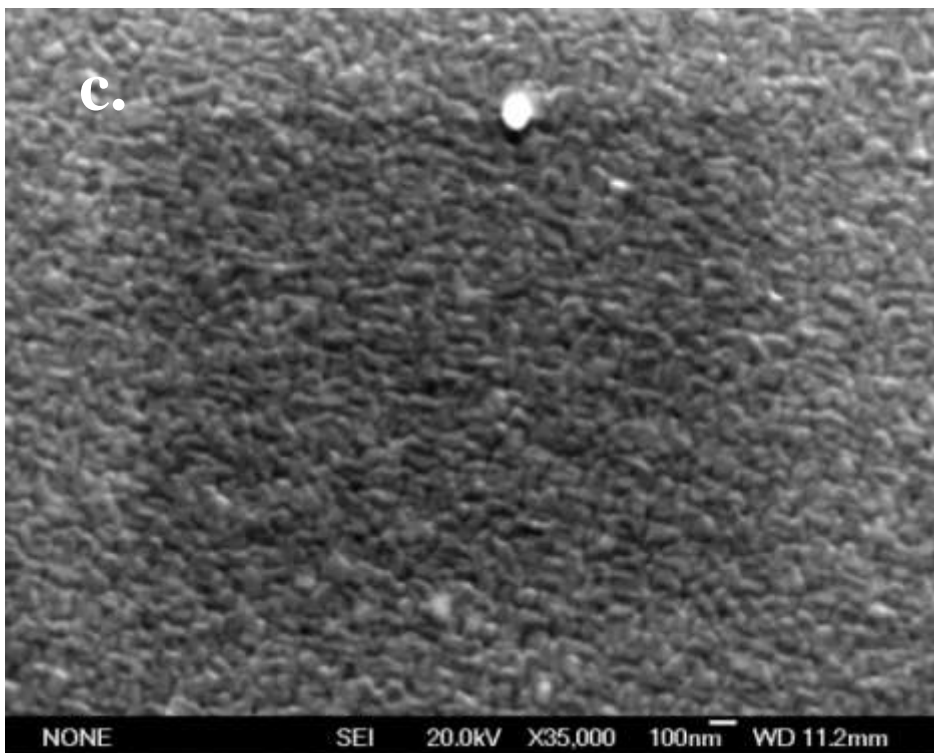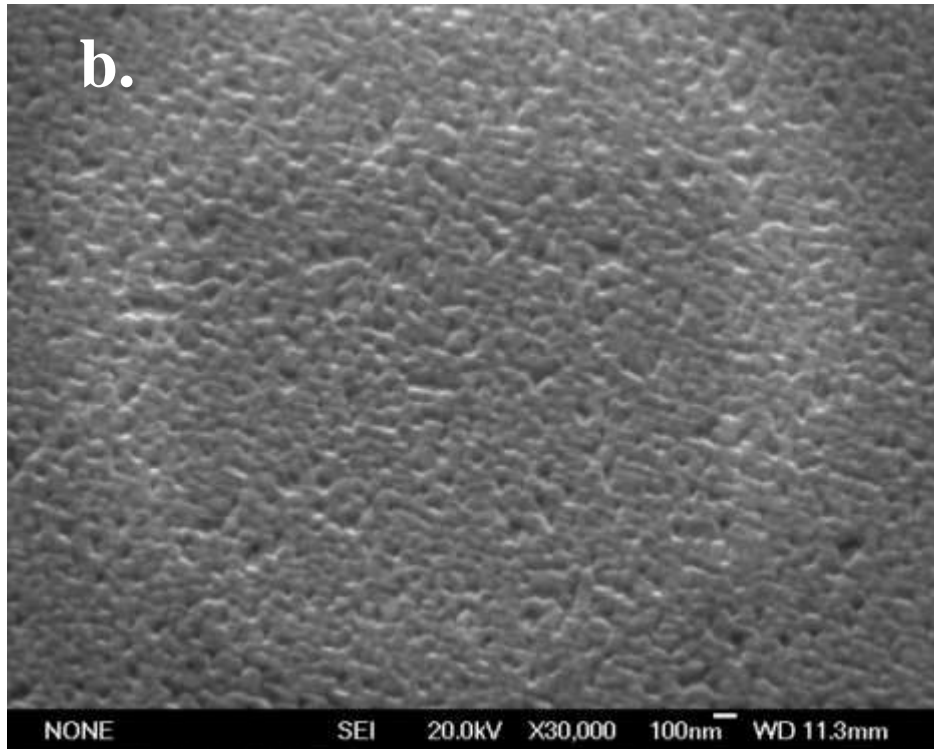
Fig.4.2.4.8 SEM images of AZO-050 on MgO(100) at position A in Fig.4.2.4.7.

a) top view, magnification of 4000; b) 30° tilt, magnification of 30,000;
c) 30° tilt, magnification of 35,000
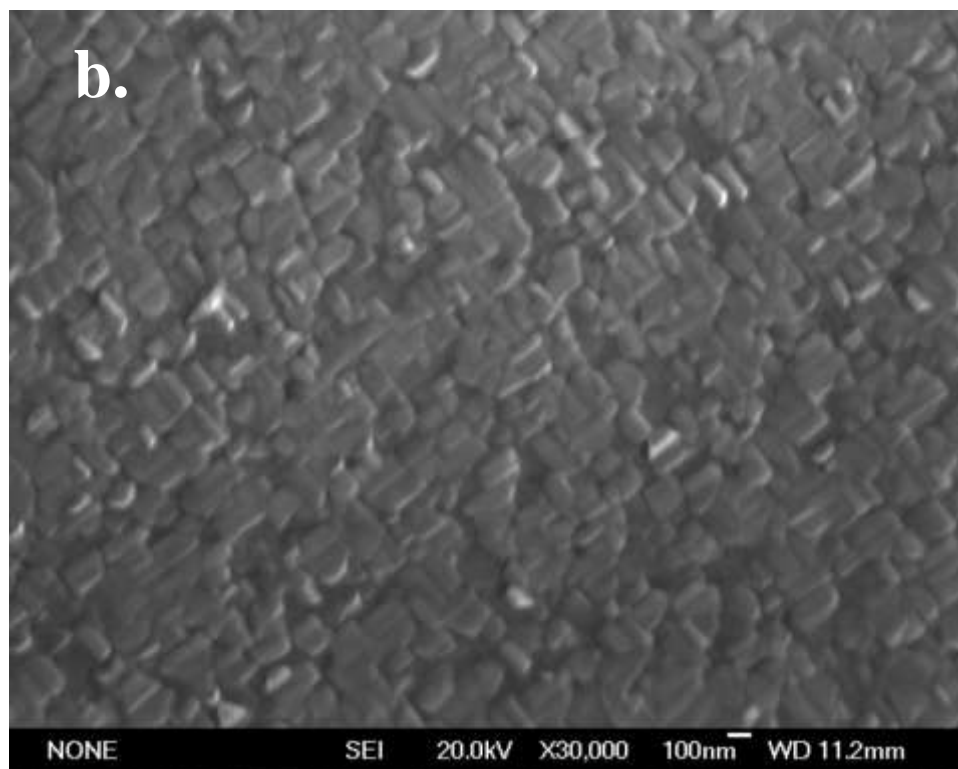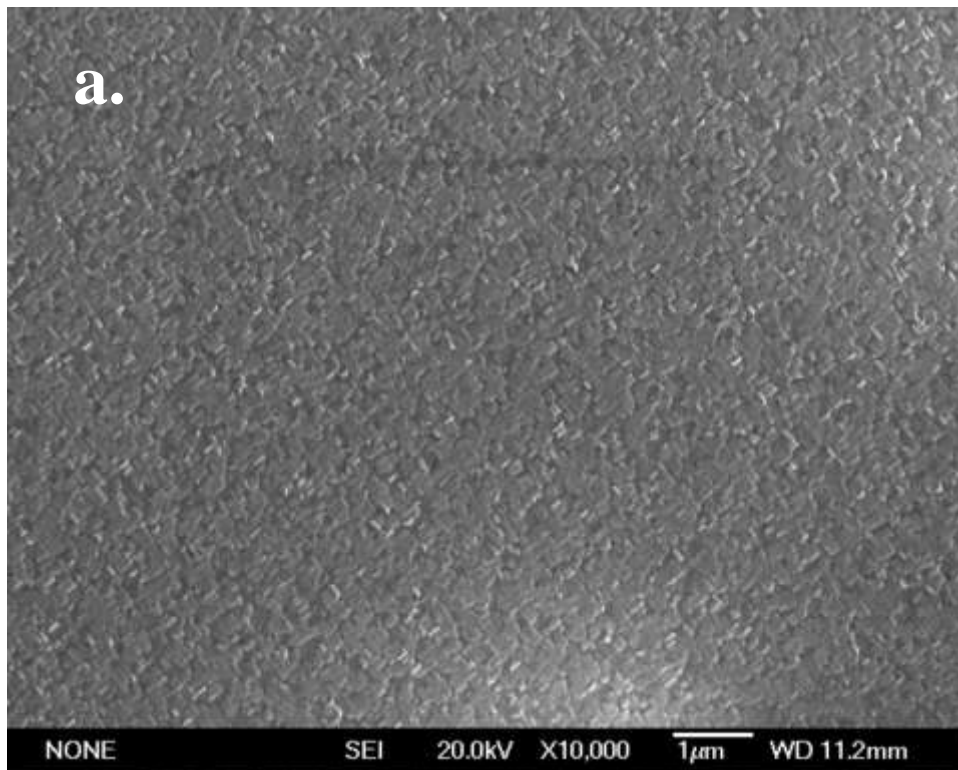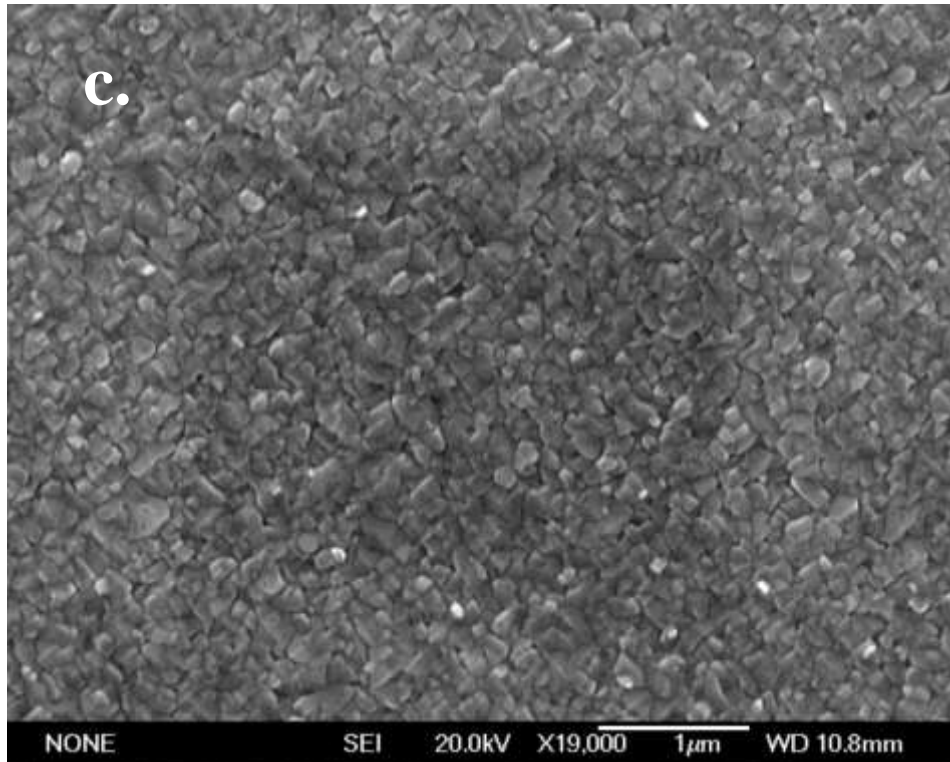
Fig.4.2.4.9 SEM images of AZO-052 on MgO(100) at position C in Fig.4.2.4.7.

a) top view, magnification of 10,000; b) top view, magnification of 30,000;
c) top view, magnification of 19,000

The heater was moved from the centre of the plume without being tilted, as shown in position B of Fig.4.2.4.7, where AZO-051 was produced. The layer shows an overall unique morphology as seen in Fig.4.2.4.10. In the grayish area **I**, two orientation deposition was produced, with widths of 300~400nm, thicknesses of 60~80nm and lengths of 800~1000nm, as shown in Fig.4.2.4.11. As for the darker shaded area **II**, the morphology is shown in Fig.4.2.4.12 Within this area the structures are formed in four directions on the surface. The area **III**, surrounding the central dotted pattern, the structures are similar to area **II**, but the quantity of nanorods within one unit area is larger and devoid of any perpendicular nanorods.

113
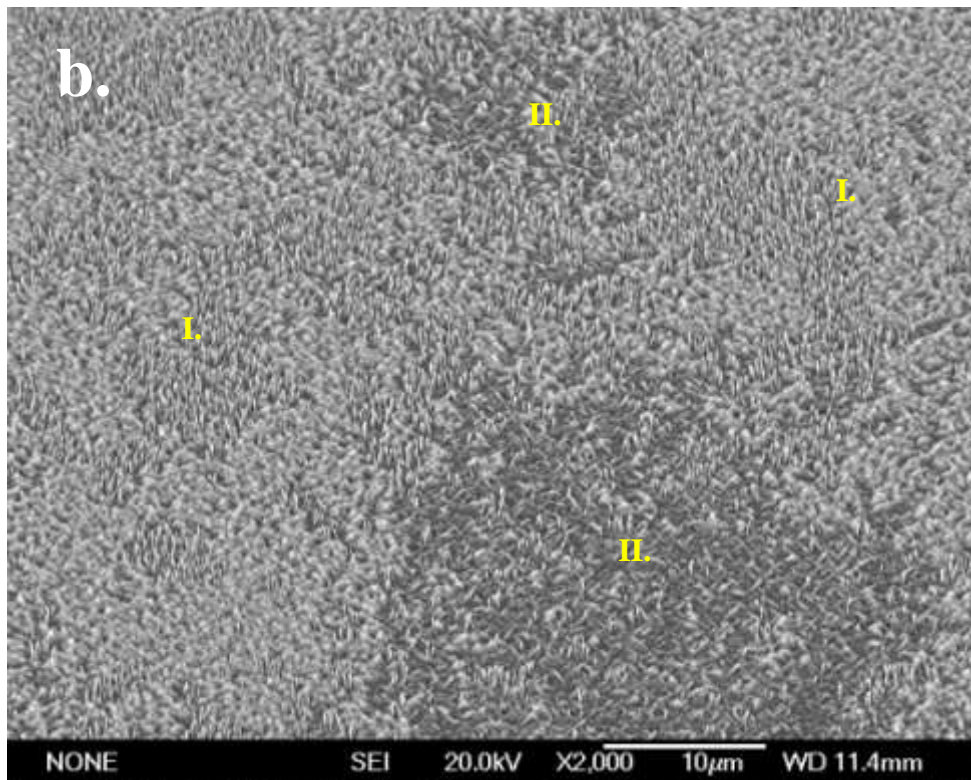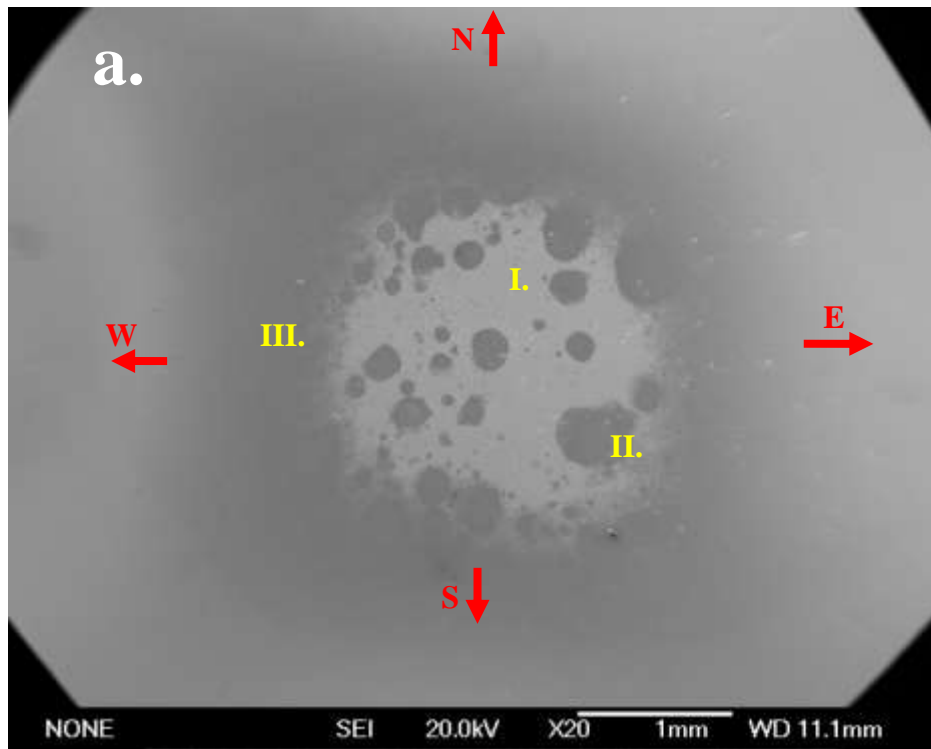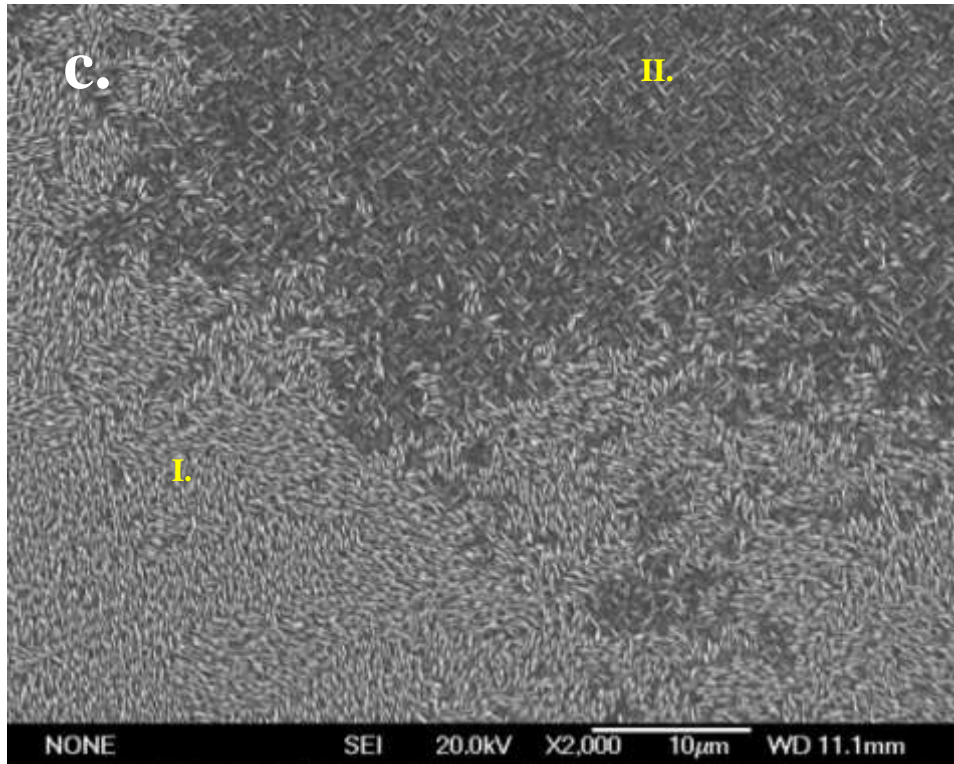
Fig.4.2.4.10 SEM images of AZO-051 on MgO(100) at position B in Fig.4.2.4.7.

a) top view, magnification of 20; b) 30° tilt, magnification of 2000;
c) top view, magnification of 2000
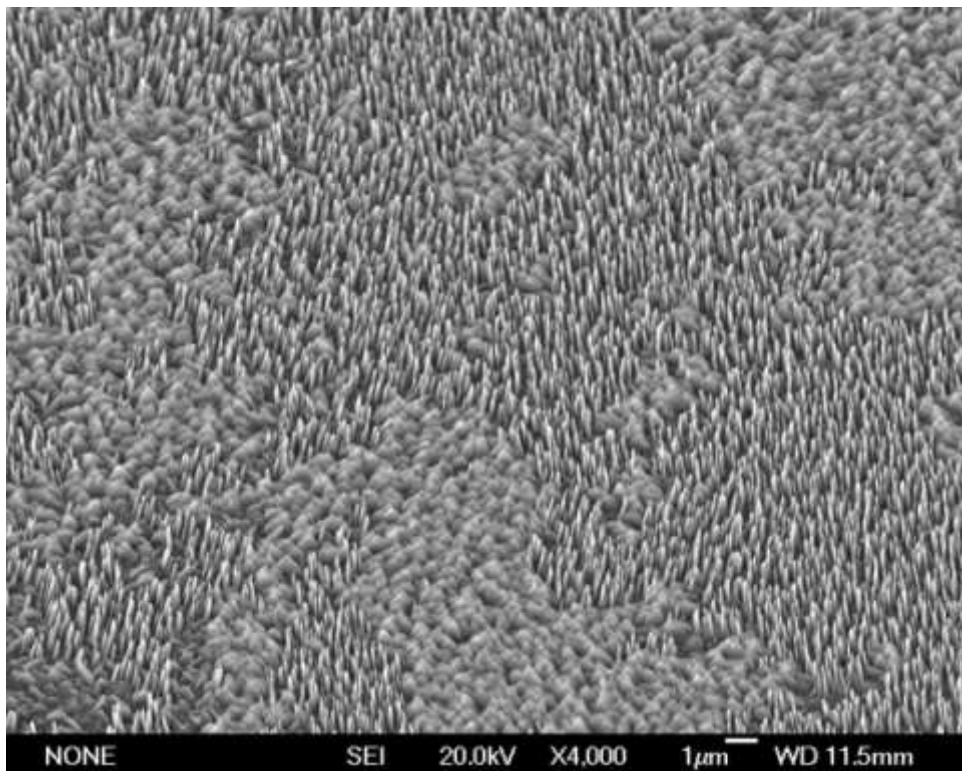
Fig.4.2.4.11 SEM image of AZO-051 on MgO(100) of area **I** in Fig.4.2.4.10., 30° tilt,
magnification of 4000
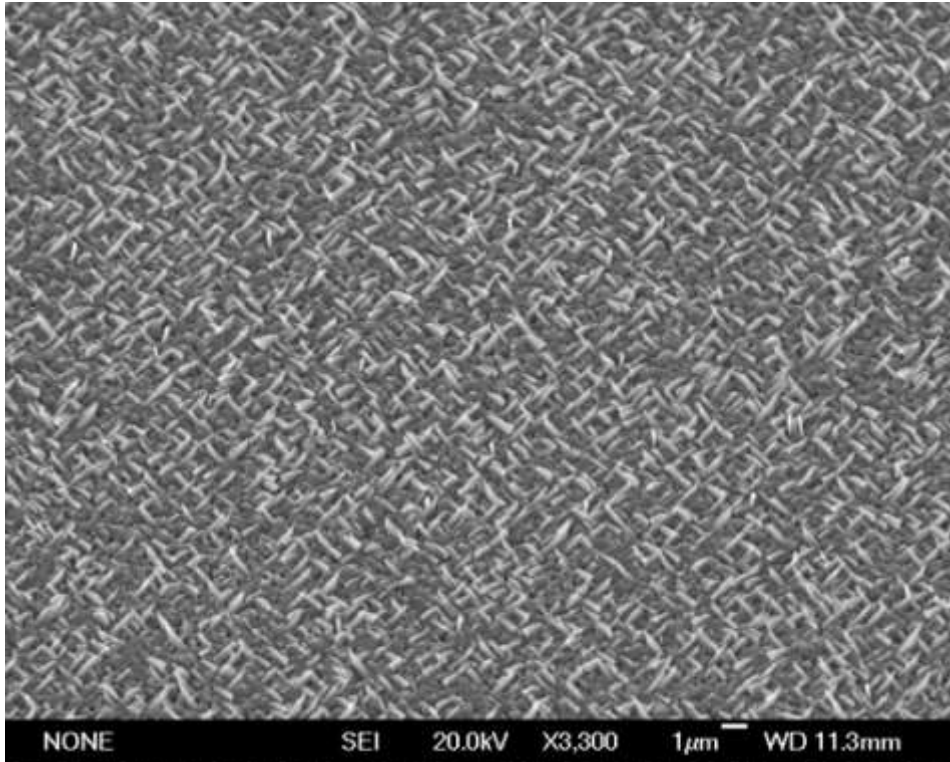
Fig.4.2.4.12 SEM image of AZO-051 on MgO(100) of area **II** in Fig.4.2.4.10., 30° tilt , magnification of 3300
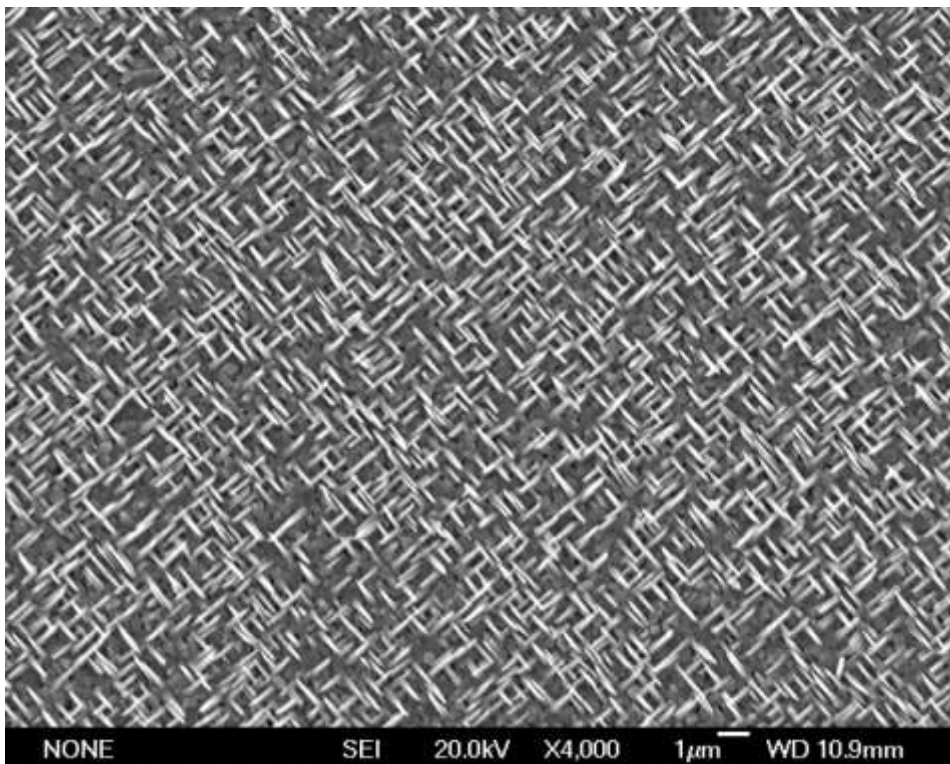
Fig.4.2.4.13 SEM image of AZO-051 on MgO(100) of area **III** in Fig.4.2.4.10., top view , magnification of 4000

When utilizing the SEM lens to scan the surface of the sample, the morphologies of the sample's four edges can been detected. Comparing the area near the edge of the sample to area **III**, the density of nanorods is larger and these nanorods are not only formed in four directions, but the presence of perpendicular nanorods can be seen between them. Also, the diameter of these nanorods have increased to 100~300nm. Very thin (diameter is between 40 to 100nm) and long (length is between 1 to 3 µm) nanowires were found only on the edge of West and East side of the sample.
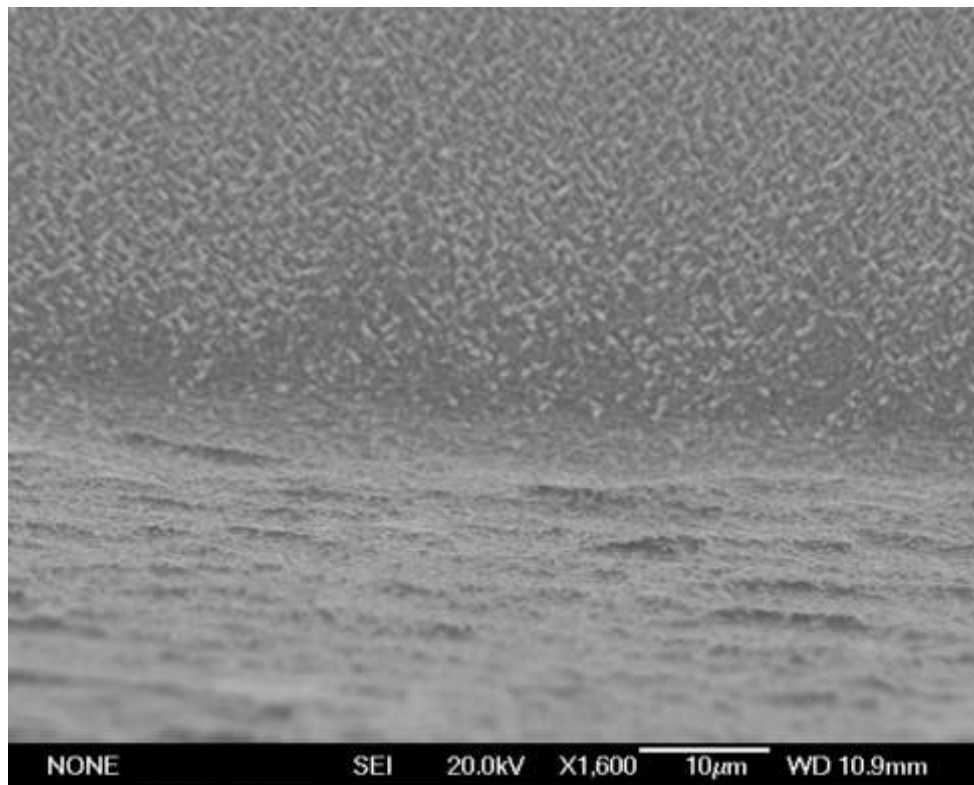
Fig.4.2.4.14 SEM image of AZO-051 on MgO(100) on South edge of Fig.4.2.4.10. , top view, magnification of 1600
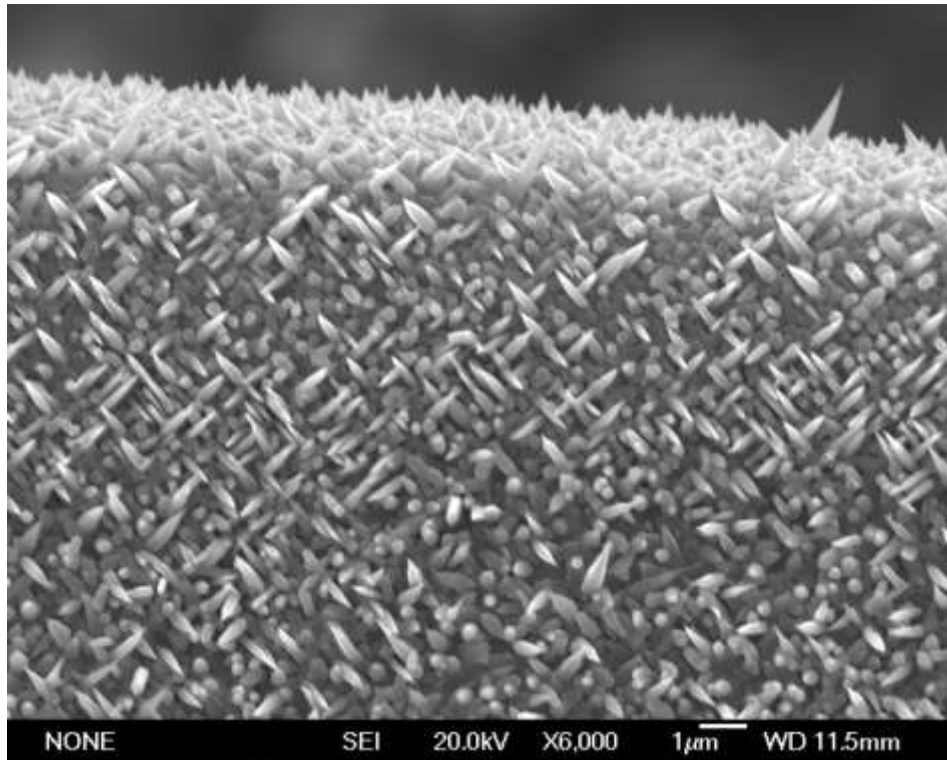
Fig.4.2.4.15 SEM image of AZO-051 on MgO(100) on North edge of Fig.4.2.4.10. , top view , magnification of 6000
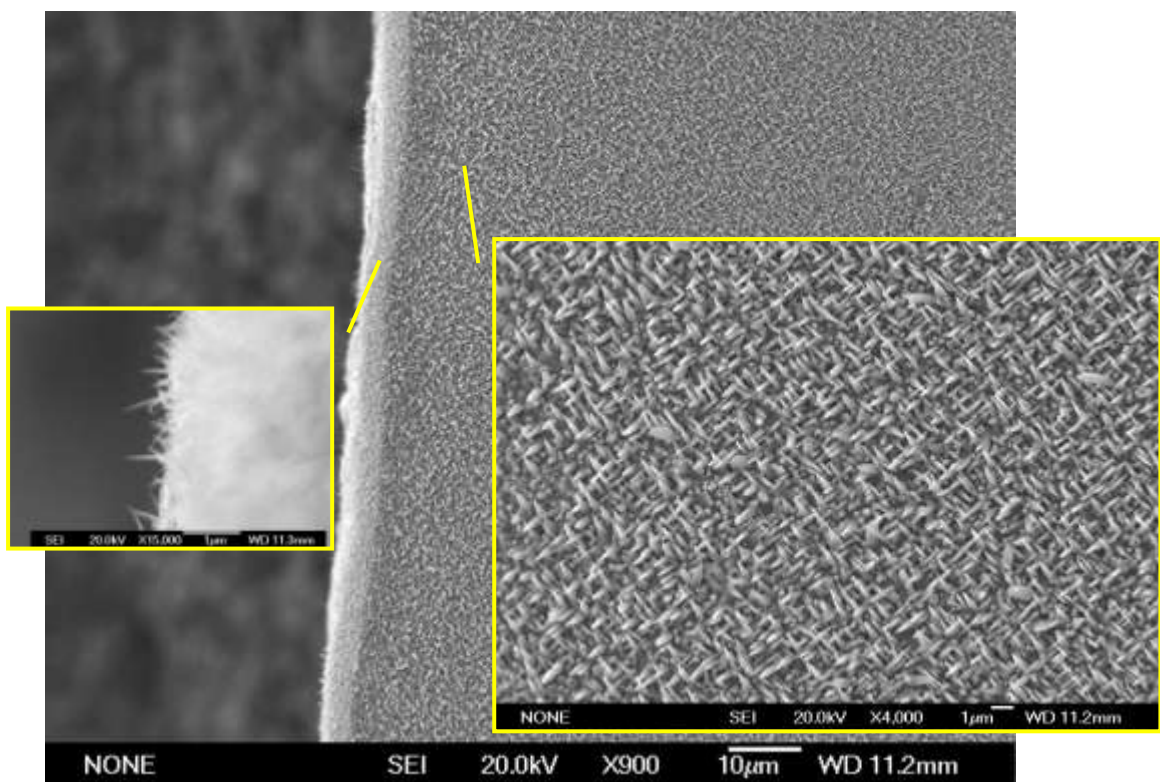
Fig.4.2.4.16 SEM image of AZO-051 on MgO(100) on West edge of Fig.4.2.4.10. , top view , magnification of 900, 15,000 and 4000
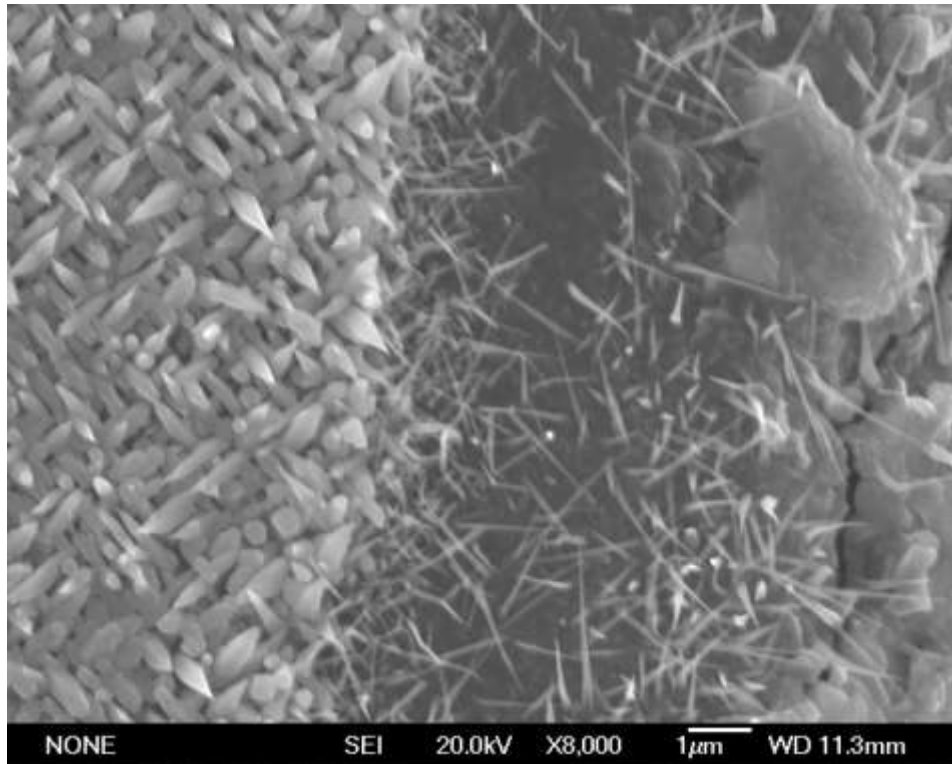
Fig.4.2.4.17 SEM image of AZO-051 on MgO(100) on East edge of Fig.4.2.4.10. , top view, magnification of 8000

In order to investigate the cause of the different morphology on various areas on AZO-051, another sample AZO-057 without a gold nanodot coating was created at position B of schematic 4.2.4.7. Nanometer sized cylinders (diameter of 380~600nm, height of 100~560nm) of ZnO were present on the central surface of the sample shown in Fig.4.2.4.18. As detected by SEM, the quantity of nanometer sized cylinders per one unit area increases while closer to the edge. The morphology gradually changes from individual cylindrical structures into a rough surface, due to the higher density of structures within the area, from the centre towards the area near the edges, as shown in Fig.4.2.4.19. Also, the quantity of perpendicular nanometer sized cylinders increase from the center of the sample to the edge of the sample. The areas near the South and the North edges are covered with similar structures, while morphologies of the areas near the East and the West edges are alike. This is most likely due to the elliptical shape of the plume, instead of being circular, as shown in Fig. 4.2.4.2.

When comparing the samples AZO-057 and AZO-023, there were notable differences due to the positioning of each of the samples (AZO-057 was placed outside the centre of the plume and AZO-023 was placed within the centre of the plume) despite having the similarity of not utilizing any gold dots on the sample. AZO-057 was found to have different morphologies in various areas throughout the sample, while AZO-023 contained a single morphology which was uniform throughout the surface of the sample. These differences are related to the even distribution of particles within the center of the plume when compared to the distribution of particles outside the central area of the plume.
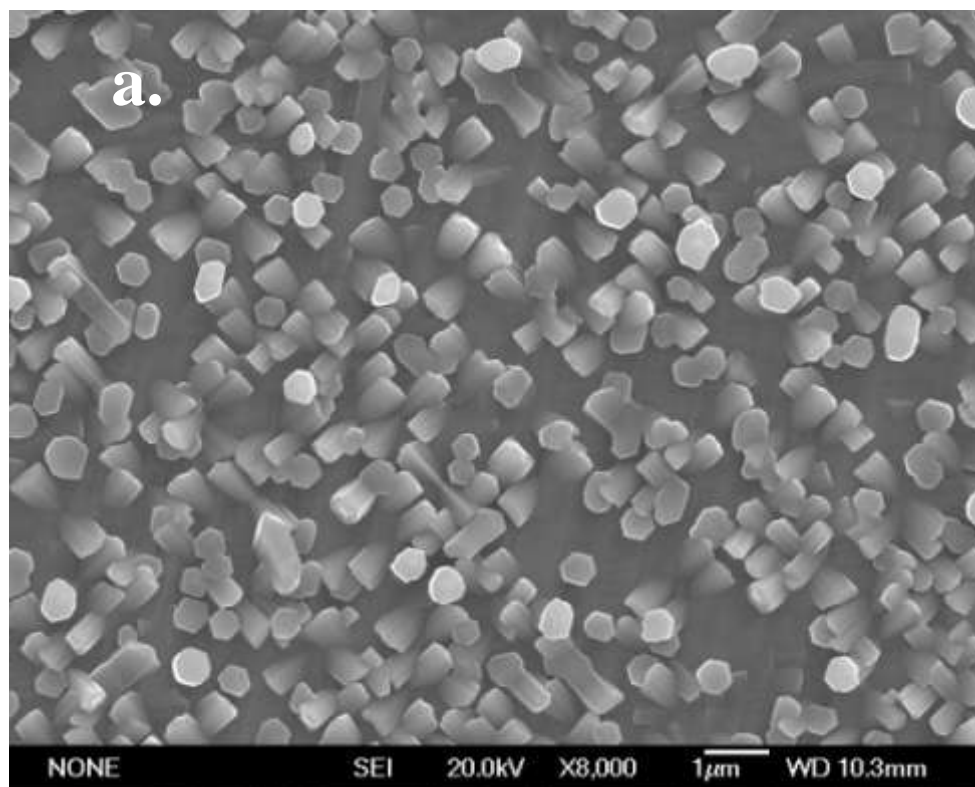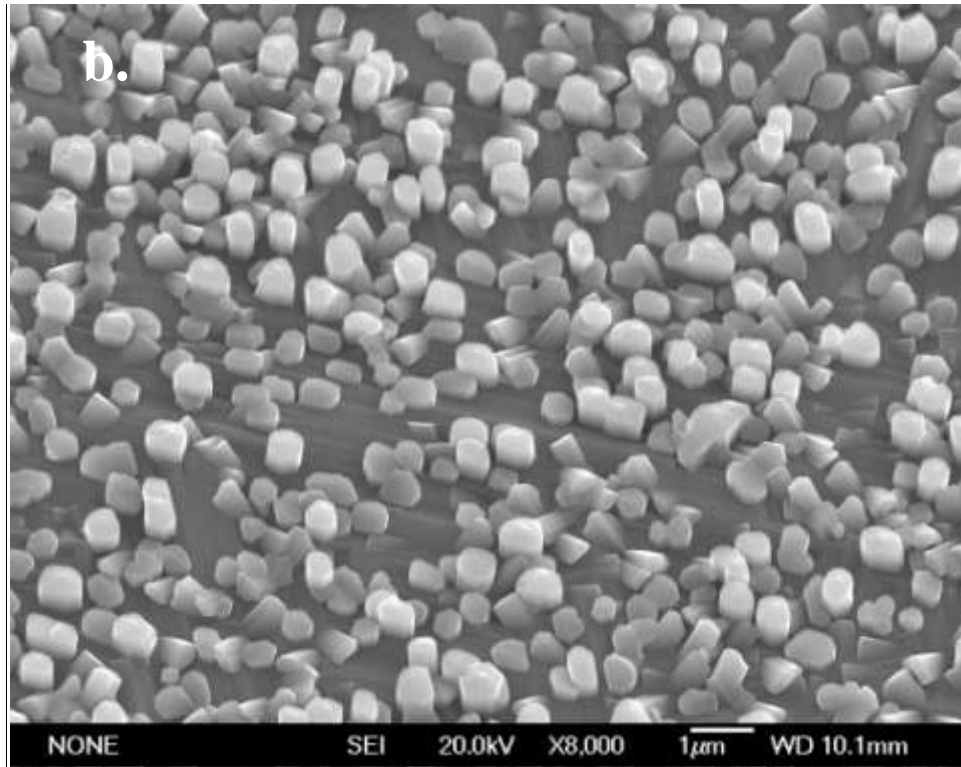
Fig.4.2.4.18 SEM images of AZO-057 without gold nanodots at position B in Fig.4.2.4.7, central morphology

a) top view, magnification of 8000; b) 30° tilt, magnification of 8000.
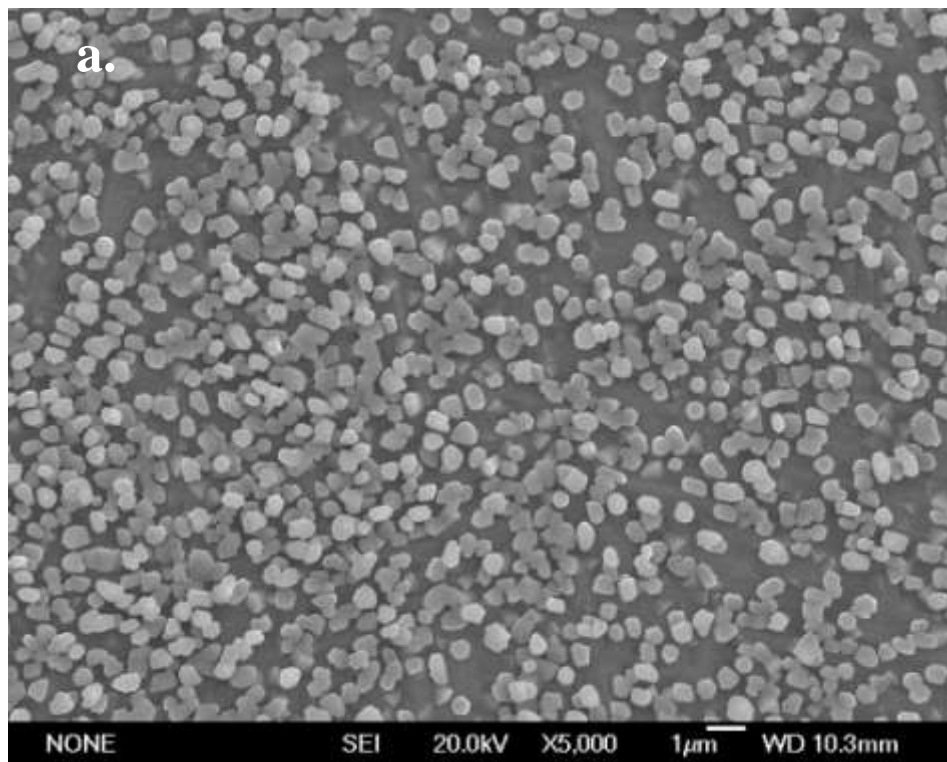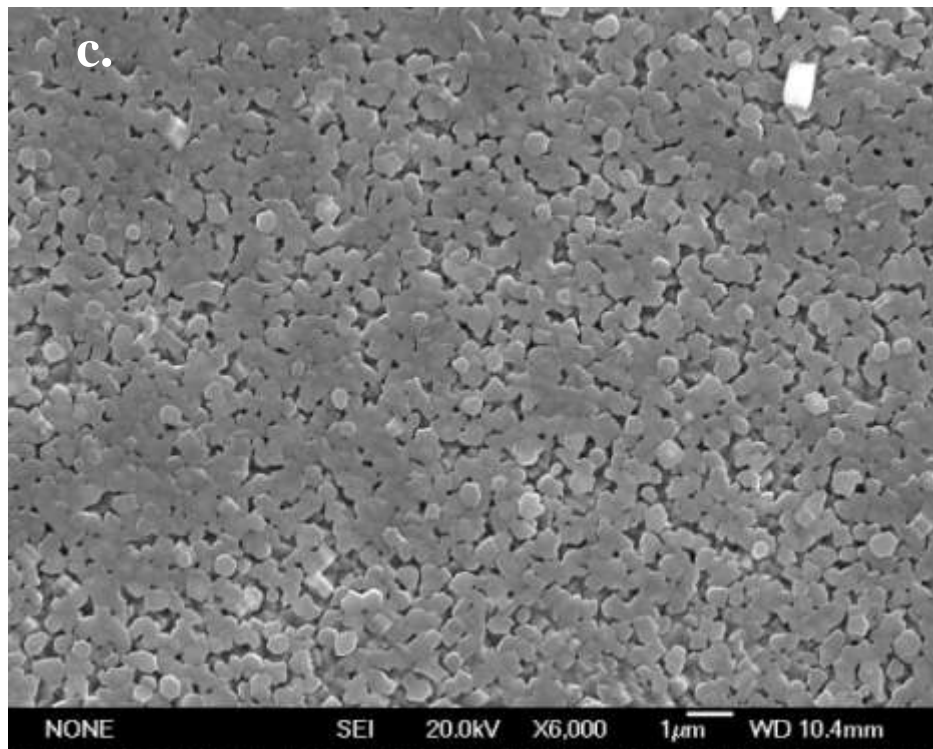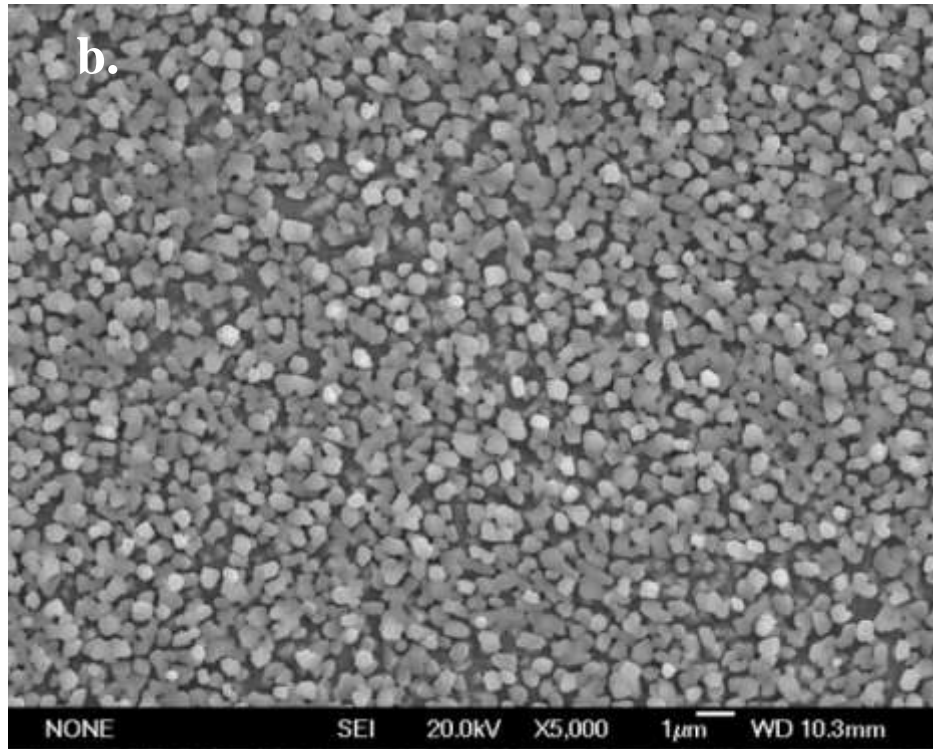
Fig.4.2.4.19 SEM images of top viewed AZO-057 without gold nanodots at position B in Fig.4.2.4.7., a)→b)→c) is from the area near the centre to the area near the north edge
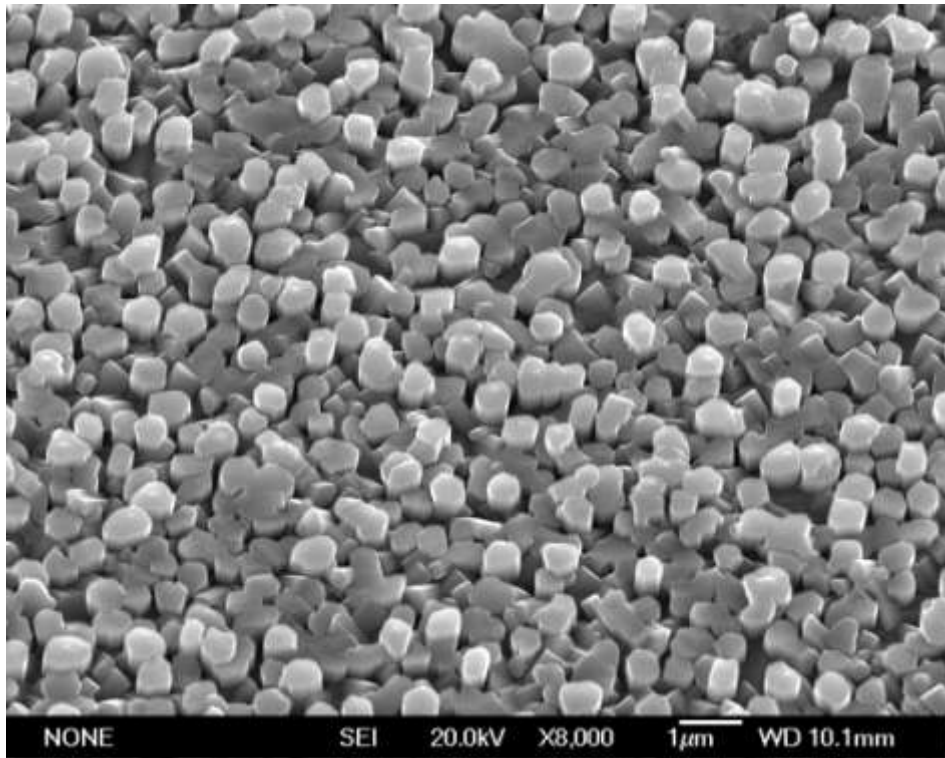
Fig.4.2.4.20 SEM image of AZO-057, 30° tilt, area between centre and south edge
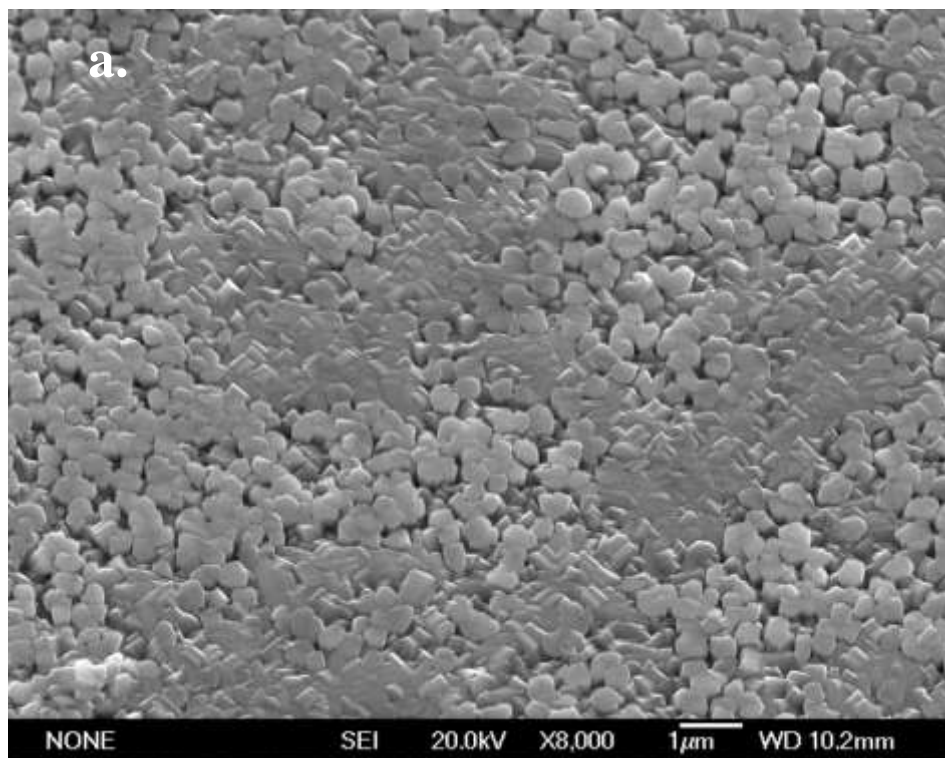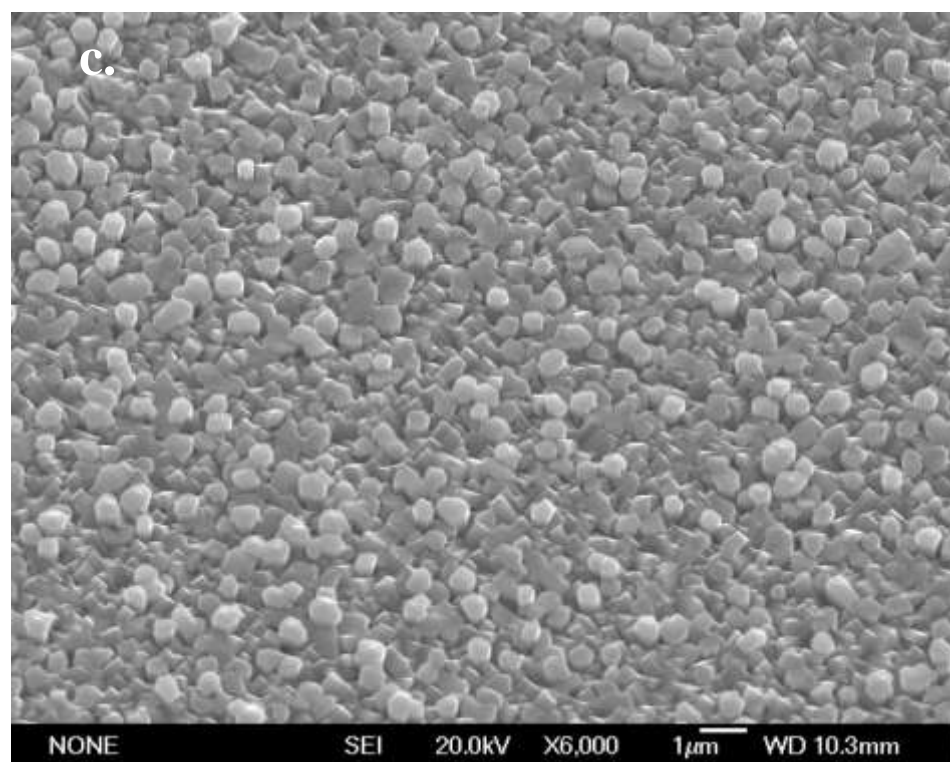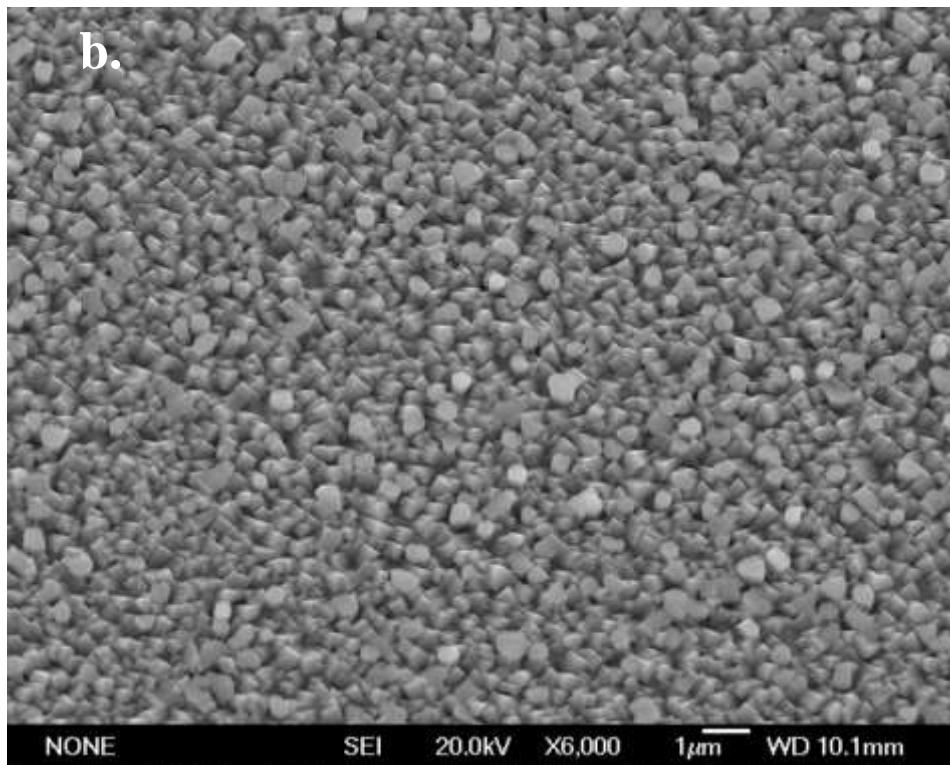
Fig.4.2.4.21 SEM images of AZO-057, 30° tilt,

a) the area near the south edge; b) the area near the west edge; c) the area near the east edge.

In the direct centre of the plume, the particles normally carry more energy and the particle energy level goes down when moving away from the centre of the plume. The growth of perpendicular nanorods requires a particular energy level, where it cannot be as high as in the centre of the plume and not as low as the edge of the plume. Higher energy results in forming parallel nanorods. The plume influences the morphologies of the samples by influencing the orientation of the deposition. Gold nanodots influence the sample's morphologies by influencing the distribution of the sizes and dimensions of ZnO's samples. The similarities of AZO-051 and AZO-057 are found in the centre of the samples. Both depositions tend to have growth in four directions as it approaches the edge. However, the distribution of orientation on both samples is quite similar. The only difference regards the diameter of the nano-structures, where AZO-051 is thin due to the gold coating and AZO-057 is thick without any gold nanodots.

The tilting of the heater was found to not benefit the growth of nanorods. This is likely due to that, when tilting the heater, the different areas of the surface has a different chance for the particles to land on the substrate from the plume. This provides a different environment for particulates' diffusion on the substrate, which does not help the growth of nanorods. The result of this can be found in one sample, where the thickness of the layer is different due to different area of the sample. In areas where it is closer to the target, the thickness is larger.

The samples having particles deposited out from the centre without being tilted have different morphologies in different areas on the substrate. This is due to the energy, of particulates, within the plume upon the surface of the substrate, used during the deposition is not as even and uniform. However, within the plume different areas of the substrate surface has different probabilities for the particles to distribute and this distribution should be symmetrical. The areas near the four edges will have a similar energy level and these areas

are much easier for the particles to distribute, which is different from the direct centre of the substrate. However, the shape of plume tends to be elliptical rather than a circular, which results in the South and North areas having a similar morphology while East and West having a similar morphology. Therefore, only thin and long nanowires only grow on the East and West edges as seen in sample AZO-051.

In conclusion, the plasma plume not only influences the nanostructure of the samples, but also the distribution of these nanostructures. Therefore, in order to optimize the best position of growing perpendicular nanorods, the best location of substrate has been chosen, as shown in Fig.4.2.4.2, marked by the blue square. Above this area is the ideal placement for the substrate near the plume for optimal nanostructure growth.

4.2.5 Influence of substrate temperature

Temperature is a parameter that can affect the crystallinity of the oxide used, which, in turn, could influence the morphology of the sample. ZnO nanowires and nanorods have been known to be very sensitive to the substrate temperature in various case studies and this is particularly true in this study. Two different types of substrates were used in three different chambers. The substrates used were single crystal of MgO(100), and glass, which is amorphous. Following preliminary depositions, the oxygen pressure was set to 1200 mTorr as a constant value, and other details are listed in the tables below.

Table 4.2.9 Detailed parameters of the samples AZO-009, 013 and 014

Sample Number	Temperature (˚C)	Substrate	Chamber number	Number of pulses on gold target (shots)	Number of pulses on ZnO target (shots)	Distance of Target-Substrate (mm)
AZO-009	**800**	MgO(100)	#1	5	5000	55
AZO-013	**750**	MgO(100)	#1	5	5000	55
AZO-014	**700**	MgO(100)	#1	5	5000	55

Table 4.2.10 Detailed parameters of the samples AZO-053, 054 and 055

Sample Number	Temperature (˚C)	Substrate	Chamber number	Number of pulses on gold target (shots)	Number of pulses on ZnO target (shots)	Distance of Target-Substrate(mm)
AZO-053	**650**	MgO(100)	#3	5	5000	55
AZO-054	**600**	MgO(100)	#3	5	5000	55
AZO-055	**500**	MgO(100)	#3	5	5000	55

Table 4.2.11 Detailed parameters of the samples AZO-066,067 and 068

Sample Number	Temperature (˚C)	Substrate	Chamber number	Number of pulses on gold target (shots)	Number of pulses on ZnO target (shots)	Distance of Target-Substrate(mm)
AZO-066	**600**	Glass	#2	5	5000	50
AZO-067	**500**	Glass	#2	5	5000	50
AZO-068	**400**	Glass	#2	5	5000	50

Table 4.2.12 Detailed parameters of the samples AZO-082 and 083

Sample Number	Temperature (˚C)	Substrate	Chamber number	Number of pulses on gold target (shots)	Number of pulses on ZnO target (shots)	Distance of Target-Substrate(mm)
AZO-082	**700**	MgO(100)	#2	5	5000	60
AZO-083	**600**	MgO(100)	#2	5	5000	60

For the sample AZO-009, shown in Fig.4.2.5.1, the substrate temperature was set at 800˚C. This caused no identifiable nanostructures to be present. When the temperature is reduced to 700˚C, a very uniform array of ZnO nanoplatelets appears. This is shown in Fig.4.2.5.3 of the sample AZO-014. The nanoplatelets formed in 4 different directions on the substrate, in Fig.4.2.5.3a, which are the top views of sample AZO-014. SEM images, with a larger magnification in Fig.4.2.5.3c, indicate that the darker region is formed by the arrayed nanoplates with one orientation, while the lighter region consists of another orientated nanoplate array. Among these nanoplatelets, crystallized granular objects and nanorods of ZnO can be seen. When the substrate temperature is set at 750˚C, a mixture of nanowires, nanorods, nanoplatelets, and crystallized granular objects are formed, as seen in Fig.4.2.5.2 of the sample AZO-013.

By reducing the temperature from 800˚C to 700˚C, the energy being provided from the heater (substrate) is reduced, as a result, more distinct nanostructures, such as nanorods, nanowires, and nanoplates begin to appear. Therefore, in order to form such nanostructures, a lower temperature would be needed.
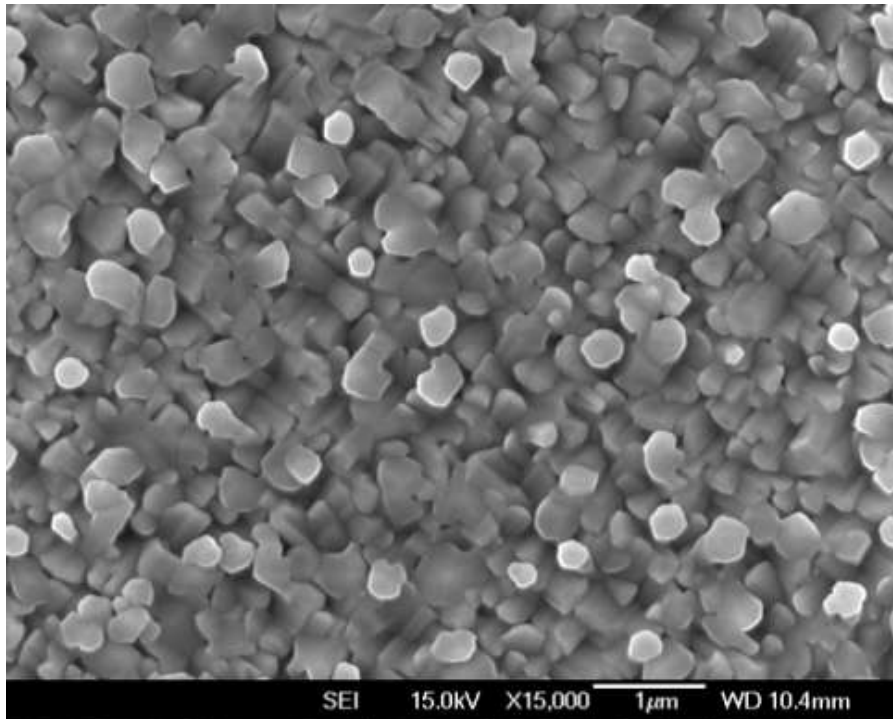
Fig.4.2.5.1 SEM image of AZO-009 on MgO(100), under 800°C and 1.2Torr oxygen pressure, with a target-substrate distance of 55mm in chamber #1, top view, magnification of 15,000
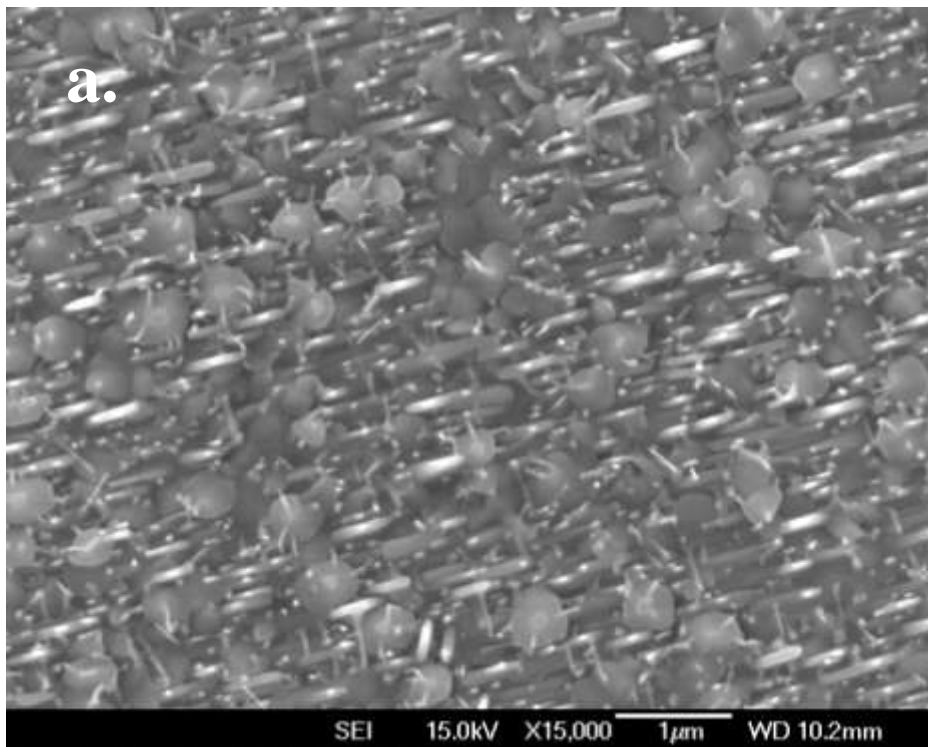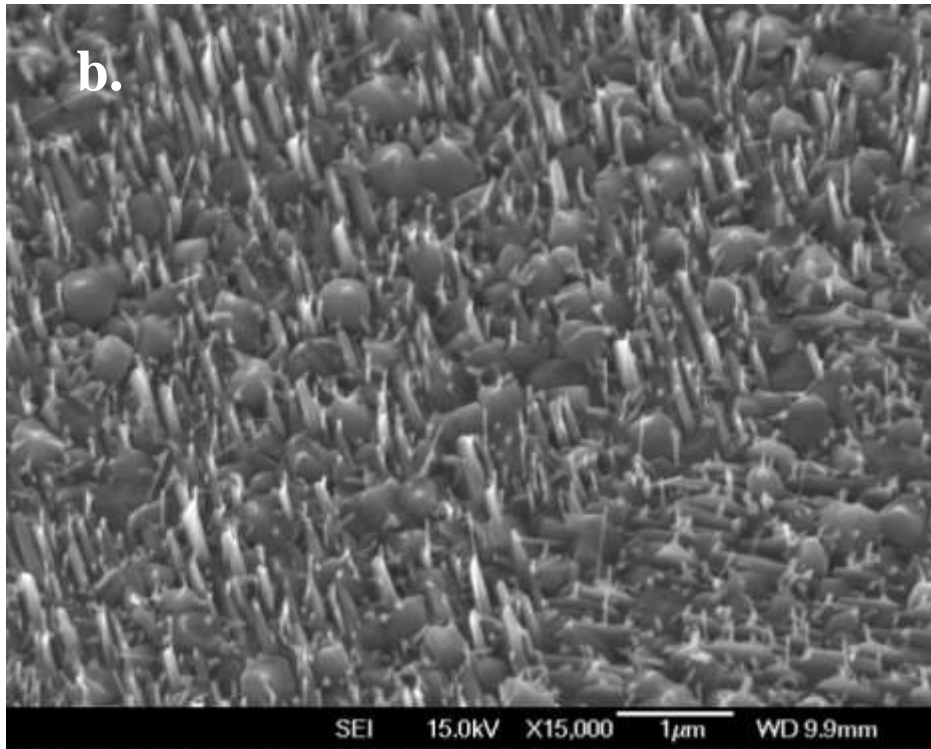
Fig.4.2.5.2 SEM images of AZO-013 on MgO(100), under 750°C and 1.2Torr oxygen pressure, with a target-substrate distance of 55mm in chamber #1,

a) top view, magnification of 15,000; b) 30° tilt, magnification of 15,000
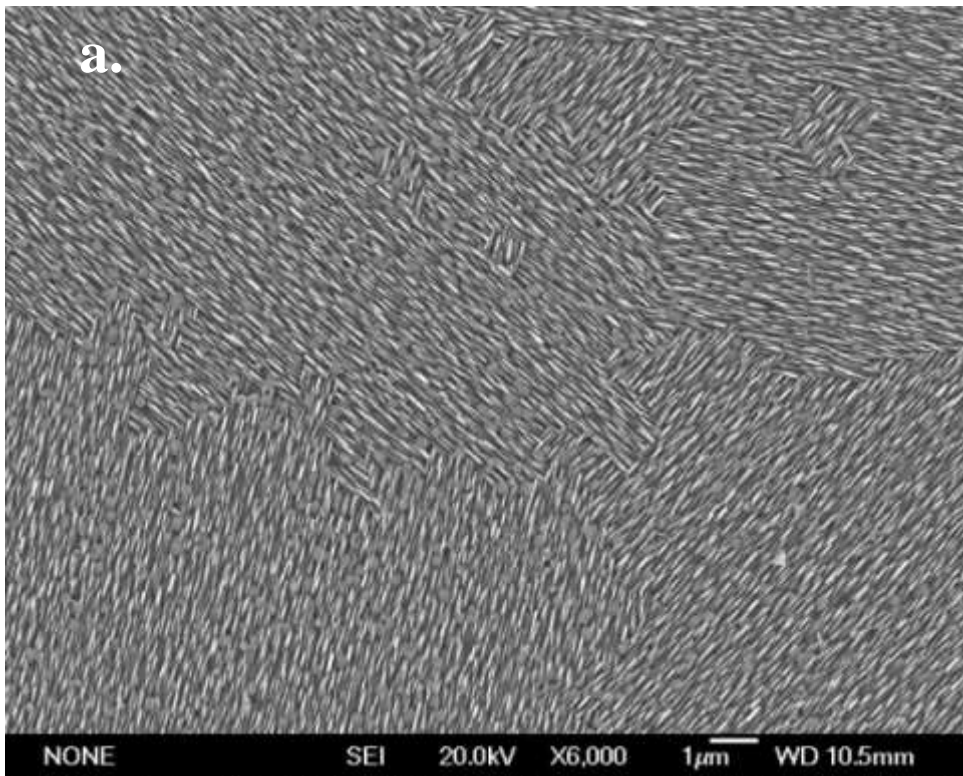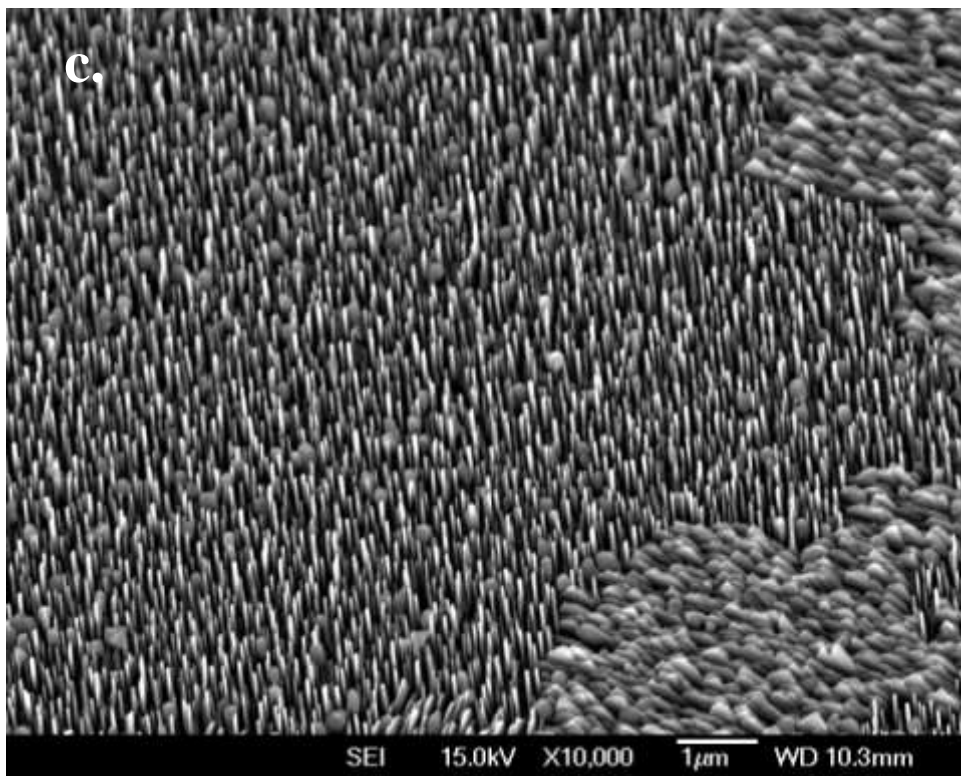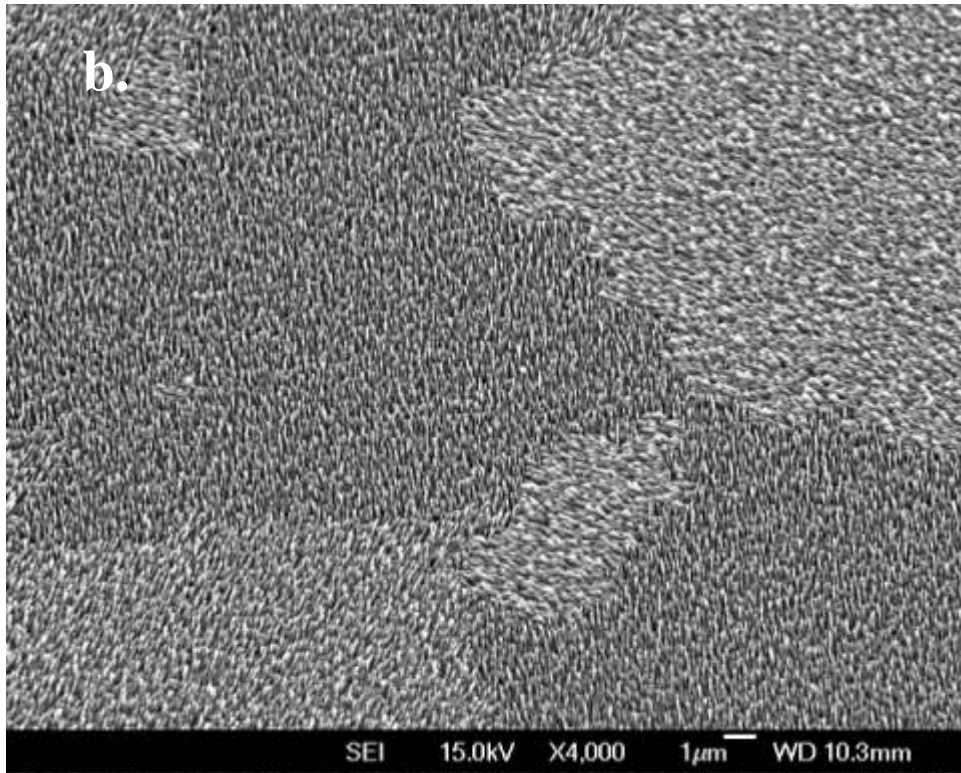
Fig.4.2.5.3 SEM images of AZO-014 on MgO(100), under 700°C and 1.2Torr oxygen pressure, with a target-substrate distance of 55mm in chamber #1,

a) top view, magnification of 6000; b) 30° tilt, magnification of 4000;
c) 30° tilt, magnification of 10,000

131

The crystalline structure of the ZnO samples AZO-013 and AZO-014 were further studied by XRD. As shown in Fig.4.2.5.4, ZnO wurtzite characteristic peaks can be seen as (100), (002), (101), (200), (004) and (202). When reducing the temperature, peaks (101) and (202) become weaker, while peaks (002) and (004) become stronger. This indicates that a lower temperature creates less complex structure.
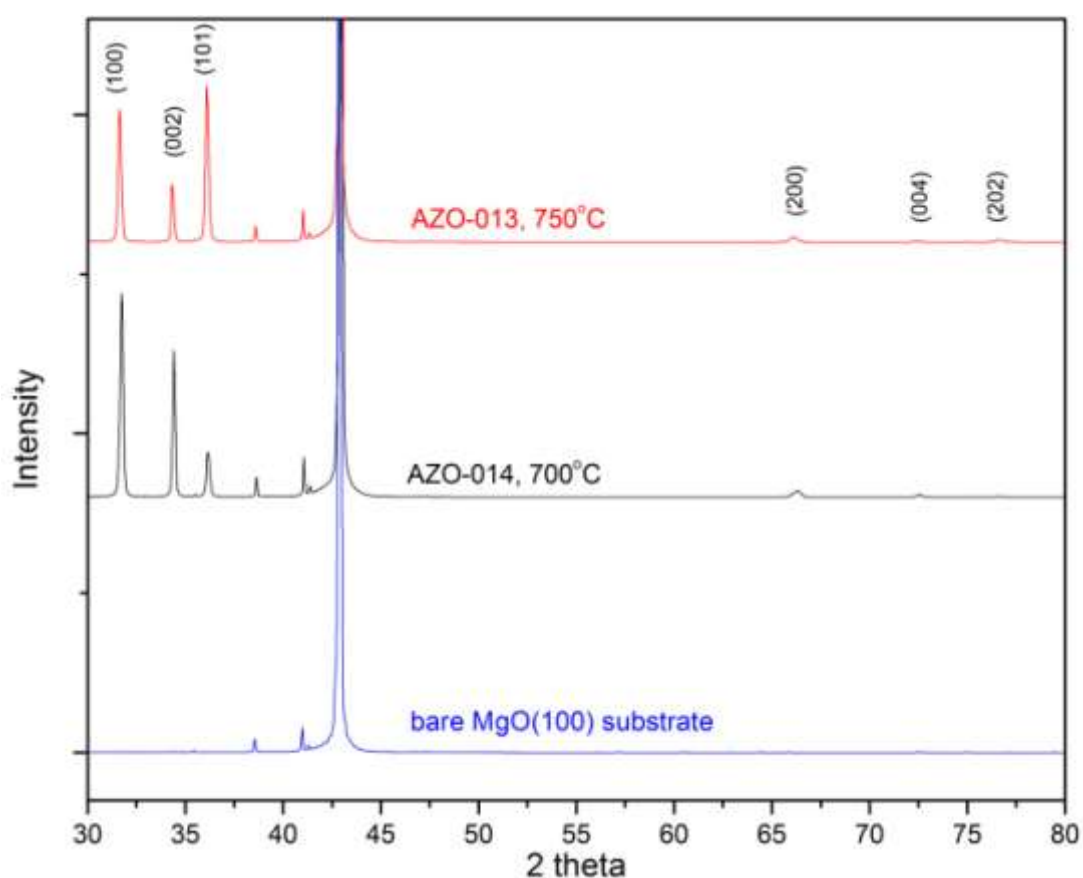
Fig. 4.2.5.4 XRD pattern of ZnO samples of AZO-013, AZO-014 and bare MgO(100) substrate

Several other depositions were conducted, with a reduction in temperature from 650°C to 500°C in chamber #3, with the details shown in Table 4.10. When the temperature was decreased from 650°C to 600°C, sample AZO-053 in Fig.4.2.5.5 and sample AZO-054

in Fig.4.2.5.6 were compared and observed. The most obvious difference, between the samples, was the quantity of perpendicular nanorods found on the substrate with the length of 550~750nm and width of 50~100nm. As discussed in the previous section, perpendicular nanorods are grown in lower energetic environment, which could also explain the situation in this case. The length of oblique nanorods do not have an obvious change in terms of length, in which the length is kept at 650nm~1.6μm in both cases. However the width becomes smaller, varying from 70~150nm to 20~100nm.

Decreasing the temperature to 500°C, sample AZO-055 displays a different morphology. ZnO nanorods orientated in random directions can be found on the surface with varying lengths from 250nm to 5.5μm and widths of 150nm~270nm. This may have been due to, under higher temperatures, it is easier for the coated gold layer to form smaller sized gold nanodots in uniform distribution due to the surface tension becoming smaller. Also in lower temperatures, the crystallinity is lower. Therefore, as a result, in lower temperatures, it is more difficult for nanorods to form and distribute evenly on the surface.
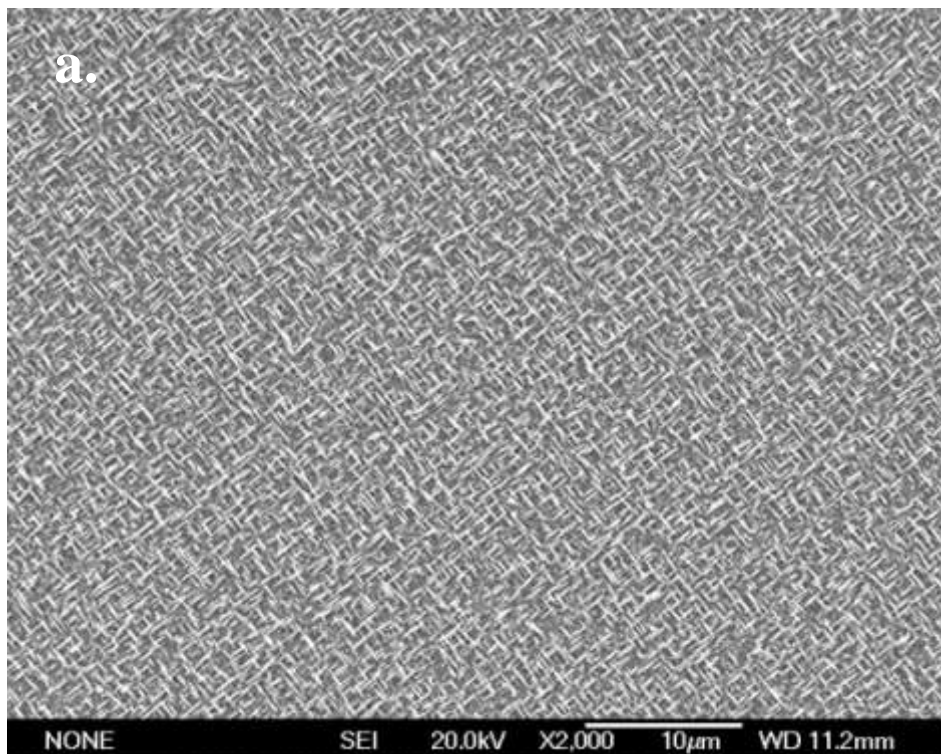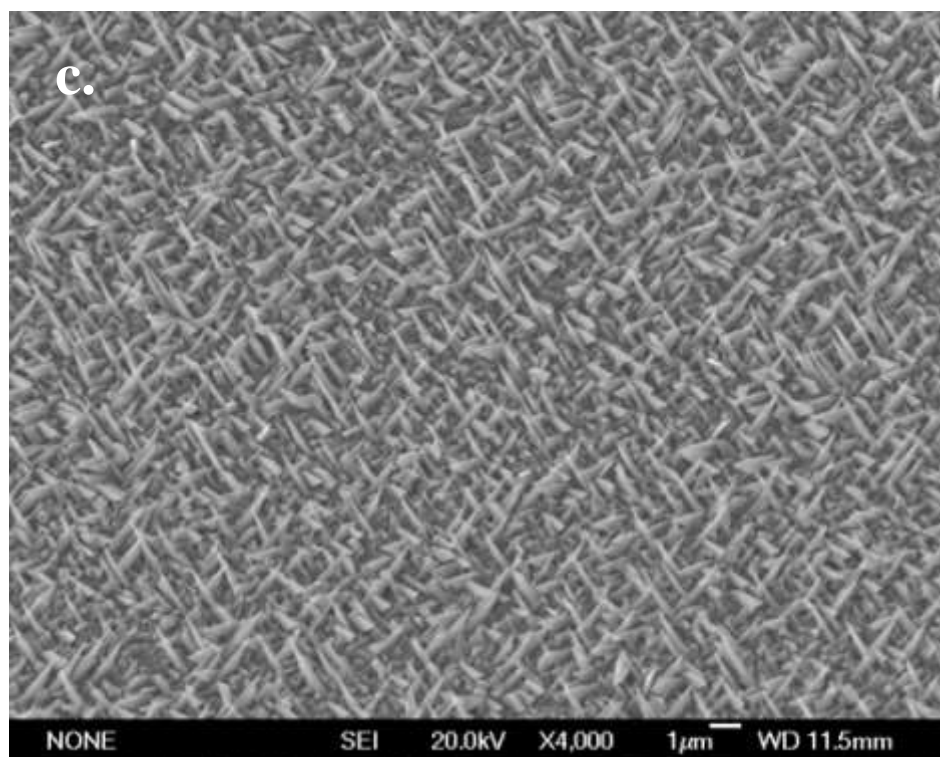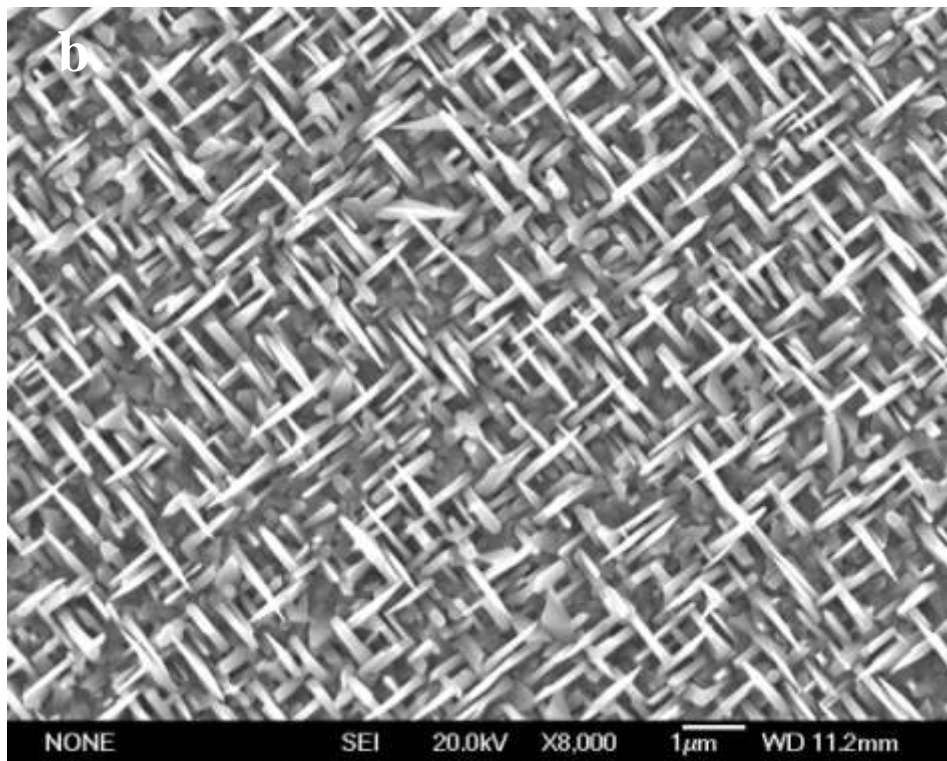
Fig.4.2.5.5 SEM images of AZO-053 on MgO(100), under 650°C and 1.2Torr oxygen pressure, with a target-substrate distance of 55mm in chamber #3,

a) top view, magnification of 2000; b) top view, magnification of 8000; c) 30° tilt, magnification of 4000

134
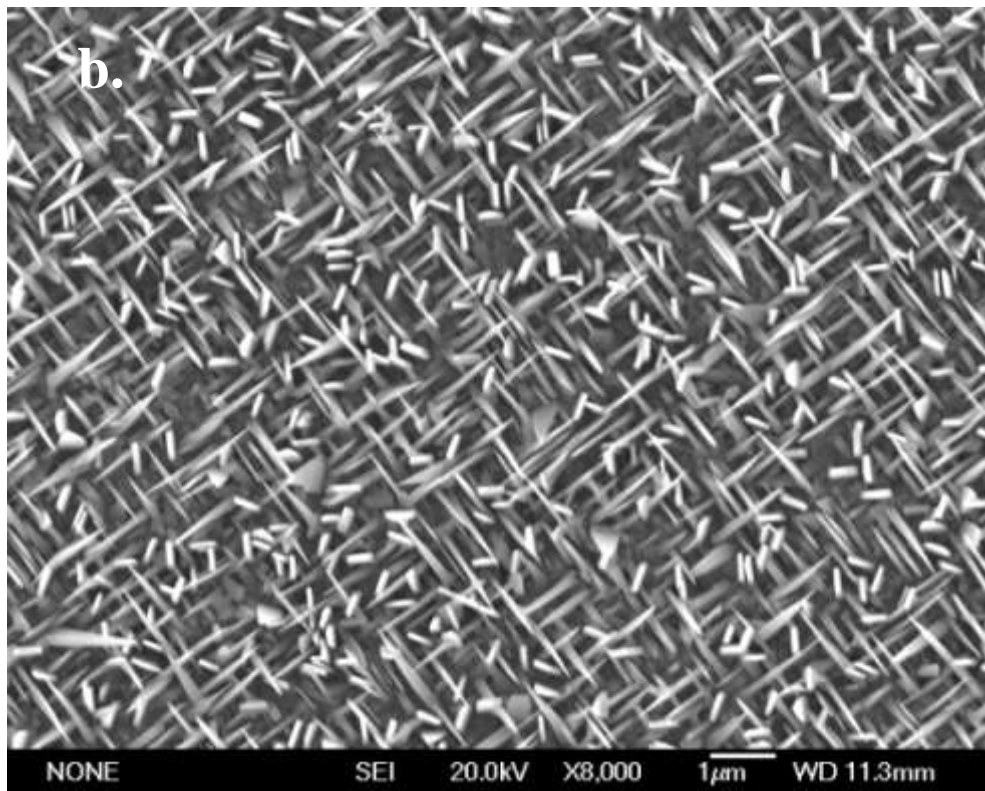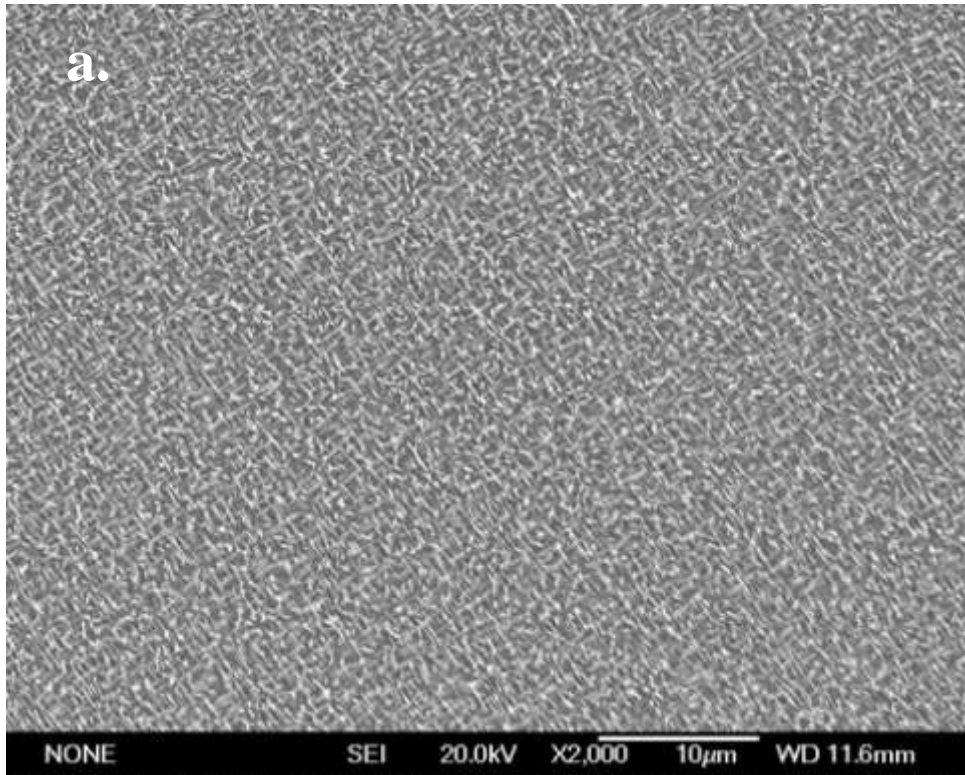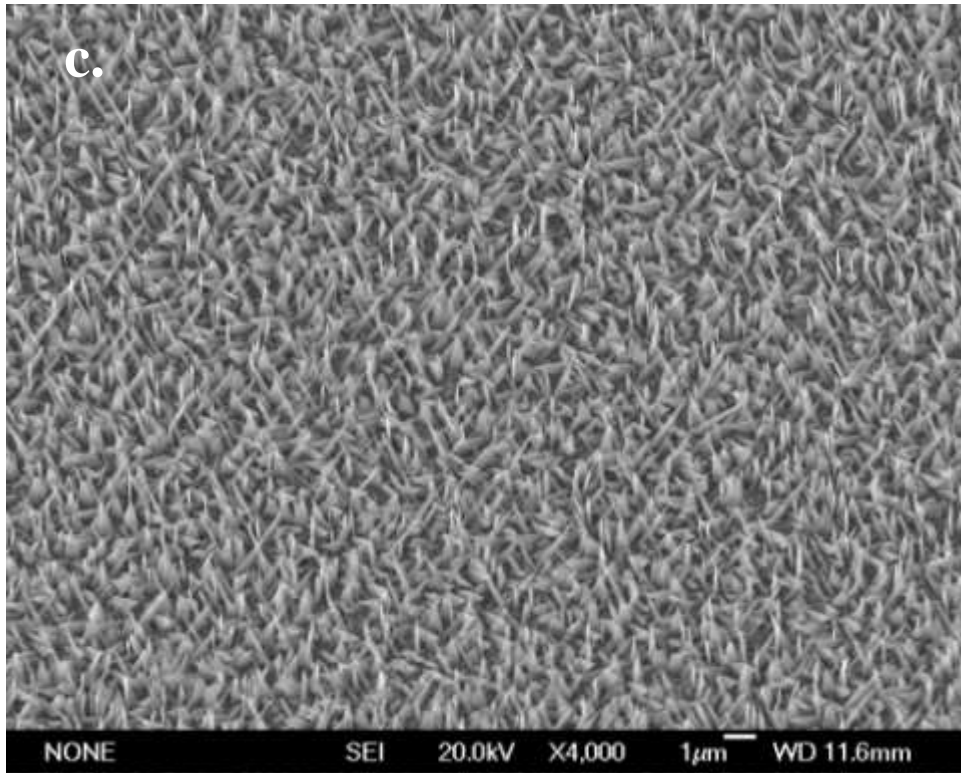
Fig.4.2.5.6 SEM images of AZO-054 on MgO(100), under 600°C and 1.2Torr oxygen pressure, with a target-substrate distance of 55mm in chamber #3,

a) top view, magnification of 2000; b) top view, magnification of 8000; c) 30° tilt, magnification of 4000

NONE   SEI   20.0kV   X3,500   1μm   WD 10.7mm

NONE   SEI   20.0kV   X8,000   1μm   WD 10.9mm
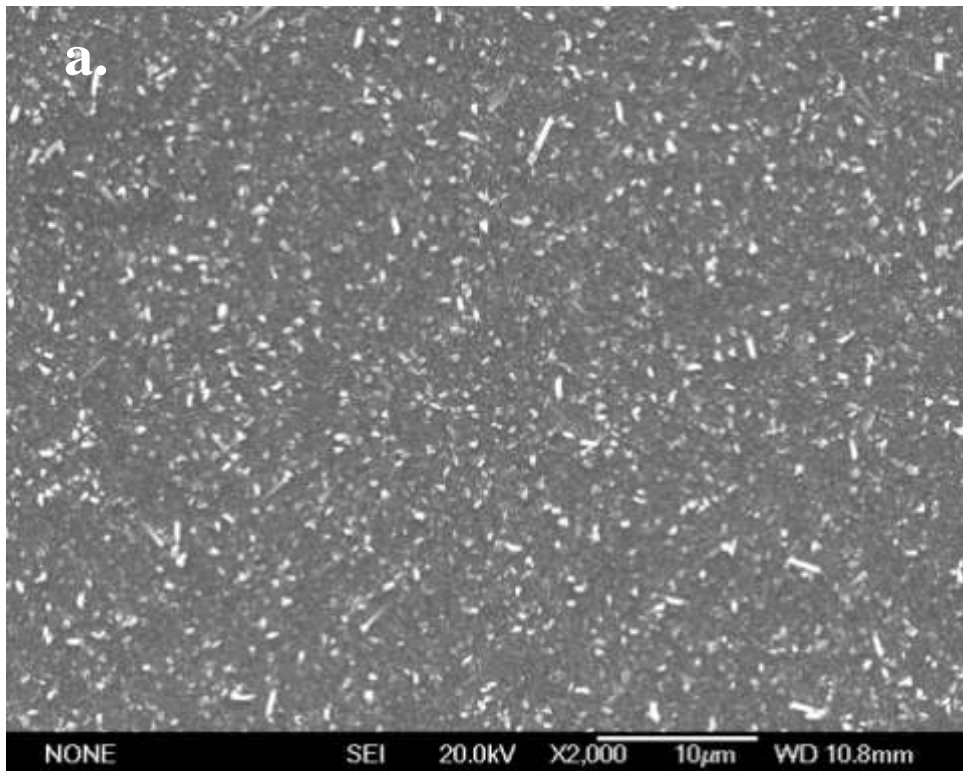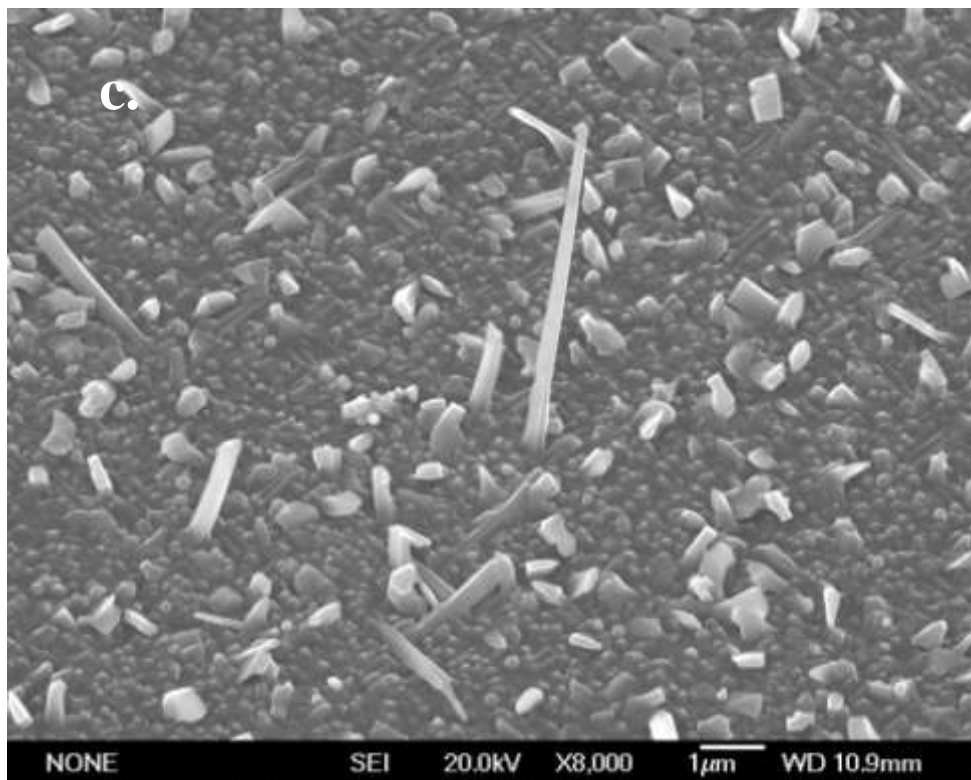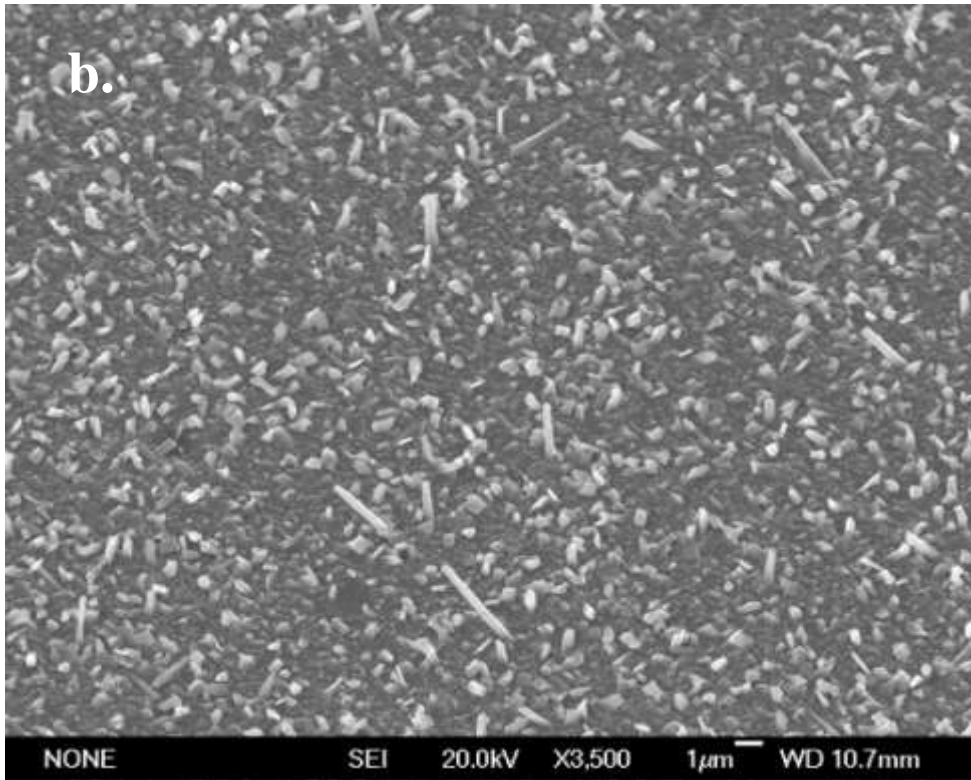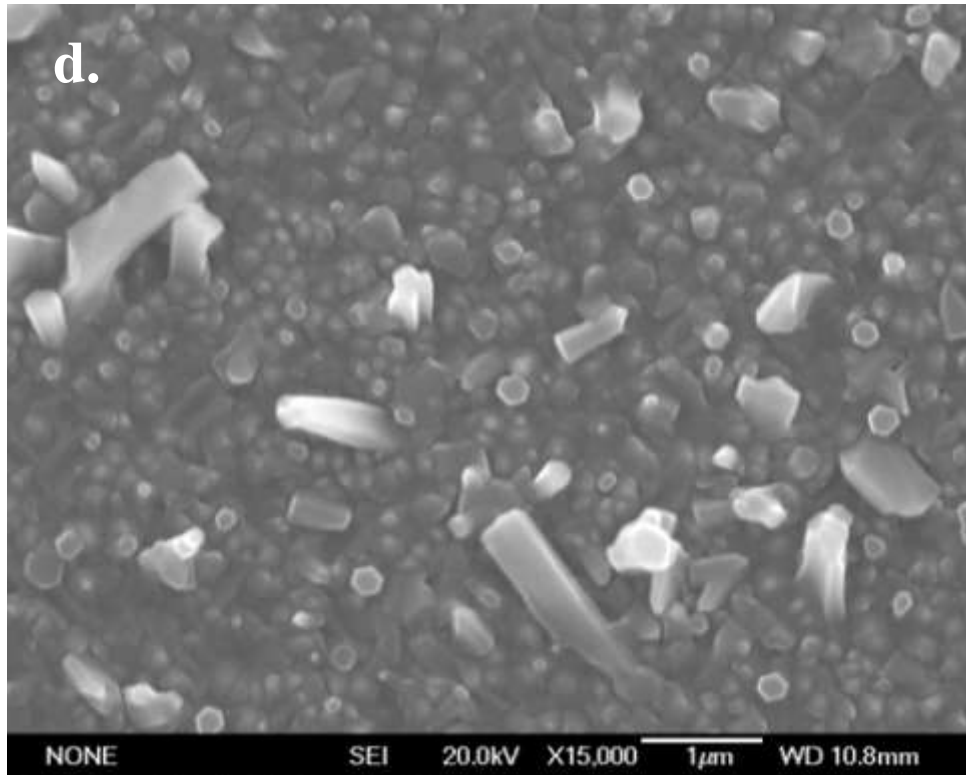
Fig.4.2.5.7 SEM images of AZO-055 on MgO(100), under 500°C and 1.2Torr oxygen pressure, with a target-substrate distance of 55mm in chamber #3,

a) top view, magnification of 2000; b) 30° tilt, magnification of 3500;
c) 30° tilt, magnification of 8000; d) top view, magnification of 15,000.

In this instance, glass was used, which is an amorphous (non-crystalline) solid material, as the substrate to investigate the influence of temperature. Since glass cannot bear as high of a temperature as MgO single crystalline substrate, the temperature was varied from 600°C to 400°C. Compared with the ZnO grown on single crystal substrate, the deposition on amorphous substrates shows nanocone structures formed in random directions instead of nanorods or nanowires formed in specific directions. As a larger sized (size of 10mm×10mm) glass substrate was used, the ZnO deposition does not show a uniform morphology as those deposited on MgO substrates over the entire substrate, as shown in Fig.4.2.5.8a. At area II in Fig.4.2.5.8b and c, intensive nanocones were produced, while approaching the area between

area II and I, shown in Fig.4.2.5.8d, the quantity of nanocones becomes less intensive. However, at area I in Fig.4.2.5.8e, the nanocones become sparse. The base width of these nanocones is between 200nm to 500nm, and the length is between 480nm to 4μm. The influence of the use of different substrates will be discussed in the next section.

Decreasing the temperature to 500°C, sample AZO-067, shown in Fig.4.2.5.9, has a similar morphology with AZO-055 in Fig.4.2.5.7. Both depositions were conducted with the same temperature, but the one on the glass substrate resulted in a smaller quantity of extreme long nanocones/ nanorods.

At 400°C, sample AZO-068, in Fig. 4.2.5.10, shows a comparatively smooth surface, without any particular nanostructures due to the low energetic environment at the lower temperature.

b.

NONE   SEI   10.0kV   X2,000   10μm   WD 8.9mm


c.

NONE   SEI   10.0kV   X8,000   1μm   WD 8.9mm
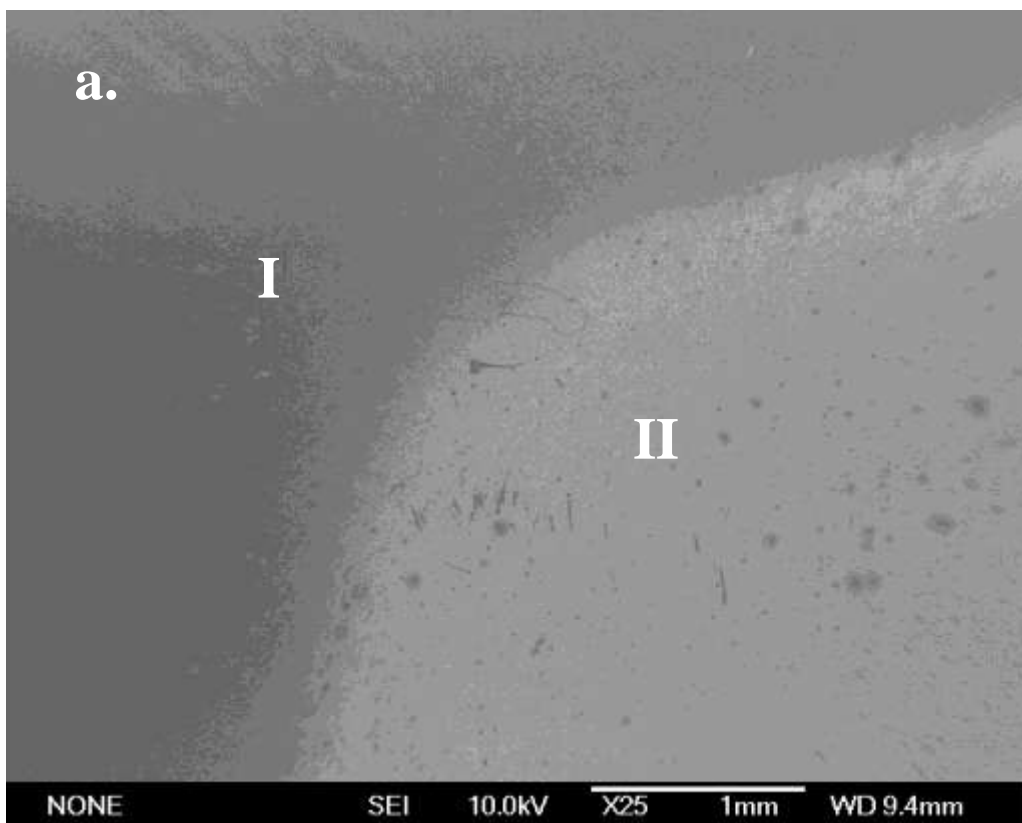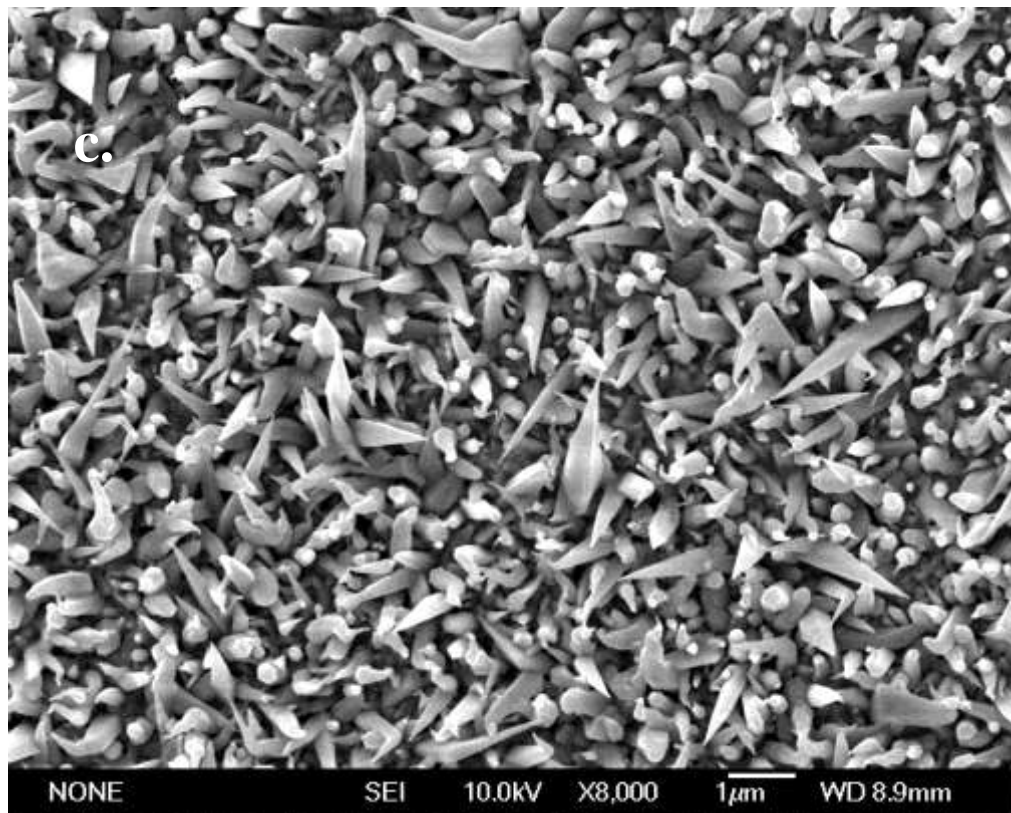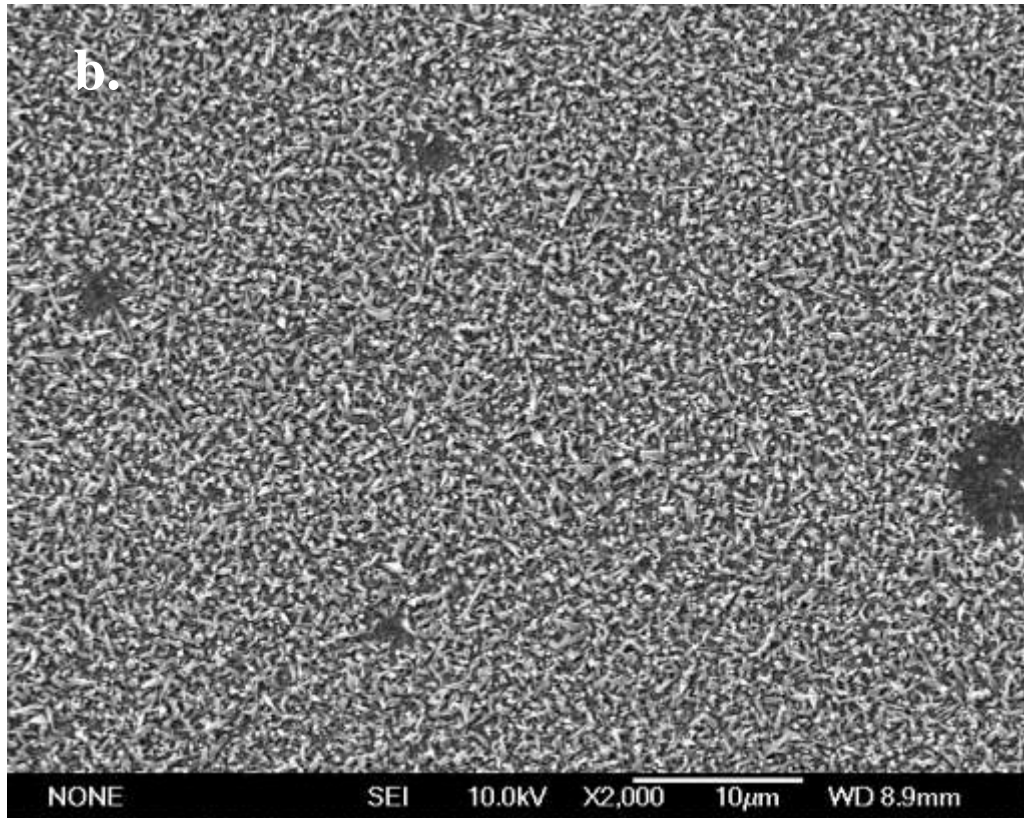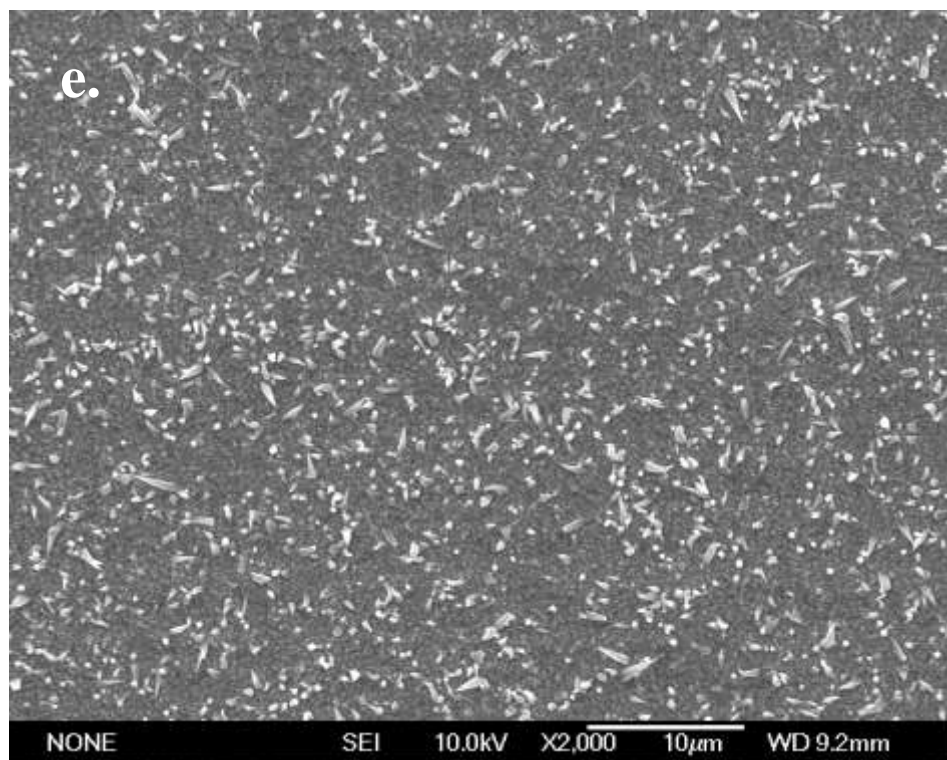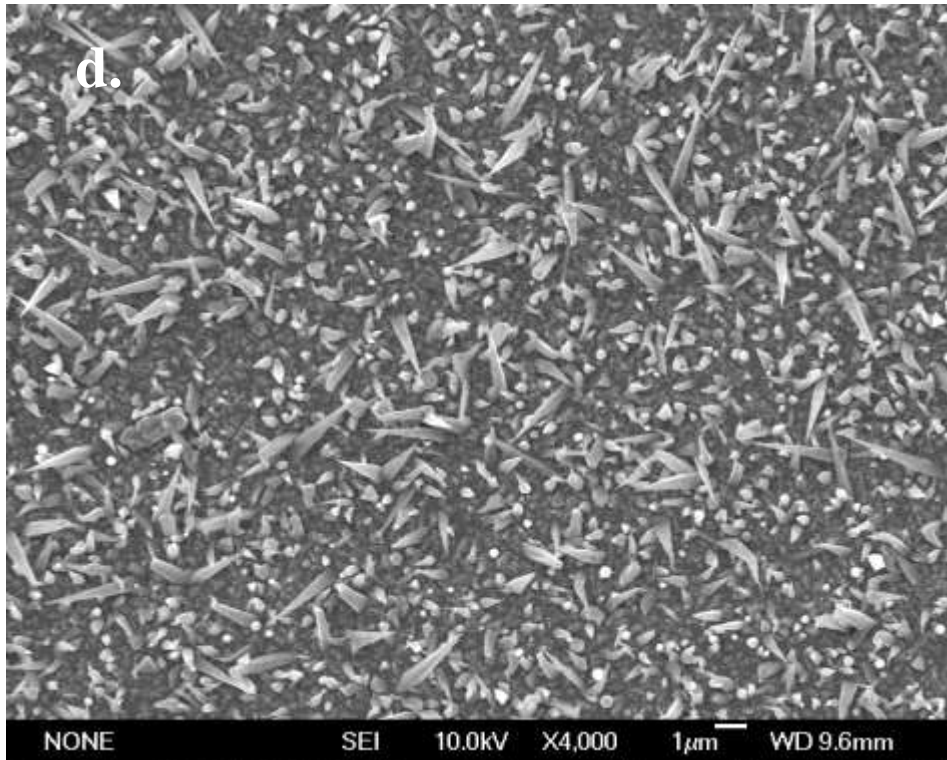
Fig.4.2.5.8 SEM images of AZO-066 on glass, under 600°C and 1.2Torr oxygen pressure, with a target-substrate distance of 50mm in chamber #2

a) top view, magnification of 25; b) top view of area II, magnification of 2000; c) top view of area II, magnification of 8000; d) top view of area between I and II, magnification of 4000; e) top view of area I, magnification of 2000.
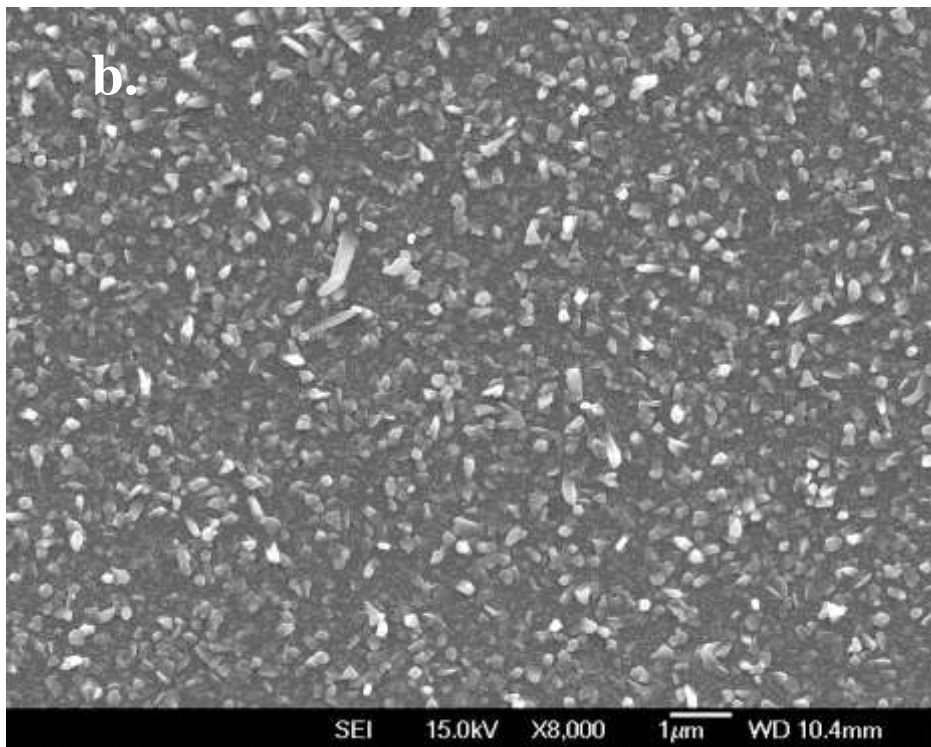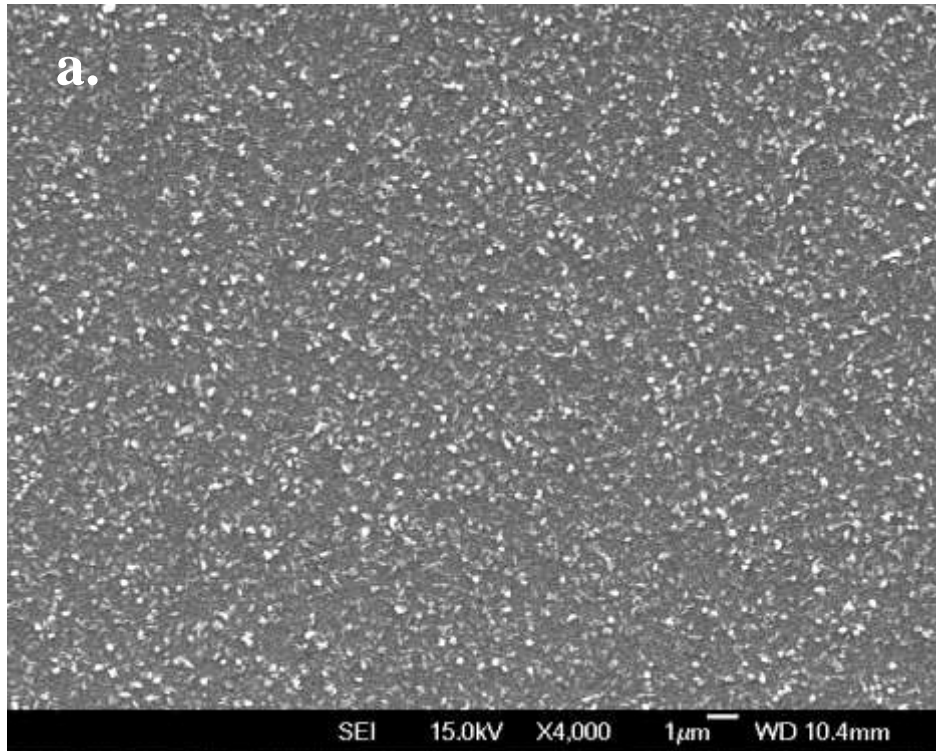
Fig.4.2.5.9 SEM images of AZO-067 on glass, under 500°C and 1.2Torr oxygen pressure, with a target-substrate distance of 50mm in chamber #2

a) top view, magnification of 4000; b) top view, magnification of 8000
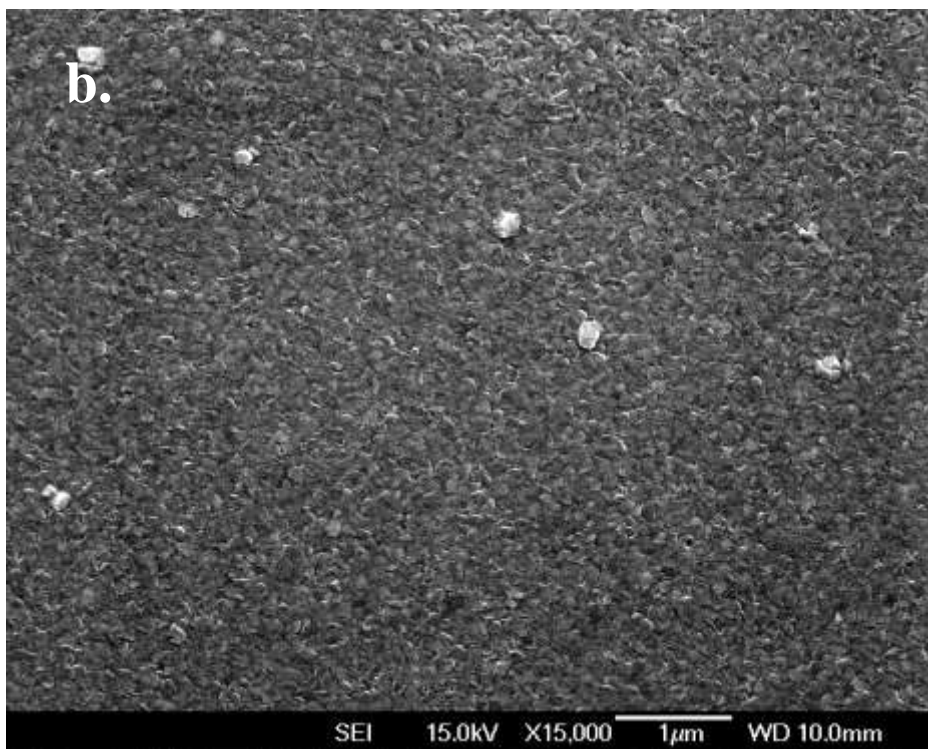
Fig.4.2.5.10 SEM images of AZO-068 on glass, under 400°C and 1.2Torr oxygen pressure, with a target-substrate distance of 50mm in chamber #2

a) top view, magnification of 8000; b) top view, magnification of 15,000

By increasing the distance of target to substrate to 60mm in chamber #2 and varying the temperature from 700°C to 600°C. At 700°C, two shaped nanostructures, sparsely distributed on the surface in different directions are shown in Fig.4.2.5.11. Perpendicular nanorods and oblique nanocones were formed. However a high density of perpendicular nanocones were observed with the deposition temperature of 600°C, shown in Fig.4.2.5.12. In both cases, the width is kept between 50nm~130nm and the length decreases from 100nm~1µm to 40nm~60nm. This change may be due to that in higher temperatures the growth speed is higher.

The influence of the distance of target to substrate will be discussed in the Influence of target-substrate distance section.
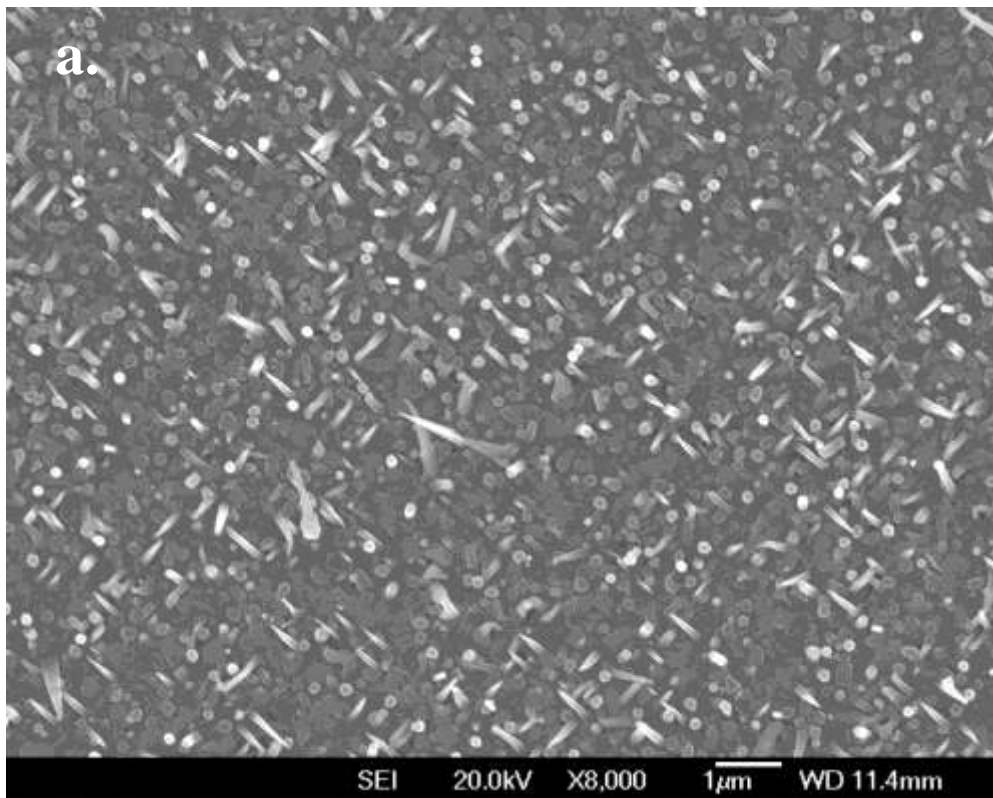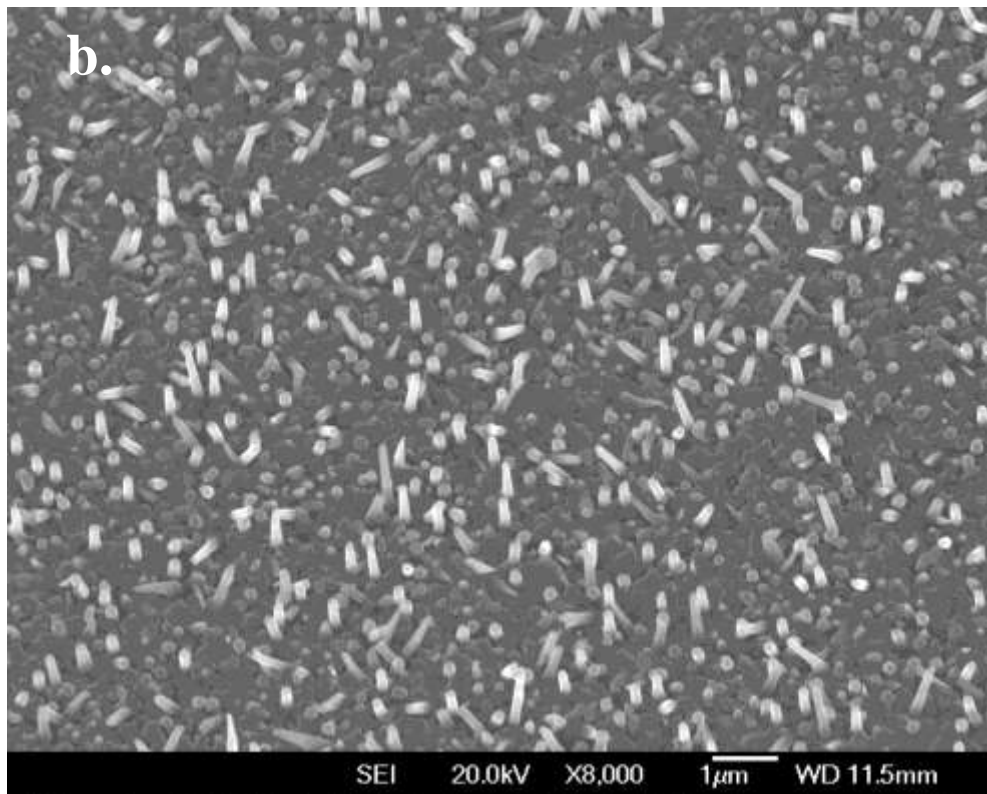
Fig.4.2.5.11 SEM images of AZO-082 on MgO(100), under 700°C and 1.2Torr oxygen pressure, with a target-substrate distance of 60mm in chamber #2

a) top view, magnification of 8000; b) 30° tilt, magnification of 8000
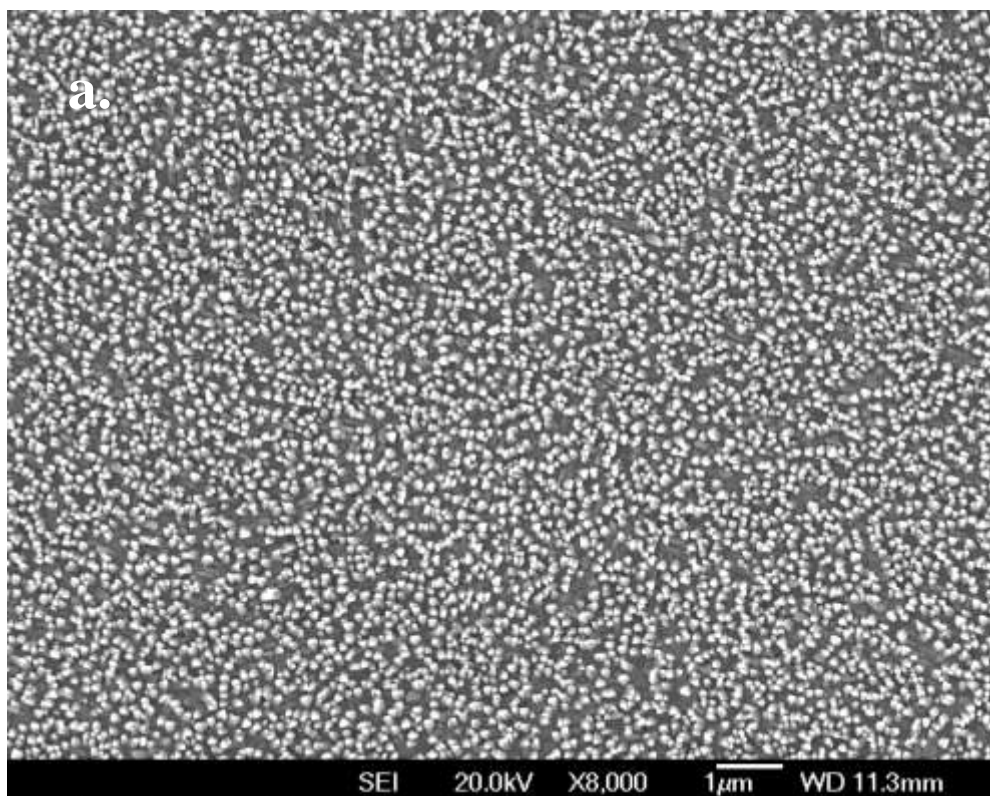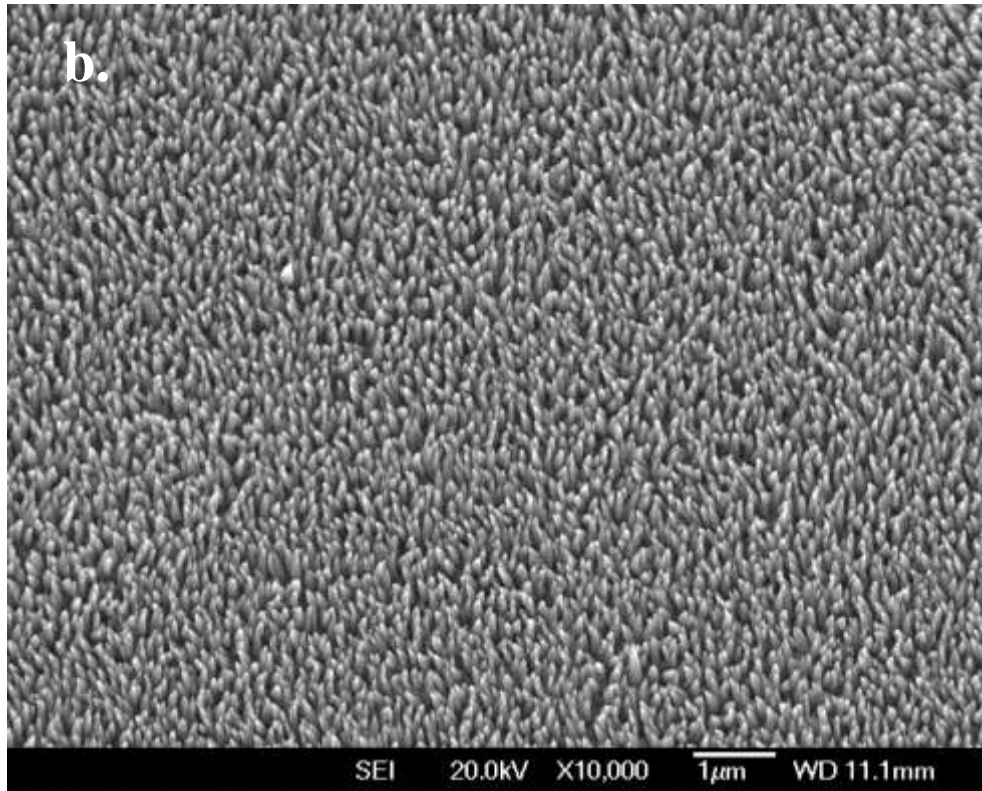
Fig.4.2.5.12 SEM images of AZO-083 on MgO(100), under 600°C and 1.2Torr oxygen pressure, with a target-substrate distance of 60mm in chamber #2

a) top view, magnification of 8000; b) 30° tilt, magnification of 10,000

In conclusion, wurtzite structured ZnO nanorods/nanocones were produced only in specific temperatures during the deposition, in which these temperatures cannot be too high or too low. Lower temperatures result in the formation of more perpendicular nanorods/nanocones. However, if the temperature is too low, the energy provided from the substrate is not high enough to form particular nanostructures. If the temperature is too high, ZnO grows in more orientations, resulting in more complex nanostructures. Therefore, from these observations it can be concluded that 600°C is the optimal temperature.

4.2.6 Influence of different substrates

Various substrates were utilized in this project in order to investigate how different substrates influence the morphology. It was also discovered that some certain parameters may not be as influential to the morphology as opposed to setting other parameters at specific values.

Table 4.2.13 Detailed parameters of the samples AZO-058 and 059

Sample Number	Chamber number	substrate	Temperature (˚C)	Number of pulses on Gold(shot)	Number of pulses on ZnO(shot)	Oxygen pressure (mTorr)	Distance of target-substrate (mm)
AZO-058	#3	MgO(100)	700	5	5000	2000	55
AZO-059	#3	MgO(001)	700	5	5000	2000	55

Table 4.2.14 Detailed parameters of the samples AZO-0691, 0692 and 0693

Sample Number	Chamber number	substrate	Temperature (˚C)	Number of pulses on Palladium (shot)	Number of pulses on ZnO(shot)	Oxygen pressure (mTorr)	Distance of target-substrate (mm)
AZO-0691	#2	Glass	600	5	5000	1200	60
AZO-0692	#2	MgO(100)	600	5	5000	1200	60
AZO-0693	#2	Si(100)	600	5	5000	1200	60

Table 4.2.15 Detailed parameters of the samples AZO-0701, 0702 and 0703

Sample Number	Chamber number	substrate	Temperature (˚C)	Number of pulses on Silver (shot)	Number of pulses on ZnO(shot)	Oxygen pressure (mTorr)	Distance of target-substrate (mm)
AZO-0701	#2	Glass	600	5	5000	1200	60
AZO-0702	#2	MgO(100)	600	5	5000	1200	60
AZO-0703	#2	Si(100)	600	5	5000	1200	60

Table 4.2.16 Detailed parameters of the samples AZO-081 and 082

Sample Number	Chamber number	substrate	Temperature (˚C)	Number of pulses on Gold(shot)	Number of pulses on ZnO(shot)	Oxygen pressure (mTorr)	Distance of target-substrate (mm)
AZO-081	#2	Al_2O_3 ceramic	700	5	5000	1200	60
AZO-082	#2	MgO(100)	700	5	5000	1200	60

MgO(100) substrates have identical crystallography to MgO(001) as the crystal structure of MgO is halite (cubic). However, comparing the layers coated on MgO(100) and MgO(001) in Fig.4.2.6.1and Fig.4.2.6.2, on MgO(100) perpendicular nanorods were formed, while on MgO(001) there were no particular nanostructures detected. XRD patterns, in Fig.4.2.6.3, also explain this phenomenon. In sample AZO-059, which was produced on MgO(001), were two main peaks of (002) and (101). The intensity of both peaks is at a similar value, while for AZO-058 produced on MgO(100), the intensity of peak(002) is extremely high when compared with other peaks of (101) and (004). This indicates that ZnO grows mainly in one orientation. The difference is related to different manufacturers, growth, and surface finishing techniques. Fig.4.2.6.4 is a corner image of AZO-059, which indicates nanowires grown on a partial MgO(001).
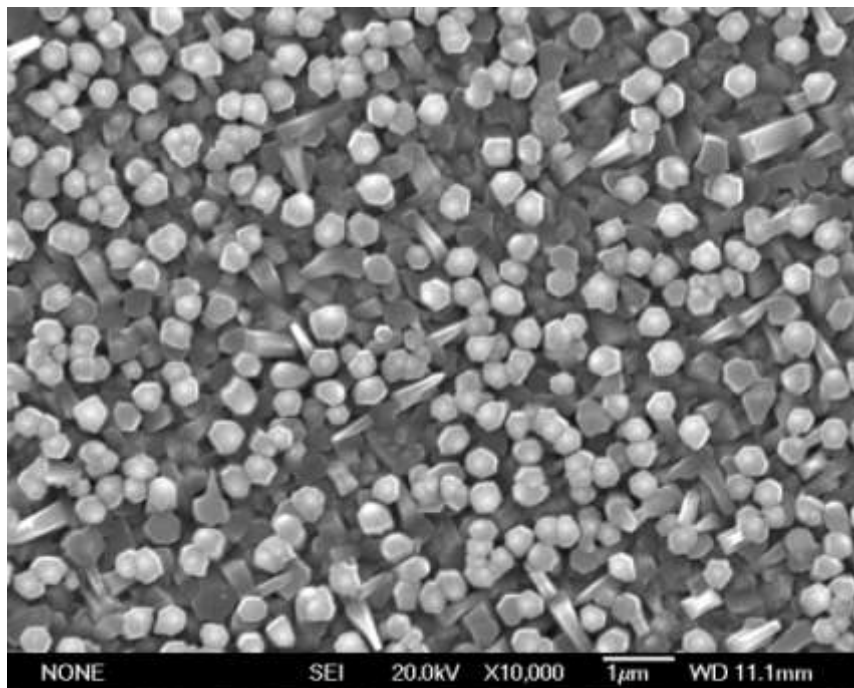
Fig.4.2.6.1 SEM image of AZO-058 on MgO(100), under 700°C and 2Torr oxygen pressure

with a target-substrate distance of 55mm in chamber #3, top view, magnification of 10,000
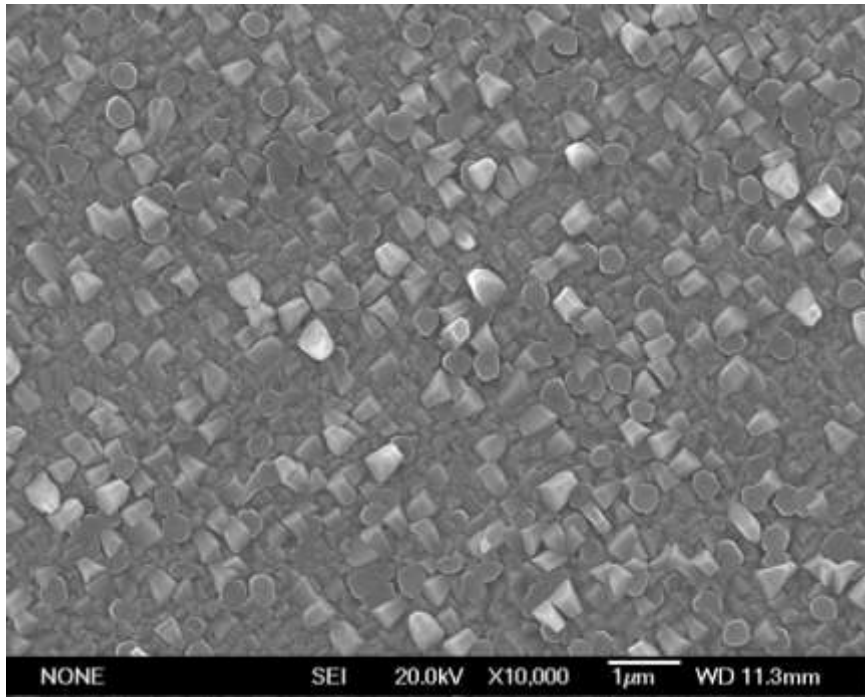
Fig.4.2.6.2 SEM image of AZO-059 on MgO(001), under 700°C and 2Torr oxygen pressure

with a target-substrate distance of 55mm in chamber #3, top view, magnification of 10,000
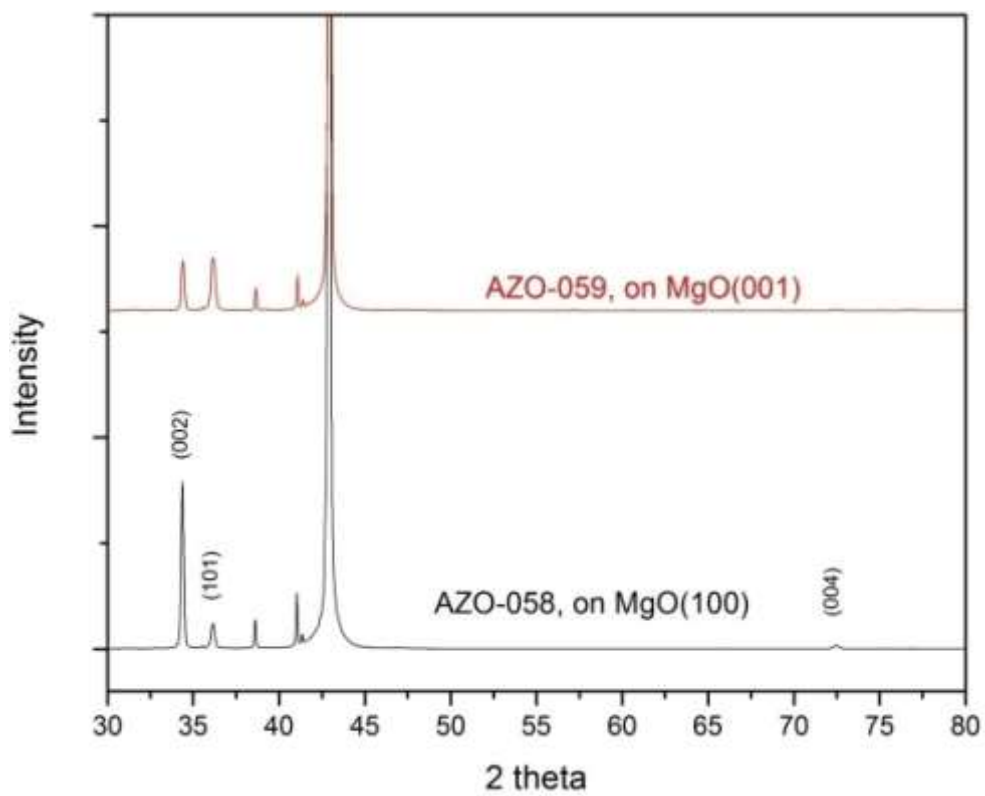
Fig.4.2.6.3 XRD pattern of ZnO samples of AZO-058, AZO-059
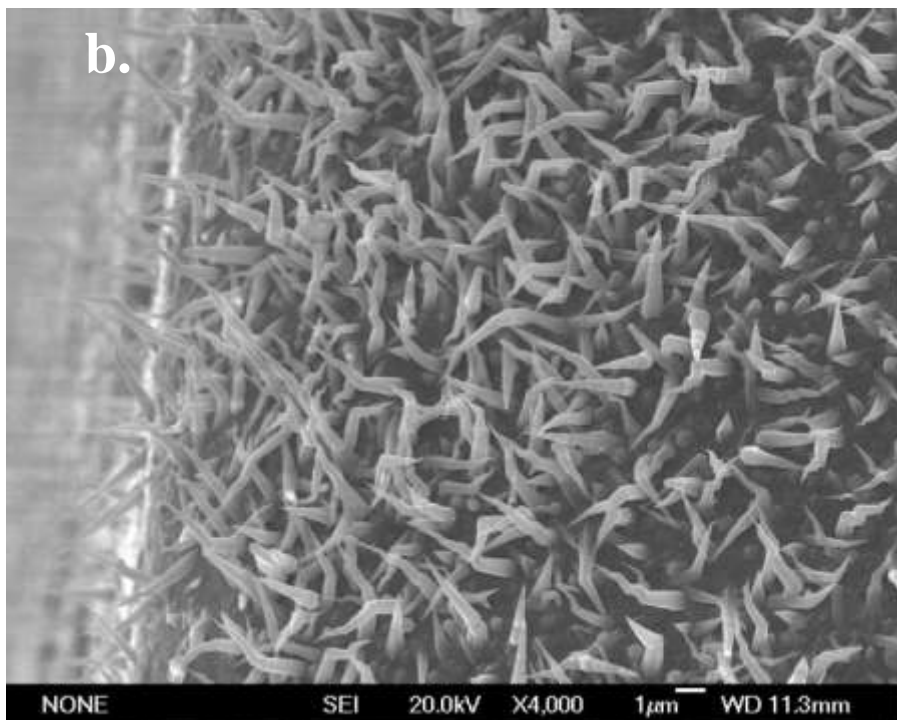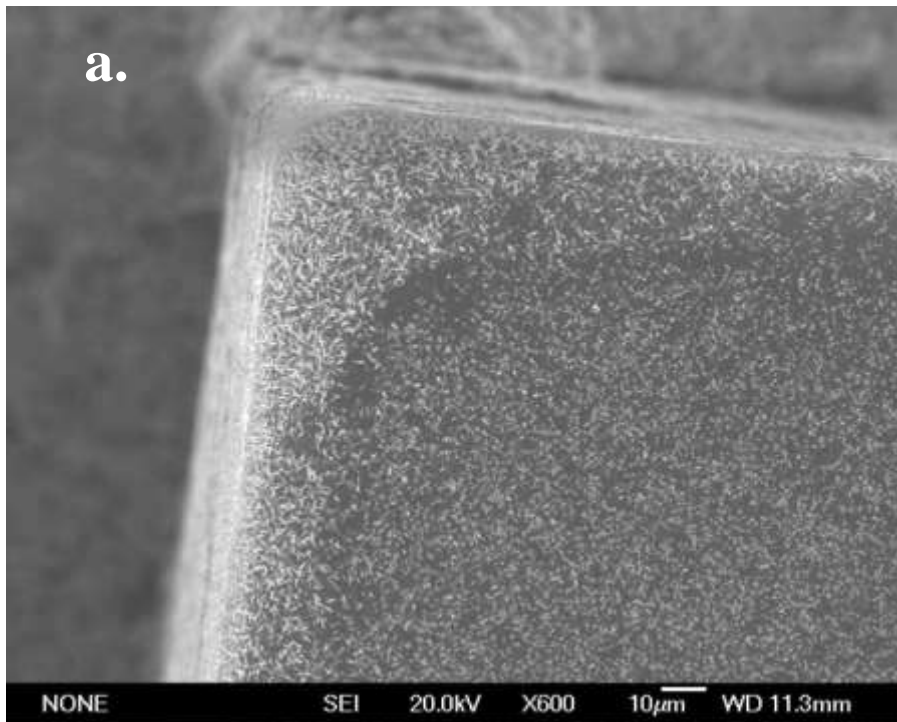
Fig.4.2.6.4 Corner SEM images of AZO-059 on MgO(001), under 700°C and 2Torr oxygen pressure
with a target-substrate distance of 55mm in chamber #3,

a) top view, magnification of 600; b)30°tilt, magnification of 4000

Samples AZO-0691 on glass, AZO-0692 on MgO(100), and AZO-0693 on Si(100) were produced by using palladium as the catalyst, instead of gold, in chamber #2. Many bulk crystals were formed in various shapes on the glass substrate, as shown in Fig.4.2.6.5. However, a large cluster of nanowires were eventually and successfully formed, evenly covering the surface on both MgO(100) and Si(100), shown in Fig.4.2.6.6 and Fig.4.2.6.7. For both samples, the morphology is very similar. The width of a single nanowire is approximately 40~60nm and length is greater than 3µm. This special morphology is different from any other ZnO samples produced in this project.
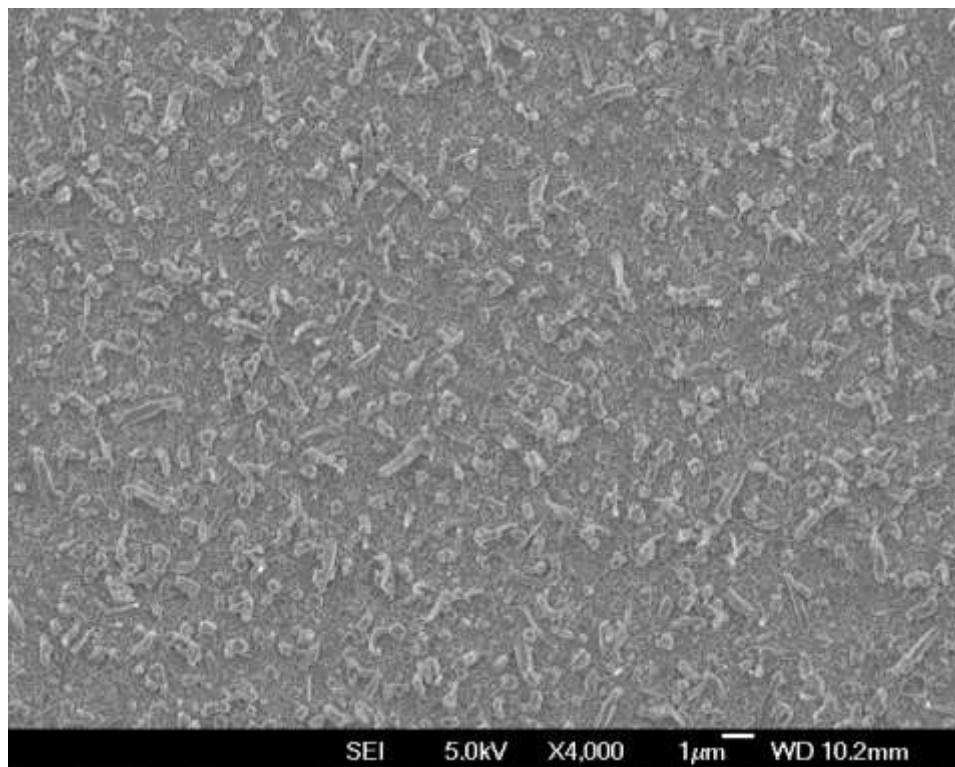
Fig.4.2.6.5 SEM image of AZO-0691 on glass, 5shots on Pd, at 600°C and 1.2Torr oxygen pressure with a target-substrate distance of 60mm in chamber #2
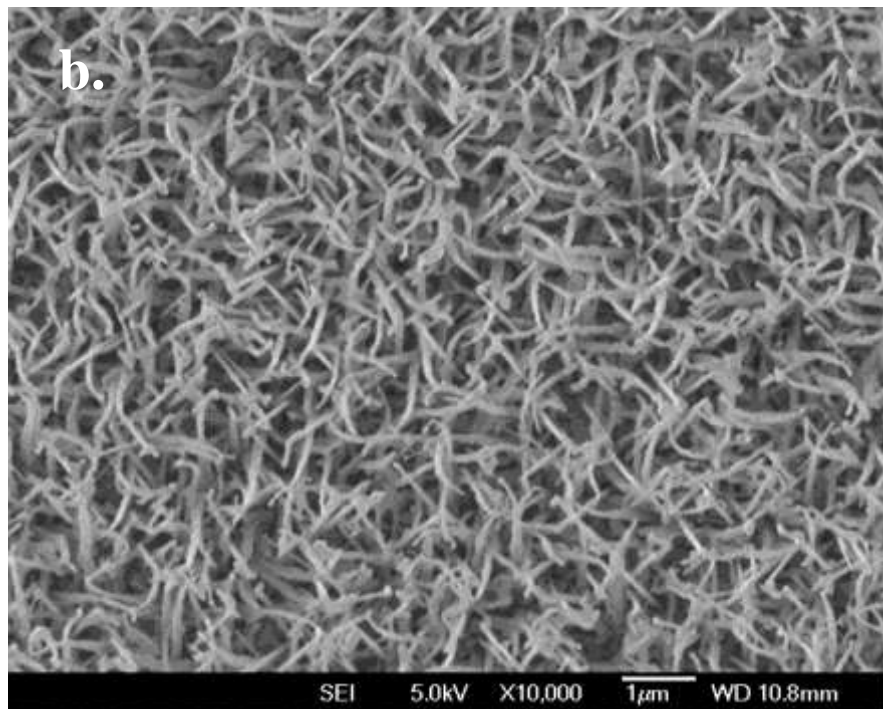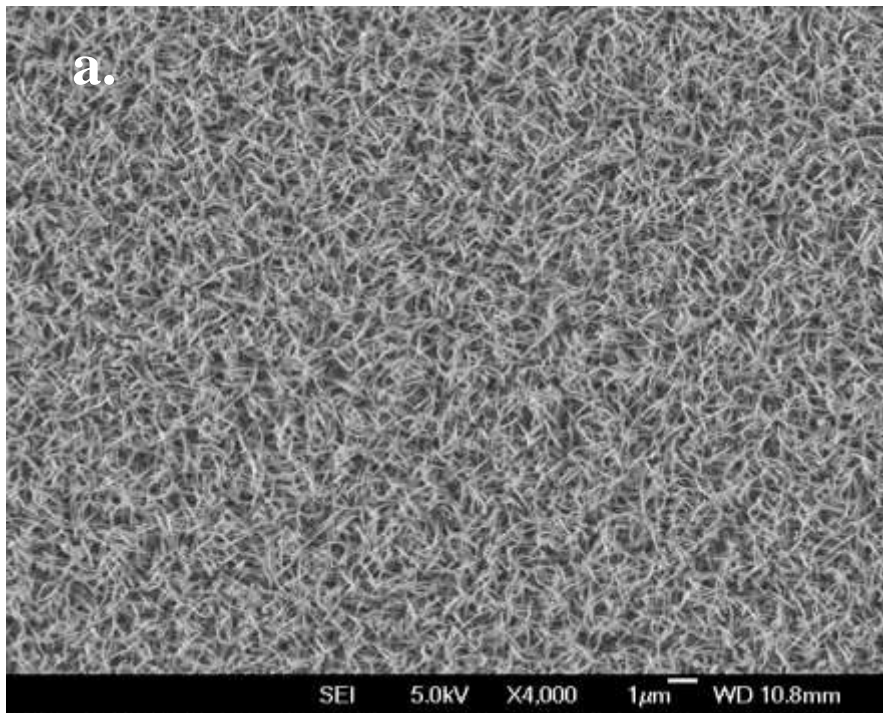
Fig.4.2.6.6 SEM images of AZO-0692 on MgO(100), 5shots on Pd, under 600°C and 1.2Torr oxygen pressure with a target-substrate distance of 60mm in chamber #2

a) top view, magnification of 4000; b)top view, magnification of 10,000
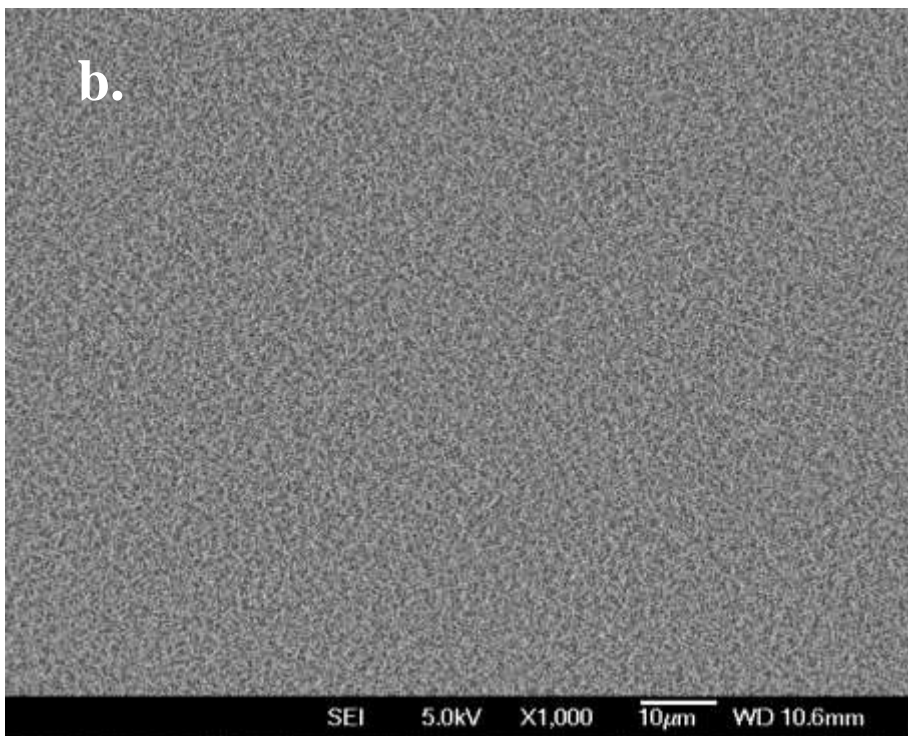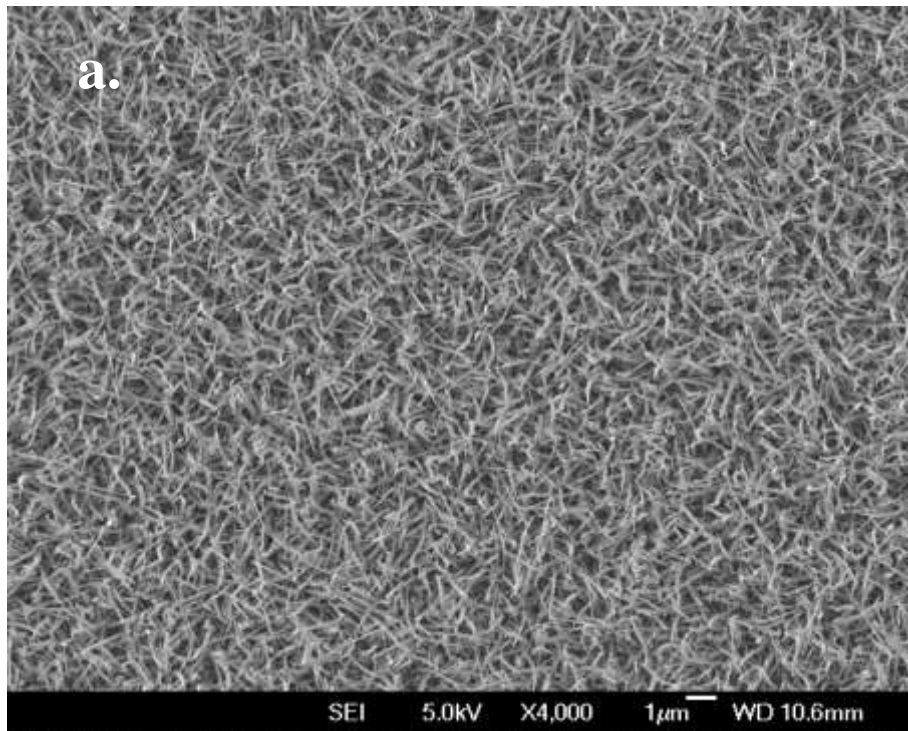
Fig.4.2.6.7 SEM images of AZO-0693 on Si(100), 5shots on Pd, under 600°C and 1.2Torr oxygen pressure with a target-substrate distance of 60mm in chamber #2

a) top view, magnification of 4000; b) top view, magnification of 1000

Samples AZO-0701, AZO-0702 and AZO-0703 were deposited in the same chamber under the same parameter settings and changing the catalyst to silver. The morphology of each sample is shown below. From the samples observed, only the layer on MgO(100) indicated a very neat crystalline growth along a-plane and c-plane as seen in Fig.4.2.6.9. The layer on Si(100) in Fig.4.2.6.10 was formed by evenly smaller sized of crystalline structures compared with those on glass. This is due to the natural properties of the substrate.
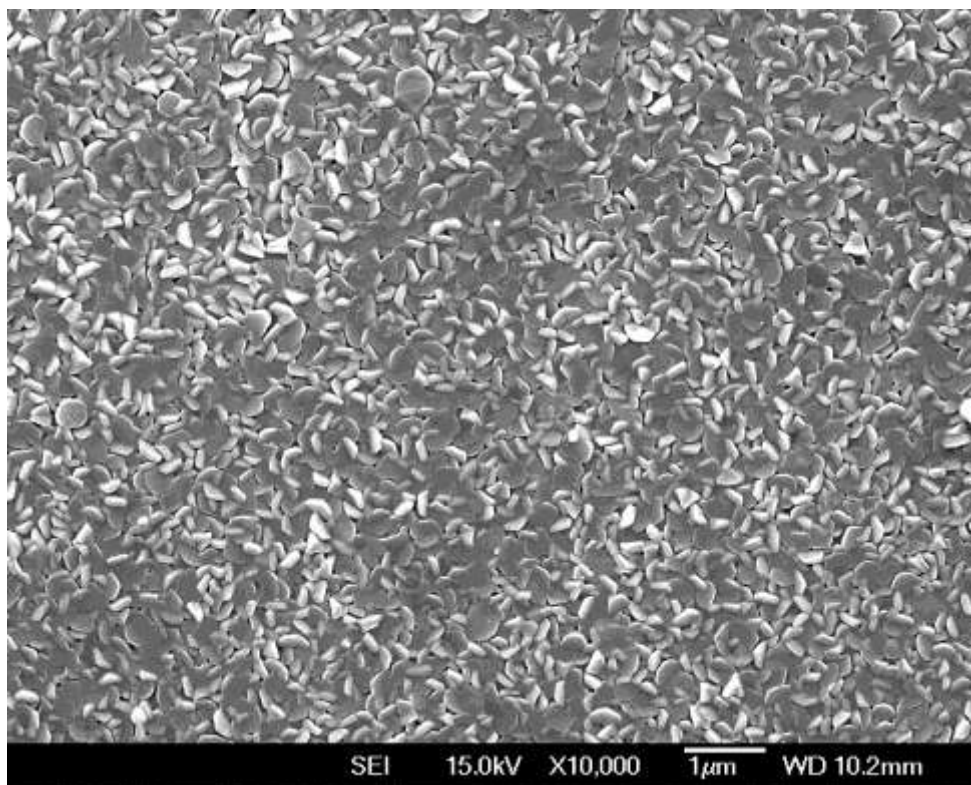
Fig.4.2.6.8 SEM image of AZO-0701 on glass, 5shots on Ag, under 600°C and 1.2Torr oxygen pressure with a target-substrate distance of 60mm in chamber #2
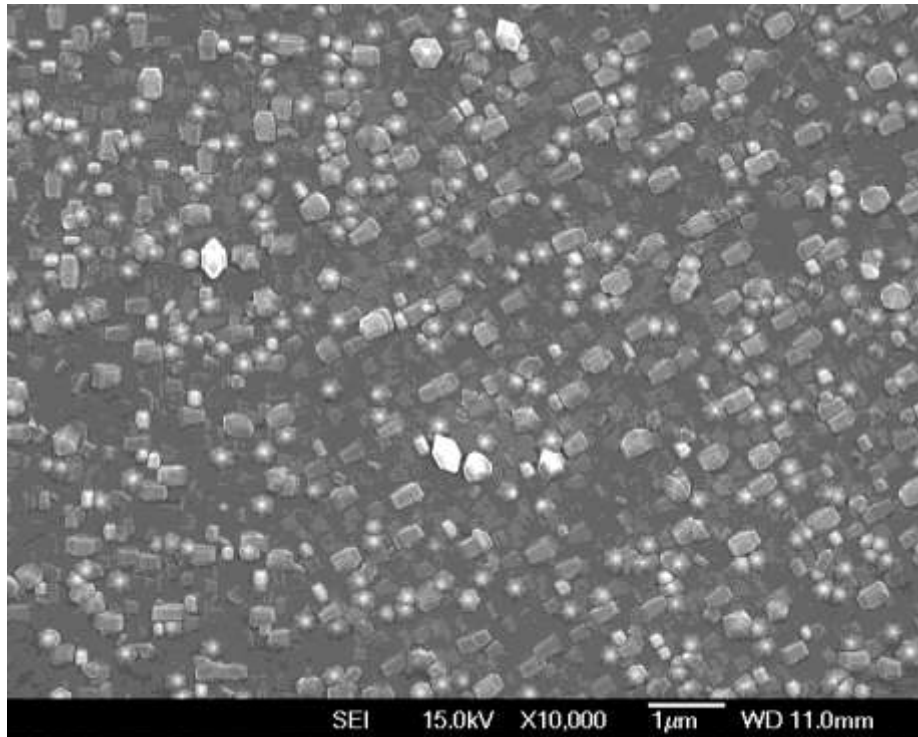
Fig.4.2.6.9 SEM image of AZO-0702 on MgO(100), 5shots on Ag, under 600°C and 1.2Torr oxygen pressure with a target-substrate distance of 60mm in chamber #2
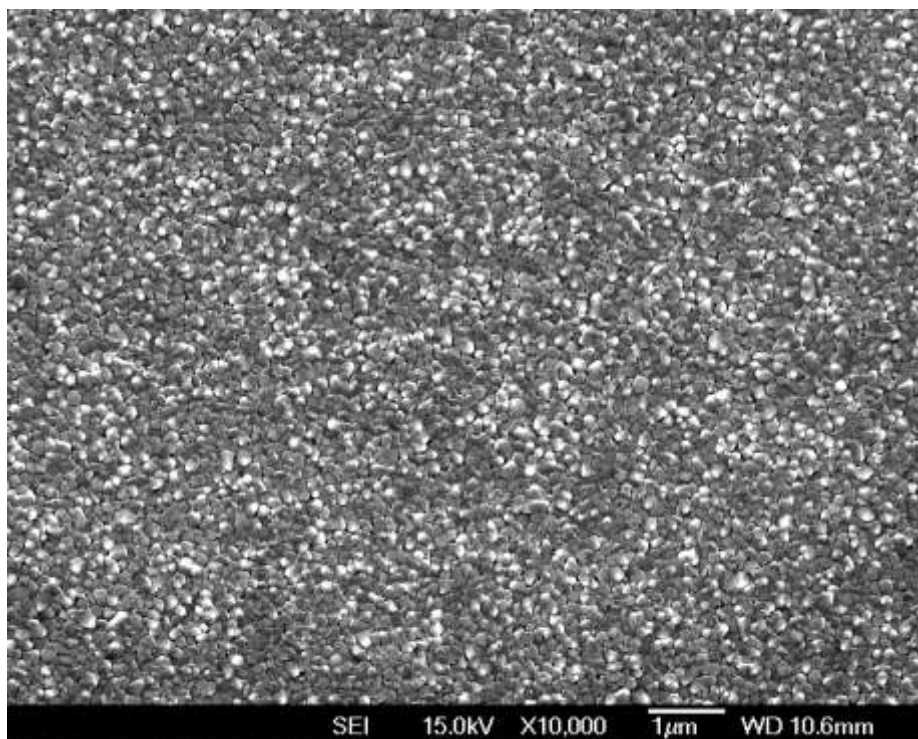
Fig.4.2.6.10 SEM image of AZO-0703 on Si(100), 5shots on Ag, under 600°C and 1.2Torr oxygen pressure with a target-substrate distance of 60mm in chamber #2

Ceramic Al_2O_3 substrates were utilized in this experiment as well. AZO-081 was produced using a one side polished ceramic Al_2O_3 (5mm×5mm) substrate in chamber #2 under 700°C with a target-substrate distance of 60mm, 5 shots on gold 5000 shots on ZnO in 1.2Torr oxygen. In order to compare the samples, sample AZO-082 was produced on MgO(100) with the same experimental parameter settings. The deposition on Al_2O_3 ceramic indicated a rough coating grown in a layer by layer growth mode, as shown in Fig.4.2.6.11.

Another interesting detail observed was that in some of the holes, on the layer, nanowires and nanorods growth was detected. These nanorods has the same dimension range of 50~130nm with those grown on MgO(100). This phenomenon is similar to the case of nanowires grown on the corner of sample AZO-059. The reason for this may be due to such an area could give a lower supersaturation compared with the area on a flat surface, which is required for one-dimensional nanostructure growth.
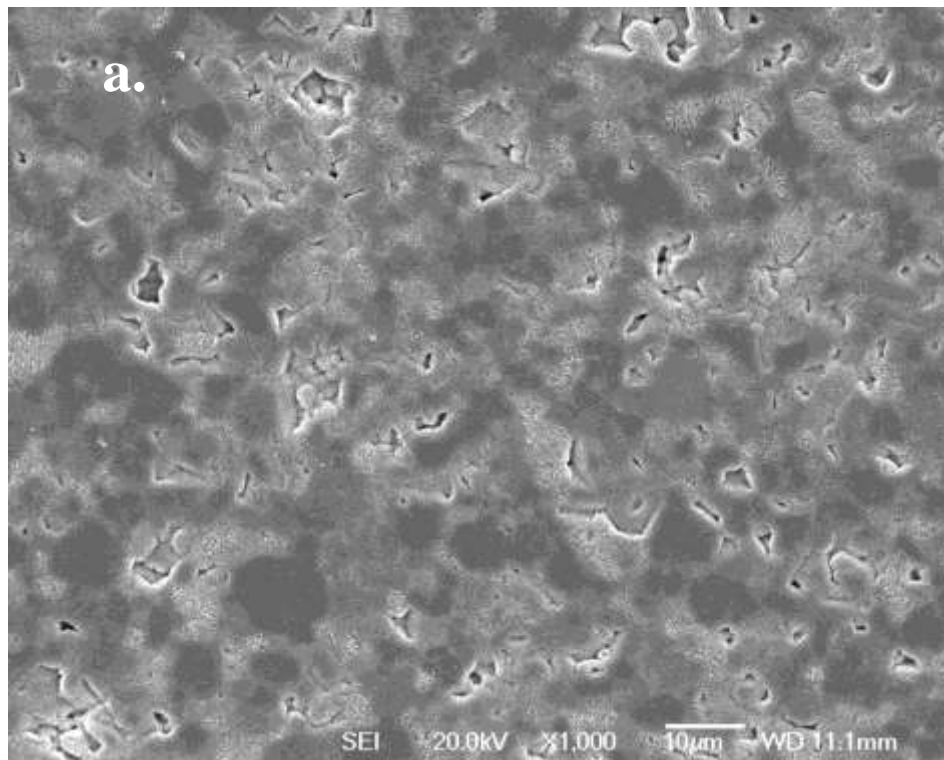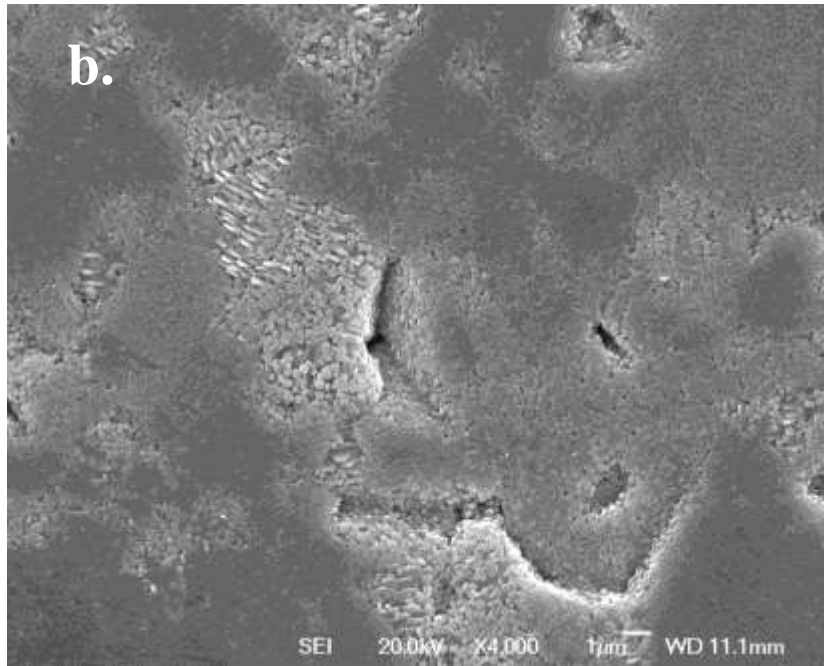
Fig.4.2.6.11 SEM images of AZO-081 on Al$_2$O$_3$ ceramic, 5shots on Au, under 700°C and 1.2Torr oxygen pressure with a target-substrate distance of 60mm in chamber #2
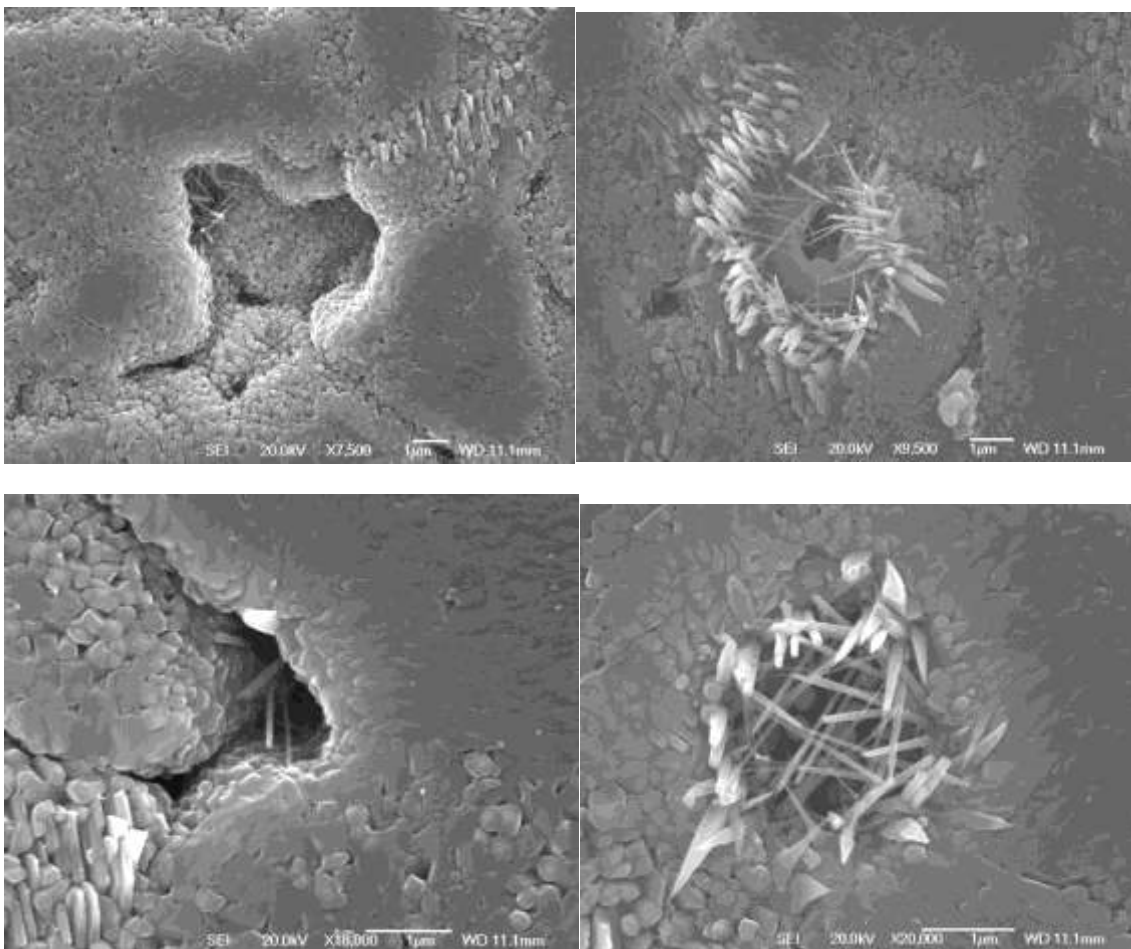
Fig.4.2.6.12 Partial SEM images of AZO-081 on Al$_2$O$_3$ ceramic, 5shots on Au, under 700°C and 1.2Torr oxygen pressure with a target-substrate distance of 60mm in chamber #2

157
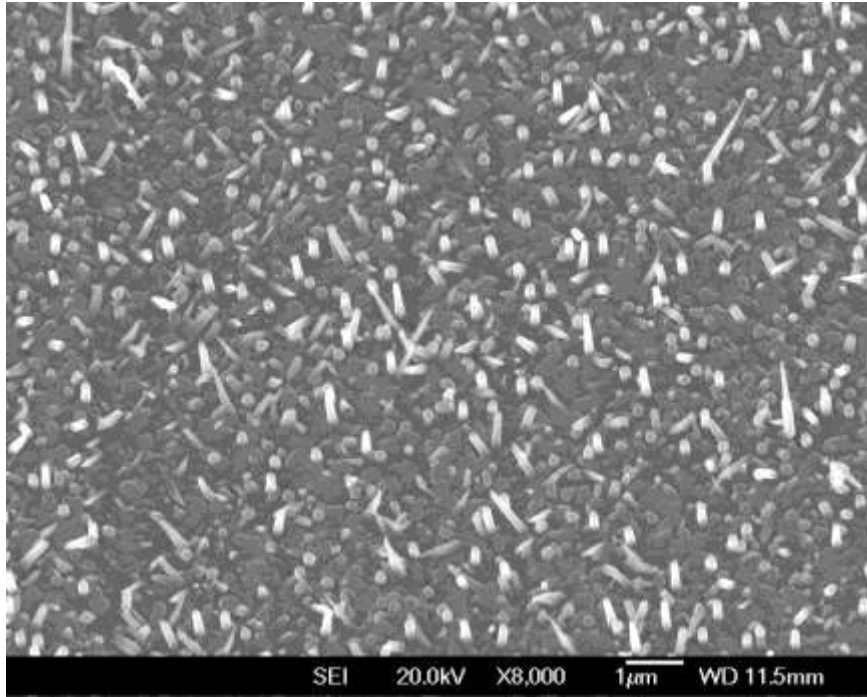
Fig.4.2.6.13 SEM image of AZO-082 on MgO(100), 5shots on Au, under 700°C and 1.2Torr oxygen pressure with a target-substrate distance of 60mm in chamber #2

From the results shown in this section, different substrates do provide a different template for nanowires growth resulting in different layer morphologies. For some orientated substrates, the coated layer tends to grow mainly in one certain orientation, which helps to form one-dimensional nanostructures. However, under some special environment, such as one that provides a low supersaturation, the differences from the substrates could not differentiate the morphologies of the deposition.

4.2.7 Influence of different metal catalysts

Many samples were produced in order to determine the best parameters to produce the ZnO nanowires with the best one dimensional morphology. It was discovered that the two crucial parameters that are key to produce ZnO nanowires. These parameters are oxygen pressure (1.2Torr) and temperature (600°C). In the previous section, another parameter was

discussed regarding the influence of different substrates. The parameter explored in this section is the influence from a metal catalyst. In order to compare this parameter, three substrates were utilized and all the other parameters were set at the same value to ensure that the morphology differences are all from the presence of the catalyst.

Table 4.2.17 Detailed parameters of the samples AZO-080812-1, 080812-2, 080812-3, 100812-1, 100812-2, 100812-3, 140812-1, 140812-2 and 140812-3

Sample Number	Catalyst (5shots)	Chamber number	Distance of target-substrate (mm)	Number of pulses on ZnO target (shots)	Substrate
AZO-080812-1	**Pd**	#2	50	5000	**MgO(100)**
AZO-080812-2	**Pd**	#2	50	5000	**STO(100)**
AZO-080812-3	**Pd**	#2	50	5000	**MgO(001)**
AZO-100812-1	**Ag**	#2	50	5000	**MgO(100)**
AZO-100812-2	**Ag**	#2	50	5000	**STO(100)**
AZO-100812-3	**Ag**	#2	50	5000	**MgO(001)**
AZO-140812-1	**Au**	#2	50	5000	**MgO(100)**
AZO-140812-2	**Au**	#2	50	5000	**STO(100)**
AZO-140812-3	**Au**	#2	50	5000	**MgO(001)**

Samples AZO-080812-1, 2, and 3 used palladium as their catalyst. The ZnO depositions on MgO(100) and also MgO(001) produced a unique morphology where the nanowires are parallel to the surface based on crystalline bulks. The average length of the nanowires grown on both MgO substrates is approximately 1.5μm. However, the nanowires, grown on MgO(001), had a thickness around 40nm. These were slightly thinner than those grown on MgO(100), whose average thickness was approximately 80nm. As discussed in the earlier sections, these differences are related to the different manufacturers. For the substrate STO(100), there were no one-dimensional nanostructures found.
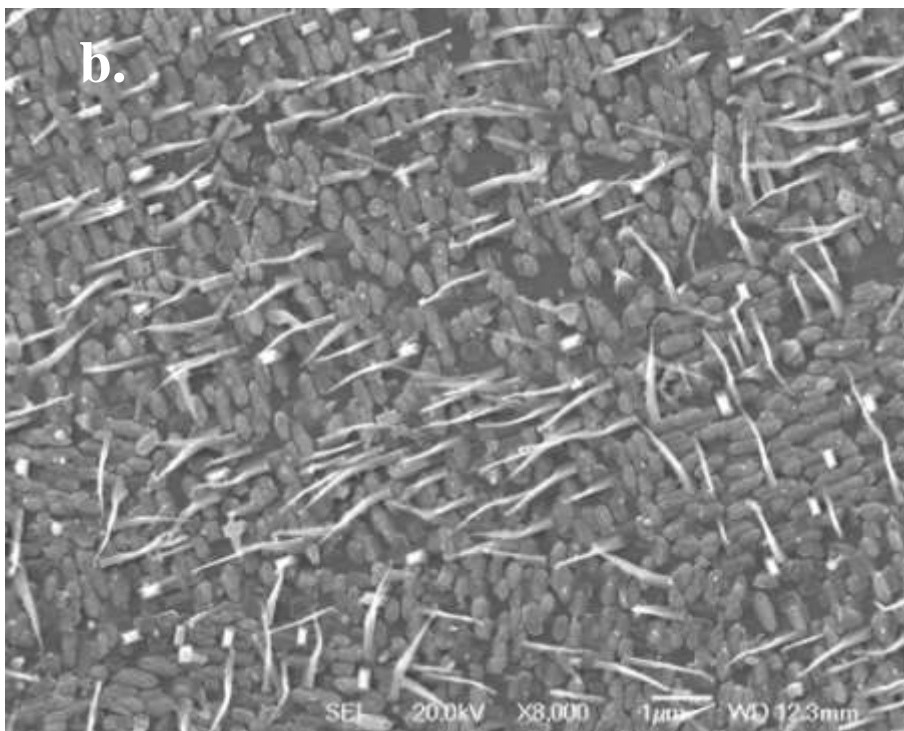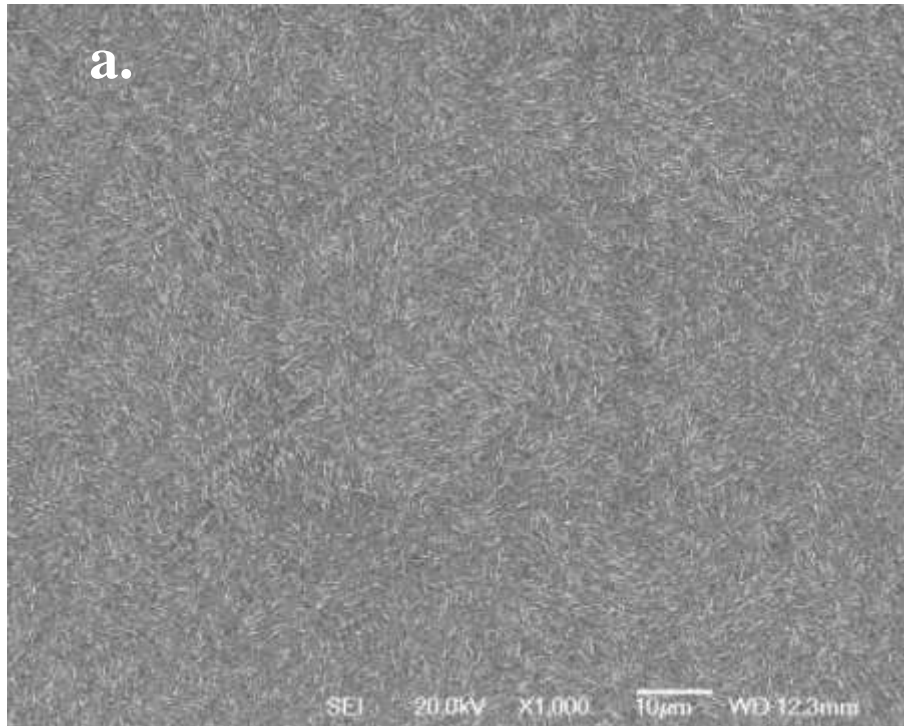
Fig.4.2.7.1 SEM images of AZO-080812-1 on MgO(100) with 5 shots on Pd

a) top view, magnification of 1000; b) top view, magnification of 8000
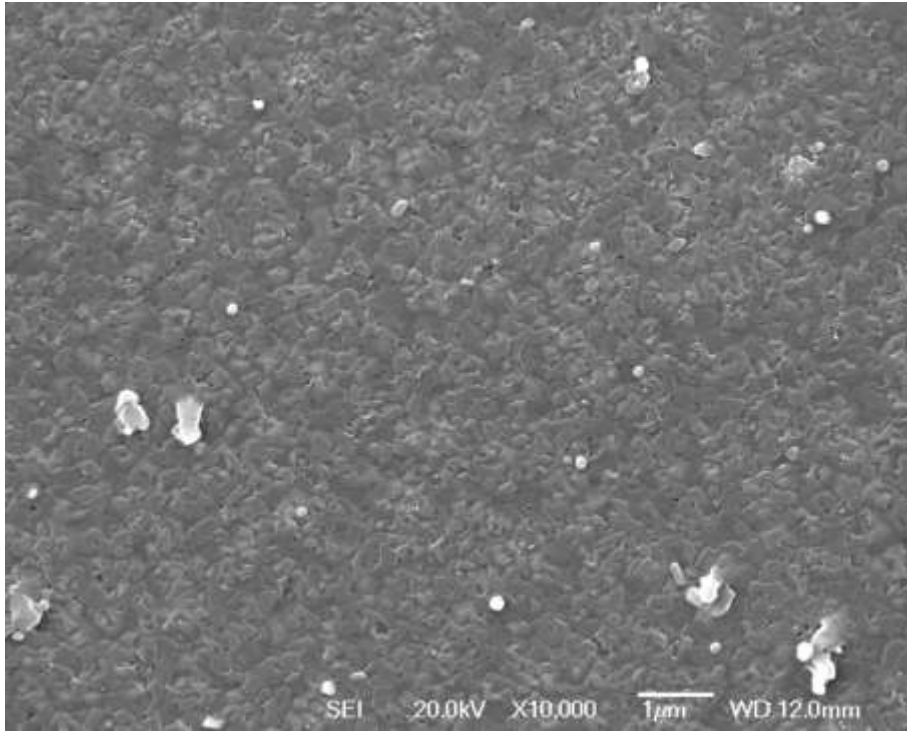
Fig.4.2.7.2 SEM image of AZO-080812-2 on STO(100) with 5 shots on Pd
top view, magnification of 10,000
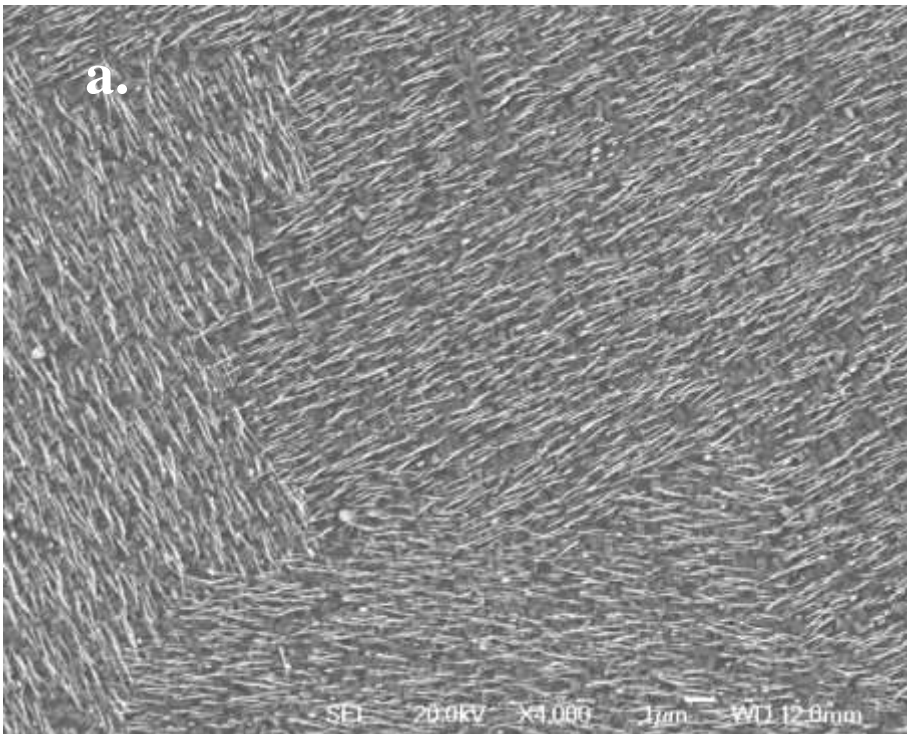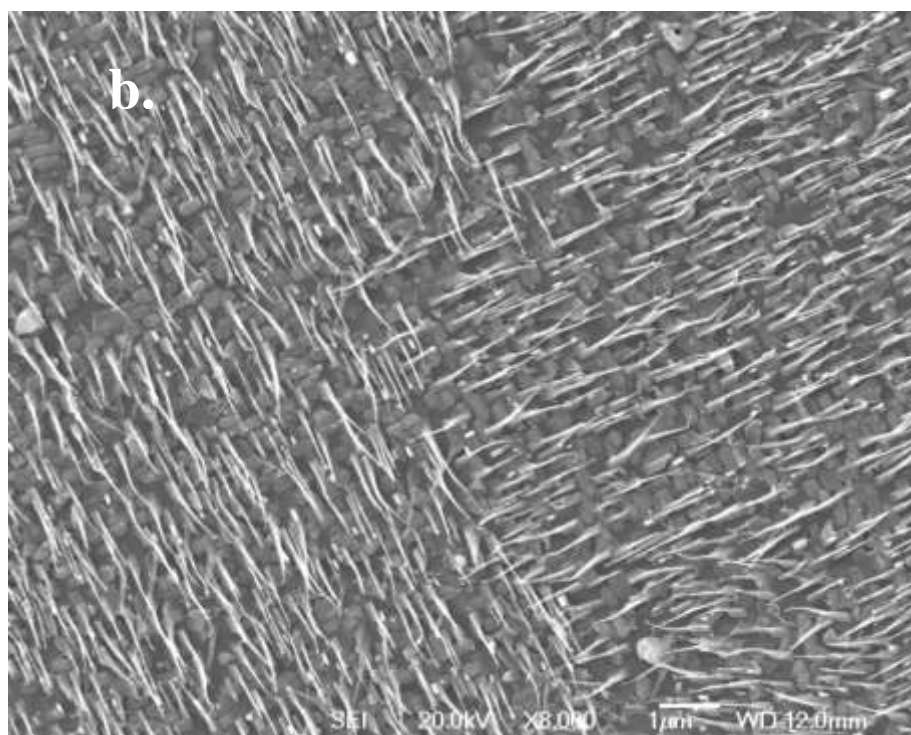
Fig.4.2.7.3 SEM images of AZO-080812-3 on MgO(001) with 5 shots on Pd

a) top view, magnification of 4000; b) top view, magnification of 8000

Unfortunately, it was determined that silver was not a good catalyst in this case. There were no particular nanostructures found on any substrates, as seen in Fig.4.2.7.4, Fig.4.2.7.5 and Fig.4.2.7.6. MgO(100) and MgO(001) indicate the same morphology. The structures present on the surface have a similar appearance with the foundation crystal in Fig.4.2.7.1 and Fig.4.2.7.3.
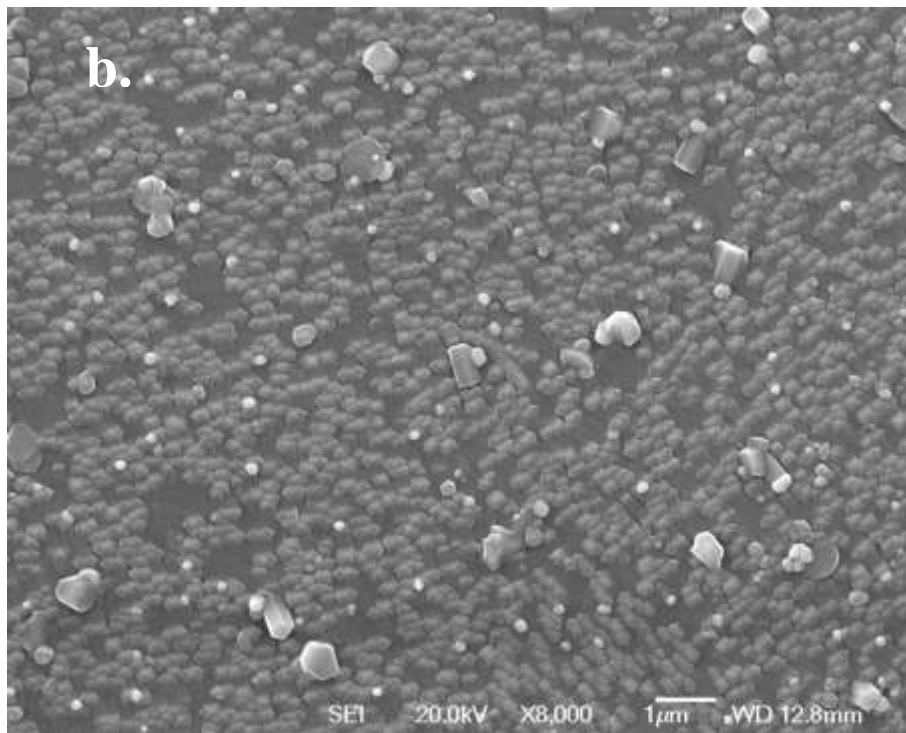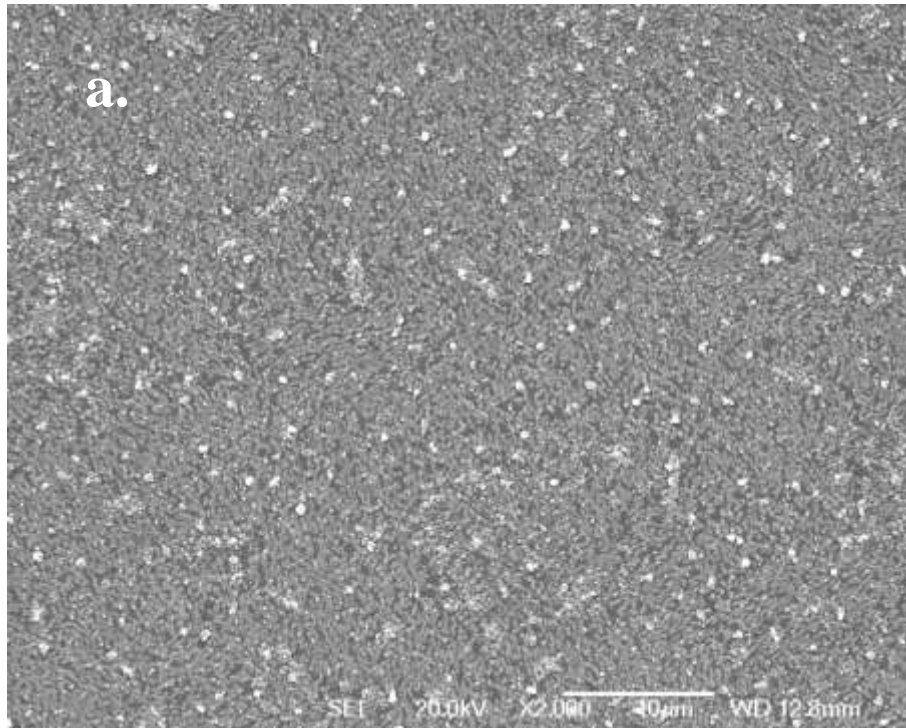
Fig.4.2.7.4 SEM images of AZO-100812-1 on MgO(100) with 5 shots on Ag

a) top view, magnification of 2000; b) top view, magnification of 8000
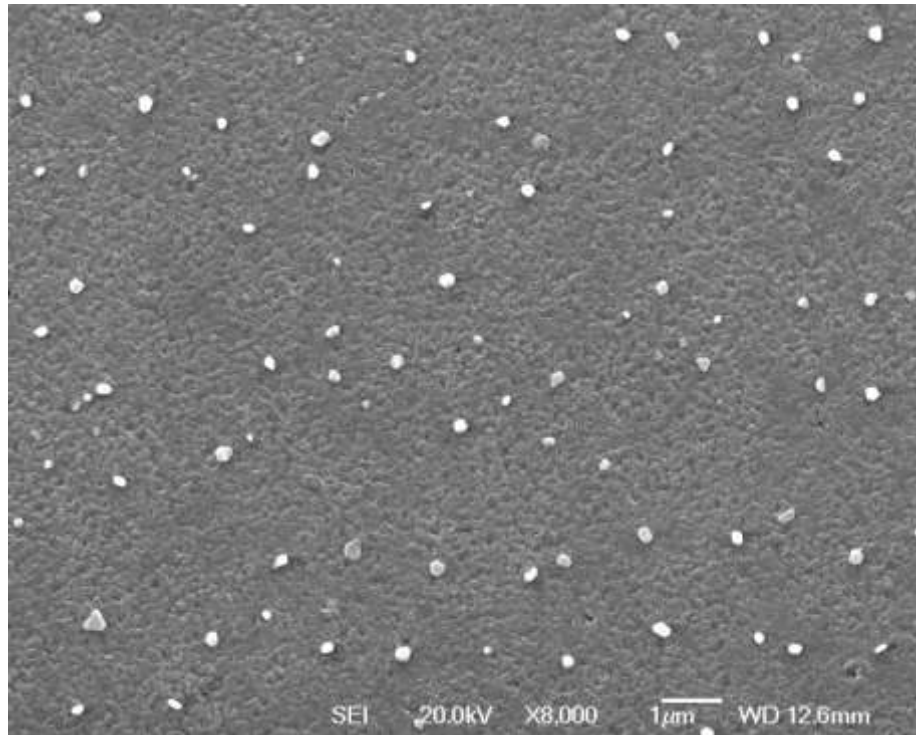
Fig.4.2.7.5 SEM image of AZO-100812-2 on STO(100) with 5 shots on Ag,
top view, magnification of 8000
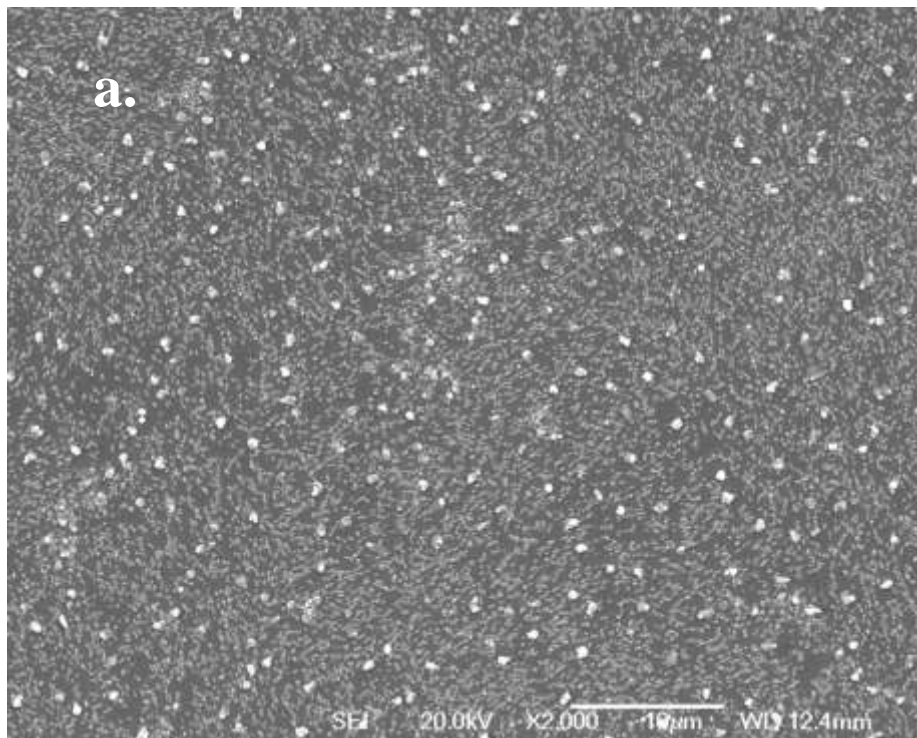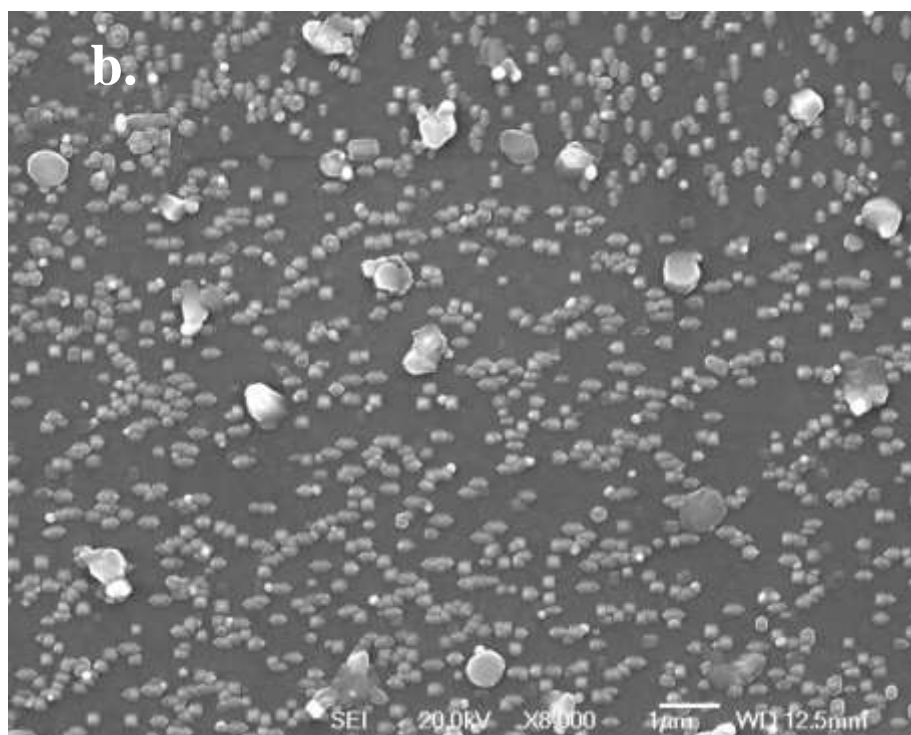
Fig.4.2.7.6 SEM images of AZO-100812-3 on MgO(001) with 5 shots on Ag

a) top view, magnification of 2000; b) top view, magnification of 8000

Gold is the most common catalyst used in one-dimensional nanostructure growth. In this case, the nanostructures observed on MgO substrates tend to grow in a more perpendicular direction compared with the catalytically assisted nanostructures from Pd, where all the nanowires are parallel to the surface. There are no bulk crystals as the nanostructures' base. Another noticeable difference is the shapes of the nanostructures grown by these two catalysts. The nanostructures grown, with Pd, are much longer, but not as straight as the nanostructures grown with Au. The nanostructures grown with Au normally have a pointed top, in the shape of a flat triangle, pyramid, or cone. In the case of gold, from the images shown in Fig.4.2.7.7 and Fig.4.2.7.9, MgO(100) was found to be a better substrate when compared with MgO(001). This is the same conclusion that can be ascertained from

165

Fig.4.2.6.1 and Fig.4.2.6.2. Also there were no particular structures found on STO(100) either.

A cluster of nanorods, in the shape resembling a sea anemone, was found on the surface of AZO-140812-1. Another cluster of nanorods, in a formation resembling a volcanic crater, was found on the surface of AZO-140812-3. The appearances of such formations seem accidental, but the cause of these formations is believed to be the same as the formations found in Fig.4.2.6.12. A hole or a large particle would be a preferable location for one dimensional nanostructure to form, since the supersaturating level is lower than those sites on the flat substrate. The particles from the plume have stronger potential with sites with the surface defects.
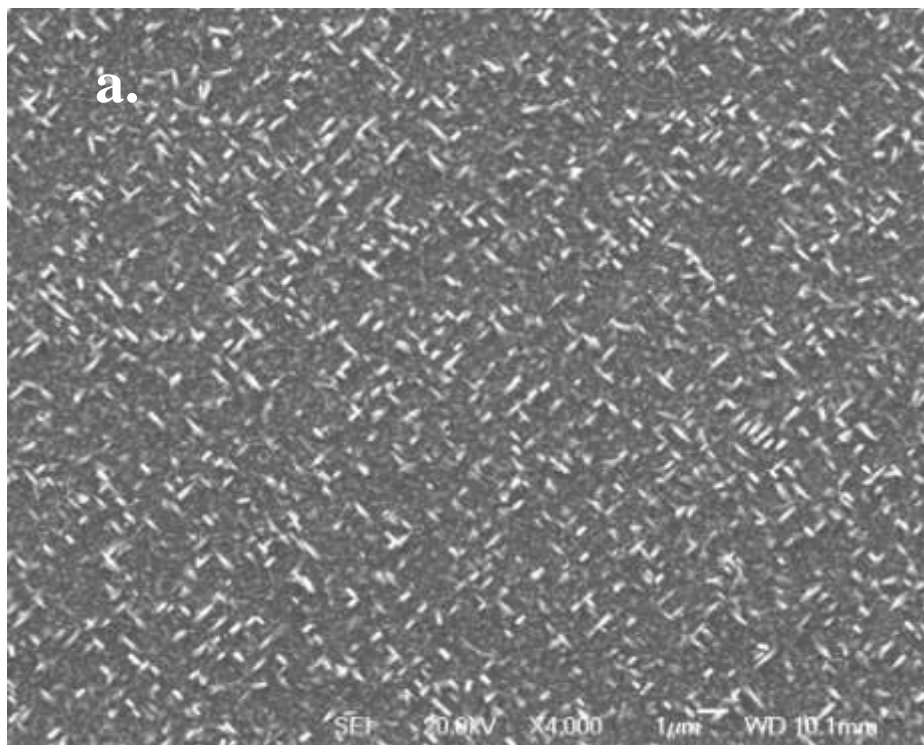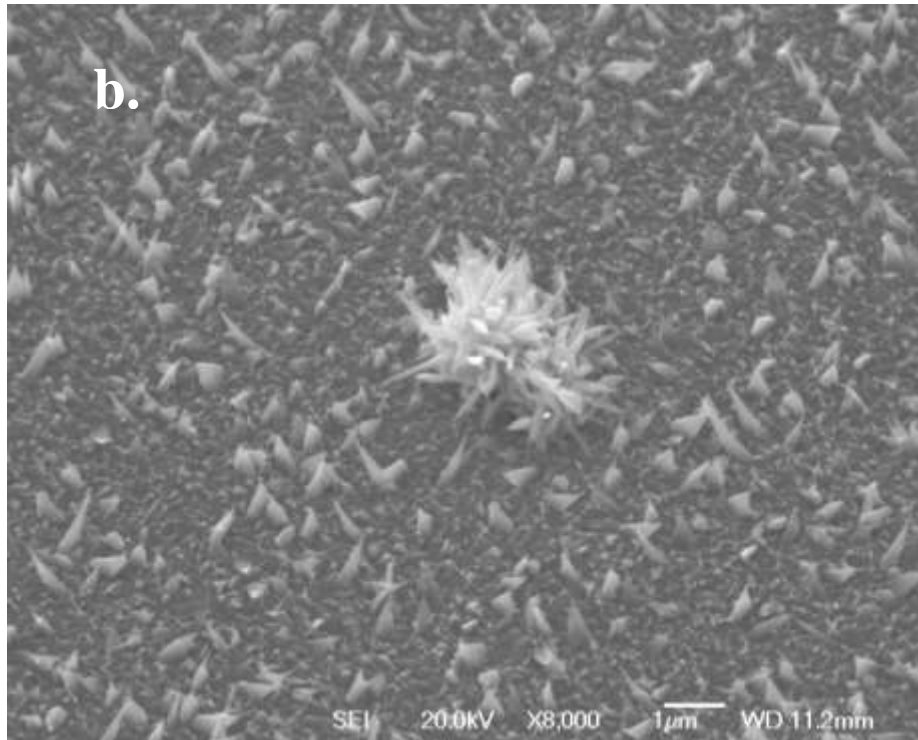
Fig.4.2.7.7 SEM images of AZO-140812-1 on MgO(100) with 5 shots on Au

a) top view, magnification of 4000; b) 30° tilt, magnification of 8000
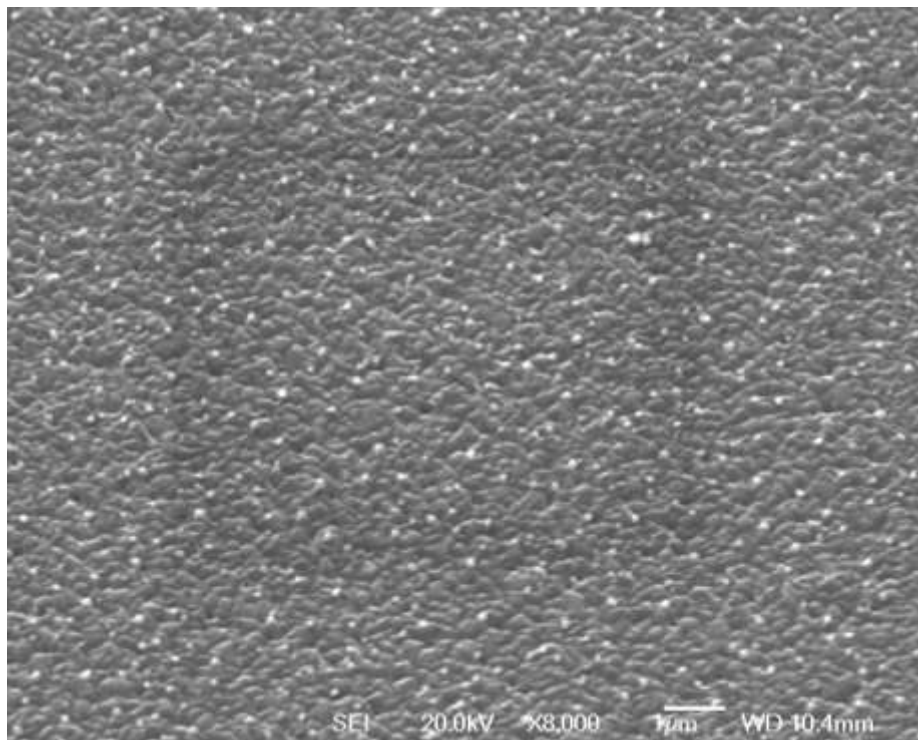
Fig.4.2.7.8 SEM image of AZO-140812-2 on STO(100) with 5 shots on Au, 30° tilt,
magnification of 8000
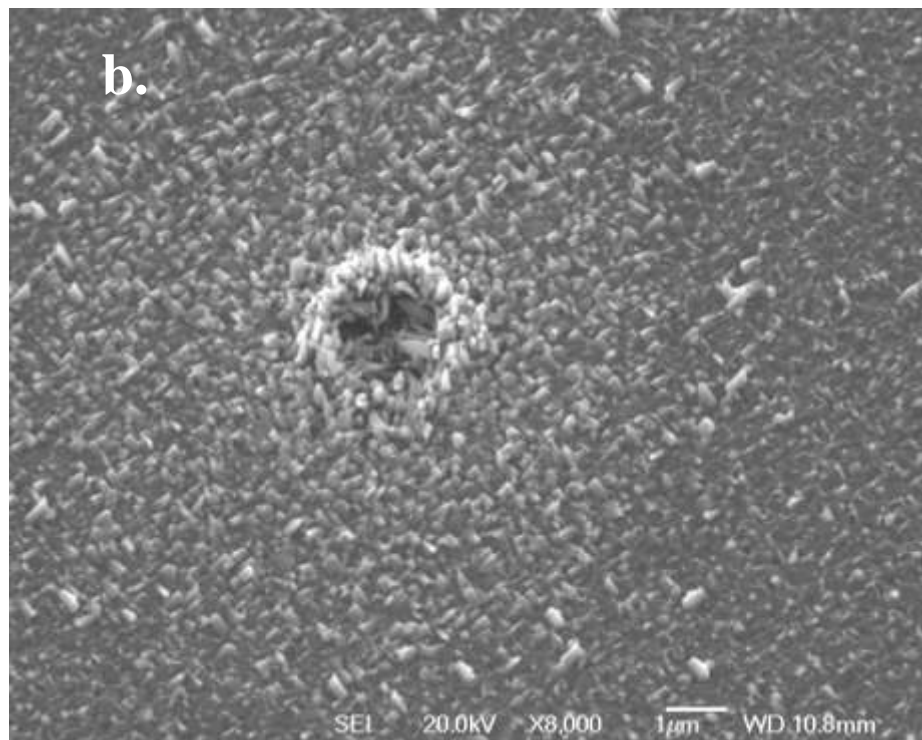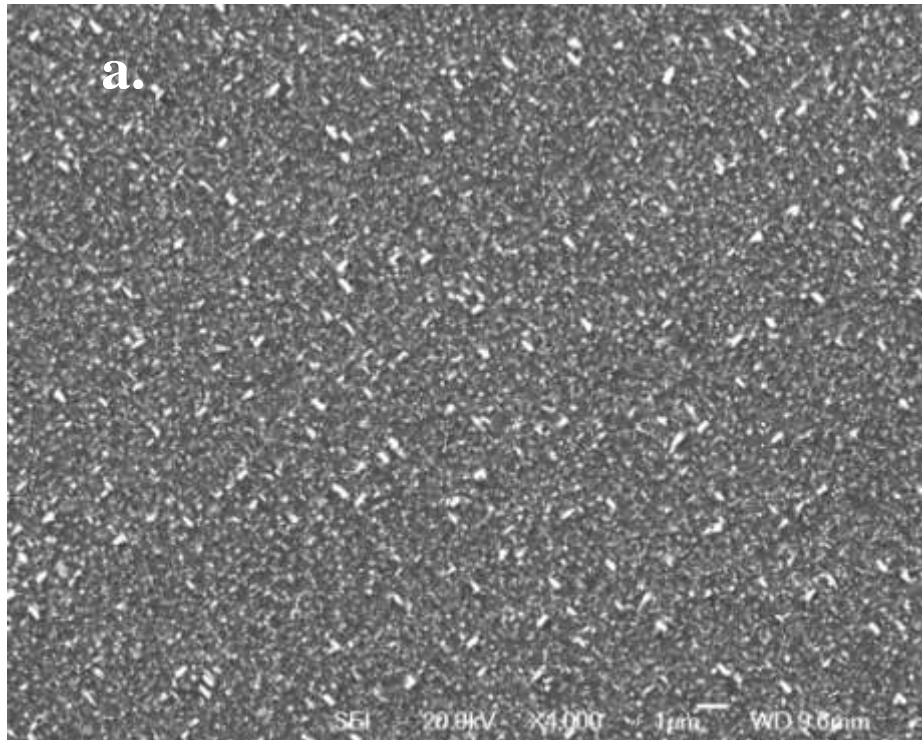
Fig.4.2.7.9 SEM images of AZO-140812-3 on MgO(001) with 5 shots on Au

a) top view, magnification of 4000; b) 30° tilt, magnification of 8000

The catalyst used can determine the nanostructures' growth mode. This is due to the metal's natural properties. Palladium- MgO substrates are a better catalyst-substrate combination for ZnO nanowires if desired results are very long, dense, but curved nanowires. Gold is a good companion with MgO subtrates, too. However, silver or STO(100) do not help in ZnO nanowires growth.

4.2.8 Influence of laser energy

Laser energy is another factor that influences the result, as it is related to the quantity, density, and the energy level of the particles in the plume. In the previous sections, particle energy is mentioned when discussing the formation of nanostructures. In this section, laser energy will be investigated on its influence on the crystallinity of nanostrucutres. The details of the samples being considered in this section are listed in the table below. The spot size is kept at $1 \times 10 mm^2$. The laser energy value in the table was measured inside the chamber. In order to keep the other parameters at the same value, all the samples were coated by 5 shots gold, with the laser energy density of 1 J/cm^2, before depositing ZnO. All samples were placed in the direct centre of the plume.

**Table 4.2.18** Detailed parameters of the samples AZO-060, 061, 062,063,064 and 065

Sample Number	Chamber number	Substrate	Temp. (˚C)	Number of pulses on Gold (with energy density)	Number of pulses on ZnO (with energy density)	Oxygen pressure (mTorr)	Distance of target-substrate (mm)
AZO-060	#3	MgO(100)	700	5(1 J/cm^2)	5000 (0.65J/cm^2)	1200	55
AZO-061	#3	MgO(001)	700	5(1 J/cm^2)	5000 (0.65 J/cm^2)	1200	55
AZO-062	#3	MgO(100)	700	5(1 J/cm^2)	5000 (0.3 J/cm^2)	1200	55
AZO-063	#3	MgO(001)	700	5(1 J/cm^2)	5000 (0.3 J/cm^2)	1200	55
AZO-064	#3	MgO(100)	700	5(1 J/cm^2)	5000 (0.15 J/cm^2)	1200	55
AZO-065	#3	MgO(001)	700	5(1 J/cm^2)	5000 (0.15 J/cm^2)	1200	55

Sample AZO-060 was produced on MgO(100) with the laser energy density of 0.65 J/cm^2. As shown in Fig.4.2.8.1, the quantity and density of perpendicular nanorods increase when approaching towards the edge, while the opposite occurs to oblique nanorods when approaching towards the edge. Decreasing the laser energy density to 0.3 J/cm^2, sample AZO-062, in Fig.4.2.8.3, displays a rough surface in the direct central area, while moving away from the centre, more parallel nanorods become present. When the laser energy density is decreased to 0.15 J/cm^2, as seen in Fig.4.2.8.5, nanocones with a thickness of 700~800nm, form on the rough surface in some areas. Some nanowires were also found on the edge in Fig.4.2.8.5c.

The substrate, MgO(001), which has identical crystallography to MgO(100) made by different manufacturers, was also used in this observation. When the laser energy density was set at 0.65 J/cm^2, as shown in Fig.4.2.8.2, parallel nanorods were concentrated in the centre of the sample. When moving away from the central area and approaching the edge, the density of perpendicular structures increase. When the energy density is reduced to 0.3 J/cm^2, in Fig.4.2.8.4 the ZnO layer tends to grow in a perpendicular direction. However, the surface is not even as some areas are not fully covered, which causes the charging effect when taking SEM images. This unevenness becomes more severe when the energy density reduced to 0.15 J/cm^2, as seen in Fig. 4.2.8.6. Some areas shows a similar morphology as the ZnO layer on MgO(100) in Fig.4.2.8.5c. Several crystal shaped nanostructures are formed in and out of the background layer, but some areas are not fully covered, while some areas are also quite rough. These differences relate to the growth and surface finishing techniques of the substrates produced by different manufactures.
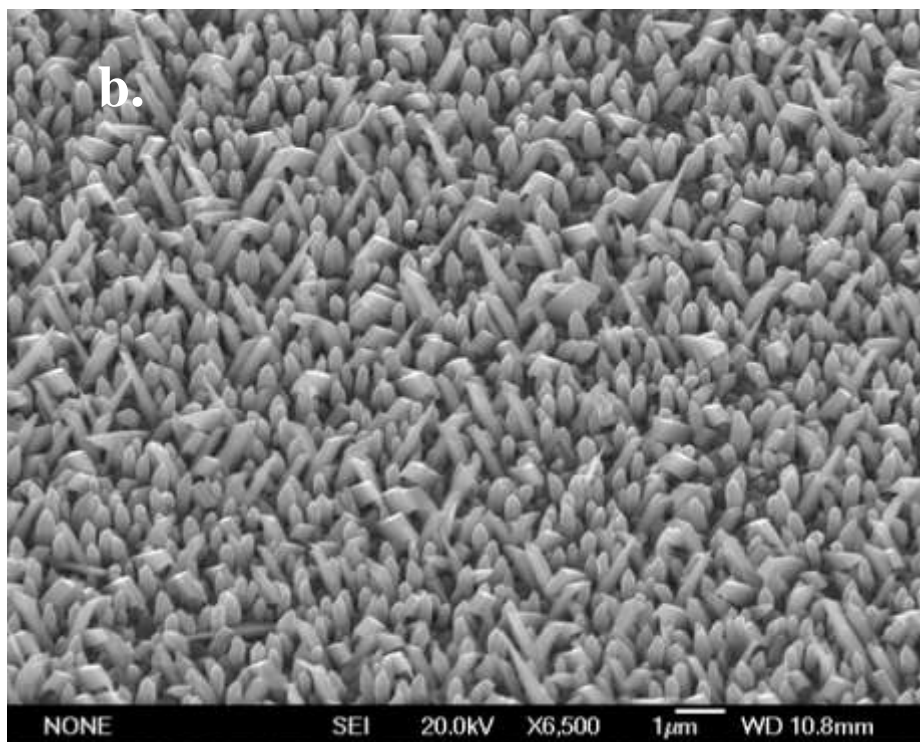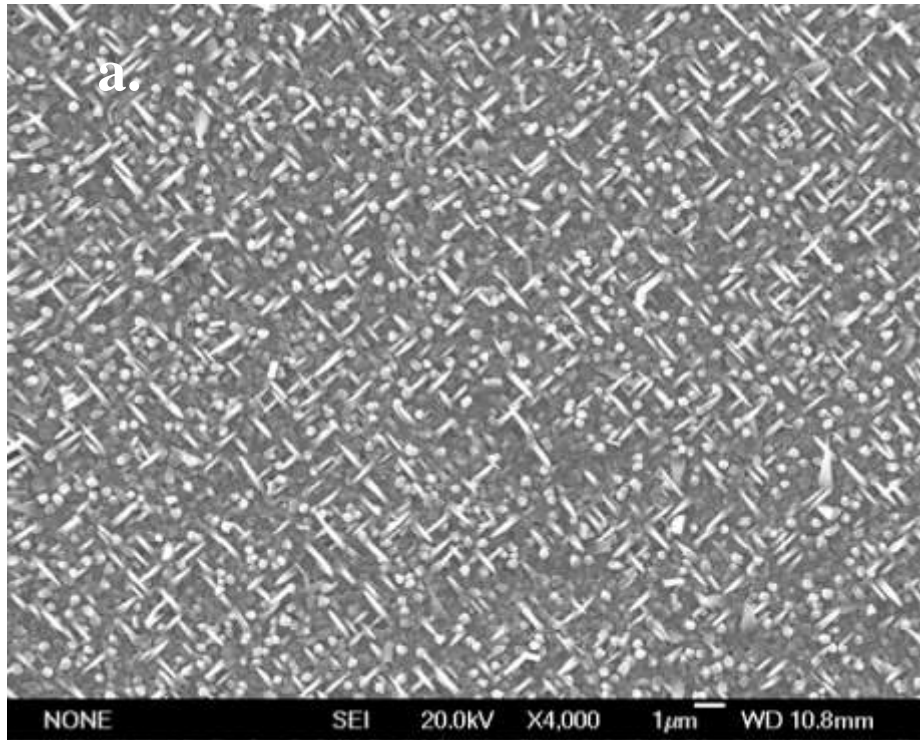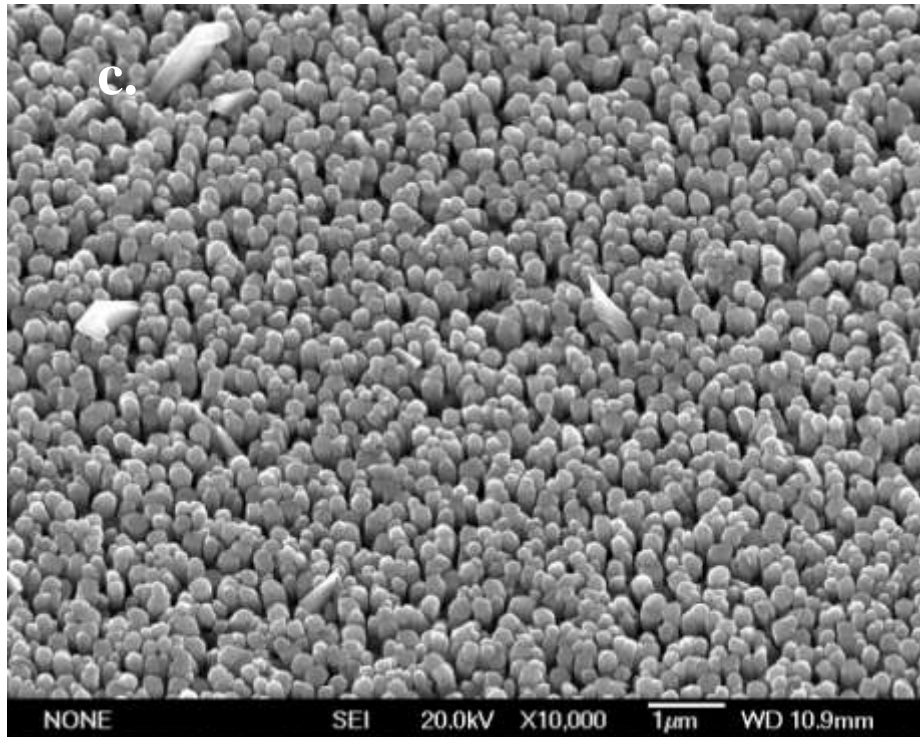
Fig.4.2.8.1 SEM images of AZO-060 on MgO(100) by 0.65 J/cm^2 laser

a) top view of direct centre, magnification of 4000;
b) 30°tilt view of area away from the centre, magnification of 6500;
c) 30°tilt view of area near the edge, magnification of 10,000
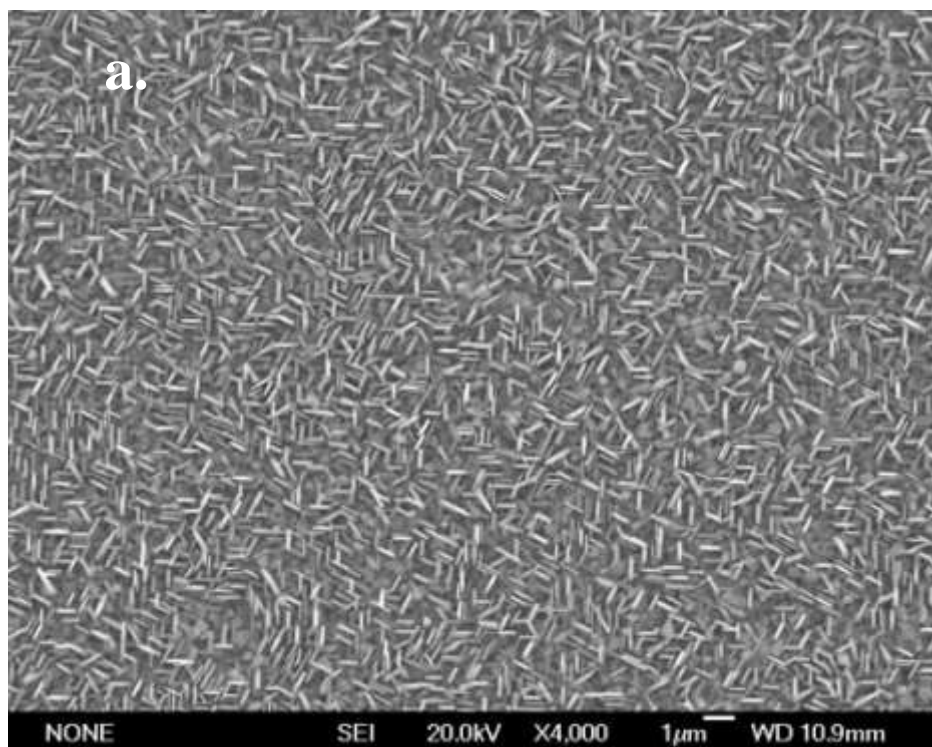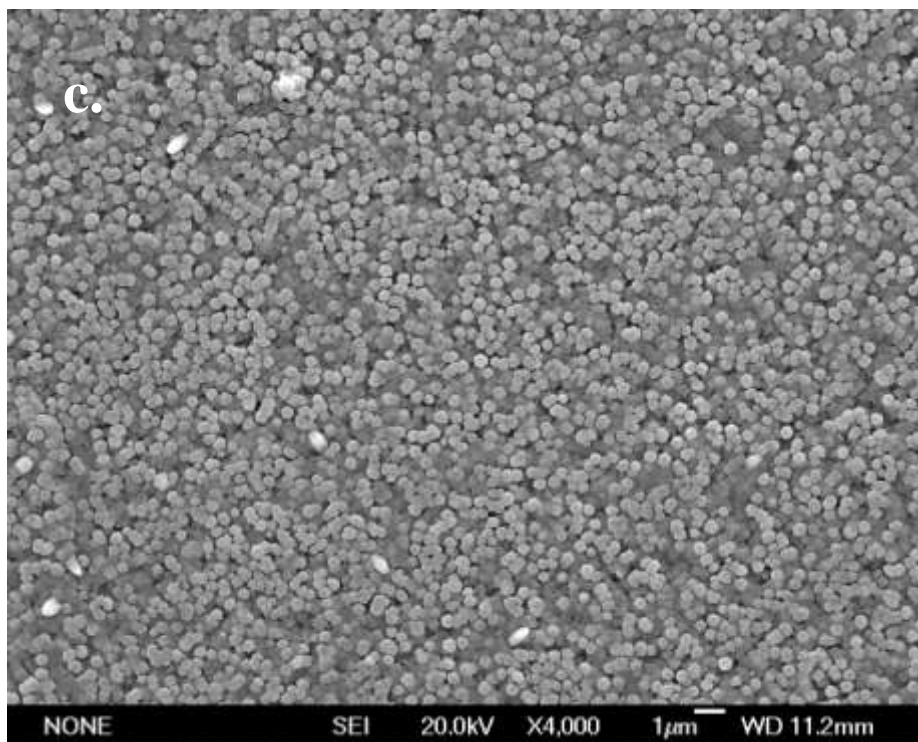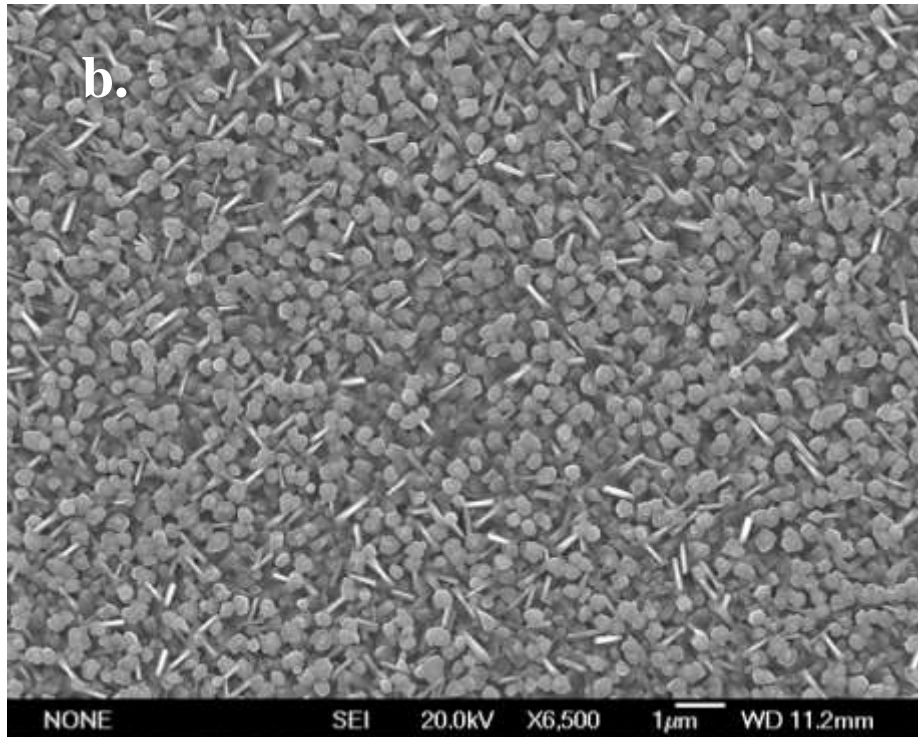
**Fig.4.2.8.2** SEM images of AZO-061 on MgO(001) by 0.65 J/cm^2 laser

a) top view of direct centre, magnification of 4000;
b) top view of area away from the centre, magnification of 6500;
c) top view of area near the edge, magnification of 4000
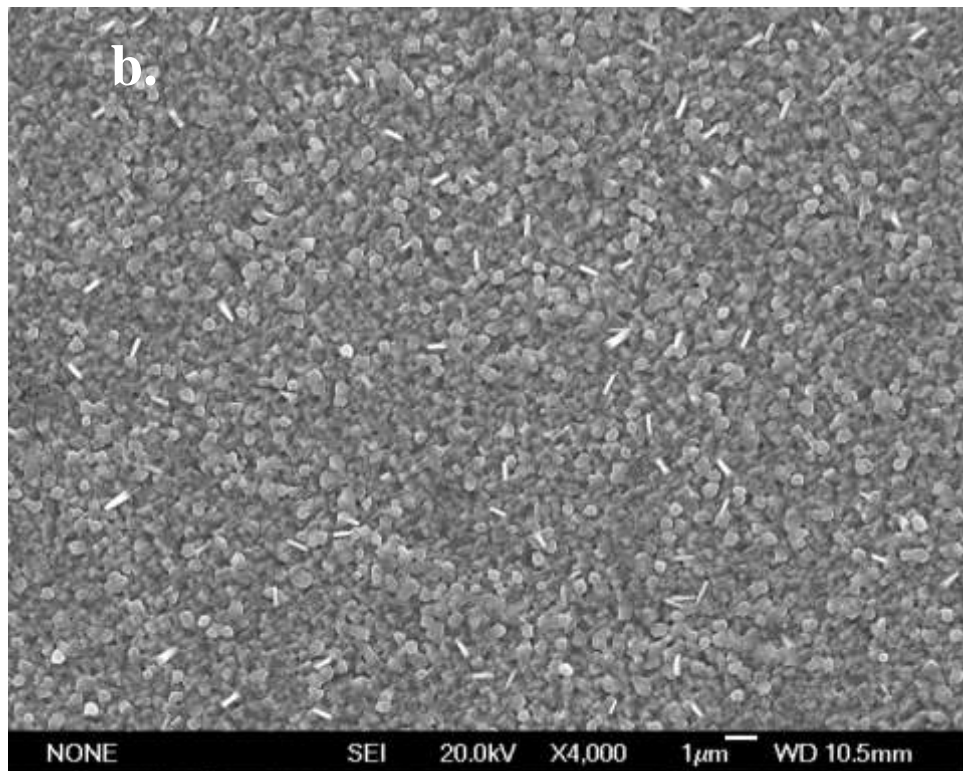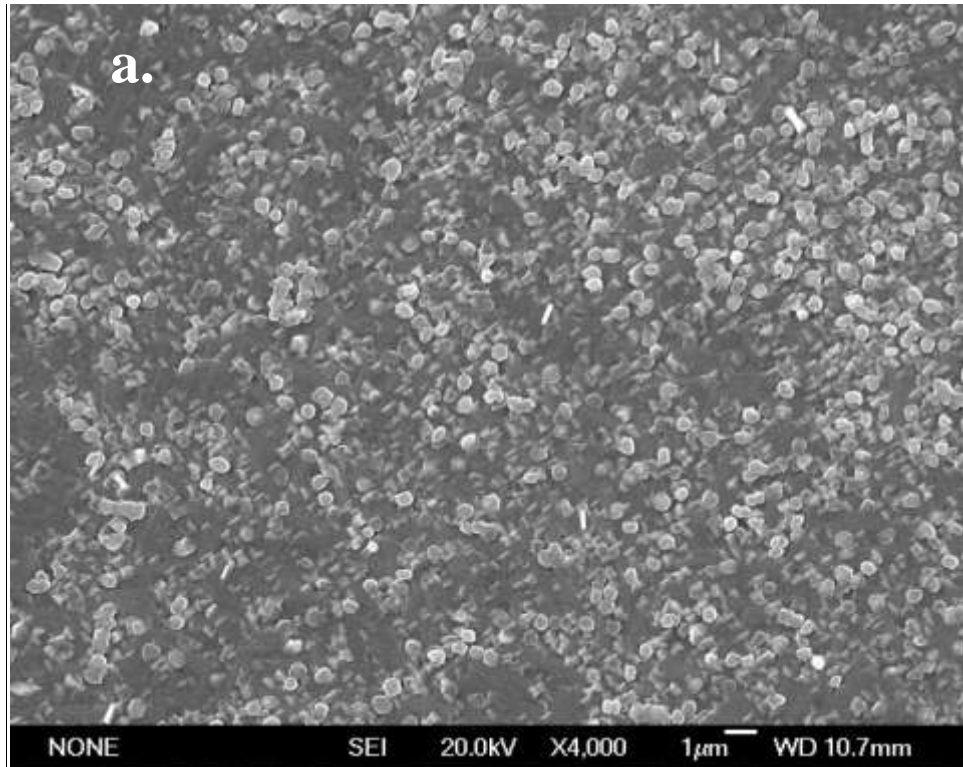
Fig.4.2.8.3 SEM images of AZO-062 on MgO(100) by 0.3 J/cm^2 laser

a) top view of direct centre, magnification of 4000;
b) top view of area away from the centre, magnification of 4000
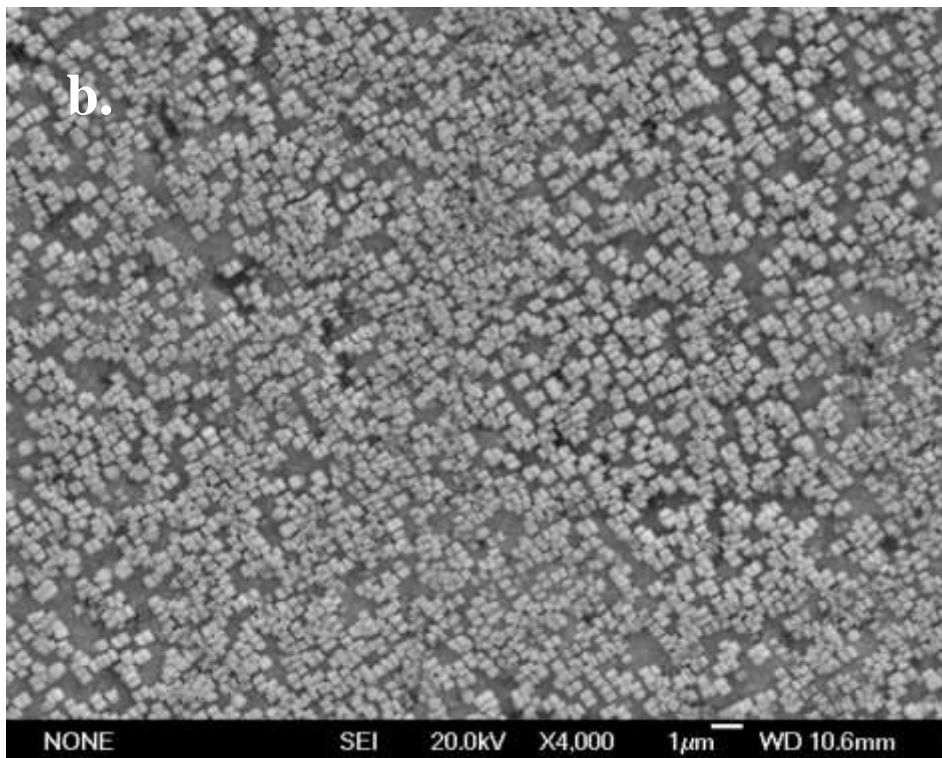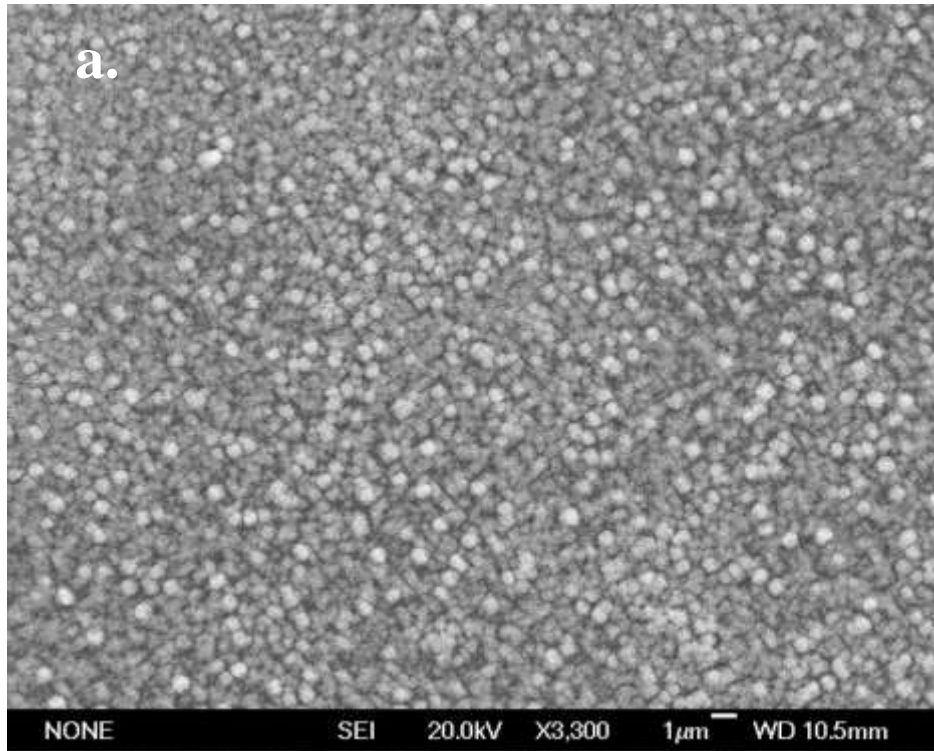
**Fig.4.2.8.4** SEM images of AZO-063 on MgO(001) by 0.3 J/cm^2 laser,

a) top view of direct centre, magnification of 3300;
b) top view of area away from the centre, magnification of 4000
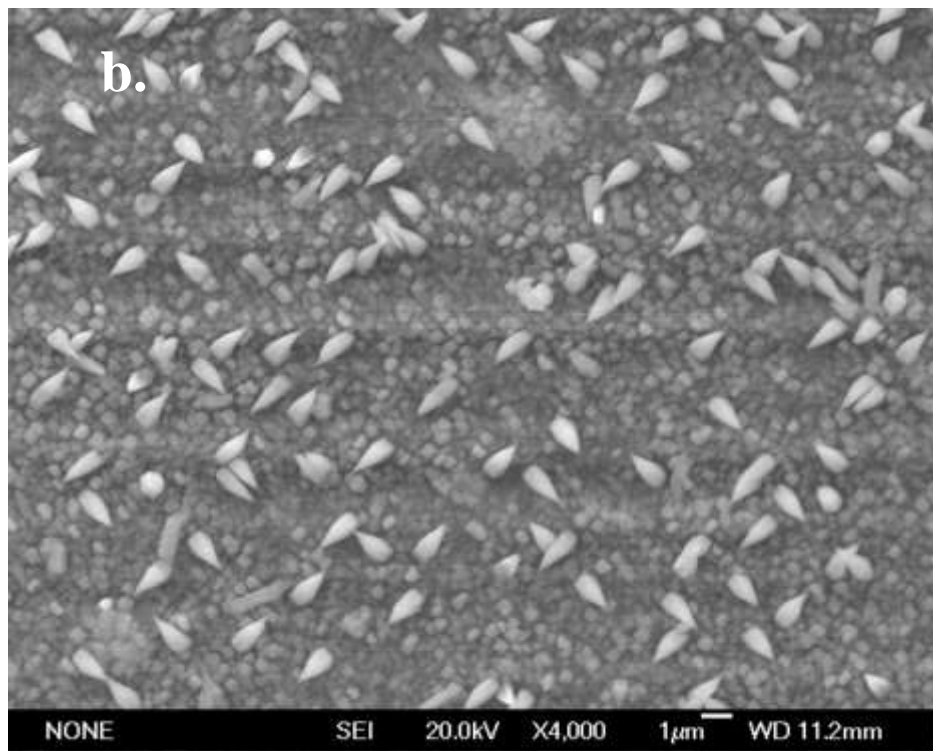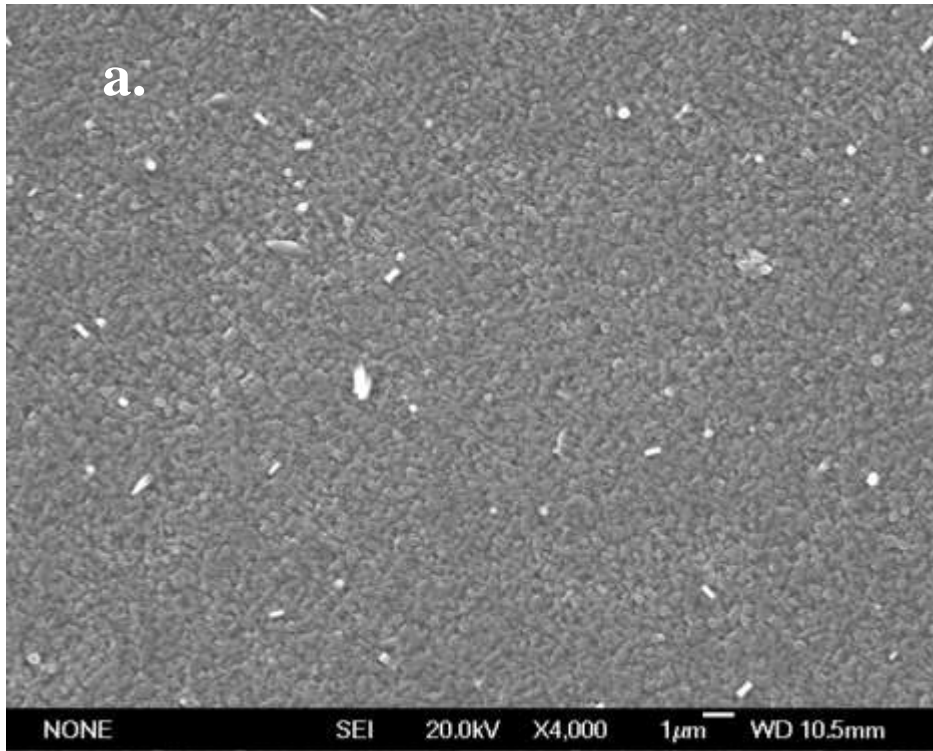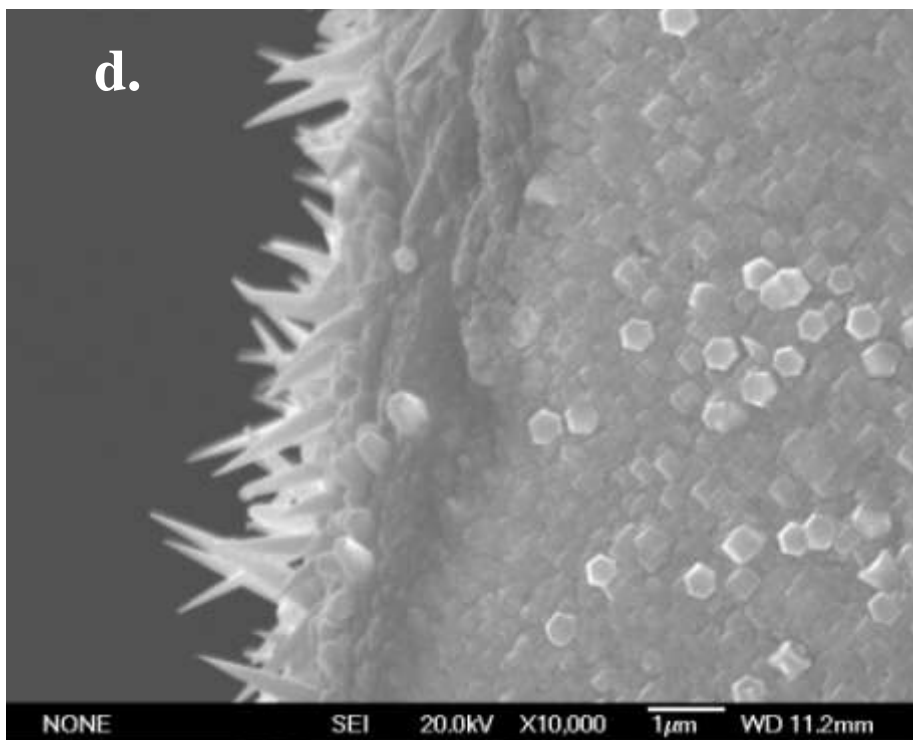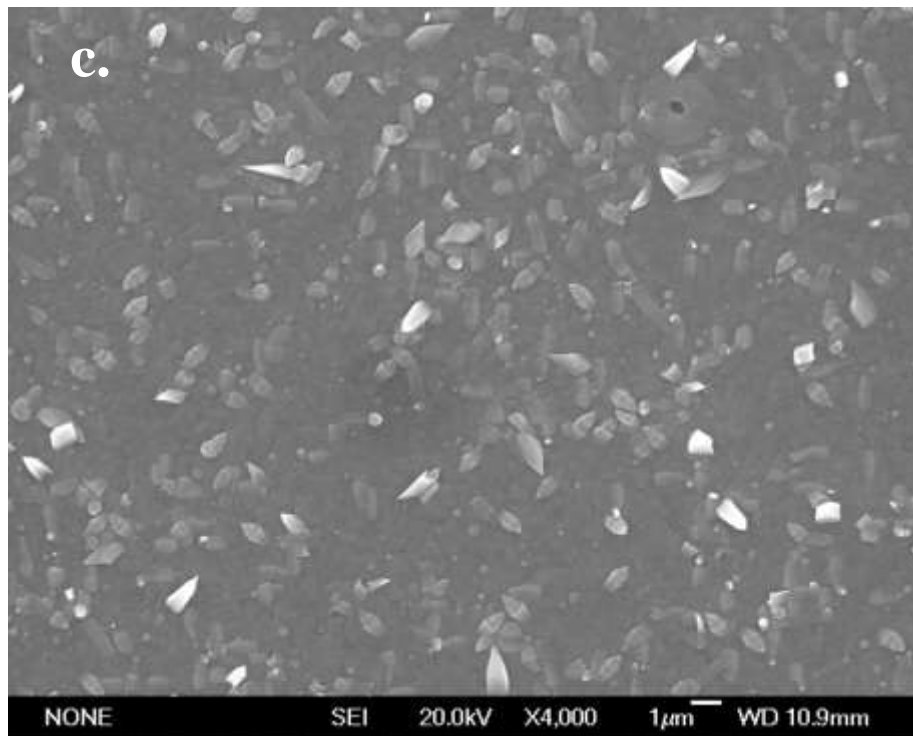
Fig.4.2.8.5 SEM images of AZO-064 on MgO(100) by 0.15 J/cm^2 laser

a) top view of direct centre, magnification of 4000;
b) top view, magnification of 4000; c) top view, magnification of 4000;
d) top view of edge, magnification of 10,000
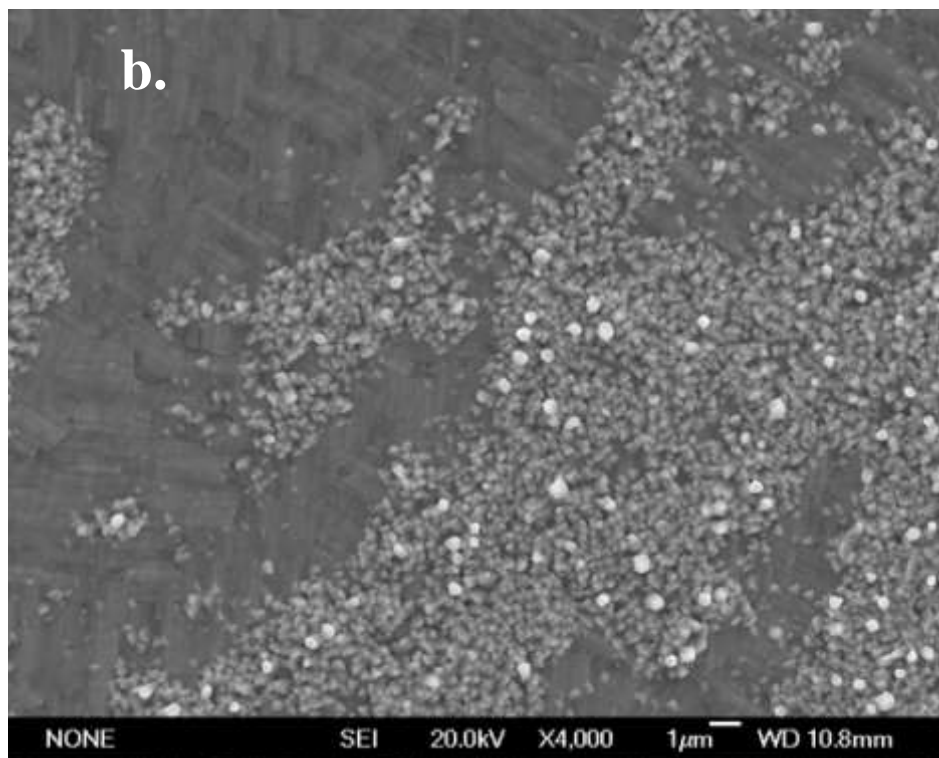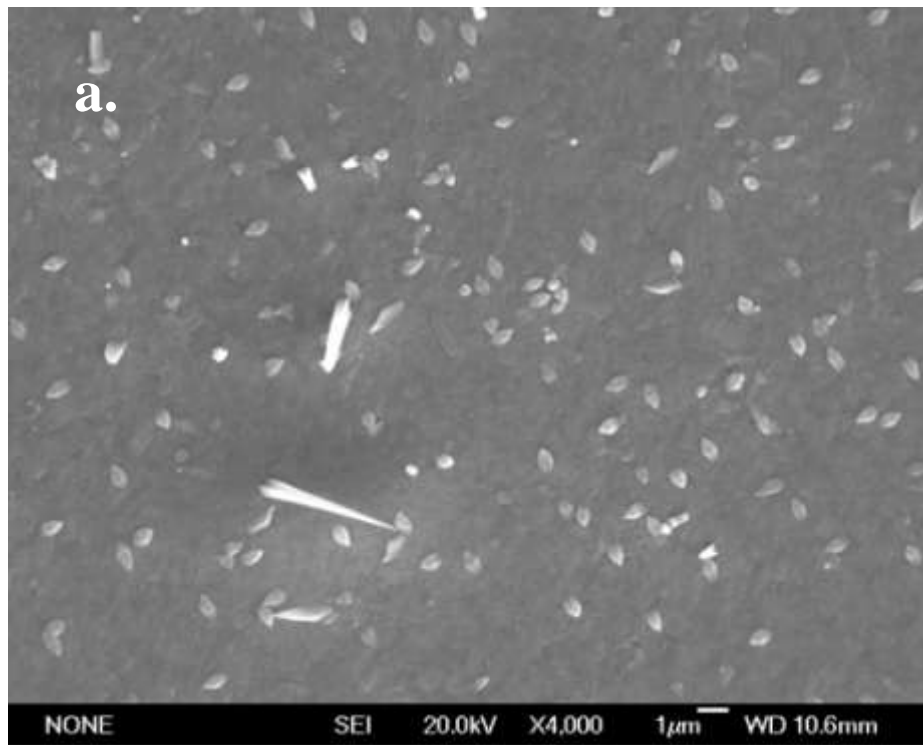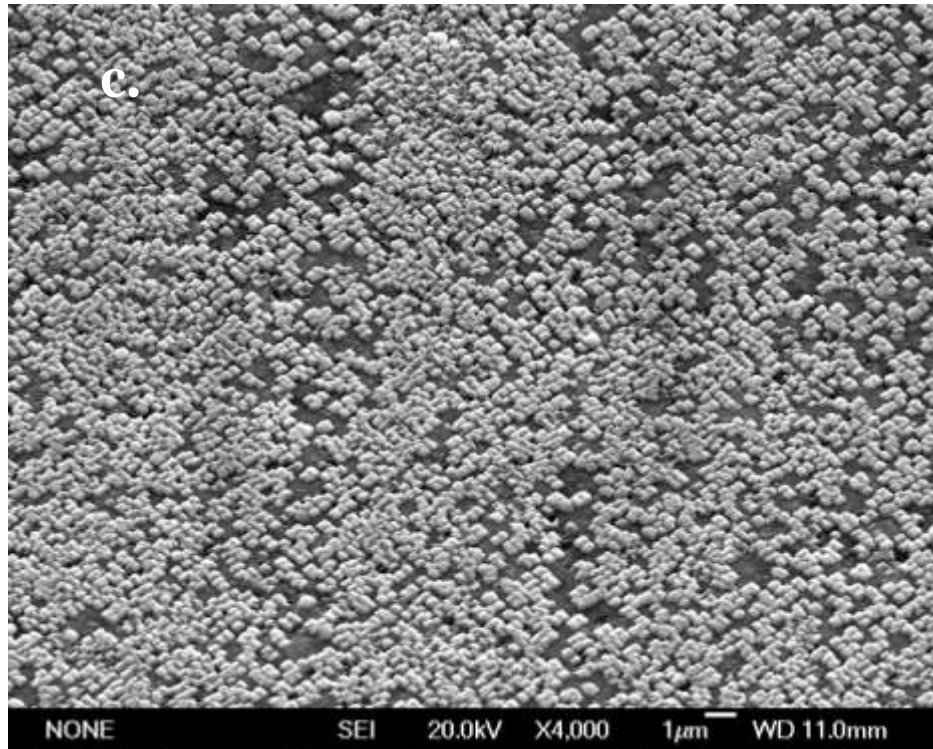
Fig.4.2.8.6 SEM images of AZO-065 on MgO(001) by 0.15 J/cm^2 laser

a) top view of direct centre, magnification of 4000;
b) top view of area away from the centre, magnification of 4000;
c) 30°tilt, area away from the centre, magnification of 4000

XRD was used to observe the central area of each sample. It was observed that, the strongest orientation was different and dependent on the energy level as indicated in Fig.4.2.8.7 and Fig.4.2.8.8. In order to clarify the preferential orientation with the increase of laser energy density, the relative intensities (100)/(101) and (002)/(101) of each sample and polycrystalline data from database were plotted in Fig.4.2.8.9 and Fig.4.2.8.10. With lower energy density, it tends to grow in the a-direction. However, at higher laser energy, it tends to grown in the c- direction.

In conclusion, decreasing the laser energy does not help in one dimensional nanostructures' growth and it also result in the unevenness of the sample's morphology.

179
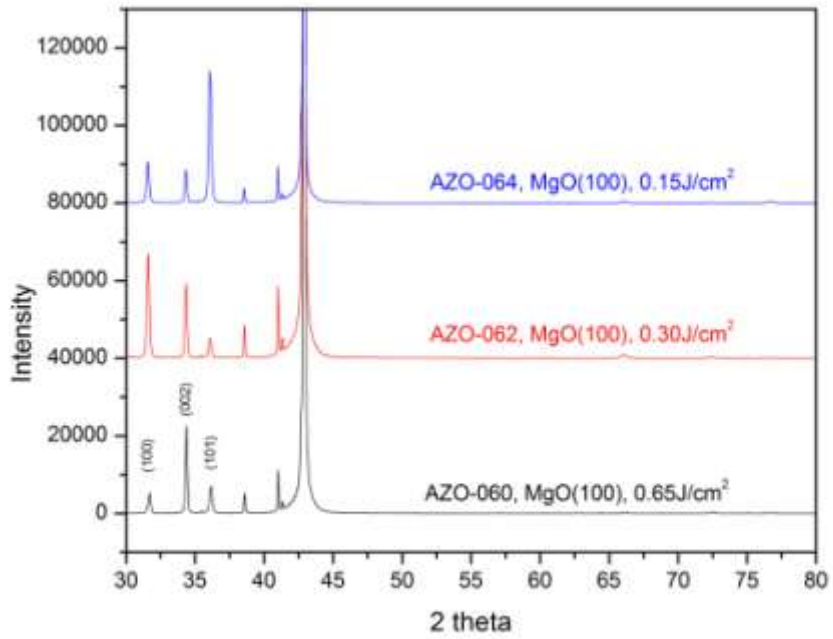
Fig.4.2.8.7 XRD patterns of ZnO grown on MgO(100)
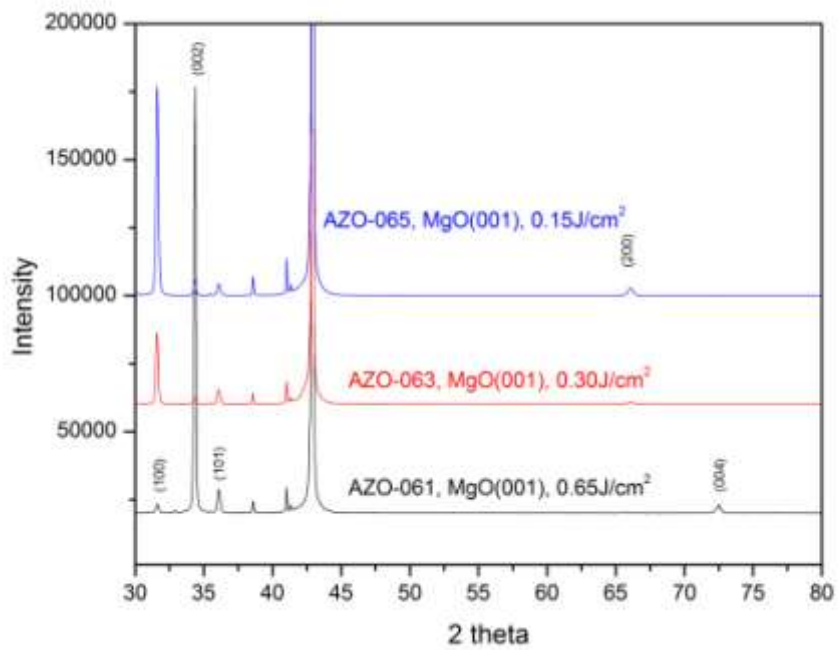
Fig.4.2.8.8 XRD patterns of ZnO grown on MgO(001)
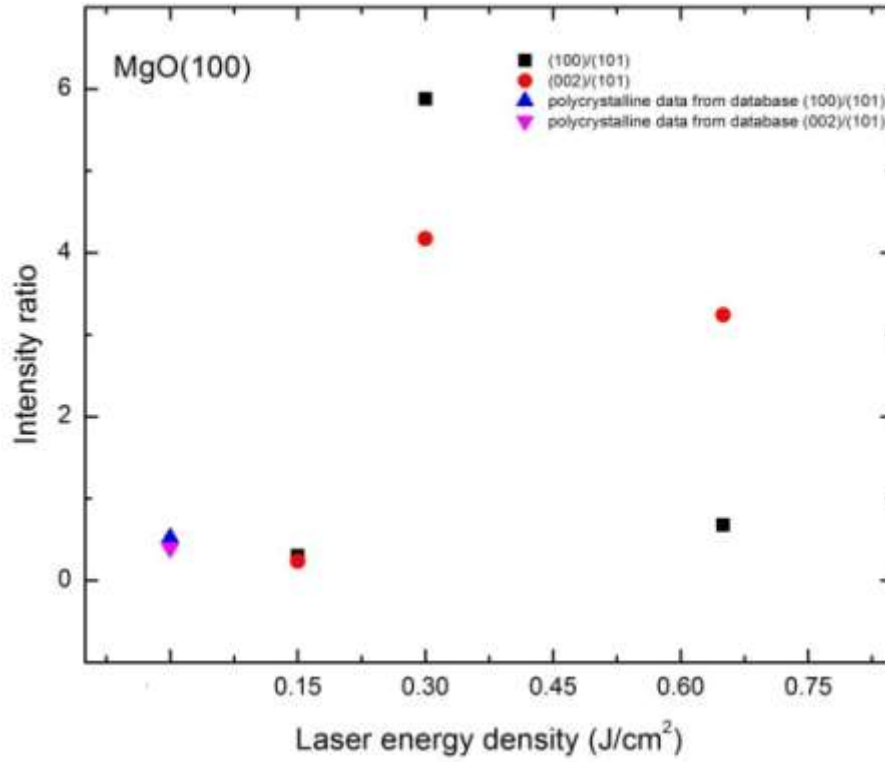
Fig.4.2.8.9 (100), (002) intensity ratio as a function of laser energy density on MgO(100) substrate
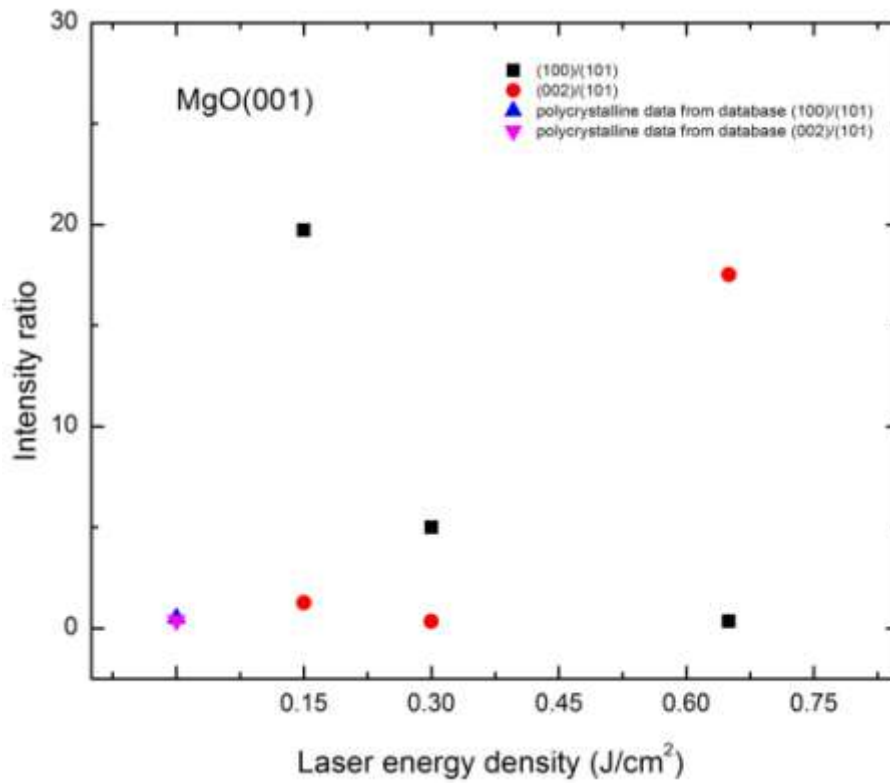

Fig.4.2.8.10 (100), (002) intensity ratio as a function of laser energy density on MgO(001) substrate

4.2.9 Influence of the target-substrate distance

4.2.9.1 Principles of effects of target-to-substrate distance

The effects of distance and ambient pressure between the target and substrate are interrelated. The scaling parameter for the plume range is E/P_0. E represents the laser pulse energy and P_0 represents the ambient gas pressure. The plume length ($L \propto (E/P_0)^{1/3\gamma}$) can be also calculated by using the scaling parameter (E/P_0) and the ratio of specific heats of the elements within the plume represented by γ. It was observed that when the distance between the target and the substrate is smaller than the plume length, the particle size and density registered no significant difference. However, as this distance increases the proportion of the smaller particles decrease and the appearance of larger particles begin to rise. This indicates that these particles are merging during flight. In a more common configuration in Fig.4.2.9.1, the substrate, positions parallel to the target, collects the laser generated flux. Therefore, the film thickness distribution can be expressed as $D(\theta) = A\cos\theta$ (derived from $f(\theta) \propto \cos\theta$) and the film volume can be expressed as $A\pi h^2/2$, where h represents the distance between the target and substrate. This leads to the conclusion that deposited films are not ideally flat and as the distance between the target and substrate vary, but it will not have any effect on the resulting thickness.

It was discovered in a previous experiment [1], as the distance between the target and substrate become closer, the result confirms a higher deposition rate and energy usage, despite the expectation of higher crystallinity from the shorter distance. Due to this observation, the thickness is directly influenced by the deposition rate and time. At specific distances between the target and substrate, the increase of depositing pulses can increase the thickness of the film by extending the time of the deposition.

TARGET

SUBSTRATE

LASER BEAM

θ: Polar angle (of ejection) measured from the target-surface normal
h: Target-to-substrate distance
φ: Angle of laser beam measured from the target-surface normal
V_x: Velocity at the X axis direction
V_z: Velocity at the Z axis direction
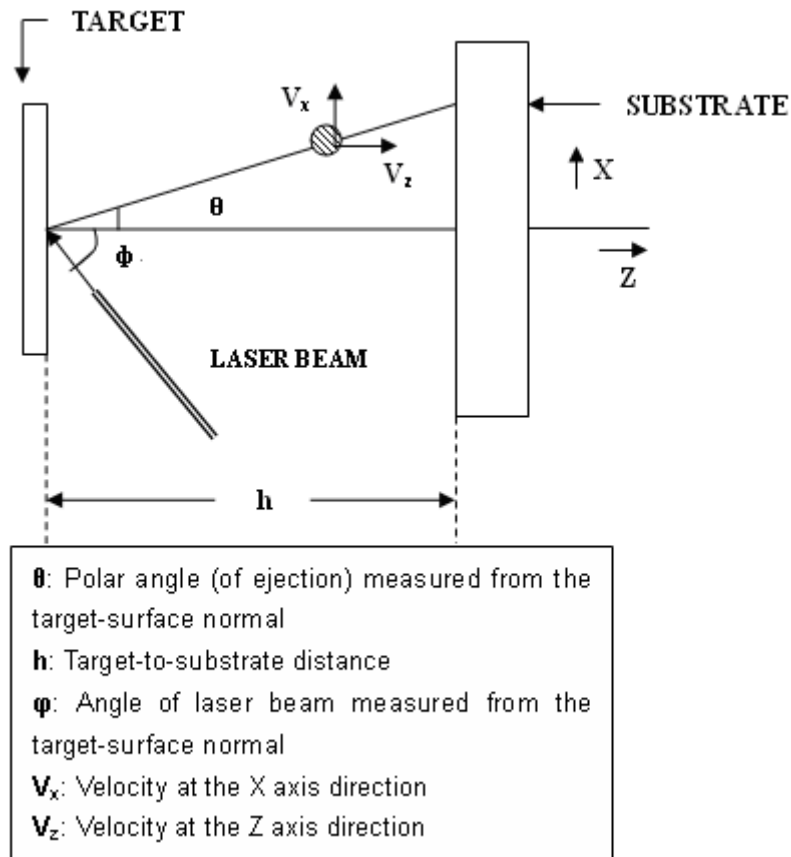
Fig.4.2.9.1 Deposition geometry [1]

4.2.9.2 Application of target-to-substrate distance

In the previous section, it was discussed that one dimensional nanostructures would need a lower energy level and a greater target-to-substrate distance, during their growth, would provide a lower deposition rate and energy. So theoretically, a greater target-to-substrate distance would help with the growth of one dimensional nanostructures under a specific temperature and oxygen pressure. The details regarding all samples taken into consideration within this section are listed in Table.4.2.19 and 4.2.20. Also, in all the samples observed the oxygen pressure was set at 1.2Torr.

**Table 4.2.19** Detailed Parameters of the samples AZO-009 and 011

Sample Number	Substrate	Temperature (˚C)	Chamber	**Distance of target-substrate (mm)**	Number of pulses on gold target(shots)	Number of pulses on ZnO target (shots)
AZO-009	MgO(100)	800	#1	**55**	5	5000
AZO-011	MgO(100)	800	#1	**65**	5	10,000

**Table 4.2.20** Detailed Parameters of the samples AZO-14812-1, 140812-2, 140812-3, 160812-1, 160812-2, and 160812-3

Sample Number	Substrate	Temperature (˚C)	Chamber	**Distance of target-substrate (mm)**	Number of pulses on gold target (shots)	Number of pulses on ZnO target (shots)
AZO-140812-1	MgO(100)	600	#2	**50**	5	5000
AZO-140812-2	STO(100)	600	#2	**50**	5	5000
AZO-140812-3	MgO(001)	600	#2	**50**	5	5000
AZO-160812-1	MgO(100)	600	#2	**40**	5	5000
AZO-160812-2	STO(100)	600	#2	**40**	5	5000
AZO-160812-3	MgO(001)	600	#2	**40**	5	5000

As indicated in the previous sections, 800°C is too high to form one dimensional nanostructures. At 800°C, sample AZO-009 in Fig.4.2.9.1, which was created with the distance of target-substrate of 55mm and with 5000 pulses, shows a rough structure without any particular nanostructures. Sample AZO-011 in Fig.4.2.9.2 was produced with 10,000 shots and increasing the target-substrate distance to 65mm. This resulted with a surface covered with bulk crystals and some nanorods which are parallel to the surface. These results indicate a greater target-substrate distance does help one dimensional nanostructure growth.
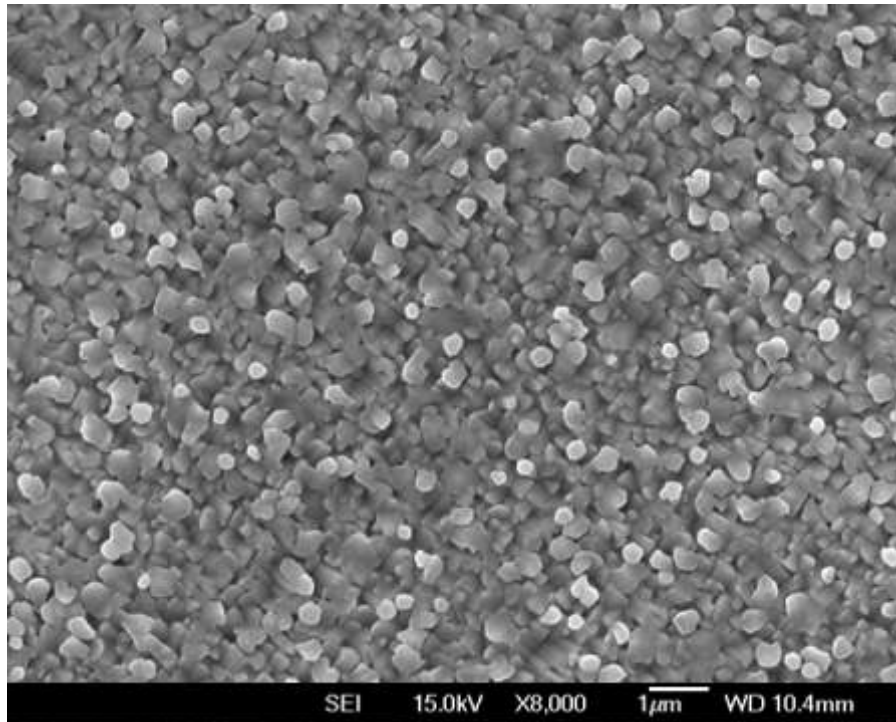
Fig.4.2.9.1 SEM image of AZO-009 on MgO(100) 800°C, 5000 shots on ZnO, with 55mm
target-substrate distance
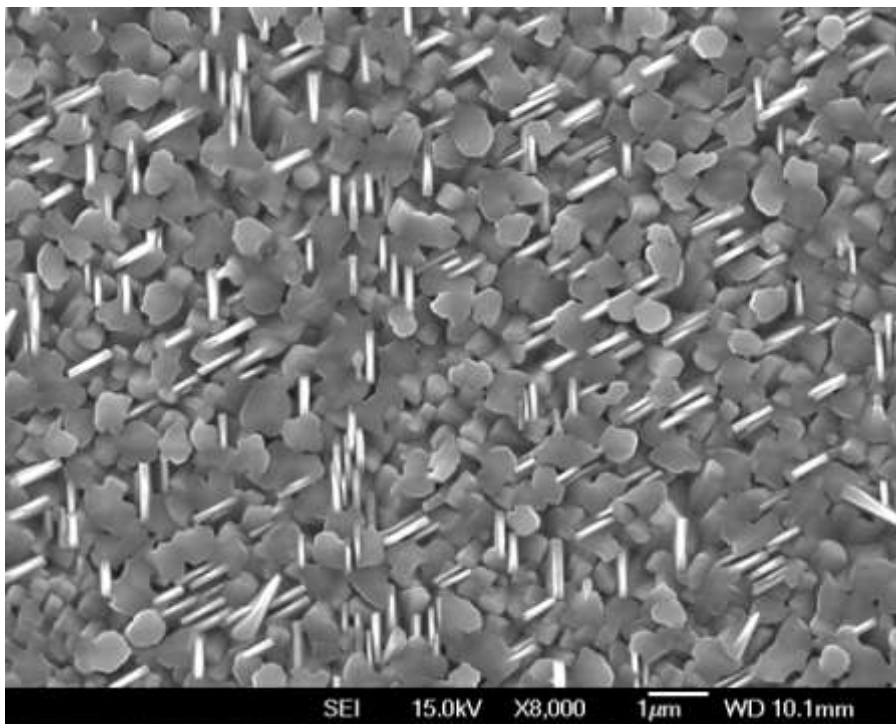
Fig.4.2.9.2 SEM image of AZO-011 on MgO(100) 800°C, 10,000 shots on ZnO, with 65mm
target-substrate distance

At a lower temperature of 600°C, on MgO(100) substrates, samples AZO-140812-1 and AZO-160812-1 were produced at target-substrate distance of 50mm and 40mm respectively. Not only do the quantity and the density of one dimensional nanostructures increase by shortening the distance, but the width of single nanorods also increase from 120~180nm to 150~280nm as well as the length increasing from 500nm~1µm to 1µm~1.5µm. As for samples AZO-140812-2 and AZO-160812-2, ZnO layers were coated on STO(100) substrates, as shown in Fig.4.2.9.5 and Fig.4.2.9.6. There were no one dimensional nanostructures present when the target-substrate distance was set at 50mm. However, when the distance was set at 40mm, nanorods and nanocones were formed, but the density and quantity of them are much lower when compared with those grown on MgO(100).
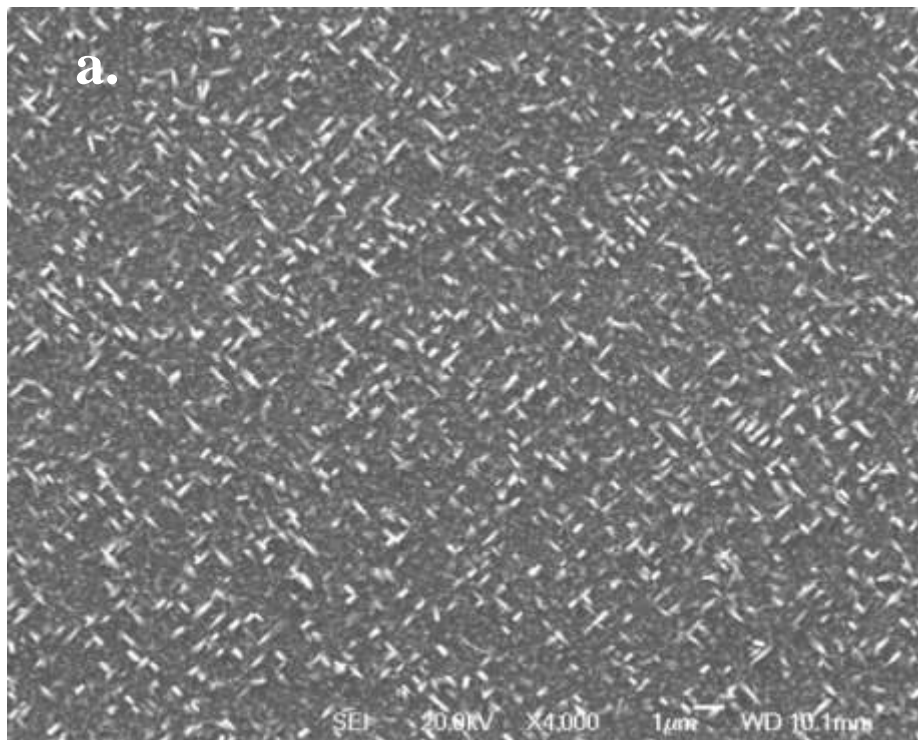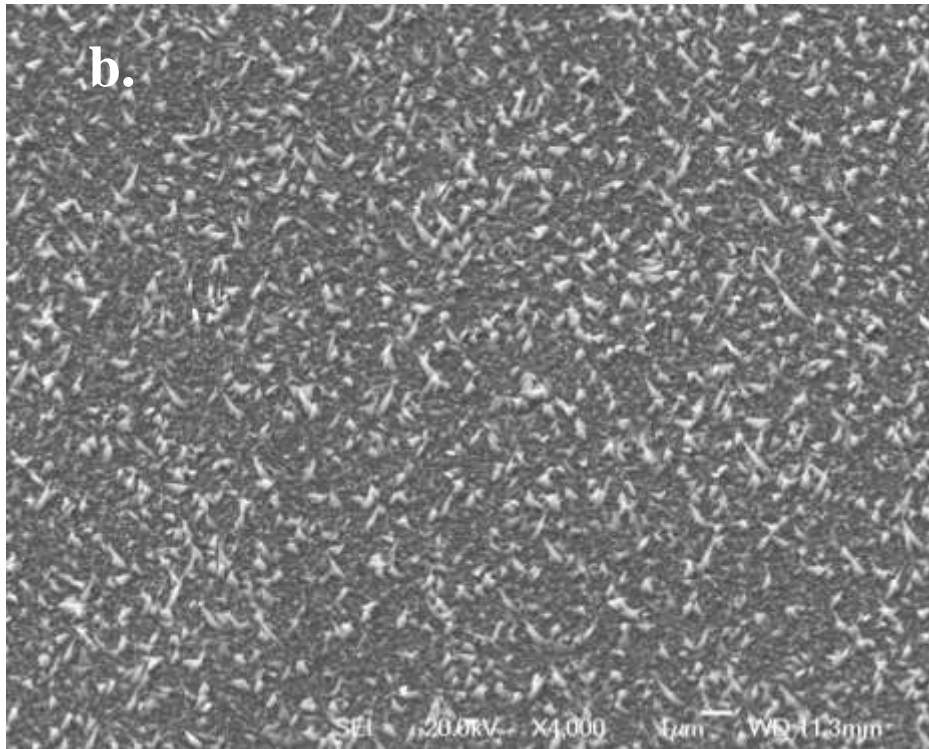
Fig.4.2.9.3 SEM images of AZO-140812-1 on MgO(100) 600°C, with 50mm target-substrate distance

a) top view, with magnification of 4000; b) 30° tilt, with magnification of 4000
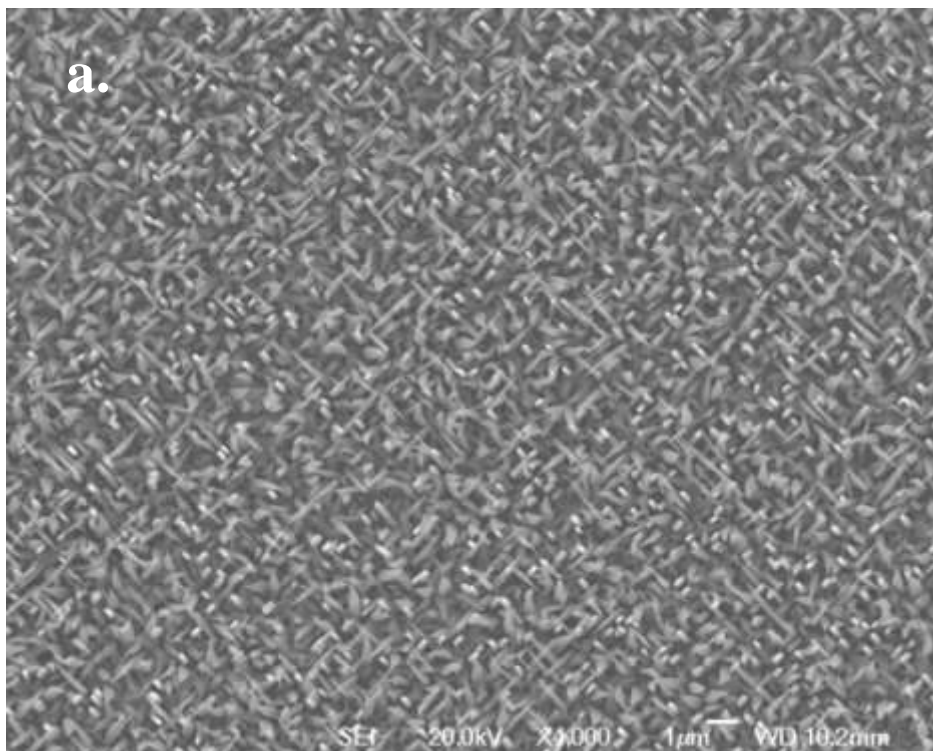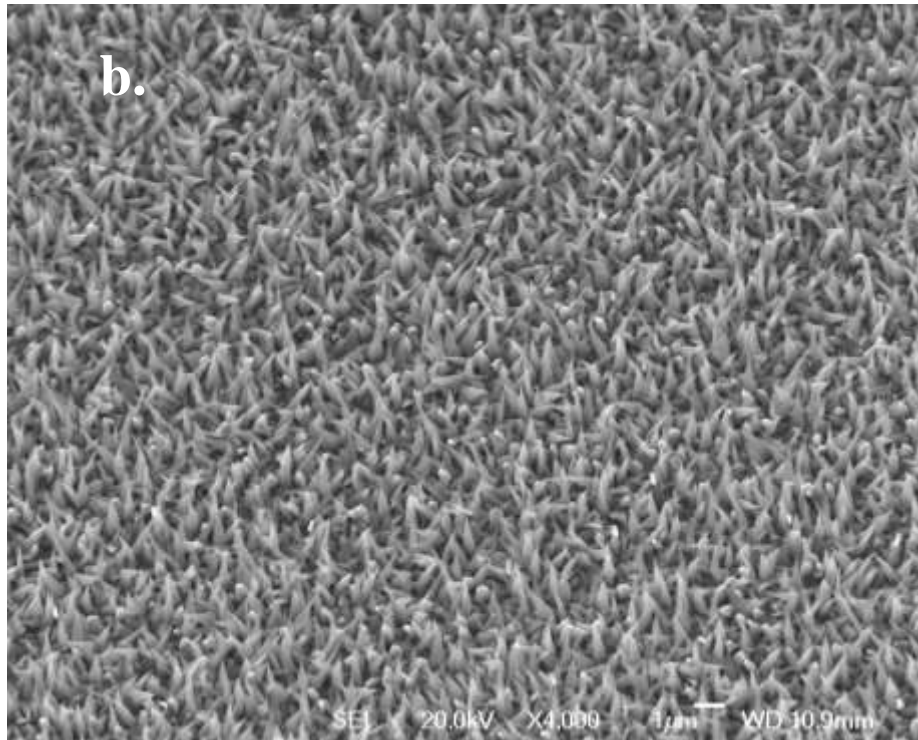
Fig.4.2.9.4 SEM images of AZO-160812-1 on MgO(100) 600°C, with 40mm target-substrate distance

a) top view, with magnification of 4000; b) 30° tilt, with magnification of 4000
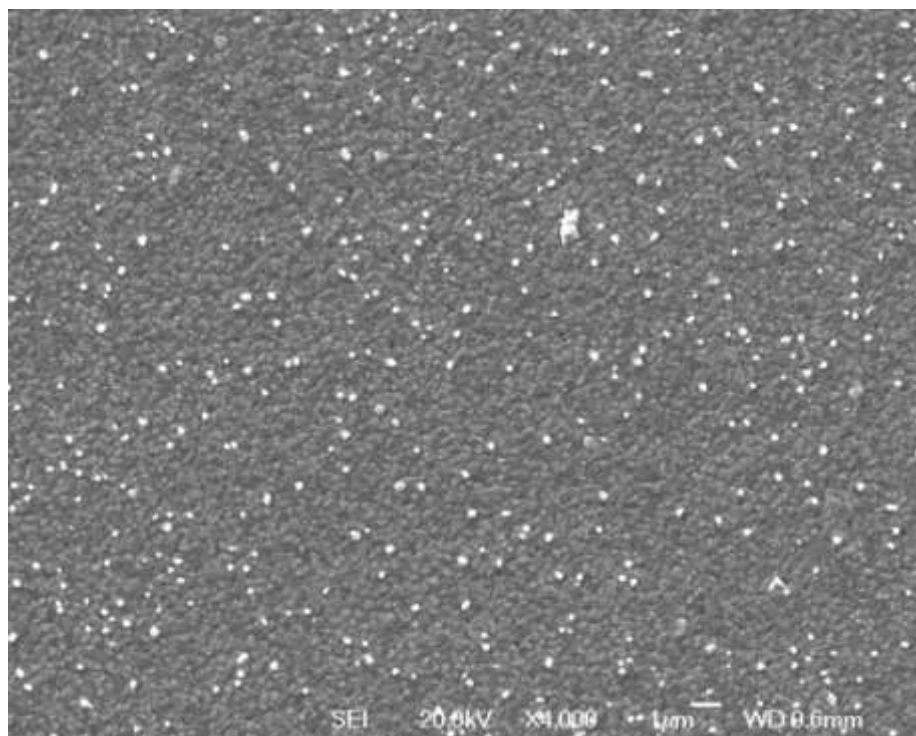
Fig.4.2.9.5 SEM image of AZO-140812-2 on STO(100) 600°C, with 50mm target-substrate distance, top view, with magnification of 4000
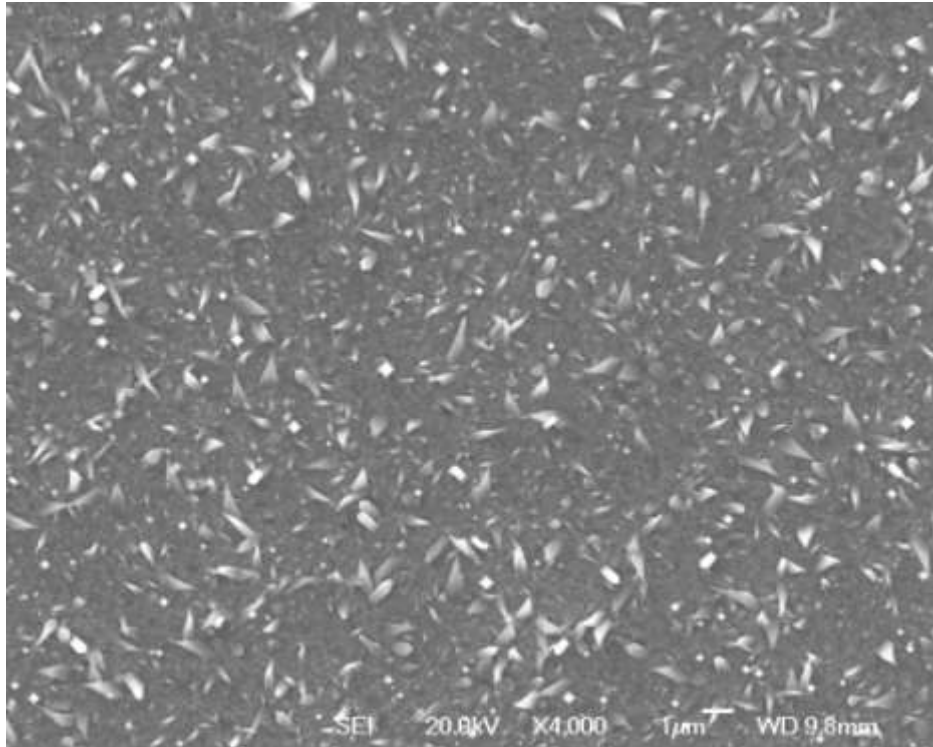
Fig.4.2.9.6 SEM image of AZO-160812-2 on STO(100) 600°C, with 40mm target-substrate distance, top view, with magnification of 4000

Samples AZO-140812-3 and AZO-160812-3, were deposited with ZnO on the substrate MgO(001). The differences between them are very similar with those differences between those produced on MgO(100). Therefore as the distance decreases, the quantity, density, width, and length of nanorods and nanocones increase.

Another observation that was noted was that on the southeast corner of both samples, the parallel nanorods, with scattered perpendicular nanorods are formed in arrays of four different directions, which is different from the other areas of the sample. This may have been due to the plume or the gas flow in the chamber.

Comparing the morphology of sample AZO-160812-1 with AZO-160812-3, the one dimensional nanostructures on MgO(100) are more straight, while on MgO(001) they are bent from the middle. This difference is due to the production process of different manufactures.

189
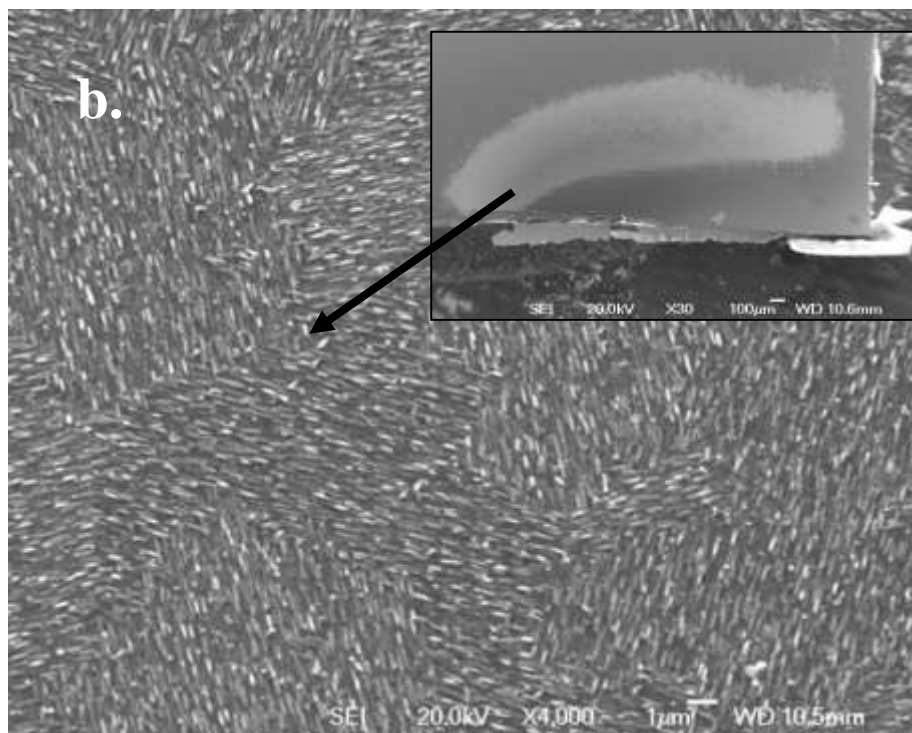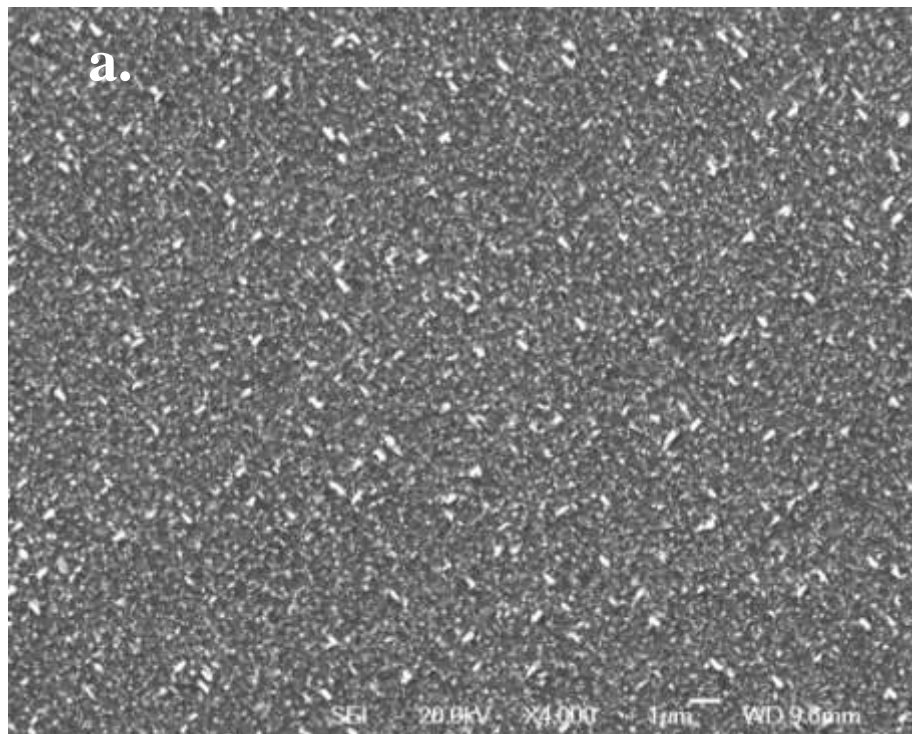
Fig.4.2.9.7 SEM images of AZO-140812-3 on MgO(001) 600°C, with 50mm target-substrate distance

a) top view, with magnification of 4000; b) top view of corner, with magnification of 30 and 4000
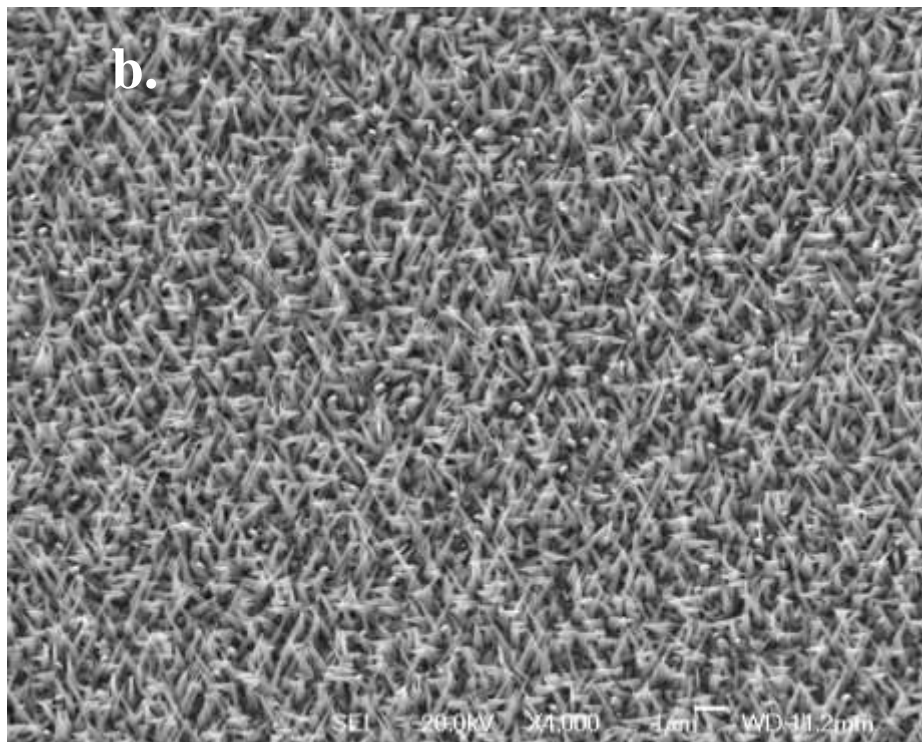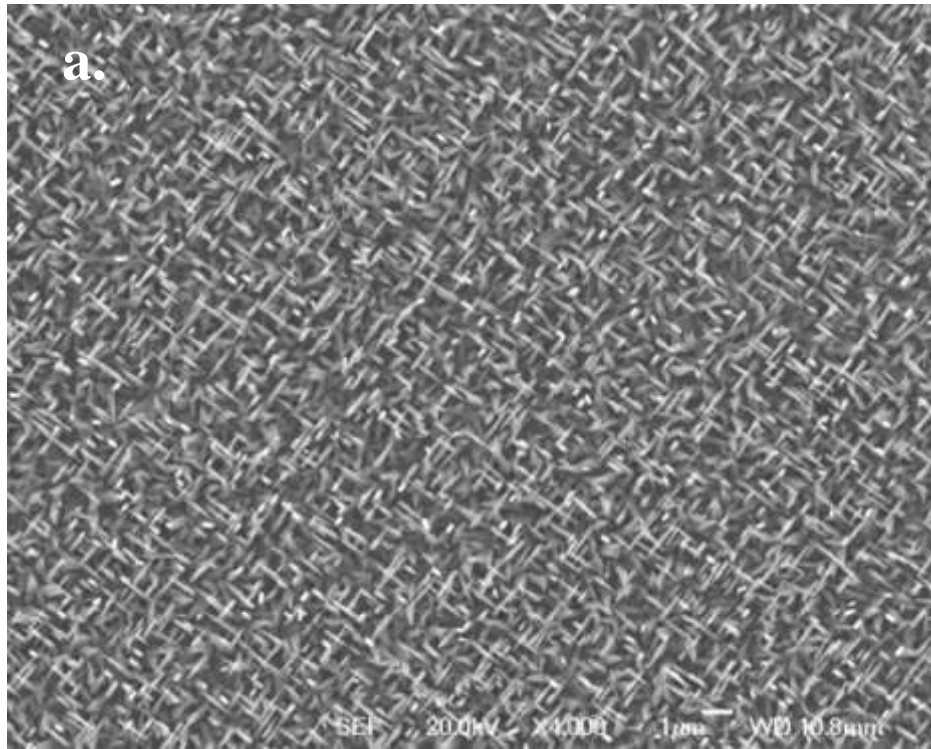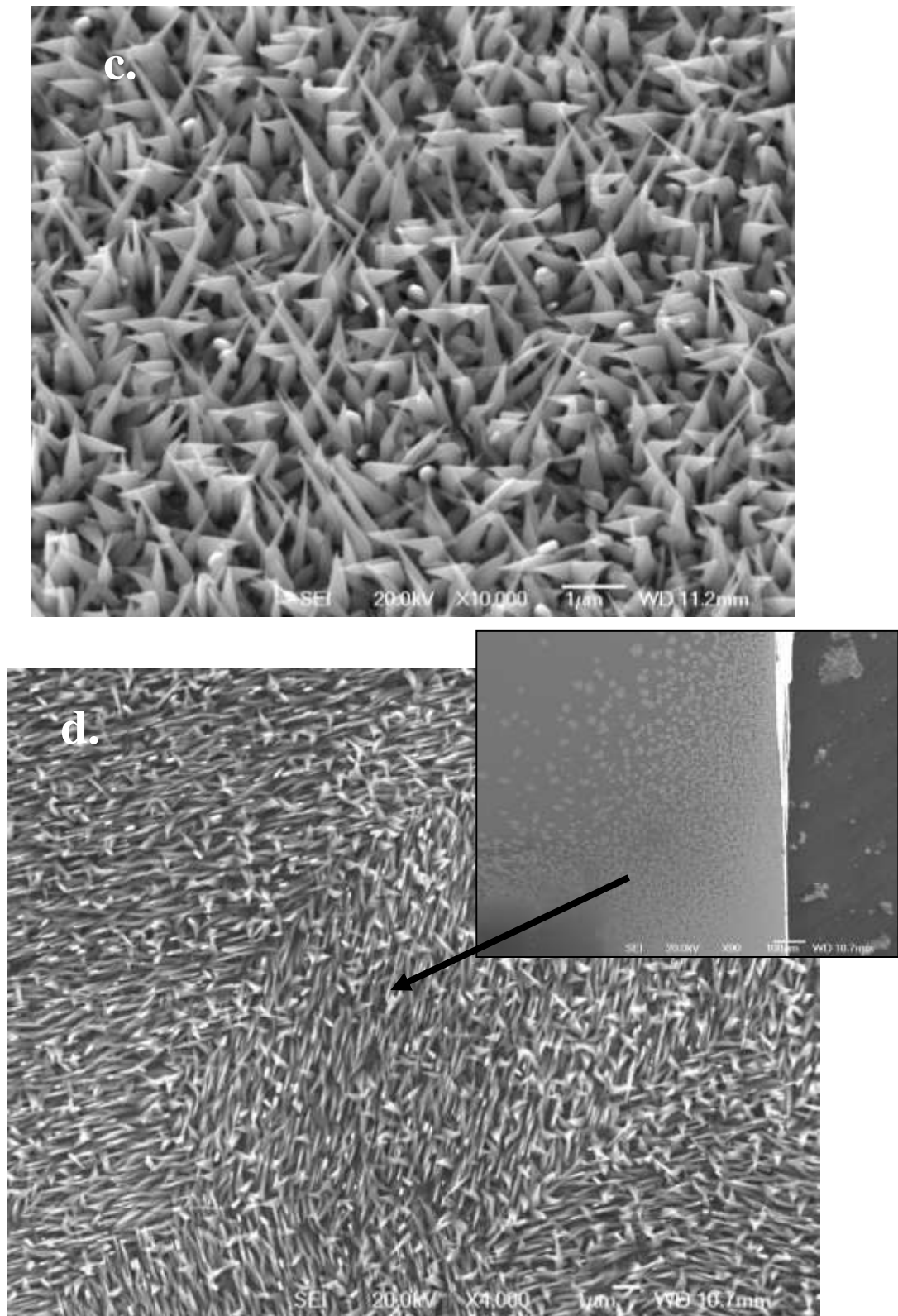
Fig.4.2.9.8 SEM images of AZO-160812-3 on MgO(001) 600°C, with 40mm target-substrate distance

a) top view, with magnification of 4000; b) 30° tilt, magnification of 4000;
c) 30° tilt, magnification of 10,000; d) top view of corner, with magnification of 90 and 4000

In conclusion, at higher temperatures, a greater target-substrate distance could be advantageous to the formation of one dimensional nanostructures. However, in lower temperatures, a shorter target-substrate distance could increase the quantity, density, width and length of one dimensional nanostructures.

4.2.10 Discussion of ZnO nanowires/ nanorods growth mechanism

There are two distinct growth modes found in the morphologies of the samples.

4.2.10.1 VLS growth

Sample AZO-001 produced in chamber #1, under laser frequency of 10Hz, indicates a typical VLS growth morphology. As shown in Fig.4.2.10.1, in which a liquid-like globule is found in the tip of nanocones and also on the grain boundaries. This is noted by the arrows in the image. However, it is difficult to confirm if the globule is from the gold layer, since the amount of gold in the sample is too small to be detected by EDS or TEM.
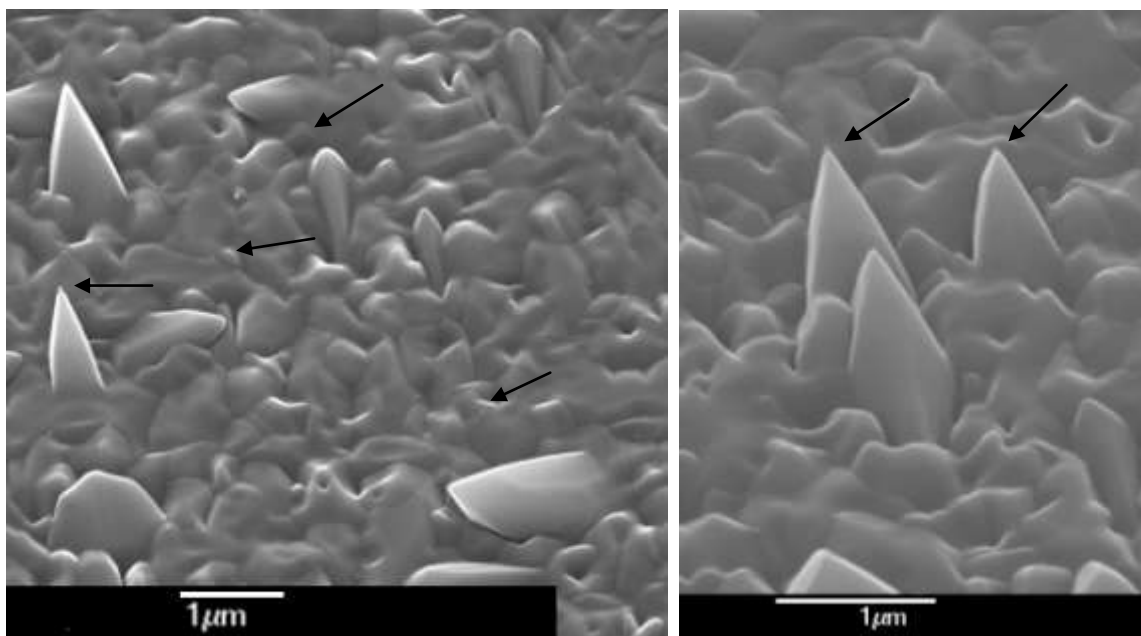
Fig. 4.2.10.1 SEM images of ZnO deposition on MgO(100) substrate with 450 mTorr oxygen partial pressure at 800˚C, 5 pulses on gold, 10000 pulses on Zn

The growth procedure is detailed in Fig. 4.2.10.2. Upon depositing gold pulses on the MgO (100) substrate with 5 pulses, the heater annealed the gold layer into a liquid state. This forms a droplet on the surface of the substrate. The particles from the ZnO target form a plume during the deposition of ZnO. These particles diffuse randomly as they arrive on the surface. On a flat surface, the particles may find different sites with different energy levels. The resulting crystal structure is due to the particle being incorporated into the structure when it diffuses to an energetically favorable site. These energetically favorable sites are associated with the gold nanodots, as they can relieve the surface tension [2]. The formation of the liquid-like globules on the grain boundaries may be caused by the dynamic conditions a PLD system

PLD is a traditional technique for producing thin-films. The particles within the PLD plasma plume may have obtained higher energy when compared with the species in other techniques. Some of the particles undergo a nucleation effect, rather than diffusing to the gold dots. In a previous study on the effect of pulses numbers on a ZnO target, it was observed that ZnO depositions tends to grow in a Volmer-Weber (island formation) nucleation and growth mode for higher temperature as 800°C. This would explain the presence of other gold dots found on the grain boundaries.
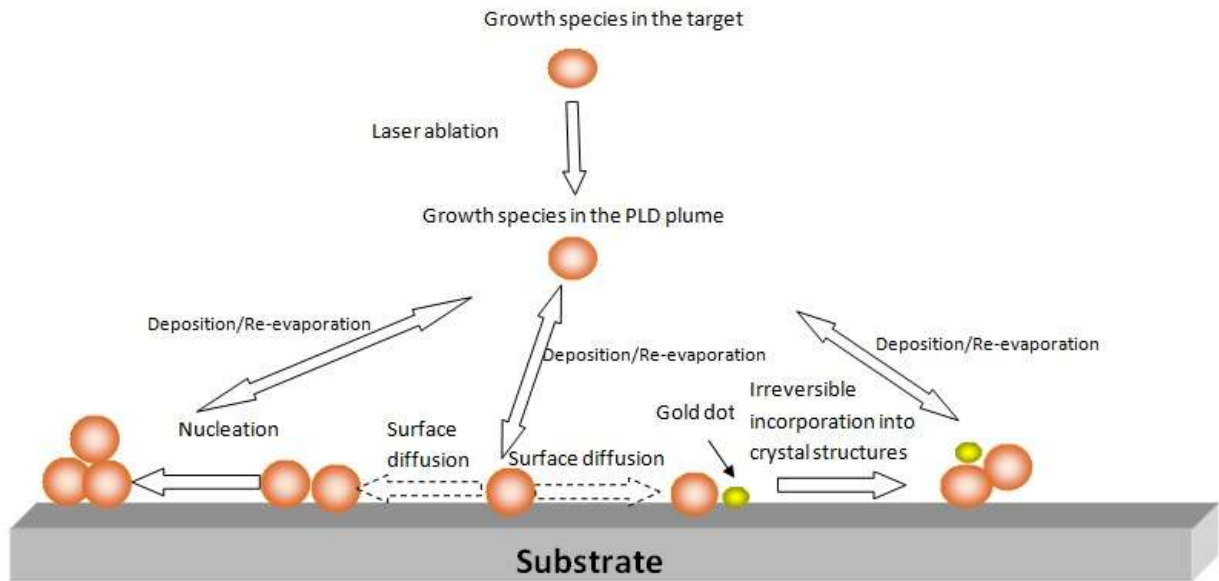
Fig. 4.2.10.2 Growth species schematic

4.2.10.2 Self-mediated growth

Another growth mechanism was found in this study of sample AZO-015, which is shown in Fig.4.2.10.3. The assumption of this growth mechanism is shown in Fig.4.2.10.4. At a suitable synthesis temperature, after the crystallized bulks are preliminarily formed, the interface between the surface of the bulks and the plume reach a supersaturating state. The sites with different energy levels distribute on the surface of the bulks. The particles within the plume may choose to diffuse onto those energetically favorable sites on the surface. Once these particles diffuse onto these sites nucleation will begin and nanowires will begin to grow.
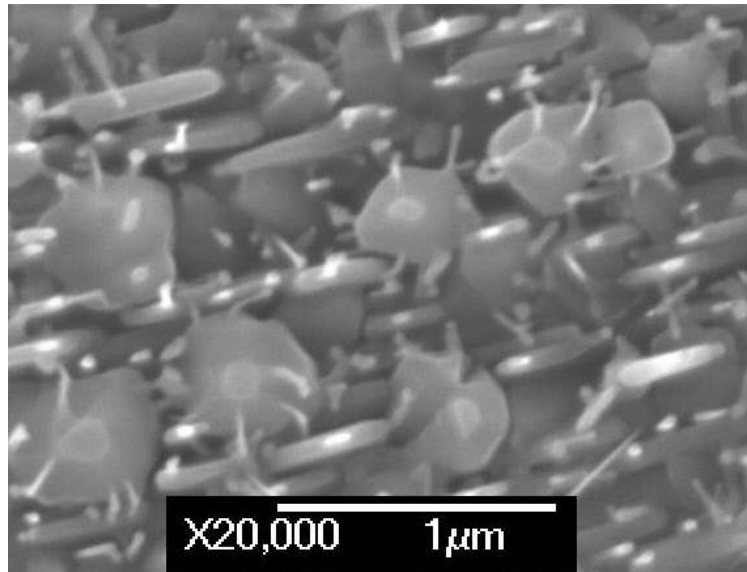
Fig. 4.2.10.3 SEM image of ZnO deposition on MgO(100) substrate with 1200 mTorr oxygen partial pressure at 750°C, 5 pulses on gold, 5000 pulses on ZnO in chamber #2.
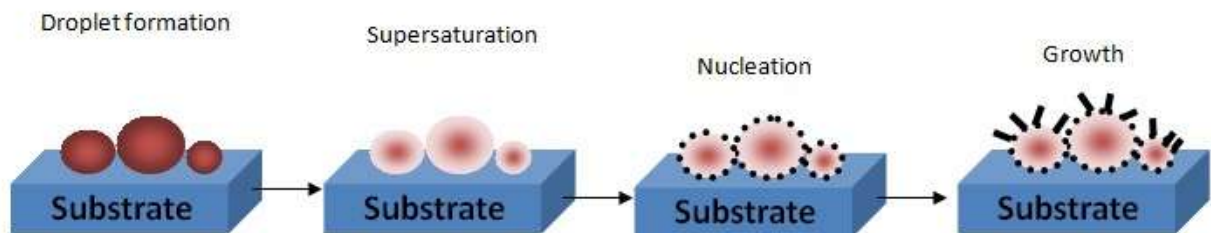
Fig. 4.2.10.4 Self-mediated growth mode

For the most ZnO samples observed, there were no indications of any obvious liquid-like globules found on the tip of nanorods or nanowires. The growth may not be according to VLS mode. However, in this study it does prove that gold nanodots do have a catalytic effect. The formation of, PLD produced, ZnO one dimensional nanostructures may combine more than one growth modes during the growth process.

4.3 In₂O₃ and SnO₂ Nanowires and Nanorods

4.3.1 Influence of substrate temperature

In the ZnO section, a proper temperature is the key parameter in order to produce one dimensional nanostructures. This is also the case for the samples in this section. Each of the samples discussed in this section, the following control parameters were utilized: laser energy density was kept at 1 J/cm^2.

Table 4.3.1 Detailed parameters of the samples of INOA-004,001 and 005

| Sample Number	Temperature (°C)	Number of pulses on Au target (shots)	Number of pulses on In₂O₃ target (shots)	Oxygen pressure (Torr)	Substrate
INOA-004	**300**	5	5000	1.2	MgO(100)
INOA-001	**500**	5	5000	1.2	MgO(100)
INOA-005	**700**	5	5000	1.2	MgO(100)

It was observed that 300°C is too low a temperature for In₂O₃ to form any particular crystalline structures. When the temperature was raised above 500°C, a very uniform array of nanorods begins to appear on the surface. As the temperature is increased to 700°C, the dimension of a single nanorod increases from 30~80nm to 70~150nm. Also the crossection of the nanostructure changes from quadrilateral shape into very well defined rectangular shape.

In the ZnO section, the areas near the edges are the areas that grow the comparative complex structures. The samples within this section also conform to this, but are situation in a different formation. In some conditions, extremely long ZnO nanowires have been found to grow at these areas. However, in the case of In₂O₃, nanorods not only cover the top surface of the substrate, but also the side of it as well. There is no obvious change on the length of nanorods, but some big bulk crystals also appear at the areas near the edge as well as on the

edge, as shown in Fig.4.3.1.2c and Fig.4.3.1.3c. The quantity of bulk crystals also decrease by increasing the producing temperature.

An attempt to separate the nanorods was conducted by using a specific process. First, a scalpel was used to scratch the coating. Then the sample was flushed by ethanol and the solution of ethanol and coating was collected. This solution then was shaken by the use of an ultrasonic cleaner. Once this was completed a pasteur pipette was used to apply a single drop of the solution onto a piece of glass. The sample was then allowed to volatilize before being further studied. A SEM image of a single In_2O_3 nanorod is shown in Fig.4.3.1.4 that was the result of this process.

In conclusion, a higher temperature is needed when producing one dimensional In_2O_3 nanostructures. Based on the observations of the samples used, the width of nanorods also increase as the deposition temperature increases.
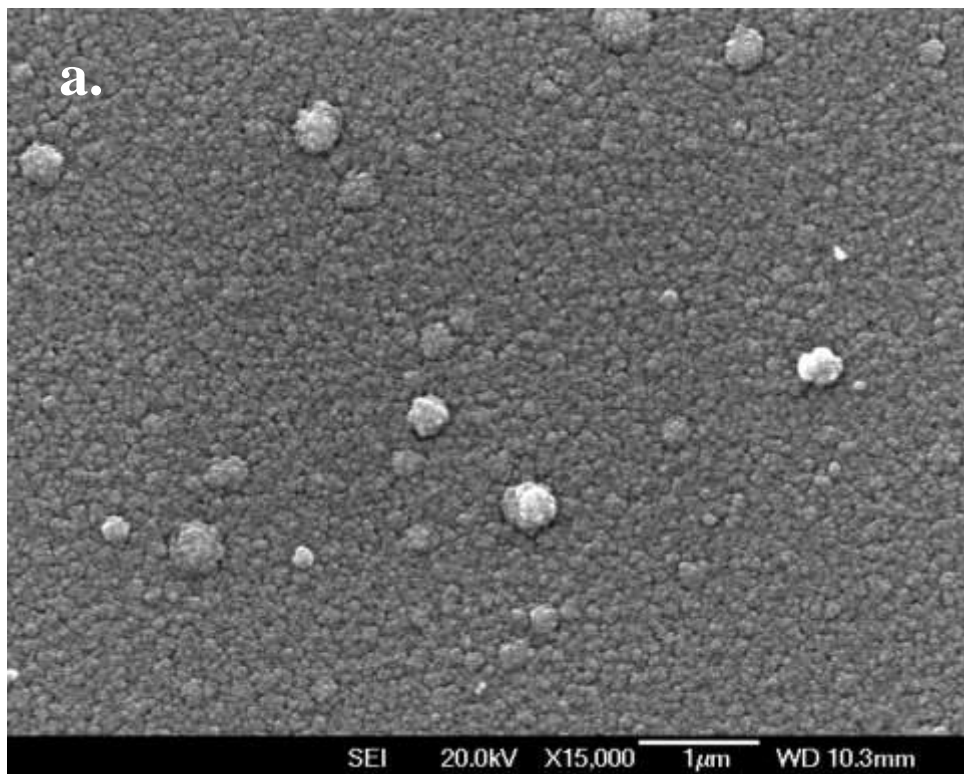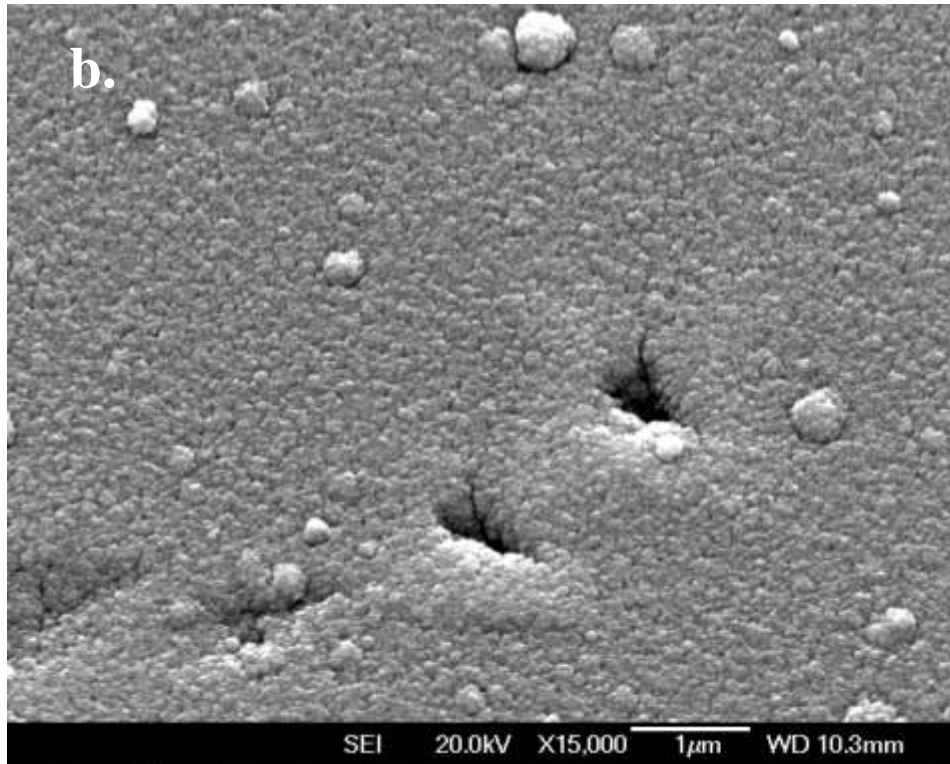
**Fig. 4.3.1.1** SEM images of INOA-004 deposited at 300°C

a) top view, magnification of 15,000; b) 25˚ tilt, magnification of 15,000
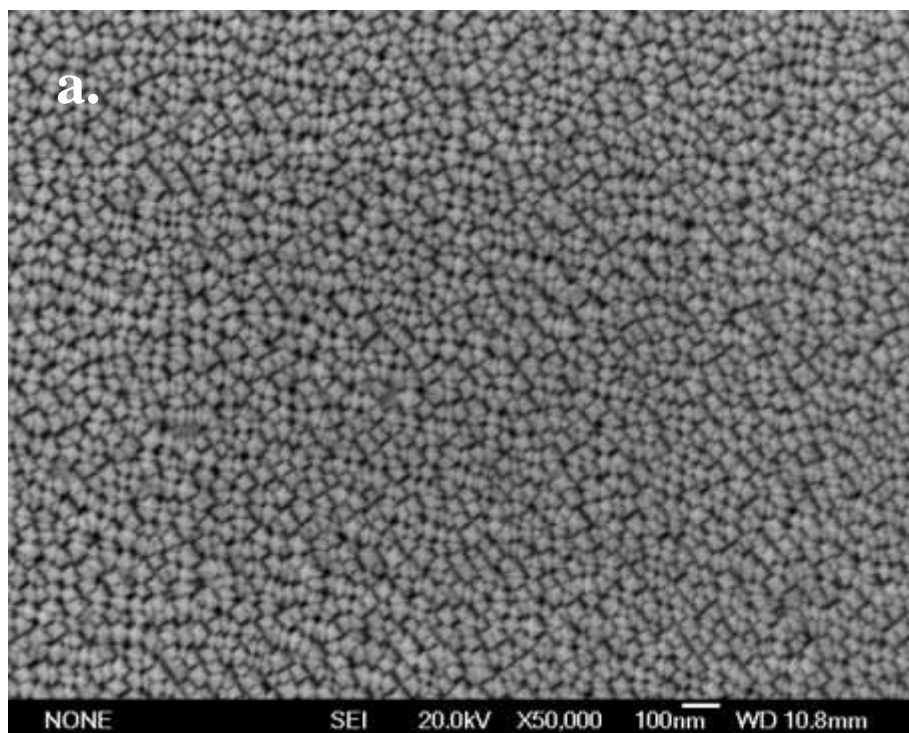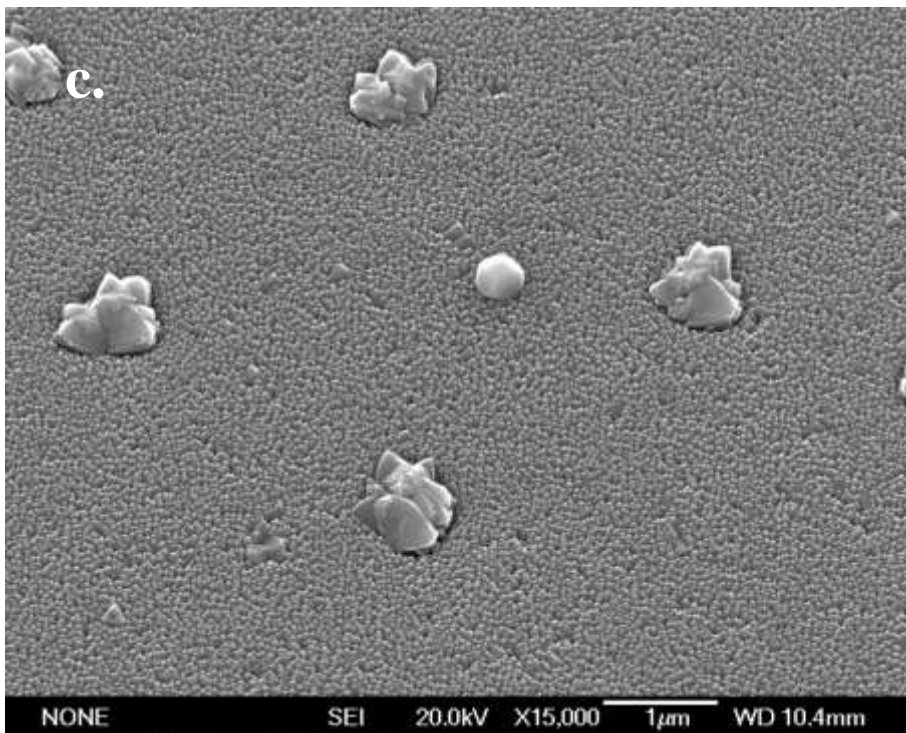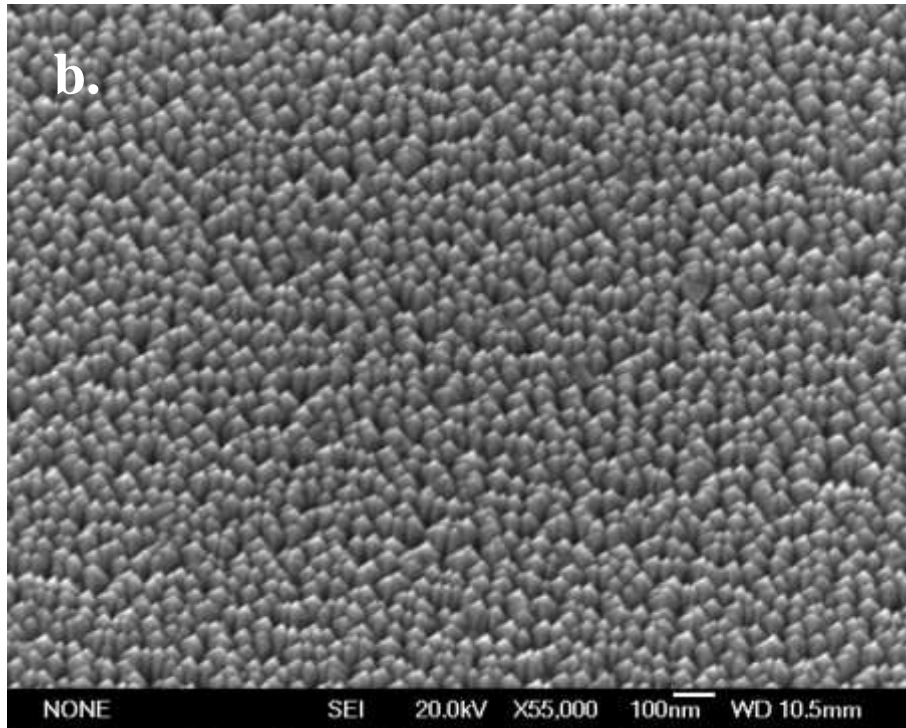
Fig. 4.3.1.2 SEM images of INOA-001 deposited at 500°C

a) top view, magnification of 50,000; b) 25° tilt, magnification of 55,000;
c) area near the edge, 25° tilt, magnification of 15,000
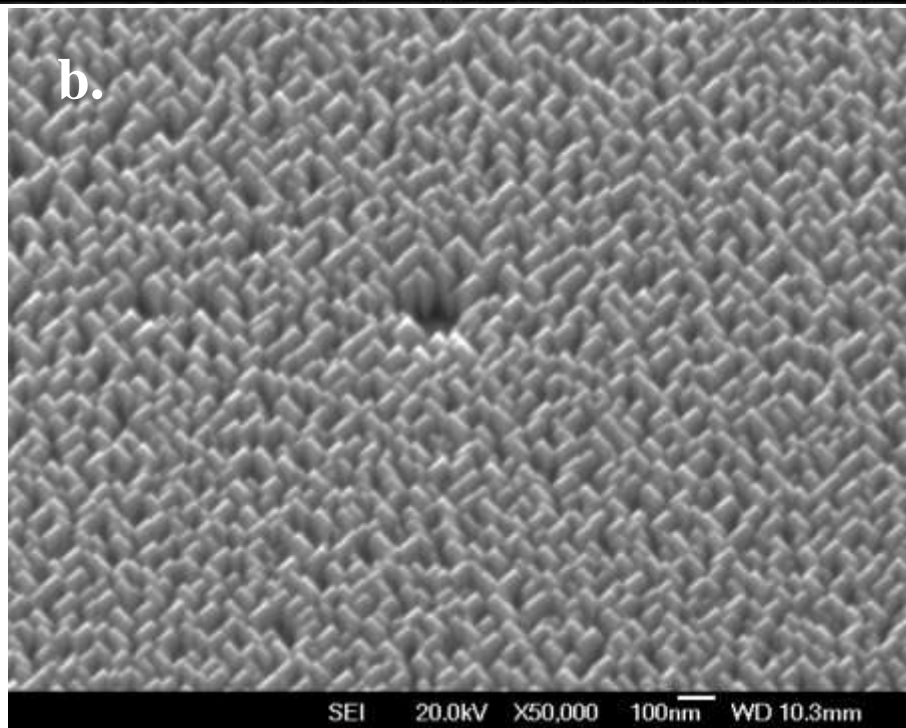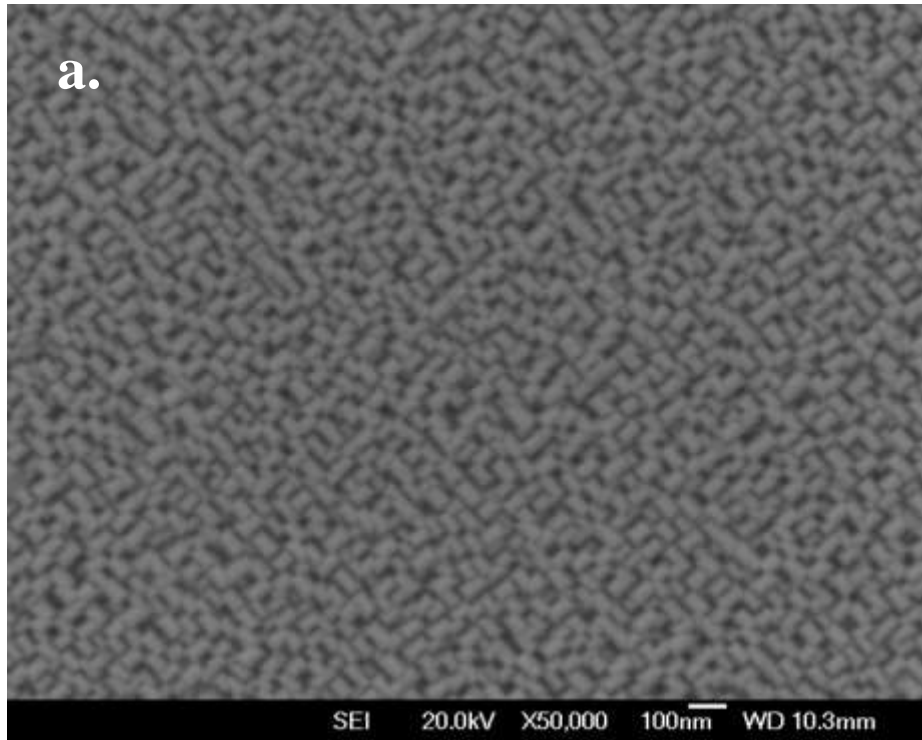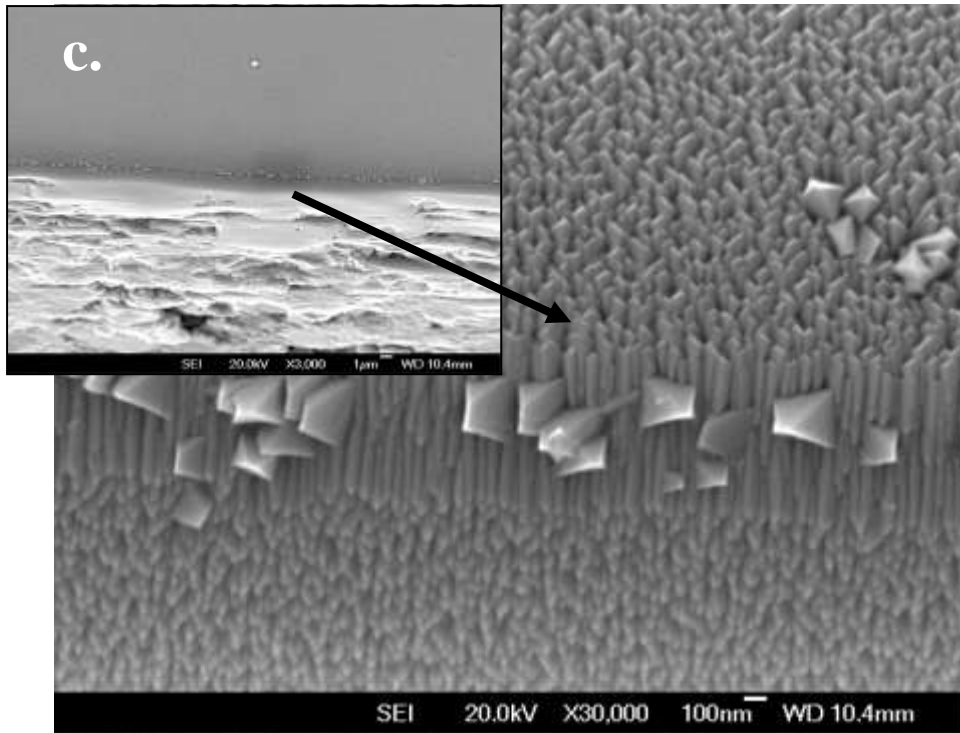
**Fig. 4.3.1.3** SEM images of INOA-005 deposited at 700°C

a) top view, magnification of 50,000; b) 25° tilt, magnification of 50,000;
c) area of the edge, 25° tilt, magnification of 3000 and 30,000

Fig.4.3.1.4 SEM image of a single nanorod

4.3.2 Influence of metal catalyst

### 4.3.2.1 Influence of gold nanodots on In₂O₃ nanorods growth

The parameters used for all the samples within this section are listed in Table 4.3.2. In addition to the listed parameters, the laser energy density was also kept at 1 J/cm^2, as a control parameter.

Table 4.3.2 Detailed parameters of the samples of INOA-053,051,002 and 003

Sample Number	Temperature (˚C)	Chamber number	Number of pulses on Au target (shots)	Substrate	Distance of Target to Substrate (mm)	Number of pulses on In₂O₃ target (shots)	Oxygen Pressure (mTorr)
INOA-053	500	#3	**0**	MgO(100)	55	5000	1200
INOA-051	500	#3	**2**	MgO(100)	55	10,000	1200
INOA-002	500	#3	**5**	MgO(100)	55	10,000	1200
INOA-003	500	#3	**25**	MgO(100)	55	10,000	1200

Sample INOA-053 was produced without any shots on the gold target. The resulting nanostructures that are formed are not uniform in shape and are also scattered throughout the sample. It can be seen that the nanostructures are also being grown in a variety of different directions. Also the nanostructures, that are formed, overlap each other. XRD patterns in Fig. 4.3.2.3 indicate that the peak (222) becomes weaker by adding 2 shots on gold target, while peak (400) becomes stronger. Therefore, it can be assumed that gold plays a factor in the growth and orientation of these nanostructures. The nanostructures formed near the edge of the sample are similar with those found on sample INOA-051. The nanostructures found near the edge are grown in a perpendicular orientation while the nanostructures near the centre have a random orientation. This occurrence is caused by the same methods used with ZnO.
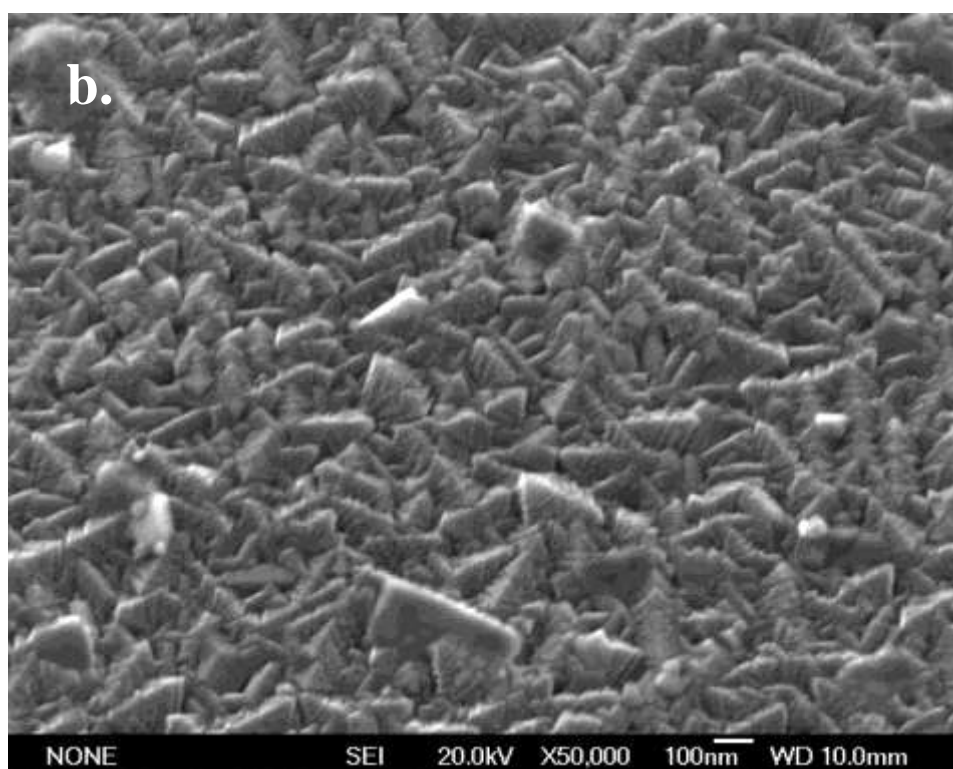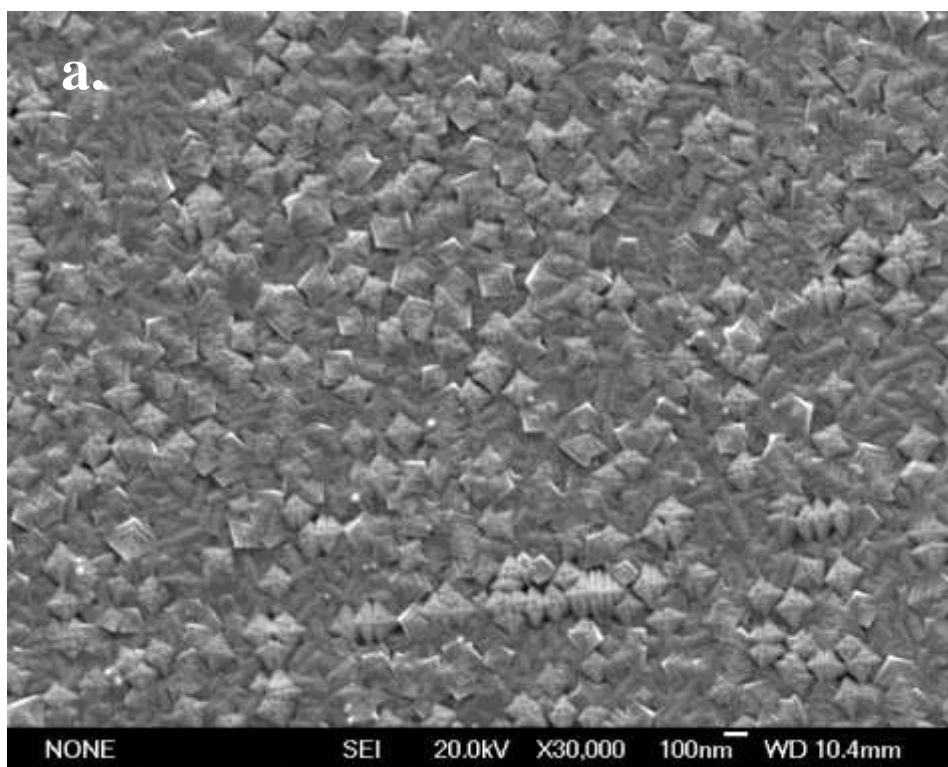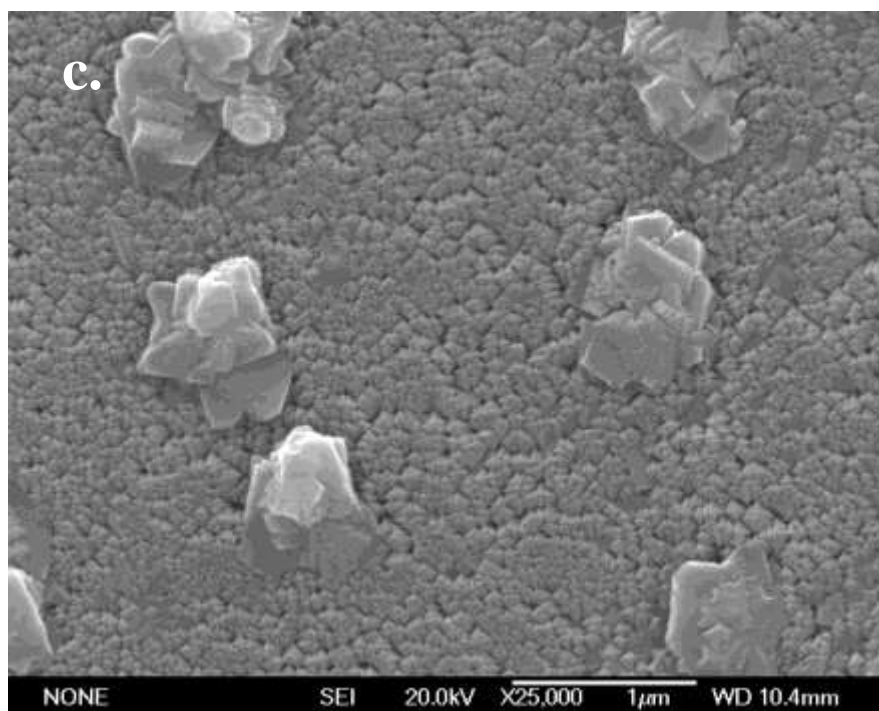
**Fig. 4.3.2.1** SEM images of INOA-053 with 0 shots on Au and 5000 shots on In_2O_3

a) top view of central area, magnification of 30,000; b) 30° tilt, magnification of 50,000;
c) top view of a corner, magnification of 25,000

The gold nanodots can release the surface tension on the sample. When the number of gold shots is too few to release the tension all over the entire surface, in some areas, In_2O_3 nanorods grow together and cannot be separated, as shown in Fig.4.3.2.2b. In the areas near the edge of the same sample, the In_2O_3 particles from the plume are crystallized into a four-leaf clover or petal shape on top of the nanorods. The detailed image, from Fig.4.3.2.2 indicates that these structures still mainly keep the one dimensional growth mode, despite being larger in size. When the gold coating is too thick to release the surface tension, the nanostructures formed are relatively uniform but there are large clusters that have grouped together to form the larger nanostructures, this phenomena is more obvious on the area near the edge. Fig.4.3.2.5a displays an example of such a nanostructure by 25 shots of gold on the substrate. When compared with Fig.4.3.2.4a, the nanostructures formed are more evenly uniform and formations of large nanostructures are not present. As for the edge areas, the In_2O_3 particles from the plume takes part into the growth of single nanorods, as shown in

4.3.2.4.b, which could explain why the average width of nanorods near the edges are larger. Therefore, it can be assumed that the optimal amount of gold shots for In$_2$O$_3$ nanorods growth must between 5 and 25 shots.

In conclusion, the fewer the gold shots, the thicker the nanostructures become. However, as the shots increase it was observed that the nanostructures became more uniform in size, but the occurrences of larger structures also were present. In order to maintain a uniform size of nanostructures formed, it was observed that the total numbers of gold shots should not be less than 5 shots and no more than 25 shots.
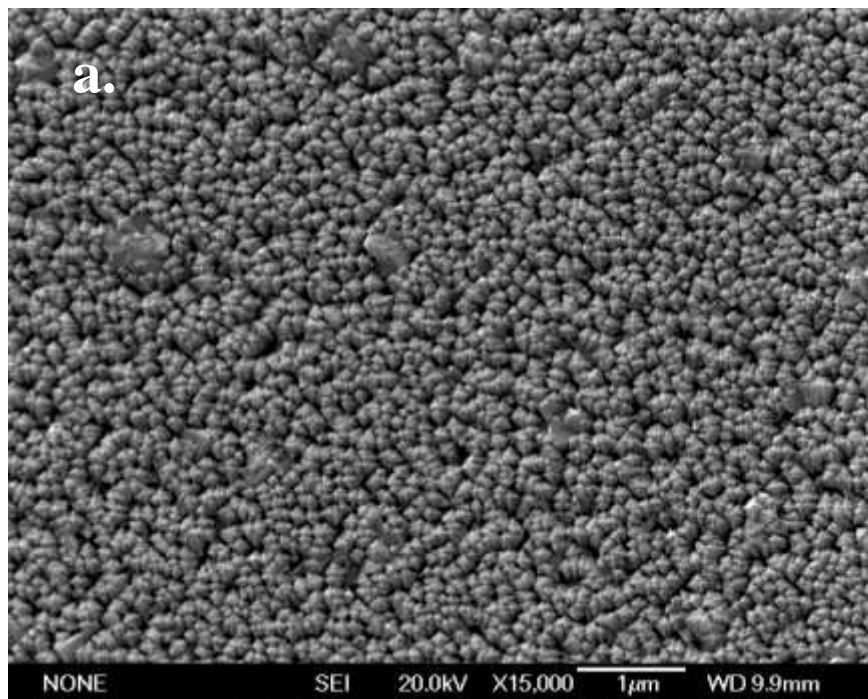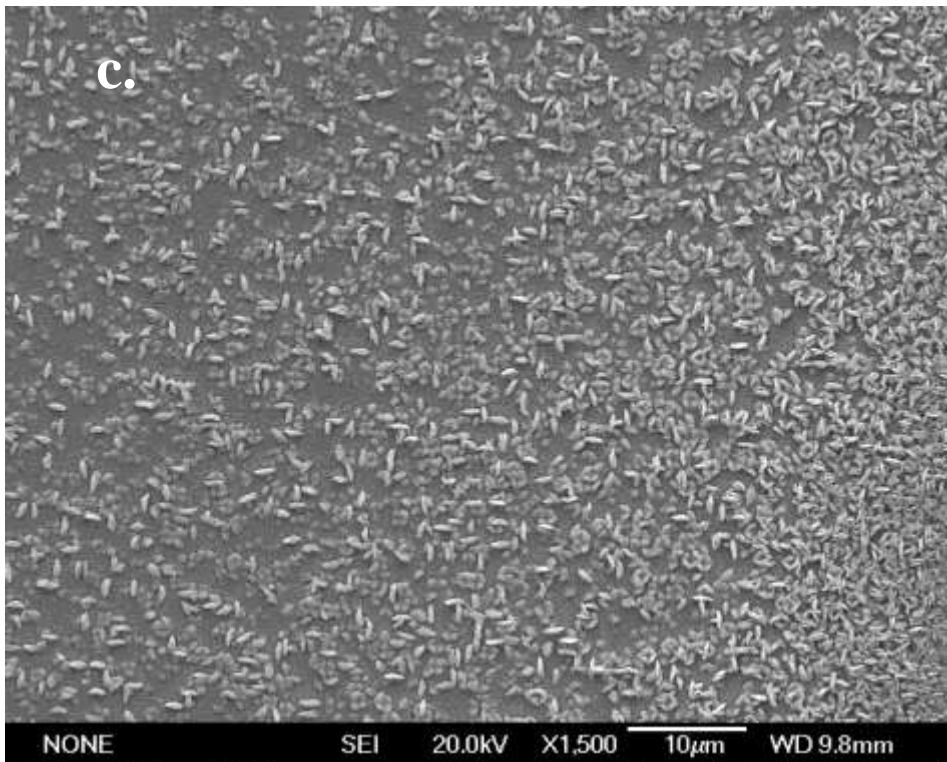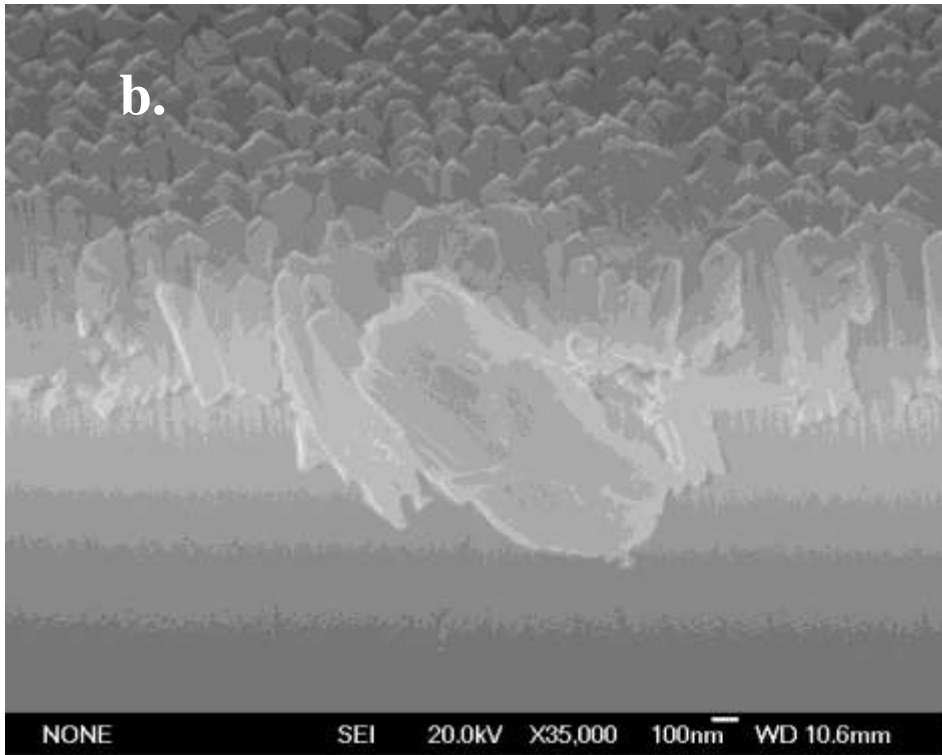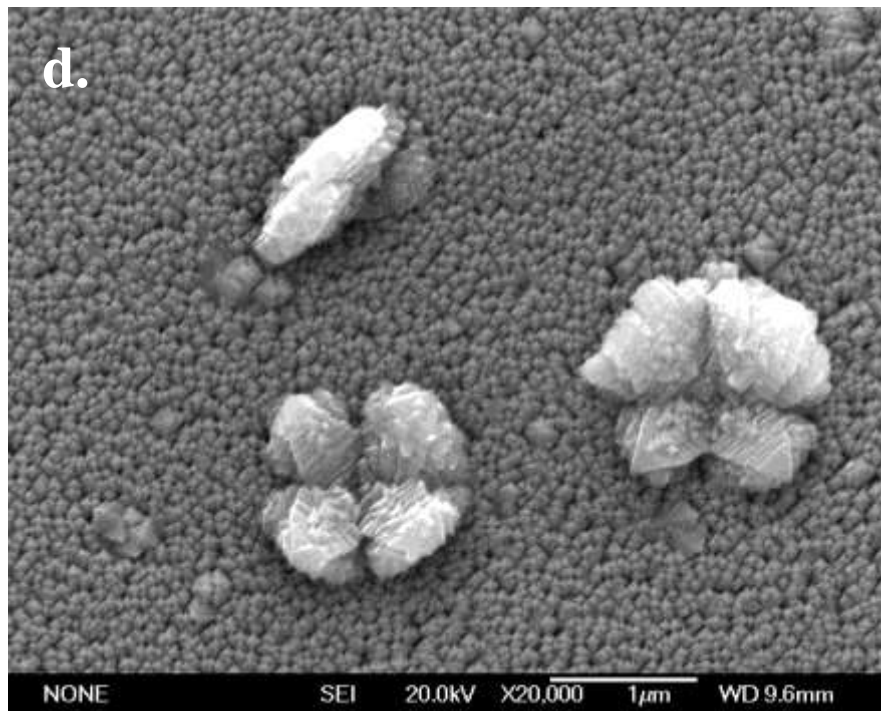
Fig. 4.3.2.2 SEM images of INOA-053 with 2 shots on Au and 10,000 shots on In$_2$O$_3$

a) top view, magnification of 15,000; b) cross-section, magnification of 35,000;
c) top view of corner, magnification of 1500; d) detail image of c.
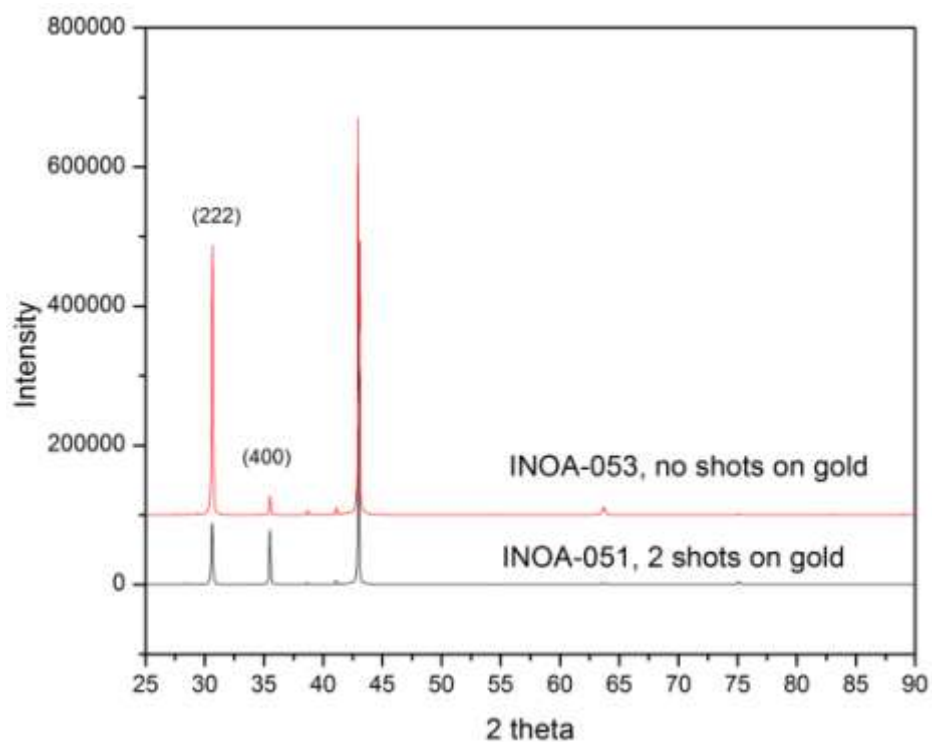
Fig. 4.3.2.3 XRD patterns of INOA-053 and INOA-051
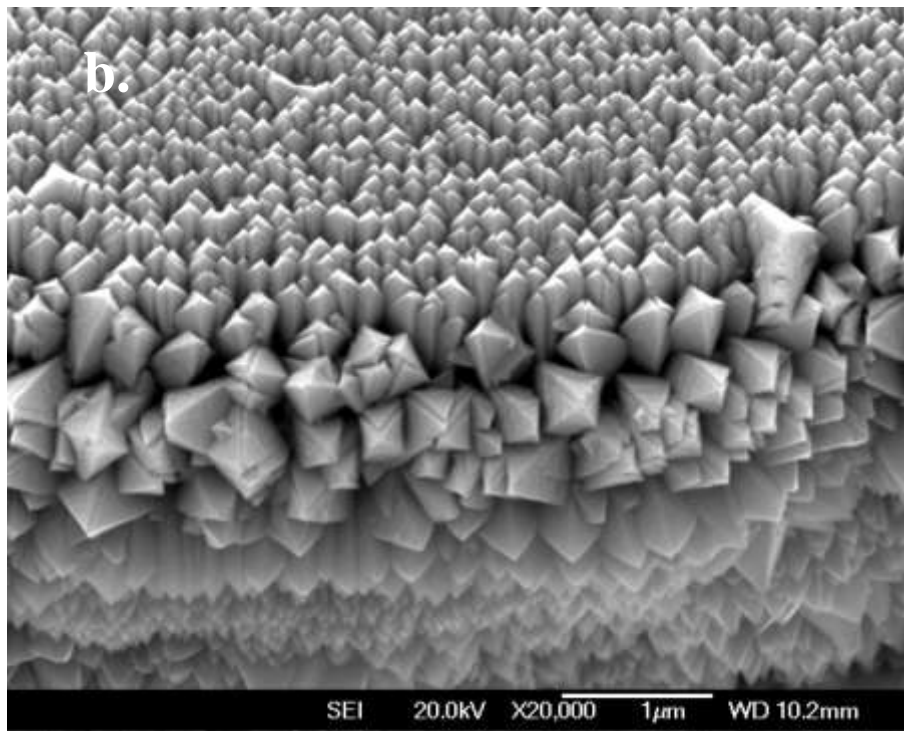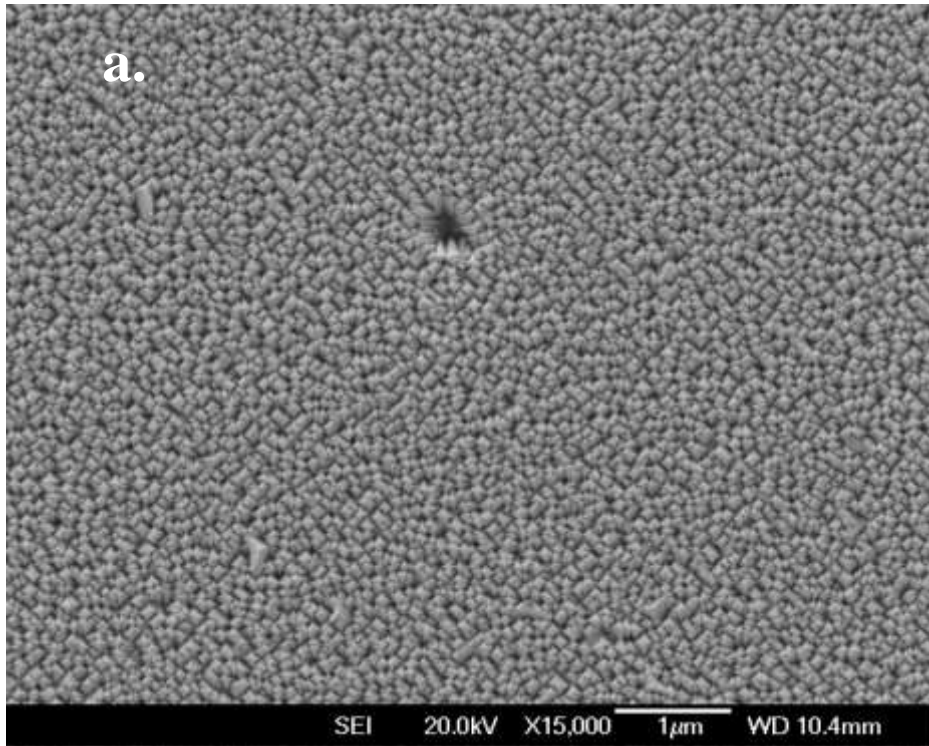
Fig. 4.3.2.4 SEM images of INOA-002 with 5 shots on Au and 10,000 shots on In_2O_3

a) top view, magnification of 15,000; b) 30° tilt view of edge, magnification of 20,000
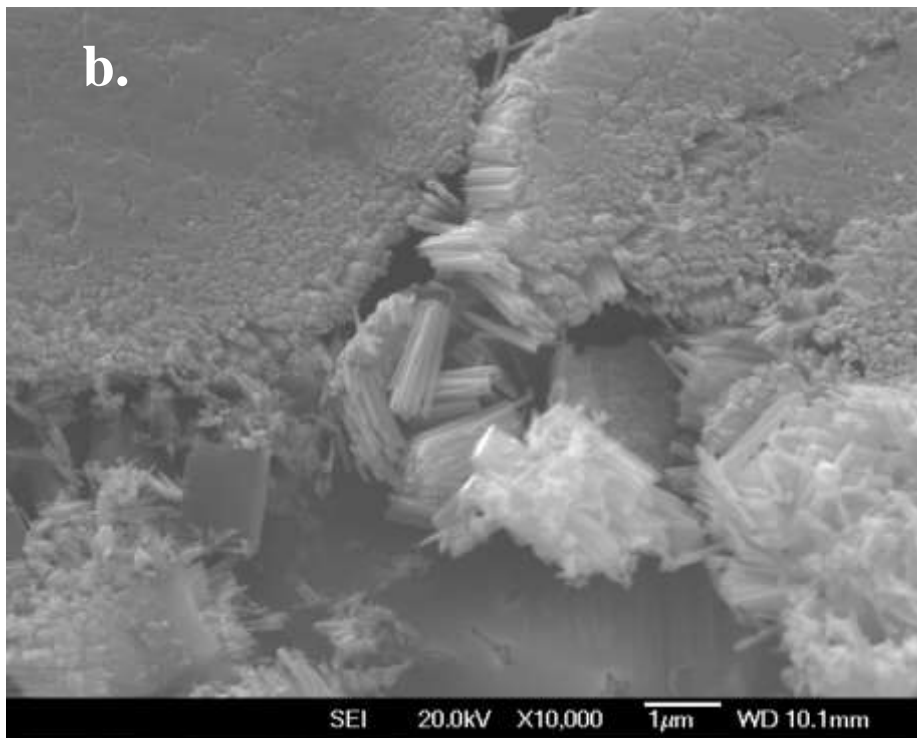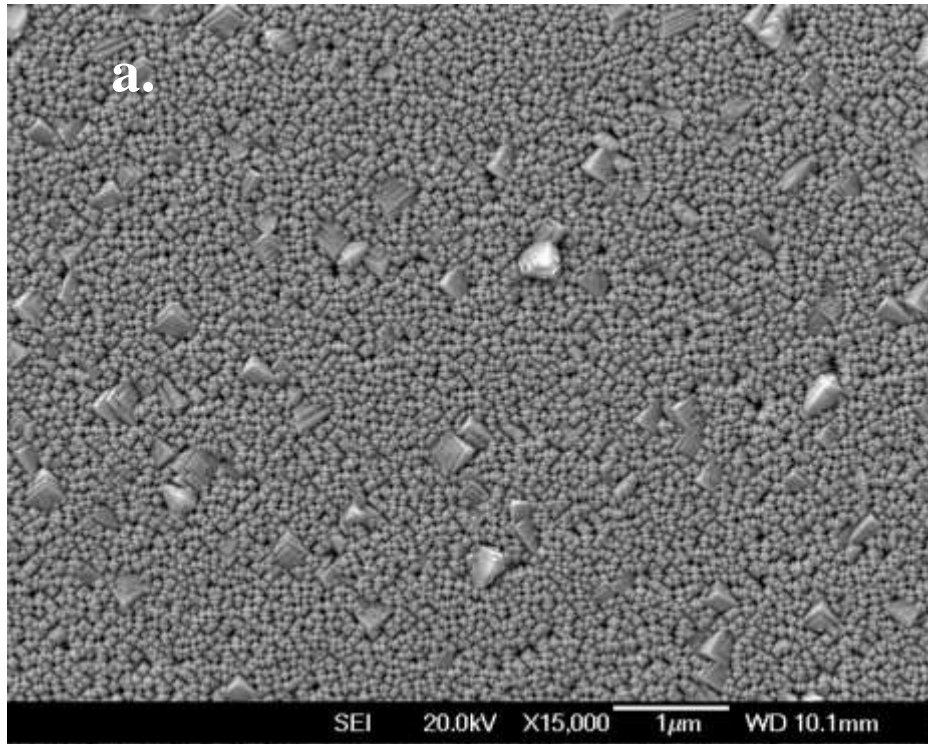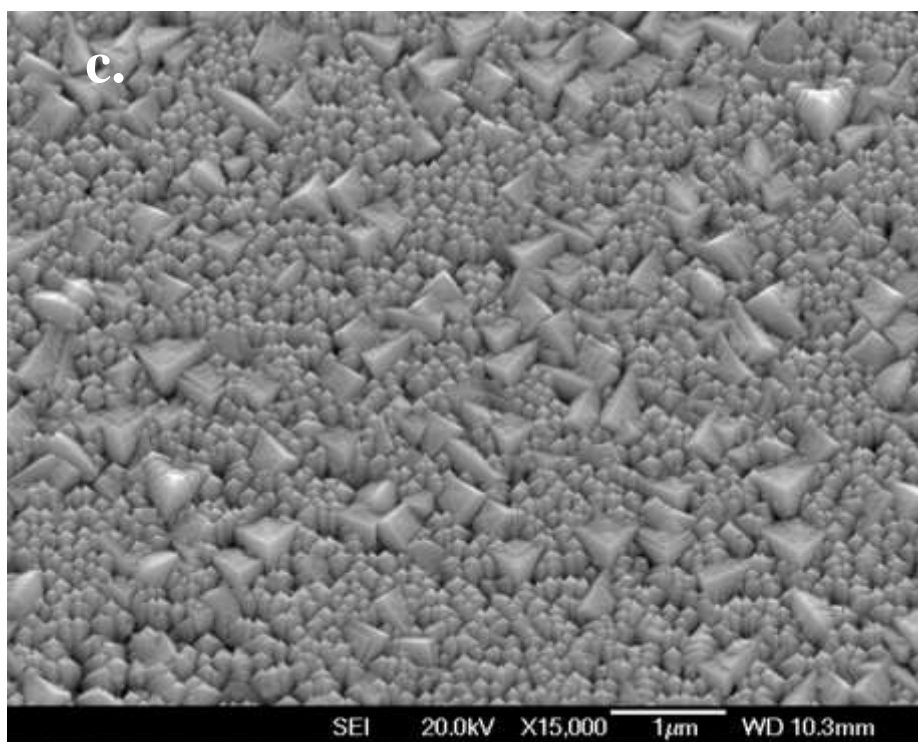
Fig. 4.3.2.5 SEM images of INOA-003 with 25 shots on Au and 10,000 shots on In$_2$O$_3$

a) top view, magnification of 15,000; b) crack area, magnification of 10,000;
c) 25° tilt view near the edge, magnification of 15,000

4.3.2.2 Influence of silver

In this section, silver was utilized as the catalyst for In$_2$O$_3$ nanorods. The samples in

this section were produced at 500°C in 1200mTorr oxygen with 1J/cm^2 on MgO(100).

Table 4.3.3 Detailed parameters of the samples of INOA-0628 and 0711

Sample Number	Chamber number	**Number of pulses on catalyst target (shots)**	Distance of Target to Substrate (mm)	**Number of pulses on In$_2$O$_3$ target (shots)**
INOA-0628	#2	**5 Au**	50	5000
INOA-0711	#2	**5 Ag**	50	5000

Comparing the width of the In$_2$O$_3$ nanorods grown by the gold catalyst (80~180nm)

and the nanorods grown by the silver catalyst (40nm to 120nm) the silver formed smaller

nanorods, shown in Fig. 4.3.2.6 and Fig. 4.3.2.7. Therefore, silver nanodots can be used as a catalyst for In_2O_3 nanorods growth.
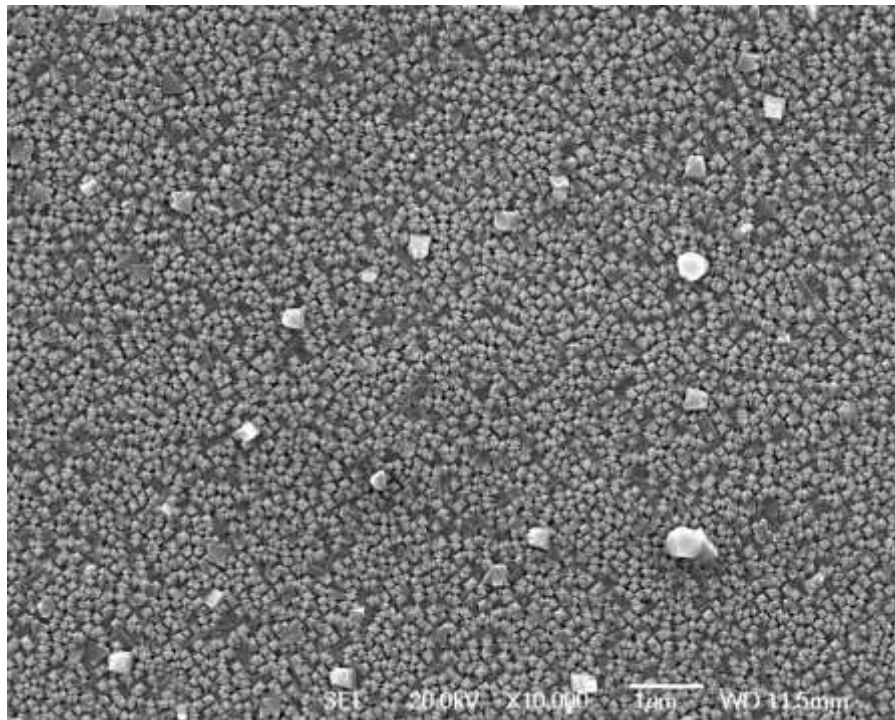
Fig. 4.3.2.6 SEM image of INOA-0628 with 5 shots on Au and 5000 shots on In_2O_3
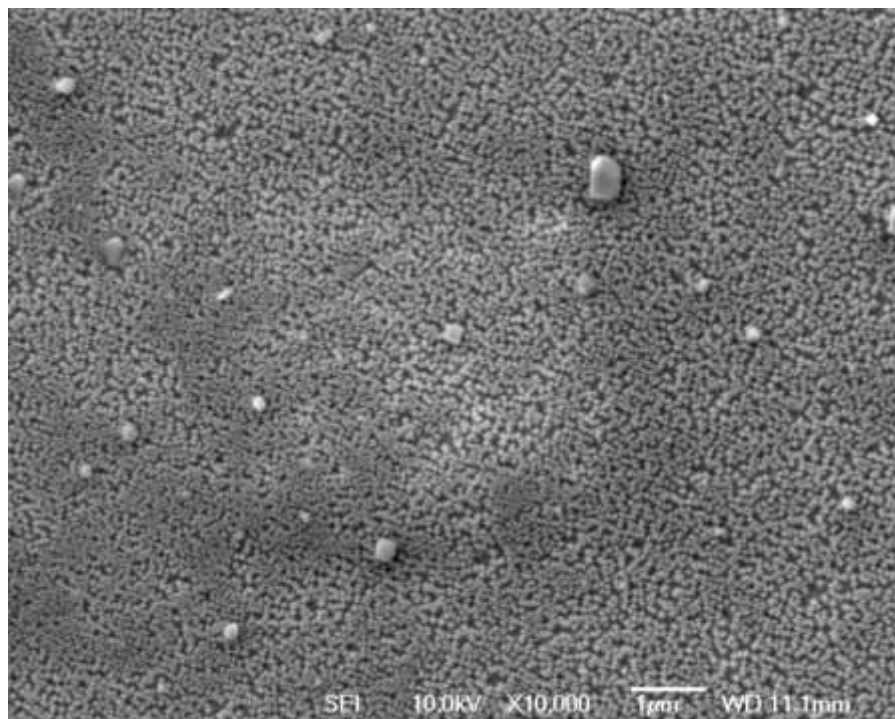
Fig. 4.3.2.7 SEM image of INOA-0711 with 5 shots on Ag and 5000 shots on In_2O_3

4.3.3 Influence of number of pulses on In$_2$O$_3$ target

In the earlier section of 4.3.2, it was observed that at the edge of the sample, average width of nanorods were larger, when compared with those grown on the central areas. As the pulses on the In$_2$O$_3$ target increase, this will also result in the increase of the average width of nanorods. Energy density was kept around 1 J/cm^2.

Table 4.3.4 Detailed parameters of the samples of INOA-006, 001 and 002

Sample Number	Temperature (°C)	Chamber number	Number of pulses on Au target (shots)	Substrate	Distance of Target to Substrate (mm)	**Number of pulses on In$_2$O$_3$ target (shots)**	Oxygen Pressure (mTorr)
INOA-006	500	#3	5	MgO(100)	55	**1000**	1200
INOA-001	500	#3	5	MgO(100)	55	**5000**	1200
INOA-002	500	#3	5	MgO(100)	55	**10,000**	1200

With 1000 shots on the In$_2$O$_3$ target, the nanorod structures begin to form. The average width of these nanostructures is around 10~30nm. At the same time the formation of large granular objects are also present.

It was observed that by depositing 5000 shots of In$_2$O$_3$, the nanorods are formed in a very uniform size of 15~50nm and length of approximately 800nm. However when the number of pulses increase to 10000, the average size of nanorods grown is between 60~100nm and the length is increased to approximately 1.5μm. Also on some areas of the surface very thick nanorods or larger structures were also present, as shown in Fig.4.3.3.3b. This is due to the growth mode of In$_2$O$_3$ nanorods, that as more In$_2$O$_3$ particles, from the

plume, join the existing structures, several smaller nanorods will form and merge into one large nanorod.

In conclusion, increasing the number of pulses on In_2O_3 will not only result in increasing the nanorods length, but also increase the average width.
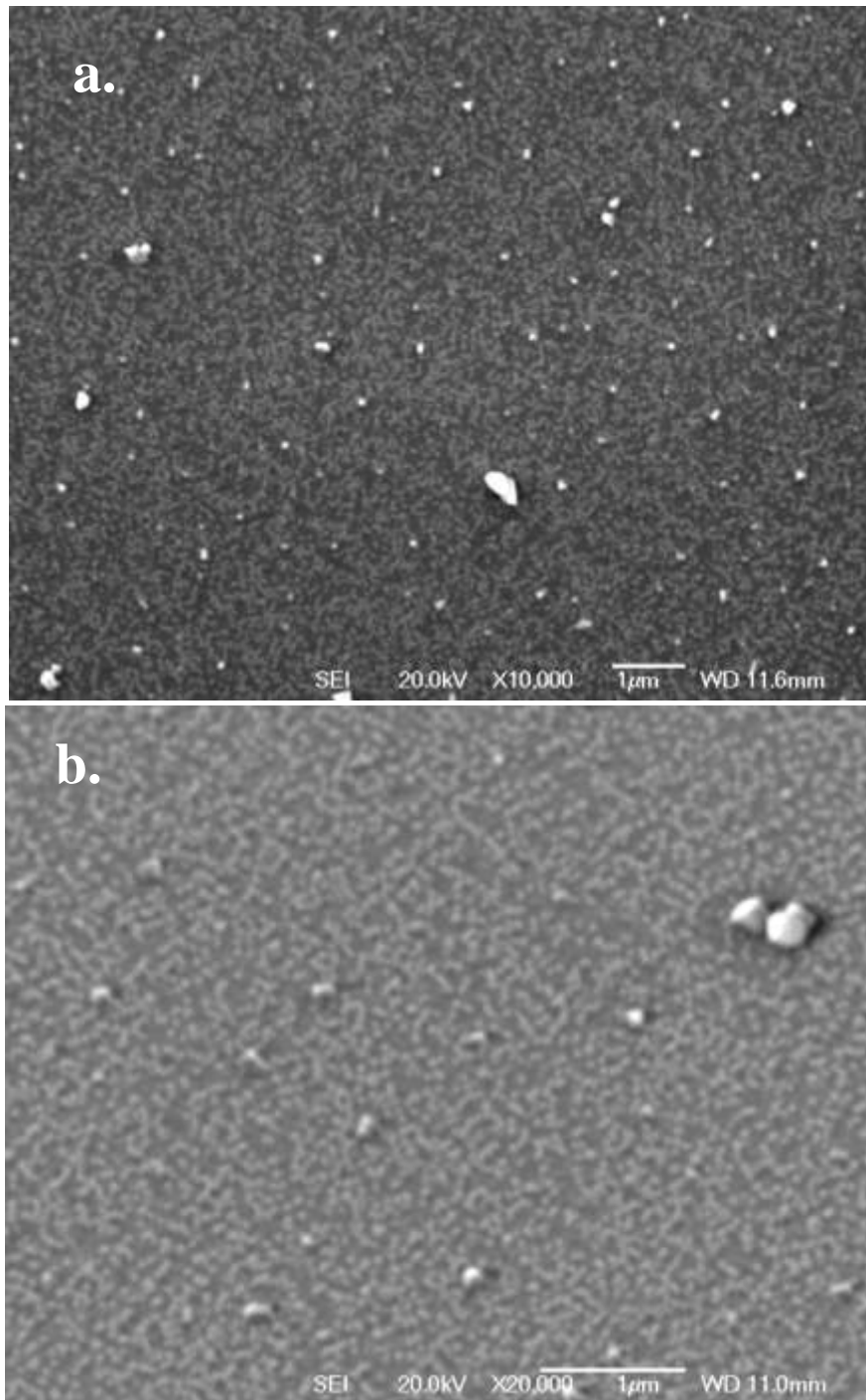
Fig. 4.3.3.1 SEM images of INOA-006 deposited with 1000 shots In_2O_3
a) top view, magnification of 10,000; b) 30° tilt, magnification of 20,000
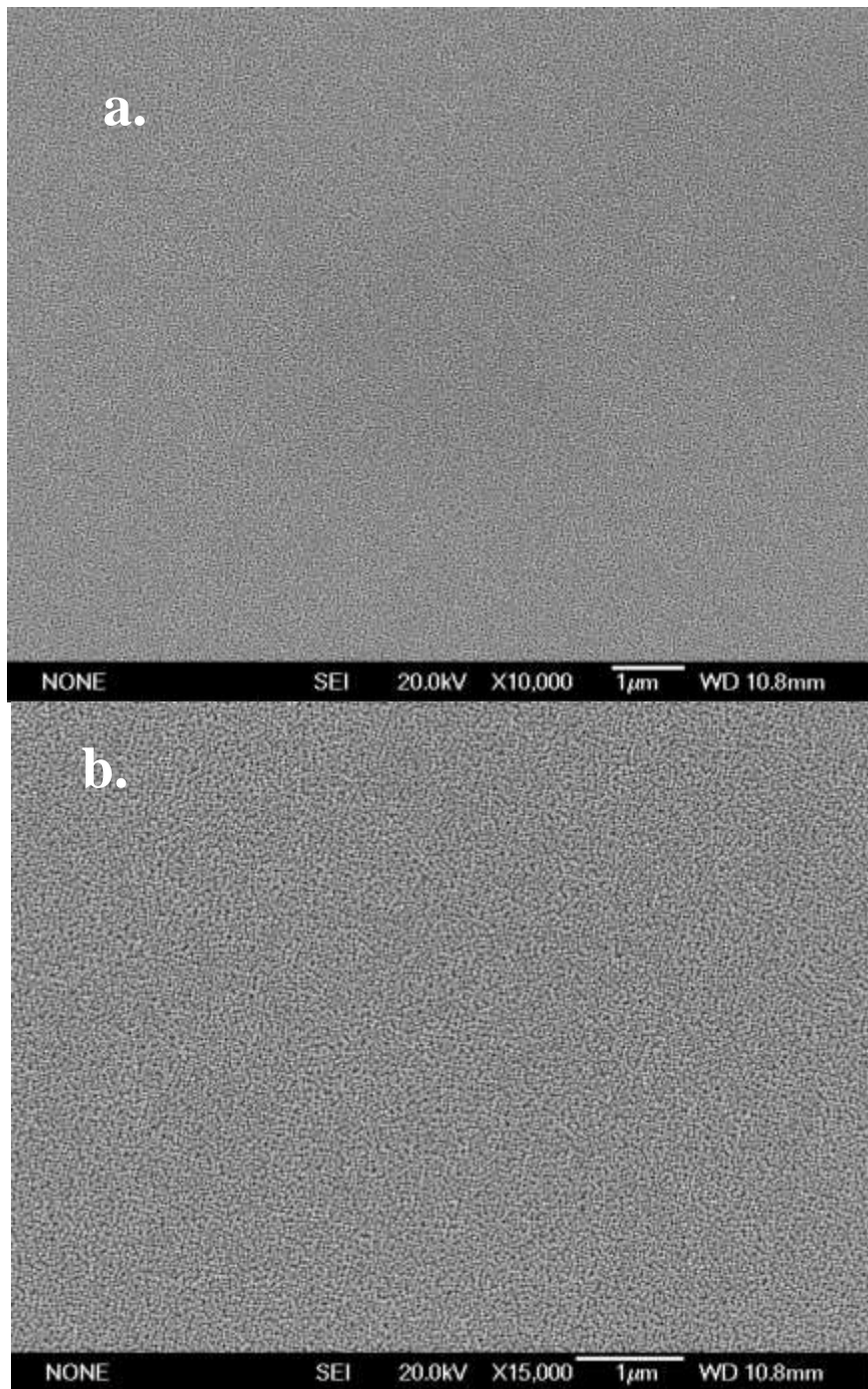
Fig. 4.3.3.2 SEM images of INOA-001 deposited with 5000 shots In_2O_3

a) top view, magnification of 10,000; b) top view, magnification of 15,000
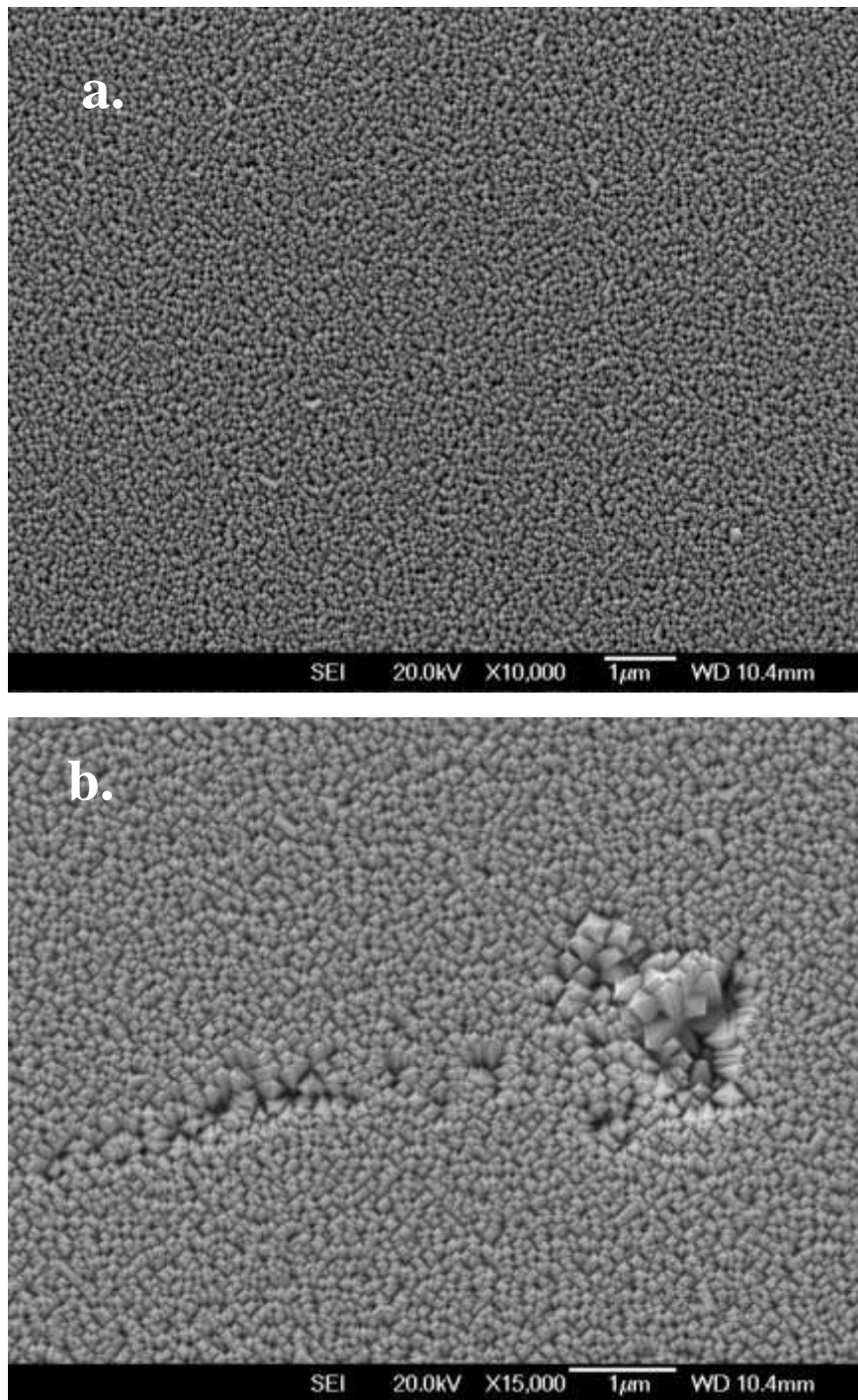
Fig. 4.3.3.3 SEM images of INOA-002 deposited with 10,000 shots In_2O_3

a) top view, magnification of 10,000; b) top view, magnification of 15,000

4.3.4 Influence of oxygen pressure

Within this section, the samples were produced with a reduction of the oxygen pressure down to 250mTorr, which is just high enough for MgO nanorods growth.

Table 4.3.5 Detailed parameters of the samples of INOA-055 and 001

Sample Number	Temperature (˚C)	Chamber number	Number of pulses on Au target (shots)	Substrate	Distance of Target to Substrate (mm)	Number of pulses on In$_2$O$_3$ target (shots)	Oxygen Pressure (mTorr)
INOA-055	500	#3	5	MgO(100)	55	5000	250
INOA-001	500	#3	5	MgO(100)	55	5000	1200

As the oxygen pressure is set at 250mTorr, when compared with sample INOA-001 shown in Fig.4.3.1.2, the average width keeps at 15~50nm, while the depressions and granular nanostructures with a size of 300~600nm are scattered along the surface of the sample. The depressions are formed because at a lower oxygen pressure fewer oxygen molecules may participate in the nanostructures' formation. Another possibility could be due to the energy level of particles in the plume being higher. The XRD patterns indicate that the crystallinity decreases by decreasing the oxygen pressure and that both peaks (222) and (400) become weaker. Peak (222) nearly vanishes. It was also observed that in some areas, the nanorods tend to grow closely together. This is caused when the oxygen pressure is lower, the surface tension becomes higher and the gold nanodots deposited at those areas are not sufficient to release the tension. Therefore, for perfect In$_2$O$_3$ nanorods growth, a high oxygen pressure is needed.
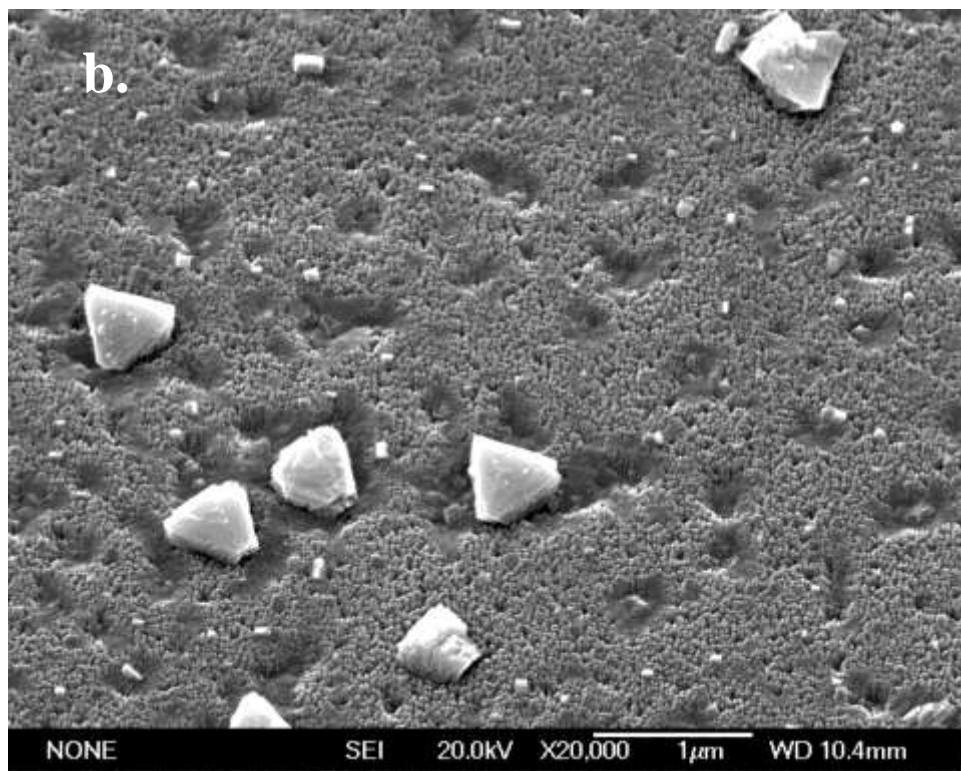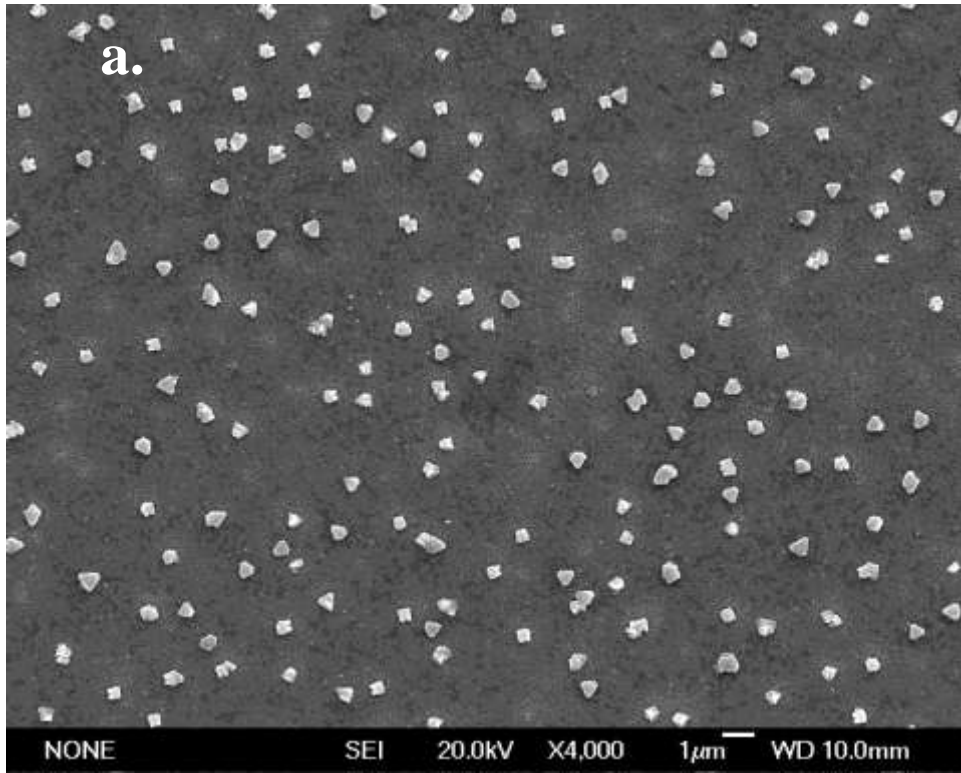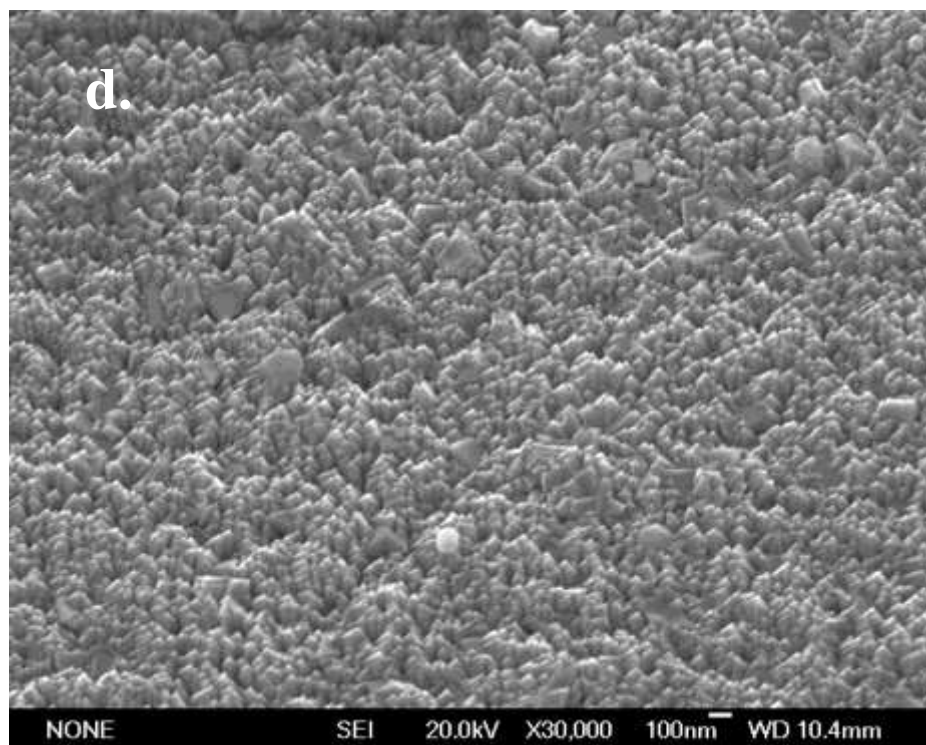
Fig. 4.3.4.1 SEM images of INOA-055 deposited in 25mTorr oxygen

a) top view, magnification of 4000; b) 30° tilt, magnification of 20,000;
c) top view, magnification of 40,000; d) 30° tilt, magnification of 30,000
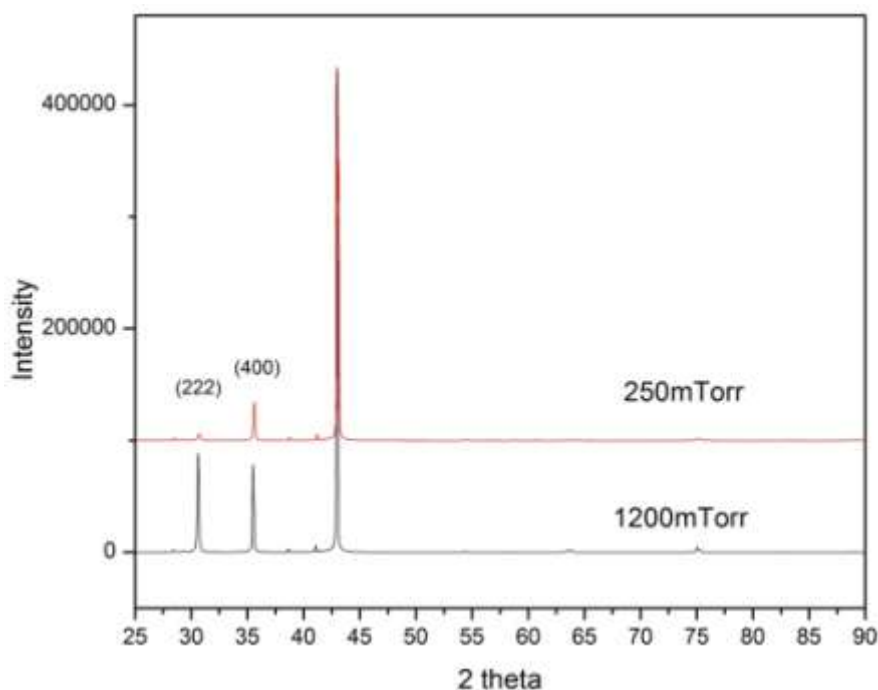
Fig. 4.3.4.2 XRD patterns comparison

4.3.5 Glass substrates

It is well-known that glass is a good substrate to produce ITO thin films. In this section a glass substrate was also used to produce In_2O_3 nanorods. The other control parameters are as shown below in Table 4.3.6.

Table 4.3.6 Detailed parameters of the sample INOA-057

Sample Number	Temperature (°C)	Chamber number	Number of pulses on Au target (shots)	Distance of Target to Substrate (mm)	Number of pulses on In_2O_3 target (shots)	Oxygen Pressure (mTorr)
INOA-057	500	#2	5	55	5000	1200

The results from this experiment yielded a few granular nanostructures formed on the surface. When compared with INOA-001, which used MgO(100) as substrate, as shown in Fig.4.3.1.2, the tips of nanorods, grown on the glass substrate, point into slightly random directions. The distribution of the widths was also larger, which ranged from 40 to 200nm.

Even though there were distinct differences, as mentioned above, glass can still be considered a good substrate for In_2O_3 growth.
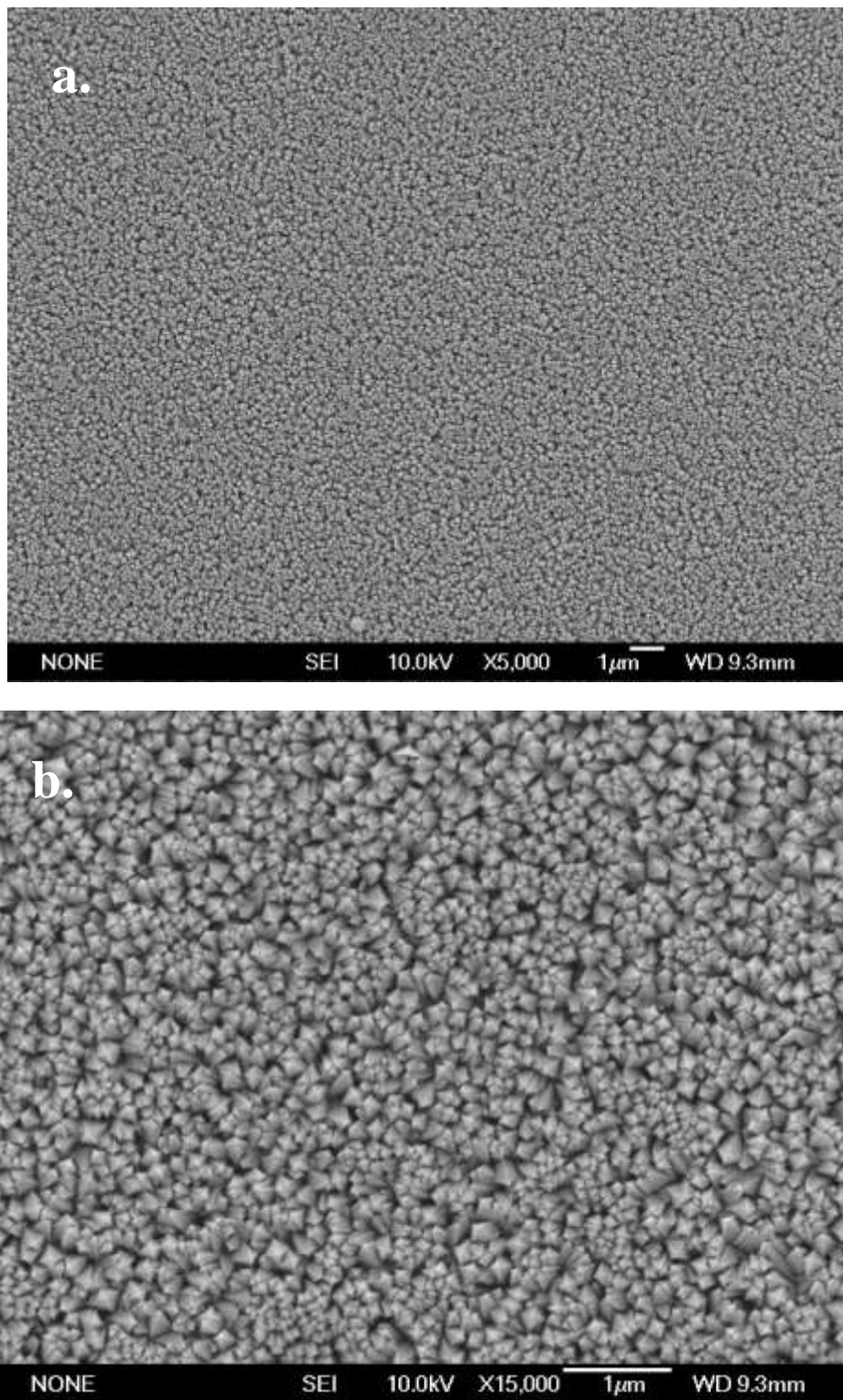
Fig. 4.3.5.1 SEM images of INOA-057 deposited on glass

a) top view, magnification of 5000; b) top view, magnification of 15,000

4.3.6 SnO$_2$ nanorods

As ITO is a solid solution of 90% In$_2$O$_3$ and 10% SnO$_2$ by weight, SnO$_2$ was also observed within this section. When comparing sample SNOA-001 and SNOA-002, it was observed that by adding 5 shots gold, larger structures were present on the surface and the nanorods formed had a width distribution that was larger, ranging from 70nm to 240nm. However, without any gold coating, fewer and smaller sized bulk crystals are present on the surface and the nanorods' width range between 70nm to 160nm.

Table 4.3.7 Detailed parameters of the samples of SNOA-001,002, 003 and 004

Sample Number	Temperature (°C)	Chamber number	Number of pulses on Au target (shots)	Substrate	Distance of Target to Substrate (mm)	Number of pulses on In$_2$O$_3$ target (shots)	Oxygen Pressure (mTorr)
SNOA-001	700	#2	5	MgO(100)	55	5000	1200
SNOA-002	700	#2	0	MgO(100)	55	5000	1200
SNOA-003	700	#2	5	MgO(100)	55	5000	550
SNOA-004	700	#2	0	MgO(100)	55	5000	550

While maintaining 5 shots on gold, but decreasing the oxygen pressure to 550mTorr, the nanorods formed had widths between 70nm to 200nm. On some areas of the surface, depressions were formed similar to the depressions that were formed in the case of In$_2$O$_3$ when the oxygen pressure is low. It was also observed that a sample that is produced without any gold nanodots and the oxygen pressure set to 550mTorr, there were no nanorod structures formed.

In conclusion, either gold nanodots must be present or a high enough oxygen pressure is needed when the temperature is set to at 700°C, in order to form SnO$_2$ nanorods.
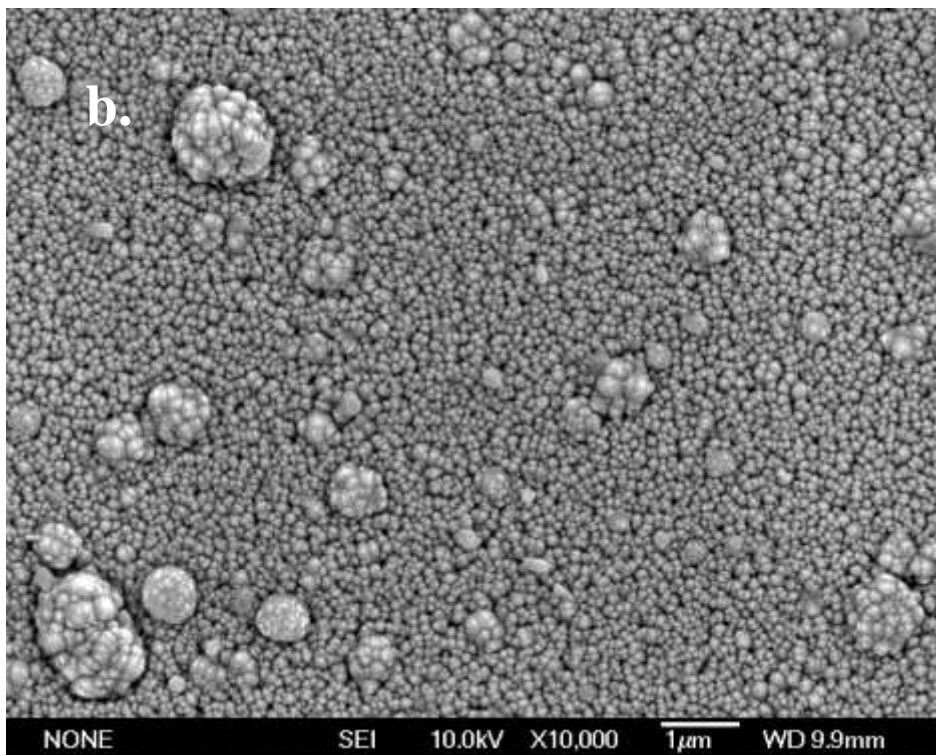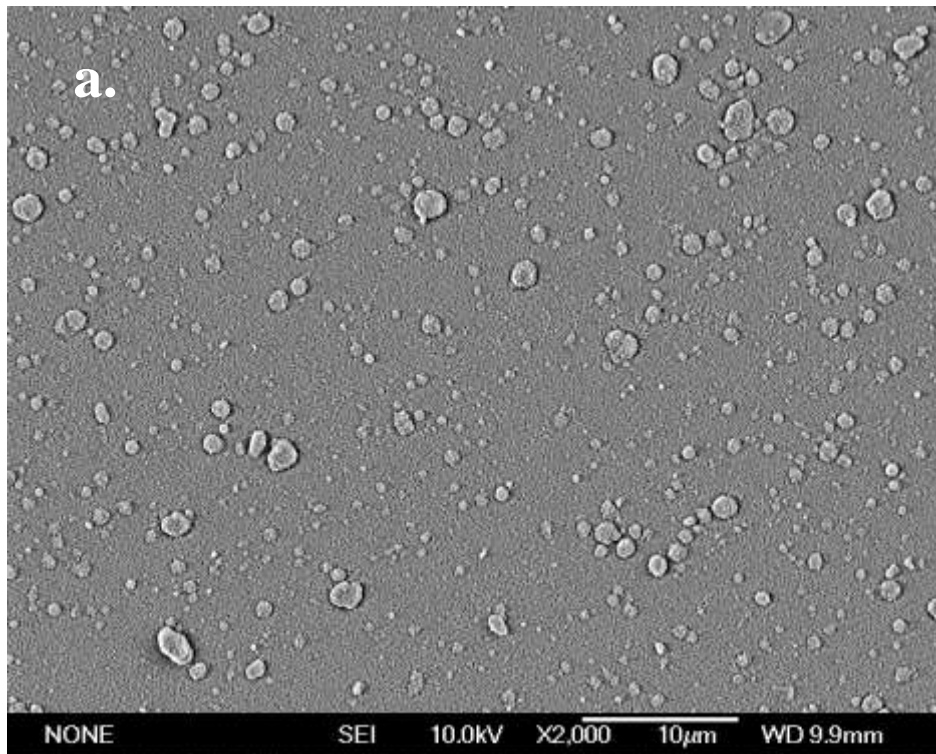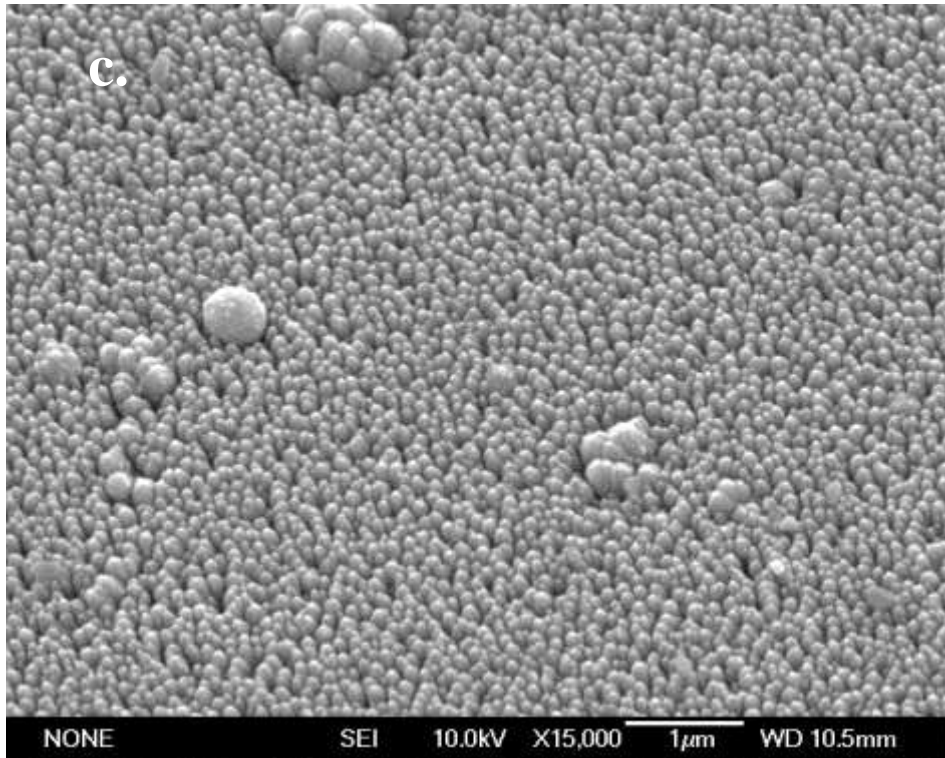
Fig. 4.3.6.1 SEM images of SNOA-001 deposited with 5 gold shots in 1200mTorr oxygen

a) top view, magnification of 2000; b) top view, magnification of 10,000;
c) 30° tilt, magnification of 15,000
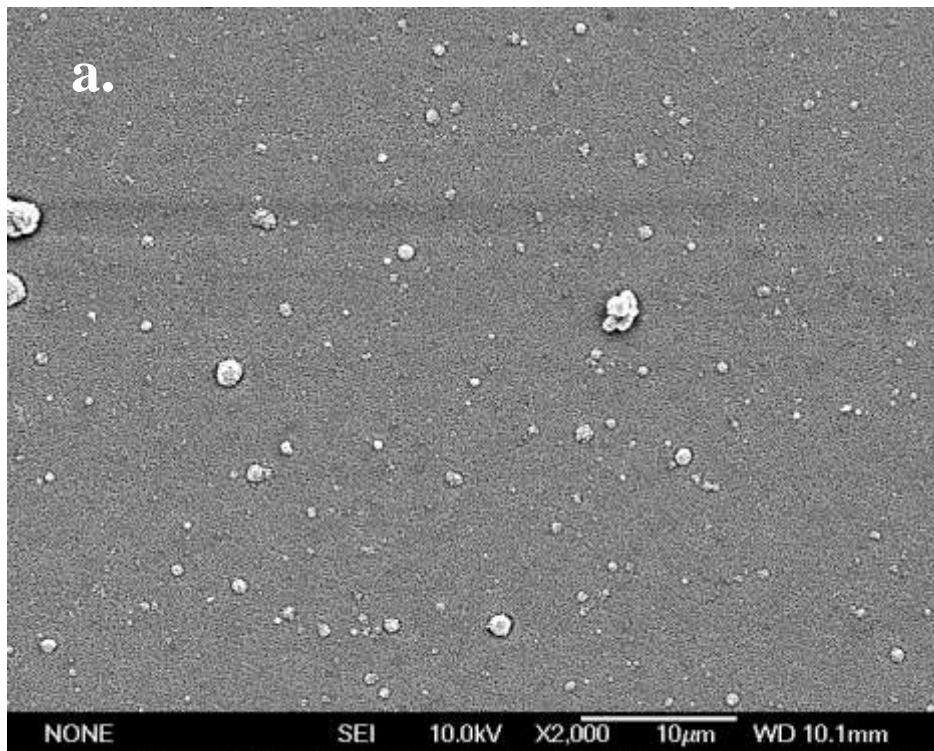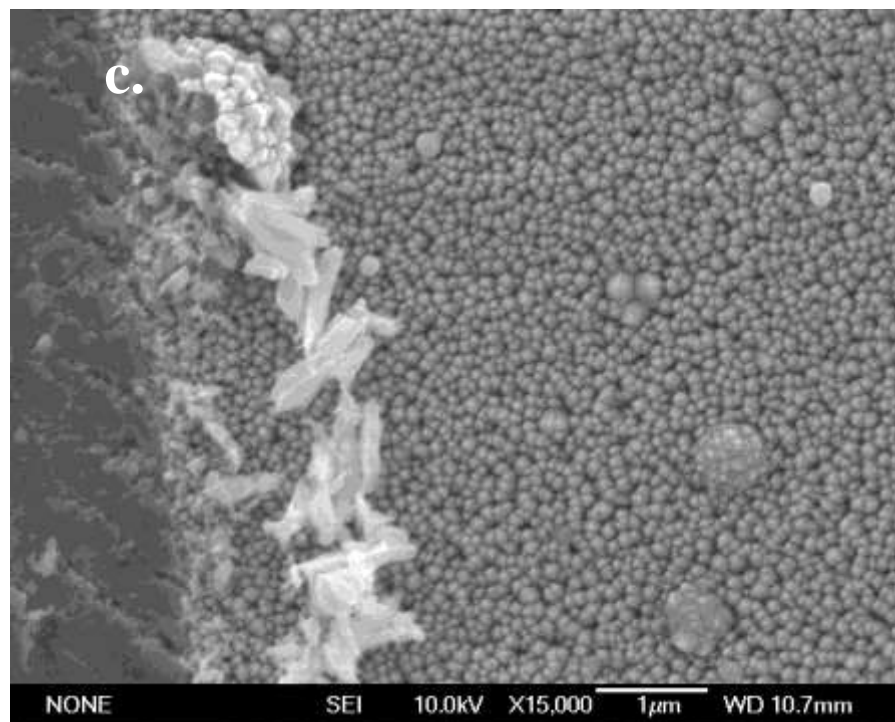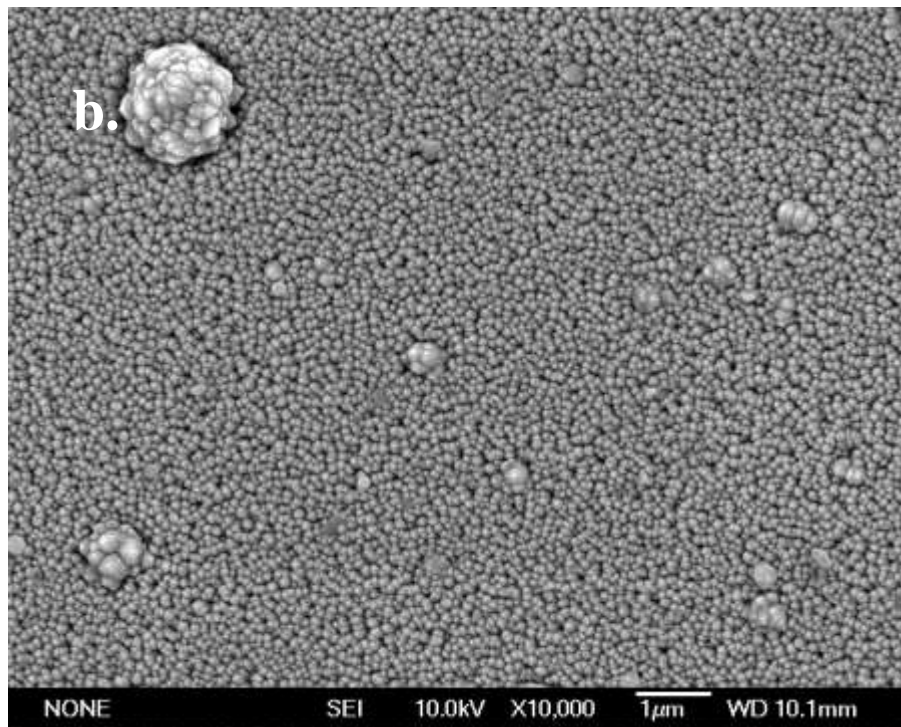
Fig.4.3.6.2 SEM images of SNOA-002 deposited without gold shots in 1200mTorr oxygen

a) top view, magnification of 2000; b) top view, magnification of 10,000;
c) top view, magnification of 15,000
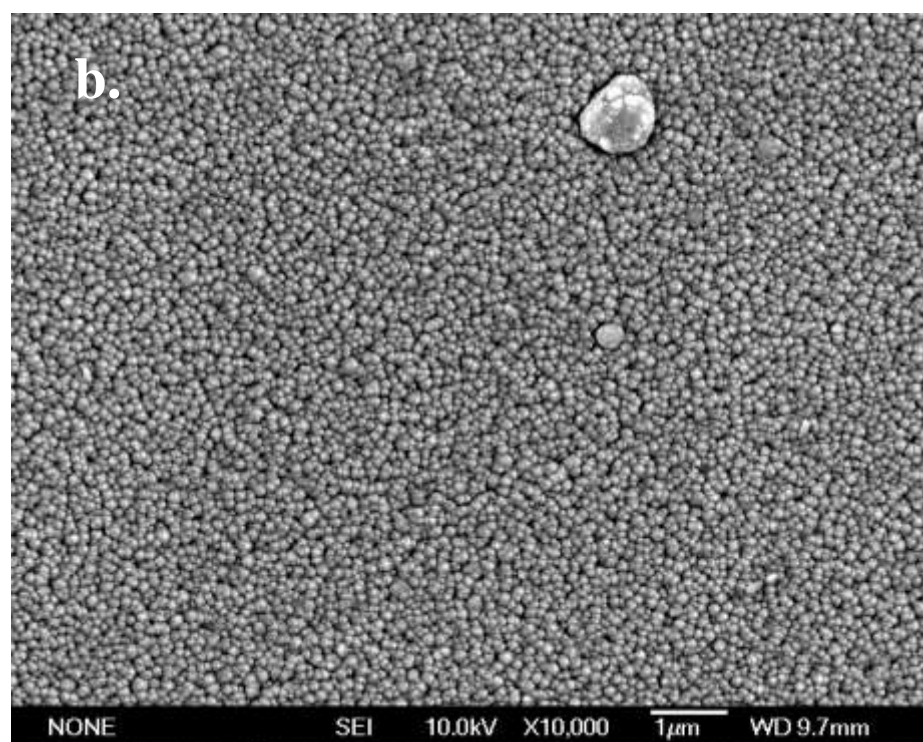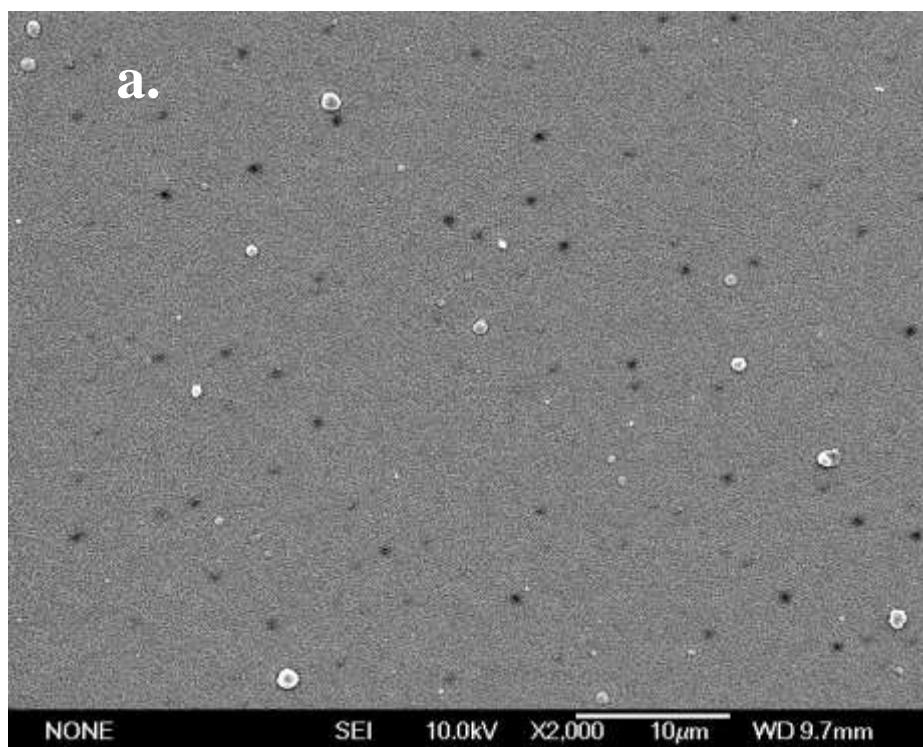
Fig. 4.3.6.3 SEM images of SNOA-003 deposited with 5 gold shots in 550mTorr oxygen

a) top view, magnification of 2000; b) top view, magnification of 10,000
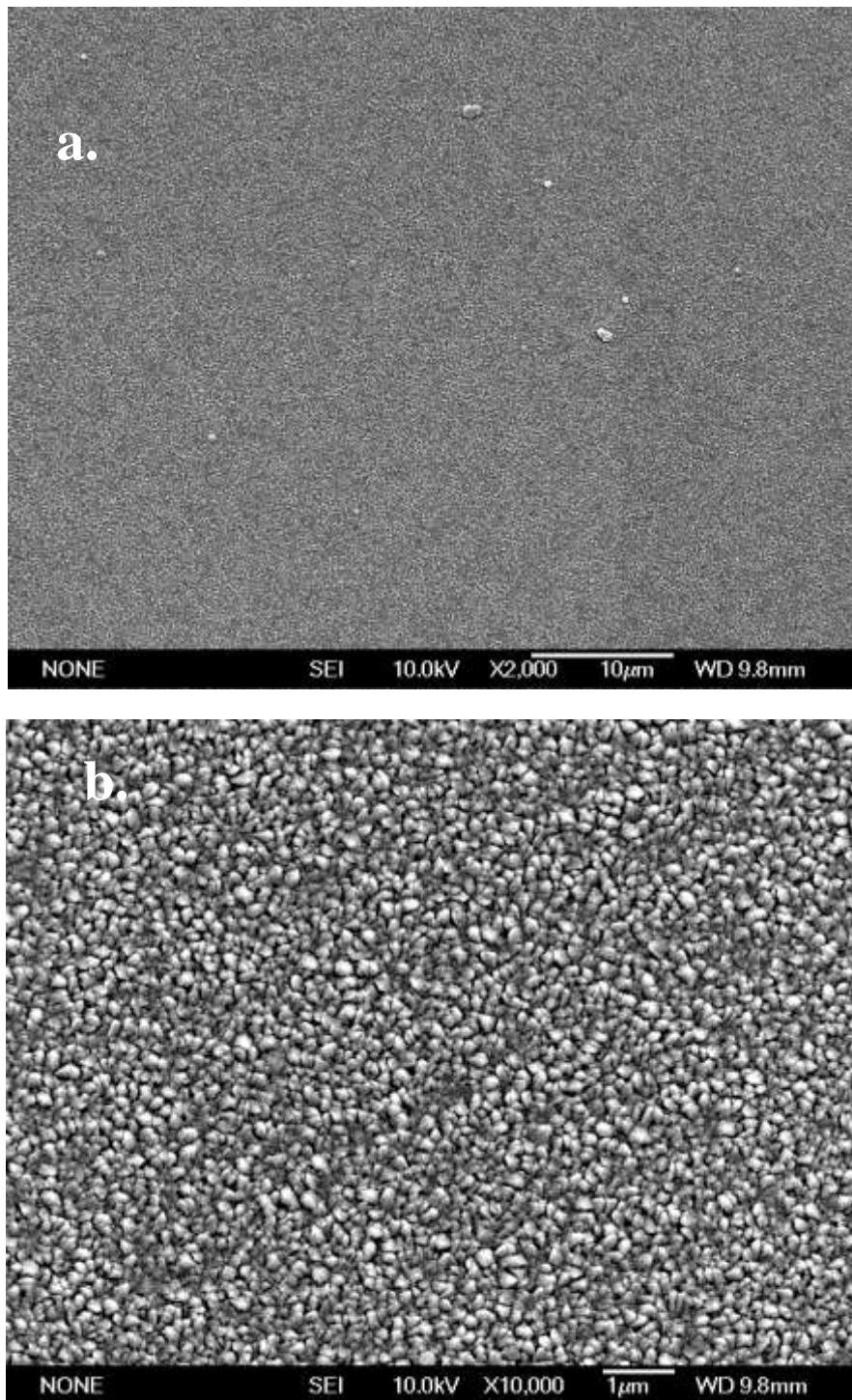
Fig.4.3.6.4 SEM images of SNOA-004 deposited without gold shots in 550mTorr oxygen

a) top view, magnification of 2000; b) top view, magnification of 10,000

4.4 Iron Oxide Nanorods

All the iron oxide samples were conducted from Fe_3O_4 target in chamber #2 with the target-substrate distance of 50mm with energy density of $1J/cm^2$. It was observed that most of the samples were an erubescent orange to gray in color. However, extending from the leading edge, a prismatic-like fringe was also noted.

Table 4.4.1 Detailed parameters of the samples FOA-001, 002, 003, 004, 005, 028, 030 and 032

| Sample Number	Temperature (°C)	Substrate	Number of pulses on Au target (shots)	Number of pulses on Fe_3O_4 target (shots)	Oxygen pressure (mTorr)
FOA-001	800	Al_2O_3 ceramic	5	10,000	1200
FOA-002	800	Al_2O_3 single crystal	5	10,000	1200
FOA-003	700	Al_2O_3 ceramic	5	10,000	1200
FOA-004	800	Al_2O_3 ceramic	5	7000	100
FOA-005	800	Al_2O_3 ceramic	0	10,000	1200
FOA-028	800	MgO single crystal	5	1000	1200
FOA-030	800	MgO single crystal	5	10,000	550
FOA-032	800	Al_2O_3 ceramic	5	10,000	550

4.4.1 Influence of substrate temperature

When comparing sample FOA-001 with FOA-003, under 800°C, iron oxide nanorods were grown in a more loose array (width of 60~180nm). However those grown under 700°C (average width of approximately 80nm) were found to have grown very close to each other.
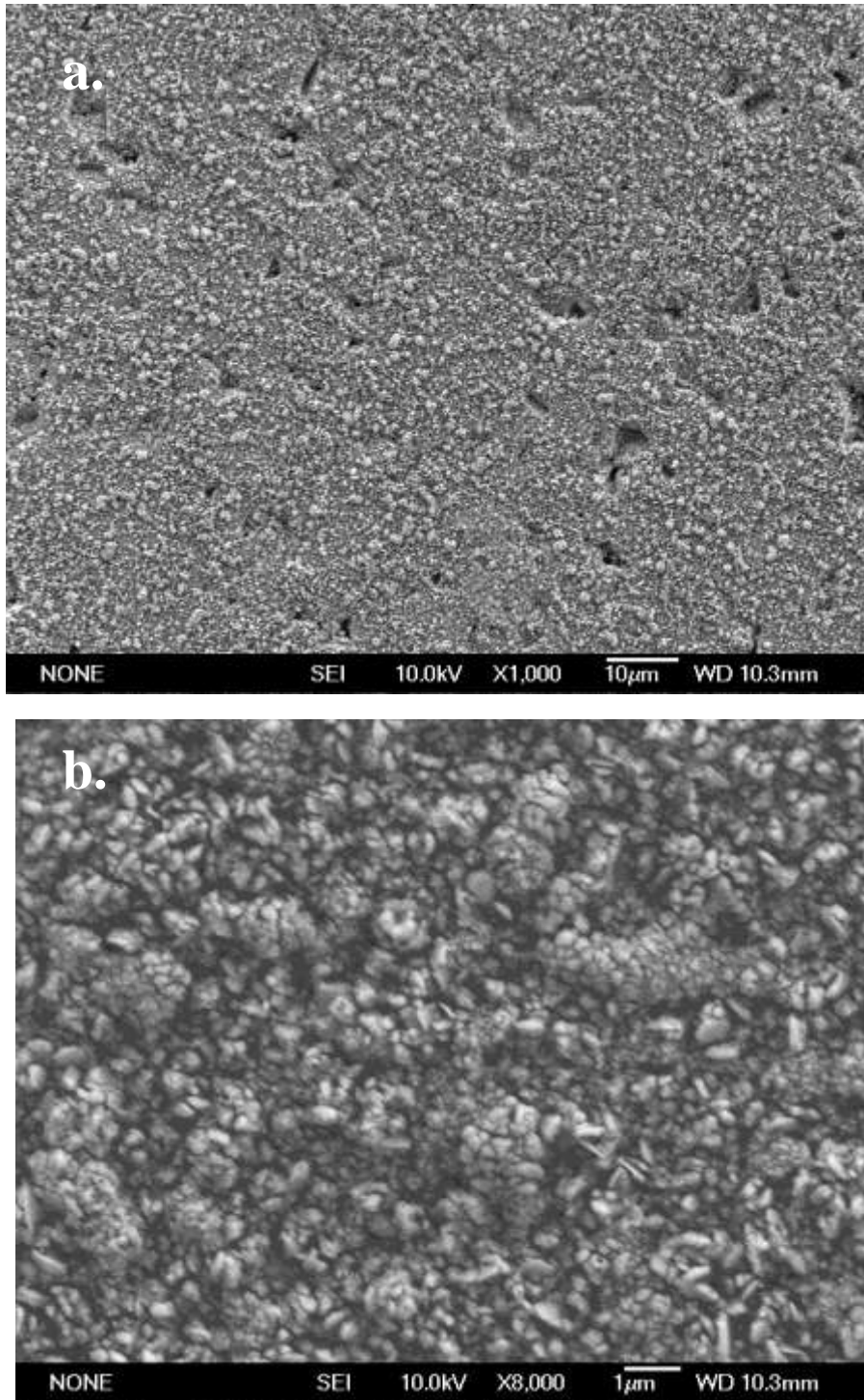
Fig. 4.4.1.1 SEM images of FOA-001 grown on Al_2O_3 ceramic, deposited by 5 shots on Au, 10,000 laser shots on Fe_3O_4, under 800°C, 1200mTorr
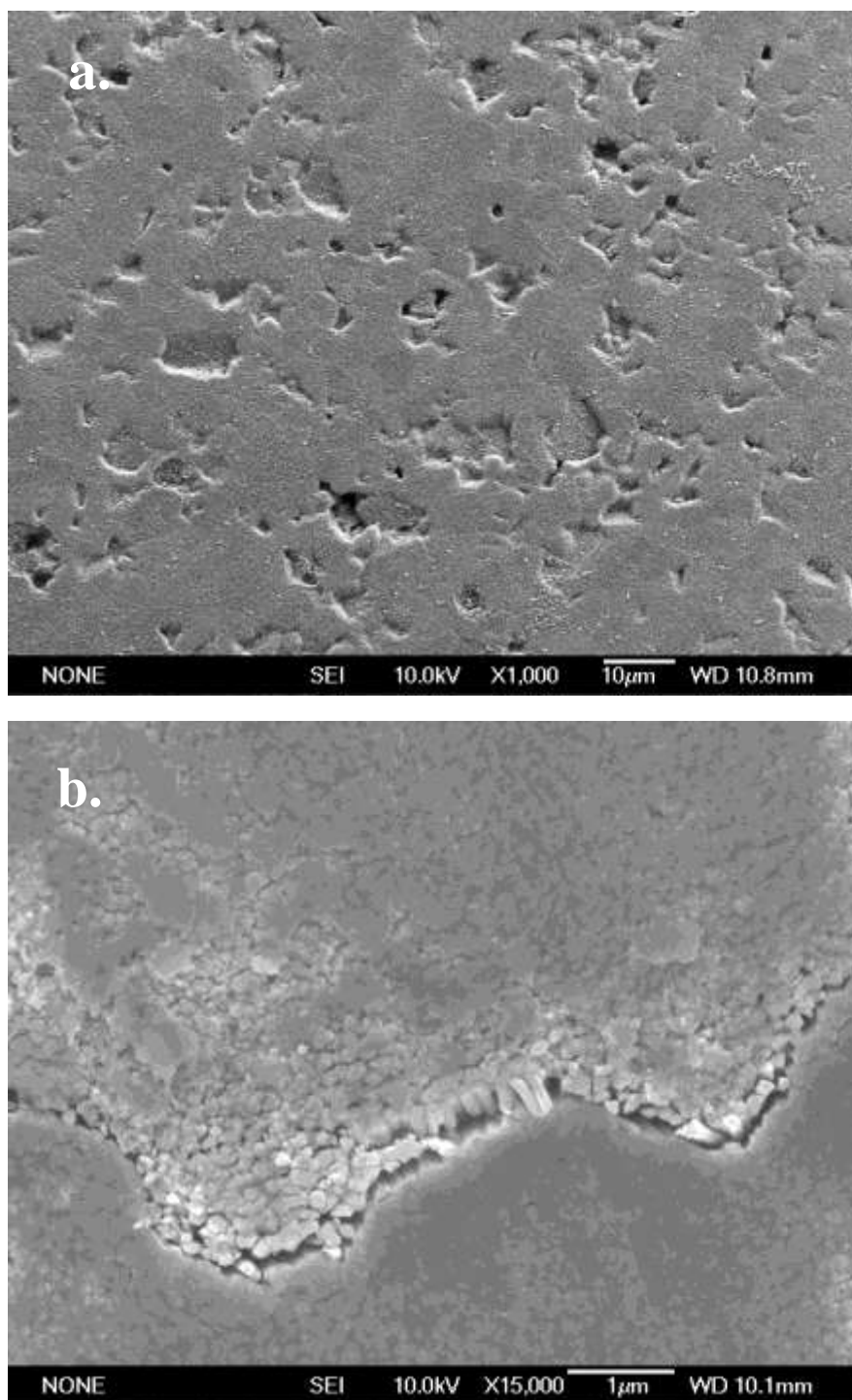
Fig. 4.4.1.2 SEM images of FOA-003 grown on Al_2O_3 ceramic, deposited by 5 shots on Au, 10,000 laser shots on Fe_3O_4, under 700°C, 1200mTorr

4.4.2 Influence of substrates

Upon comparing Fig.4.4.1.1 with Fig.4.4.2.1, it was observed that like other oxide nanorods, iron oxide nanorods grown on single crystal substrates are more uniform and neat

compared with those grown on ceramic or amorphous glass substrates. Iron oxide nanorods grown on Al_2O_3 single crystal perpendicularly were found to have an average width of 120nm, while those grown on ceramic substrate had a wider distribution of width and, in some areas, were found to have grown closely to each other in a group.

It was observed that when comparing the morphologies on two different single crystals, iron oxide nanorods were formed parallel to MgO(100) substrate, but were grown perpendicularly on Al_2O_3 single crystal. This difference is due to the substrates' lattice parameters.
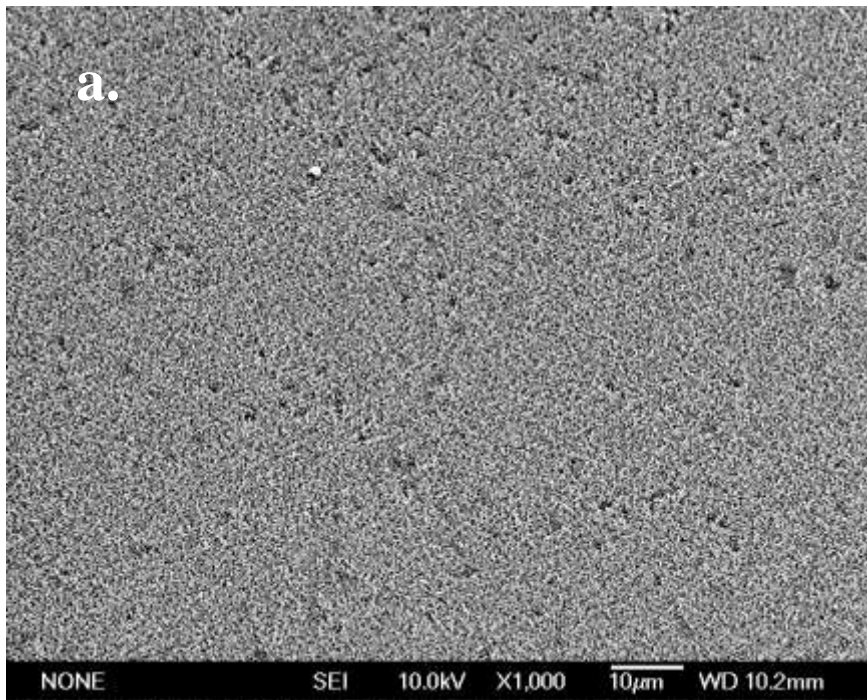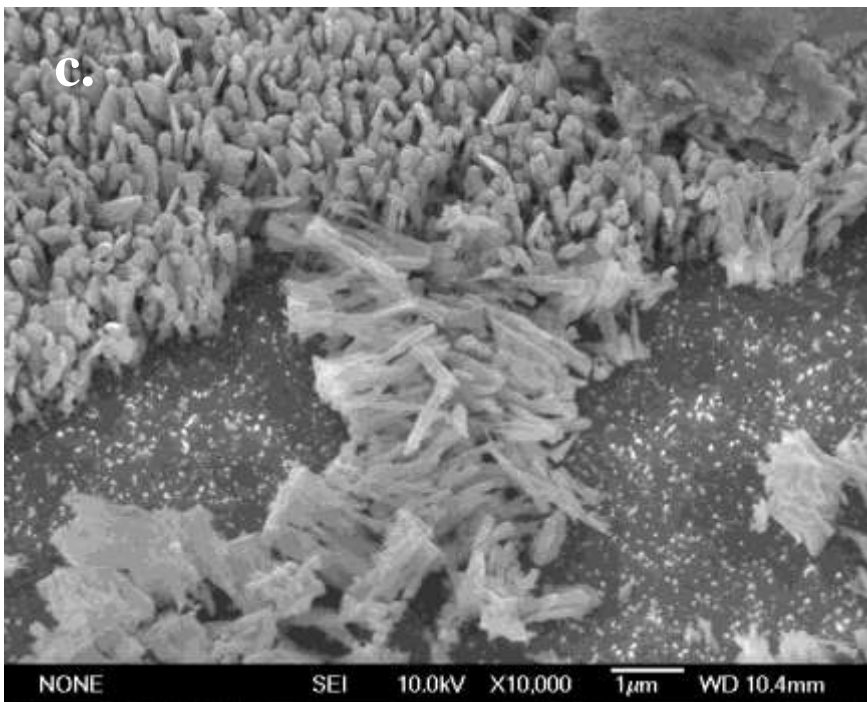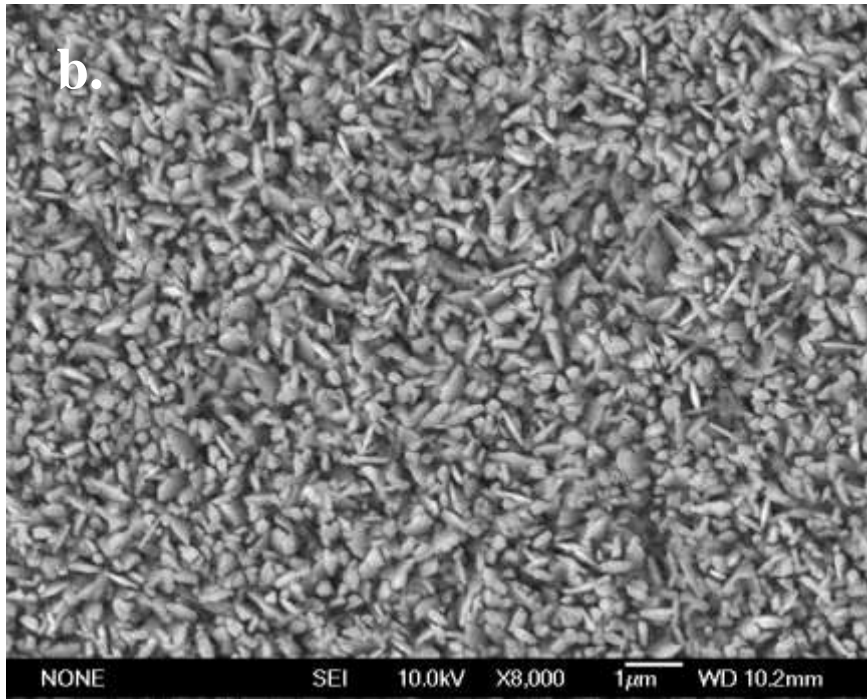
Fig. 4.4.2.1 SEM images of FOA-002 grown on Al_2O_3 single crystal, deposited by 5 shots on Au, 10,000 laser shots on Fe_3O_4, under 800°C, 1200mTorr
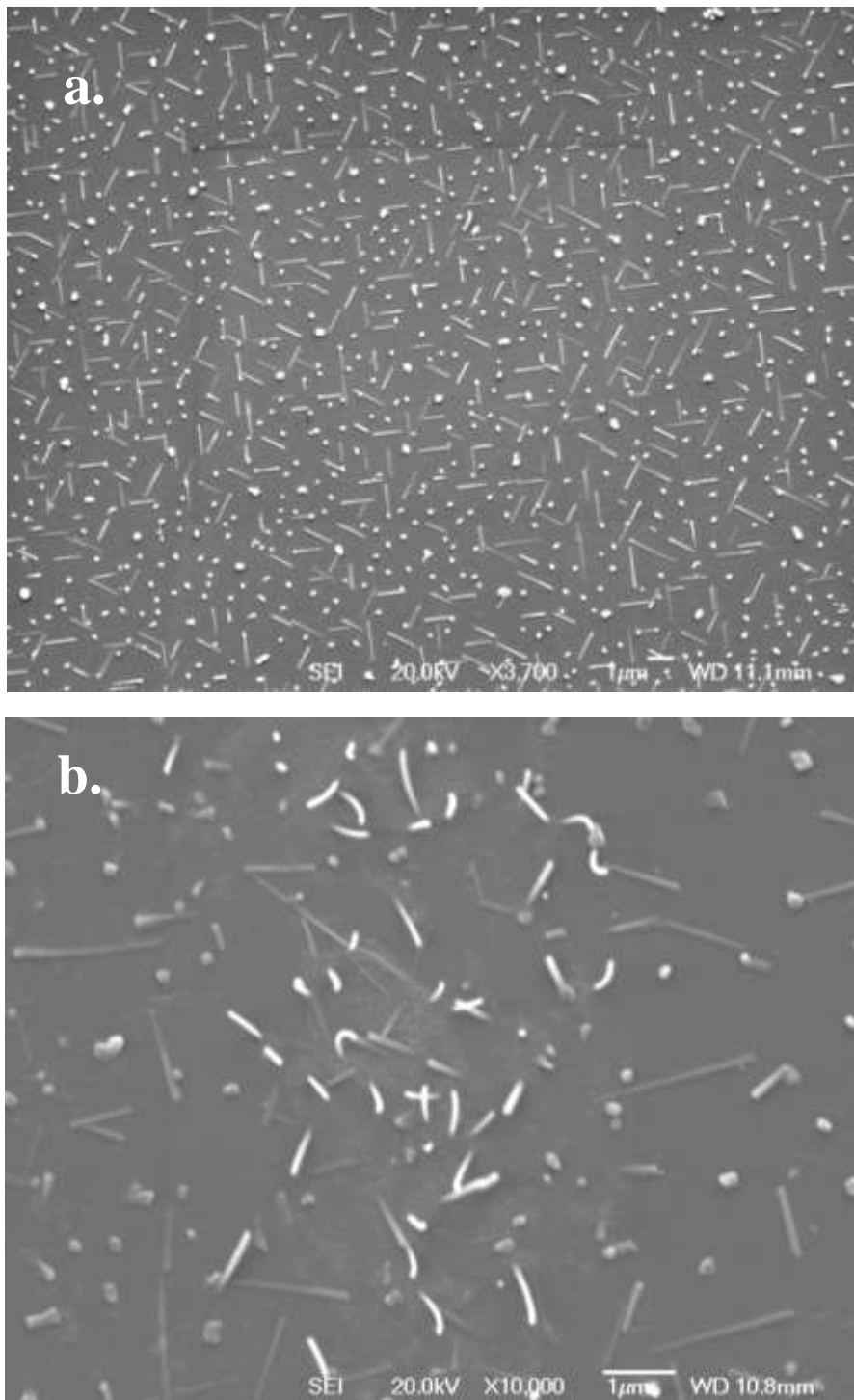
Fig. 4.4.2.2 SEM images of FOA-028 grown on MgO single crystal, deposited by 5 shots on Au, 1000 laser shots on Fe_3O_4, under 800°C, 1200mTorr

4.4.3 Influence of gold

Without the presence of any gold nanodots, the sample produced shows a rough surface with different grain boundaries. However, there is no indication of one dimensional growth mode on the surface.
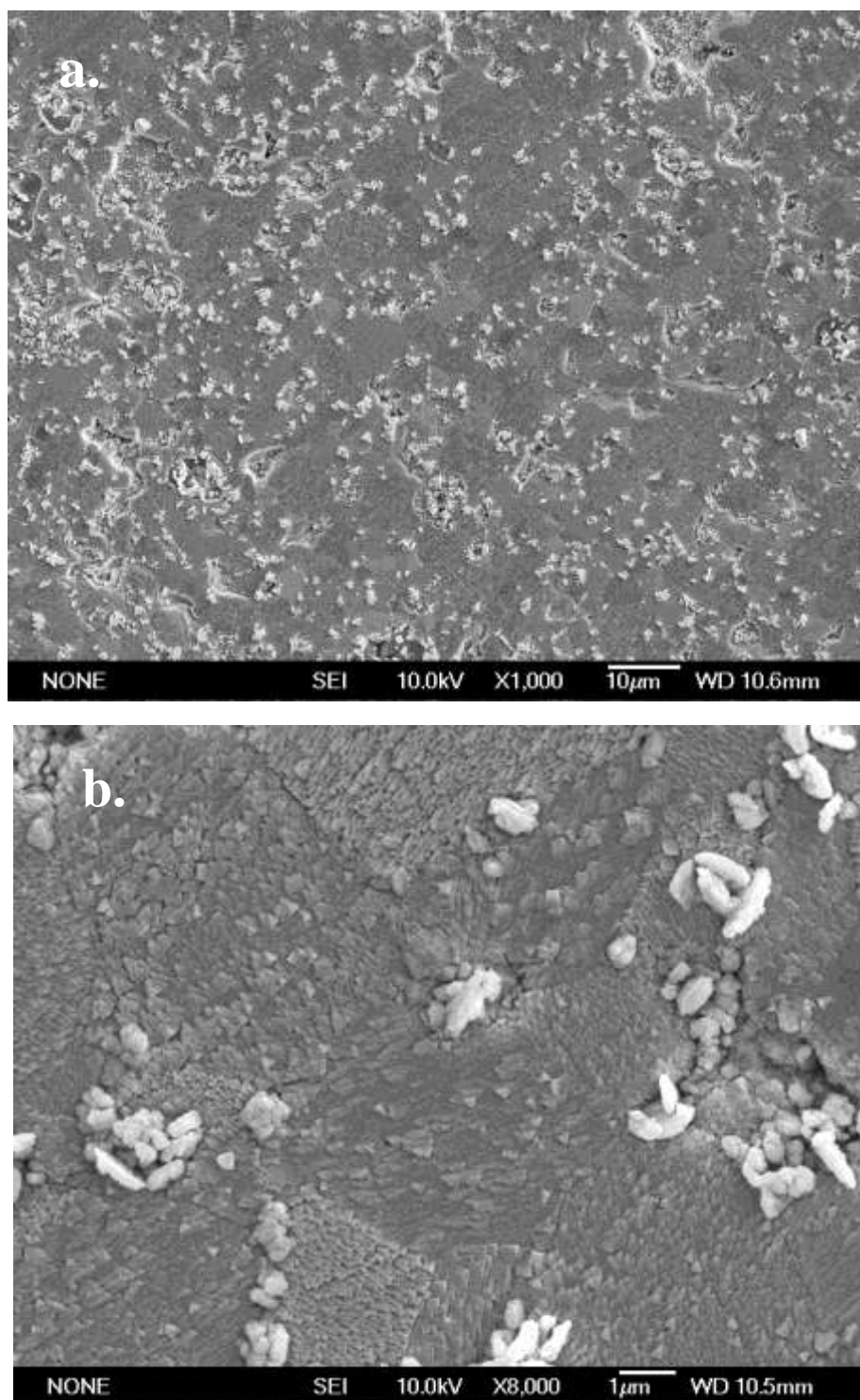
Fig. 4.4.3.1 SEM images of FOA-005 grown on Al_2O_3 ceramic, without Au, 10,000 laser shots on Fe_3O_4, under 800°C, 1200mTorr

4.4.4 Influence of oxygen pressure

Fig.4.4.4.3, Fig.4.4.4.1 and Fig.4.4.1.1 were utilized and observed to compare the layers deposited on the ceramic substrate. It was observed that the surface of the samples became rougher as the oxygen pressure increased. There was no one dimensional nanostructure found on the surface in lower oxygen pressure. However, in lower oxygen pressure, a lot of granular structures were formed in the holes. This is due to the same reason for ZnO nanorods forming in the holes of sample AZO-081, as shown in Fig.4.2.6.12

MgO single crystal substrate, in a lower oxygen pressure of 550mTorr, did not indicate any perpendicular or parallel nanorods. Pores are scattered throughout the surface and structure is very tight, which indicates that there are no packed nanorods.
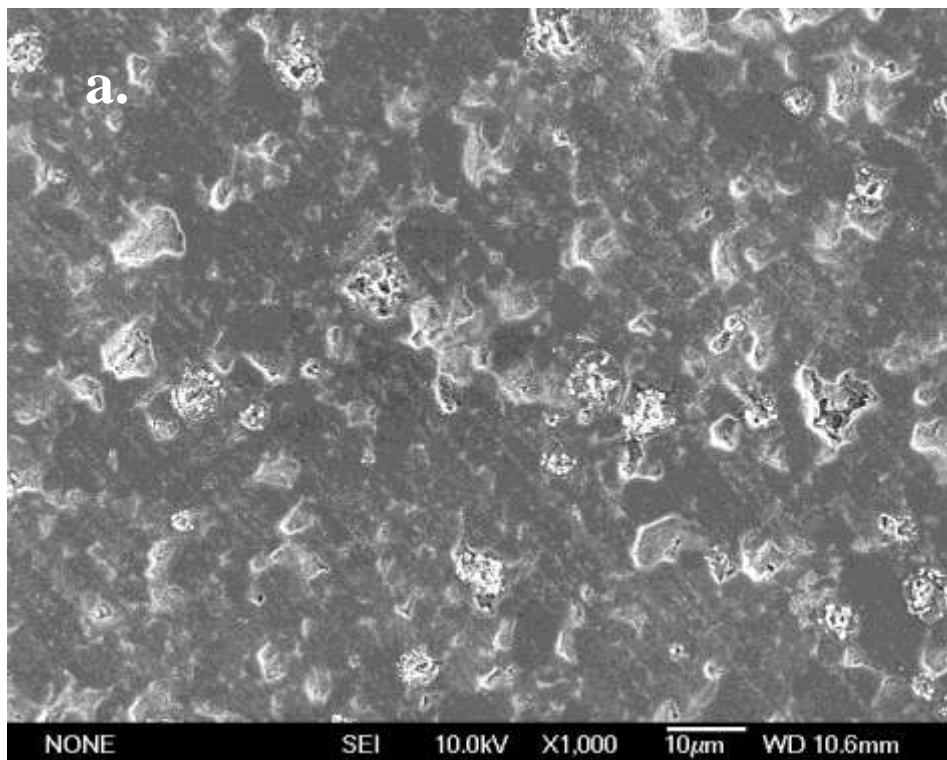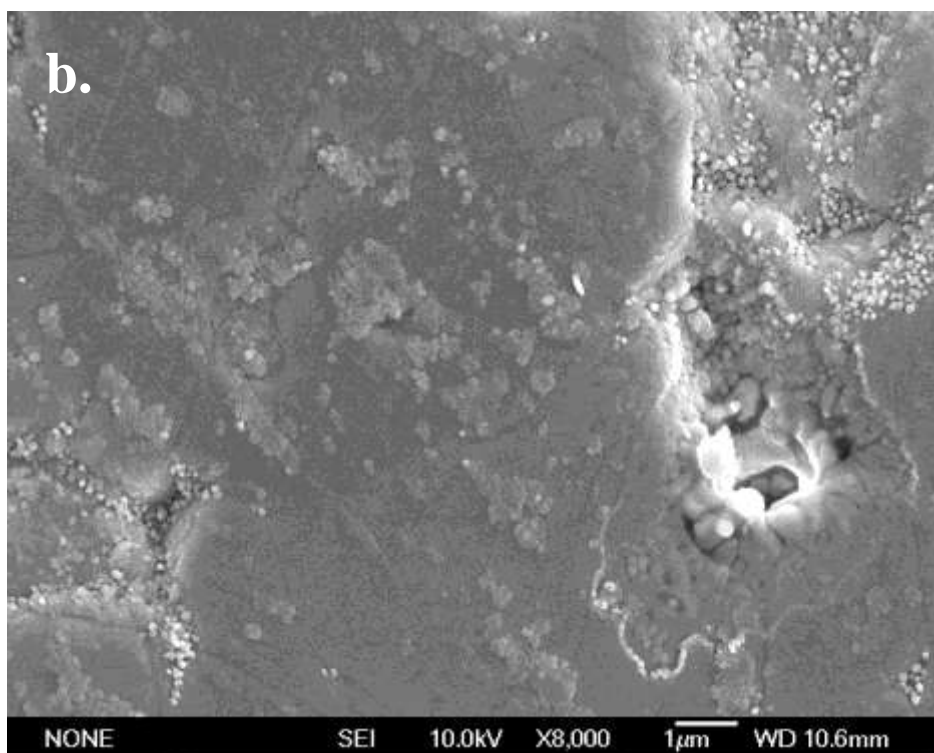
Fig. 4.4.4.1 SEM images of FOA-004 grown on Al_2O_3 ceramic, with 5 shots Au, 7000 laser shots on Fe_3O_4, under 800°C, 100mTorr
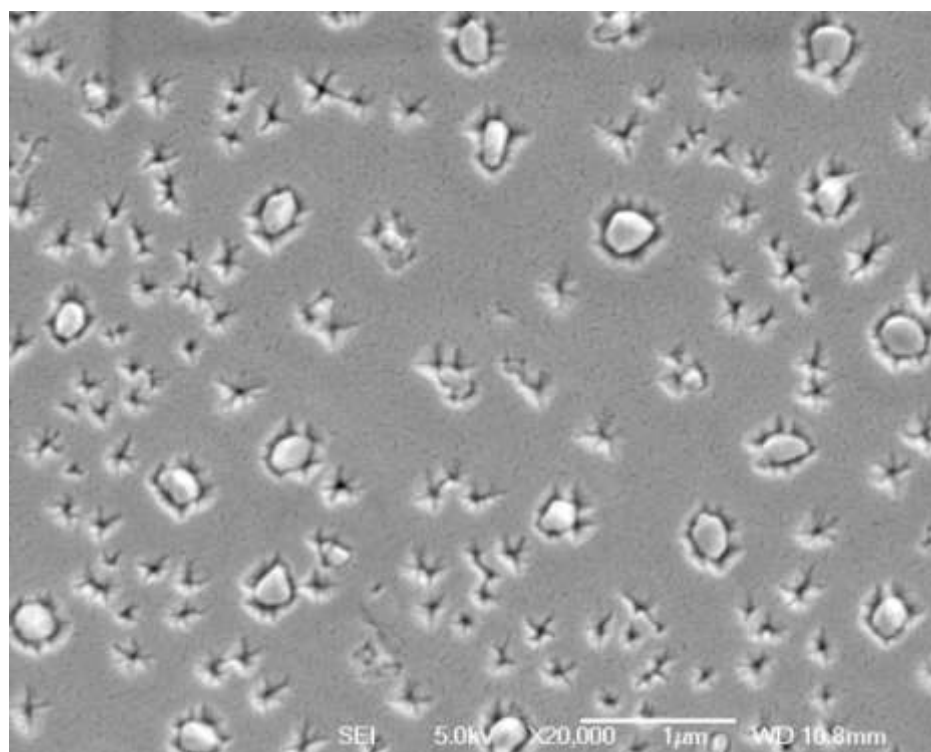
Fig. 4.4.4.2 SEM image of FOA-030 grown on MgO(100), with 5 shots Au, 10,000 laser shots on Fe_3O_4, under 800°C, 550mTorr
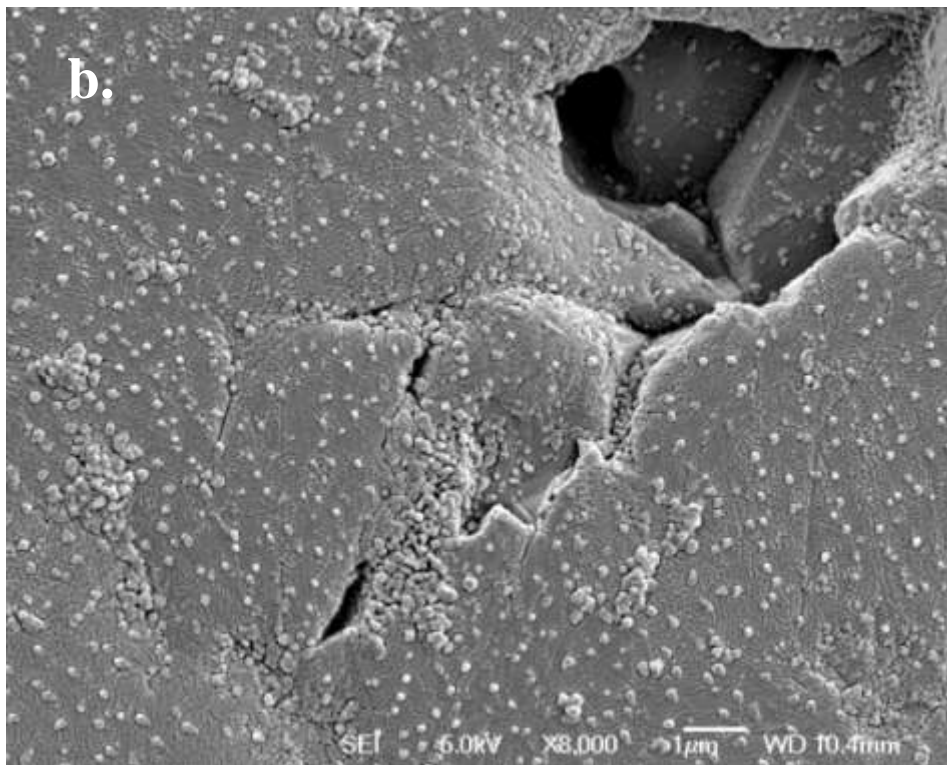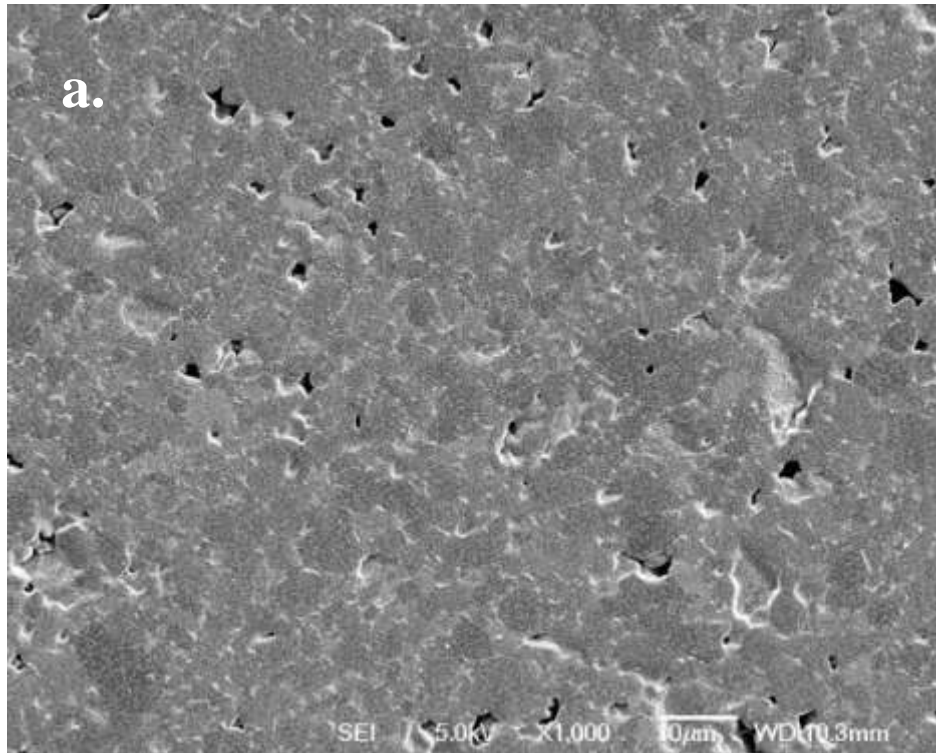
Fig. 4.4.4.3 SEM images of FOA-032 grown on Al_2O_3 ceramic, with 5 shots Au, 10,000 laser shots on Fe_3O_4, under 800°C, 550mTorr

It would not be expected that Fe_3O_4 nanorods would be produced from the Fe_3O_4 target, as Fe_2O_3 would be the preferred material grown under those conditions. However no evidence for the presence of Fe_2O_3 has been observed by XRD.

In conclusion, iron oxide nanorods can be successfully produced with the gold nanodots assistance in high oxygen pressure. The substrate's lattice parameters will determine nanorods growth direction.

References

[1] Ye Wang, Fabrication and characterization of ITO thin films on flexible plastic substrated deposited by pulsed laser deposition, (2007), Mphil thesis, University of Birmingham

[2] G. Z. Cao, Nanostrcutures and nanomaterials: synthesis, properties and applications, Imperial college press (2004) 129

[3] Douglas B. Chrisey, Graham K. Hubler, Pulsed Laser Deposition of Thin Films, (1994) John Wiley & Sons, Inc.

[4] P. H. Buffat and J. P. Borrel, Size effect on the melting temperature of gold particles, Phys. Rev. A 13(1976) 2287.

Chapter 5

Conclusions and Future Work

5.1 Conclusions

One dimensional nanostructures of MgO, ZnO, In$_2$O$_3$, SnO$_2$ and iron oxide were successfully produced by using different PLD systems. The detailed parameters of these samples have been collected in Table 5.1. Straight MgO nanorods and nanowires were formed perpendicular on the substrate of MgO(100) with a square cross section. In$_2$O$_3$ and SnO$_2$ nanorods were formed in groupings perpendicular to the substrate. The aspect and direction of iron oxide nanorods are determined by different substrates. ZnO contained the most variety of nanostructures in different shapes and sizes, but were dependent on different parameters.

5.1.1 Catalyst

In order to grow one dimensional nanostructures, it was determined that a metal catalyst is necessary for all the oxides in this project, except in the case of SnO$_2$. The following observations were noted in the following samples without any gold nanodots: MgO would form rough surface with overlapped nanostructures on MgO(100). Iron oxide was found to have a rough surface formed by different orientated grain boundaries on the ceramic Al$_2$O$_3$ substrate. ZnO was observed to have a smoother surface decorated with crystallized granular objects on the MgO(100) substrate. While In$_2$O$_3$ would have uneven shaped and overlapped nanostructures in various directions on MgO(100). However, SnO$_2$ formed more uniform nanorods with fewer and smaller sized bulk crystals present on the surface.

The catalyst used can determine the shape of the nanostructure. It was also observed that Pd can assist in the formation to produce very long, dense and curved ZnO nanowires. However, Au forms shorter and straight nanorods when 5000 shots are used on ZnO target. Another notable observation was that Ag does not help in ZnO one dimensional

nanostructures growth. Ag nanodots result in thinner In_2O_3 nanorods when compared with gold.

The number of pulses on a catalyst target influences differently on different oxides. Increasing the shots on gold target would increase the width of MgO nanorods, but by increasing the number of gold pulses, the distribution of the sizes and dimensions of ZnO nanorods become smaller. However, in the case of In_2O_3, retaining the total number of gold shots between 5 shots and 25 shots is critical, as any less than 5 shots or more than 25 shots would result in thicker, larger and uneven nanostructures.

5.1.2 Oxygen pressure

A high oxygen pressure is necessary for the most oxides in this study, except MgO, which can form uniform nanorods in 120mTorr. In the cases of SnO_2 and In_2O_3, within oxygen pressure of less than 550mTorr, would result in the present of depressions and granular nanostructures on the surface. In lower oxygen pressure of 550mTorr, iron oxide could not form any one dimensional nanostructures. In the case of ZnO, higher oxygen pressure directly affects the growth of various nanostructures. Regardless of the oxygen pressure, lower temperatures will result in uneven or non-uniform structures, but a lower temperature is necessary for ZnO nanorods growth.

5.1.3 Number of pulses on target

MgO nanorods grow separately from one another. As the number of pulses of MgO increase, this will result in increase of the length of the nanorods without significantly increasing the planar dimension. In regards of the grouping growth nanorods of In_2O_3, increasing the number of pulses will not only increase the length of the nanorods, but also the average width, so long as there are sufficient gold nanodots present. If the gold amount is not sufficient, the excess In_2O_3 will nucleate into other structures on top of the nanorods. The

shapes and forms of ZnO structures are many and varied. Under higher temperatures, increasing the number of pulses on the ZnO target, tends to be the Volmer-Weber (3D island) growth mode, while under lower temperatures, the growth tends to be the Stranski-Krastanov growth mode.

5.1.4 Temperature

One dimensional ZnO nanostructures were produced only in specific temperatures, which cannot be too high or too low. If the temperature is set too low, then the energy provided from the substrate will not be sufficient. However, if the temperature is set too high, the ZnO grows in several different orientations, resulting in more complex nanostructures. It was discovered that 600°C is the optimal temperature for ZnO. Reducing the temperature from 800°C to 700°C, it was observed that iron oxide nanorods would grow from a loose array into a compact array of nanorods. A temperature higher than 500°C is needed when producing In_2O_3 nanorods. As the temperature increases, In_2O_3 nanorods become more uniform and the average width also increases.

5.1.5 Plasma plume

ZnO nanostructures are more sensitive to the plasma plume when compared with the other oxides. The plasma plume not only influences the nanostructure of the ZnO samples, but also the distribution of these nanostructures. The blue square, marked in Fig. 4.2.4.1 is the ideal substrate placement for optimal nanostructure growth.

5.1.6 Substrate

It has been proven that, in this study, different substrates provide a different template for nanowires growth resulting in different layer morphologies. Due to the different manufacturers and surface finishing techniques for MgO(100) and MgO(001) substrates, in

242

regards to ZnO, using gold as catalyst, more nanowires were found growing parallel to the substrate on MgO(100). However, by using Palladium, significantly more, as well as longer, ZnO nanowires were found on MgO(001). It was also observed that iron oxide nanorods grew perpendicularly on Al_2O_3 substrate, but grew parallel on the MgO single crystal substrates.

For some orientated single crystal substrates, the coated layer tends to grow mainly in one specific orientation, which helps to form uniform one-dimensional nanostructures. Glass can also be considered as a substrate option for ZnO, In_2O_3 and SnO_2 when the requirement for the uniformity of nanorods is low. In the case of ZnO, it was also discovered that, under some specific environments, in some areas that provide low supersaturation, the differences from the substrates do not differentiate the morphologies of the deposition.

5.1.7 Laser energy

Decreasing the laser energy does not help in the one dimensional nanostructure growth in the case of ZnO. $1J/cm^2$ is the optimized energy density.

5.1.8 Target to substrate distance

In this study, target to substrate distance was only studied in the case ZnO. It was discovered that at higher temperatures, a greater target-substrate distance may help with the formation of one dimensional nanostructures. However, in lower temperatures, where the ideal environment to produce one dimensional nanostructures is present, a greater target-substrate distance could only decrease the quantity, density, width and length of the nanostructures.

243

Table 5.1 Detailed parameters of the samples using MgO, ZnO, In$_2$O$_3$, SnO$_2$, and iron oxide

Oxide	Number of pulses on catalyst	Number of pulses on oxide	Temp (°C)	Energy density (J/cm^2)	Oxygen pressure (mTorr)	Target-substrate distance (mm)	Substrate	One dimensional nanostructure length (nm)	One dimensional nanostructure width (nm)
MgO	0	25000	800	1.15	120-165	58	MgO(100)	-	-
	5/Au	10000						100-200	20
	5/Au	60000						1000	20
	25/Au	60000						1000	100
ZnO	5/ Pd	5000	600	1	1200	50	Si(100)	1200-1500	40-80
	5/ Pd		600			50	MgO(100) &(001)	1200-1500	40-80
	-		-				STO(100)	-	-
	5/ Ag		600			60	-	-	-
	0		700			50	MgO(100)	-	-
	5/ Au		700			50	MgO(100)	500-1000	30-230
	5/ Au		650			50	MgO(100)	550-1600	70-150
	5/ Au		600			50	MgO(100)	650-1600	20-100
	5/ Au		600			50	Glass	480-4000	200-500
	5/ Au		500			50	MgO(100)	250-5500	150-270
	5/ Au		700			60	MgO(100)	100-1000	50-130
	5/ Au		600			60	MgO(100)	40-60	50-130
	20/ Au		700			50	MgO(100)	800-1000	50-170
In$_2$O$_3$	0	5000	500	1	1200	55	MgO(100)	-	-
	2/ Au	10000	500			55	MgO(100)	1500	150-450
	5/ Au	5000	300			55	MgO(100)	-	-
	5/ Au	5000	500			55	MgO(100)	1000	30-80
	5/ Au	5000	500			55	Glass	1000	40-200
	5/ Au	10000	500			55	MgO(100)	1500	200-350
	5/ Au	5000	700			55	MgO(100)	1000	70-150
	25/ Au	10000	500			55	MgO(100)	1500	150-650
	5/ Au	5000	500			50	MgO(100)	1000	80-180
	5/ Ag	5000	500			50	MgO(100)	1000	40-120
SnO$_2$	0	5000	700	1	1200	55	MgO(100)	1000	70-160
	5/ Au		700		1200	55	MgO(100)	1000	70-240
	0		700		550	55	MgO(100)	-	-
	5/ Au		700		550	55	MgO(100)	1000	70-200
Iron oxide	0	10000	800	1	1200	55	Al$_2$O$_3$ ceramic	-	-
	5/ Au	10000	800		1200	55	Al$_2$O$_3$ ceramic	1000	60-180
	5/ Au	10000	800		1200	55	Al$_2$O$_3$ single crystal	1500	200-300
	5/ Au	7000	800		100	55	Al$_2$O$_3$ ceramic	-	-
	5/ Au	1000	800		1200	55	MgO single crystal	2000	30-60
	5/ Au	10000	700		1200	55	Al$_2$O$_3$ ceramic	700	80

5.2 Future work

Additional applications, using the produced nanostructures in this study, need to be developed in future work. Also the details of each material growth mode need to be studied further.

5.2.1 Catalyst

The influence of gold nanodots affecting these oxides growth mode could be studied by TEM. It will be very crucial to obtain the detailed TEM images of the crossection of nanorods with the substrate in order to understand how the first layer grows on the substrate.

Pd or any other metal, such as Pt and Pb, may be a proper catalyst for In_2O_3 and as well as other oxides, but this needs further investigation. The influence of increasing gold shots in the case of iron oxide would also be a topic which needs to be studied in the future.

5.2.2 Oxygen pressure

A lot of semiconductors' properties are related to the oxygen vacancy. However, higher oxygen pressure results in lack of sufficient oxygen vacancies. One of future objectives will be to produce even and uniform one dimensional nanostructures containing sufficient oxygen vacancies. There are two methods: using argon or a mix gas of argon and oxygen, decreasing the target to substrate distance when reducing the oxygen pressure. Currently in chamber #2, the closest distance is 40mm. To produce a sample with even and uniform nanostructures, reducing the turbo pump working frequency and gently introduce gas during the process of deposition is another factor. Moving the gas pipe opening to the bottom of chamber #2 could result in more even structures, because when comparing the three chambers, chamber #1 and especially chamber #3 could produce samples with more even

structures since the gas pipe openings in these two chambers are at the bottom of the chamber.

5.2.3 Number of pulses on target

The effect of increasing the number of pulses on SnO_2 and iron oxide is not quite clear, though it can be assumed that it may result in increasing SnO_2 nanorods' length and width, since SnO_2 nanorods are also formed in similar groupings as In_2O_3. This needs to be further investigated in the future. As for iron oxide nanorods, as study that varies the number of pulses at different temperatures can also be considered as a research direction.

5.2.4 Laser energy

Additional research in this topic should also cover the effects of decreasing the oxygen pressure or decreasing the target to substrate distance, when decreasing the laser energy. This may result in more oxygen vacancies in the one dimensional nanostructures.

5.2.5 Others

With the exception of introducing more oxygen vacancies, doping into the nanorods is another important topic that needs to be studied, in more detail, in the future. This may prove useful as there are many useful properties of semiconductors that are derived from oxygen vacancies and doping.

ITO could be studied in the future. However, ITO needs to be produced in an environment that contains a very low oxygen pressure (2~10mTorr). However, this oxygen pressure level is too low to form one dimensional nanostructures. Argon or a mixture of oxygen with argon is highly suggested for future study of ITO.

There are some limitations by using the available facilities to investigate the properties or applications of nano-sized one dimensional structures. As this field is still considered to be at the cutting edge of scientific research, it is still far away from maturity. At this stage, it can be studied by using the methods of thin films study. Spectrum study could be considered as another direction for future study. It should be noted that avoid using silver paste on the substrate and two sized polished substrates is highly suggested. Also it assumes due to their large surface to volume ration, one dimensional nanostructure functional oxides such as ZnO and In_2O_3 can be utilized into applications in nanoscale sensor, which can be developed in the future.

As MgO nanorods were successfully produced, based on these nanorods, further applications should be developed, such as coating YBCO or other multiple oxides, as thin layers, outside these nanorods and study their properties.